PETROGRAPHIC AND GEOCHEMICAL EVIDENCE FOR THE ORIGIN OF PHOSPHORITES AND PHOSPHATE ROCKS FROM THE WEST COAST OF SOUTH AFRICA

XAVIER N MIDDLETON

Submitted in fulfilment of the requirements of the degree of
MASTER OF SCIENCE
in the
Department of Geological Sciences
Faculty of Science
University of Cape Town
December 2003

DECLARATION

I, **Xavier N Middleton**, submit this thesis in fulfilment of the requirements for the degree of Master of Science (MSc) in Geology. I claim that this is my original work and that it was conducted under the supervision of Dr J Compton. No part of this research has been submitted in the past, or is being submitted, for a degree at another university.

Signed by candidate

Xavier N Middleton

ACKNOWLEDGMENTS

I would like to express my sincerest appreciation and gratitude to the following people and institutions that helped to make the completion of this study a possibility;

- Dr John Compton of the Department of Geological Sciences, who patiently guided and encouraged me and offered invaluable academic and practical assistance in the field and in the laboratory.

- Dr John Rogers of the Department of Geological Sciences, for numerous discussions on phosphorites, sedimentology and more importantly the enigma of the deposit at Langebaanweg.

- Ms Pippa Haarhoff and the friendly staff at the West Coast Fossil Park, for allowing access to the deposit.

- Ms Leigh Sonn for her kind words and compassionate support, especially when the going got "tough".

- The Sedimentology workshop for weekly discussions and providing a platform to discuss the findings of this research.

- UCT postgraduate Scholarship office and the NRF (National Research Foundation) for the financial support, without which this project would not have been completed.

- Special thanks are also due to my close friends and family for their encouragement.

Thank you.

SYNOPSIS

The onshore marine phosphorite and aluminium phosphate deposits of Varswater Quarry (near Langebaanweg), Bomgat (near Hoedjiespunt), Kreefte Bay and Konstabelkop were studied to determine the origin of the various deposits. Langebaanweg is situated 110 km north-north west of Cape Town in the southwestern Cape. It is roughly 13 km north-east of Saldanha Bay and 21 km south of the mouth of St Helena Bay. The Bomgat exposure is situated on the Hoedjiespunt Peninsula at Saldanha Bay. It is approximately 2 km south of Saldanha. Konstabelkop is approximately 15 km south-south east of Saldanha, whereas Kreefte Bay is approximately 4 km west of Konstabelkop. The main phosphate bearing units within the Varswater Quarry include the Pelletal Phosphorite member and the Gravel member. Both units are found within the Varswater Formation.

The Pelletal Phosphorite member is composed of consolidated phosphorite lenses and unconsolidated fossiliferous phosphatic sands. Petrographic analysis of the Varswater phosphorites reveals that the Pelletal Phosphorite member and the Gravel member are composed of predominantly rounded to well rounded quartz grains, phosphatised shell fragments (PSh) and peloidal phosphorite (Pph). Unlike the Pelletal Phosphorite member, the Gravel member contains only occasional phosphatised shell fragments. The Pelletal Phosphorite member also contains minor amounts of phosphatised echinoid spines and occasional partially digested (dissolved) phosphatised foraminifera. The Bomgat phosphorites are composed of various well to poorly preserved phosphatised bioclasts (bryozoan remains, echinoderm fragments (mostly ossicles), mollusc shell fragments (typically gastropods and bivalves) and occasional benthic foraminifers). The phosphate from the Gravel member and Pelletal Phosphorite member was determined to be francolite, whereas the mineralogy of the Bomgat phosphorites was determined by XRD to be dahllite. The mineralogy of the aluminium phosphate deposits is either crandallite or varsicite. The mineralogy is consistent with the weathering of igneous rocks by the leaching of guano by meteoric water, resulting in the aluminium phosphates.

The rare-earth elements (REE) and trace-element abundances of the phosphate and phosphorite deposits of the southwestern Cape have been studied in order to characterise the various deposits. The rare-earth element and trace-element abundances and distributions for the phosphorites and phosphate rocks have been measured by inductively coupled plasma – mass spectroscopy (ICP-MS) and laser ablation inductively coupled plasma – mass spectroscopy (LA-ICP-MS). The REE are normalised to Post-Archaean average Australian shale (PAAS). The PAAS-normalised REE distribution patterns of the offshore and onshore marine phosphorites show flat, heavy REE (HREE) enriched, relative to light REE (LREE) patterns, whereas the distribution patterns of the aluminium phosphate deposits from Kreefte Bay are "toothed".

The phosphatic components (peloids, biogenic and carbonate fluorapatite (CFA) cement) within the Gravel member phosphorite show very similar REE distribution patterns. The phosphatic components within the Pelletal Phosphorite member show significantly different REE distribution patterns. The CFA cement and the peloids are similar with flat HREE-enriched patterns, whereas the phosphatised shell fragments show HREE-enriched patterns. It is therefore possible to distinguish between the various components within the phosphorite and phosphatic sands from the Pelletal Phosphorite member.

Cerium anomalies were determined for the various phosphorite and phosphate rocks. Generally, the phosphorite and phosphate rocks show slightly negative to positive Ce-anomalies. Ce-anomalies have been applied in numerous studies as a palaeoredox indicator,

and, according to the Ce-anomalies found in the phosphorites, it appears that the deposits gained their REE under suboxic conditions.

The chemical variability amongst the various phosphorites was investigated. In terms of the trace-elements (including the REEs), the Pelletal Phosphorite member and the Gravel member show similar trace-element abundances. This was determined by bi-variant scatterplots (or binary plots). The similar trace-element distribution indicates that the Pelletal Phosphorite member is indeed an erosional remnant of the underlying Gravel member.

Further work should be carried out using stable isotopes (e.g. C, O, S, and Sr) as rare-earth elements are not an alternative to isotope studies. Further research should attempt to develop the REE and trace-element data set and possibly attempt comparisons of other offshore phosphorite deposits (i.e. the concretionary phosphorites from Walvis Bay) with the onshore sedimentary phosphate deposits. Future research should also attempt to understand the extent of phosphorite alteration, preferably using stable isotopes (C and O). Additional research needs to be done on the aluminium phosphate deposits of the Posberg peninsula, concerning major oxides, and trace-elements.

GLOSSARY OF TERMS AND ABBREVIATIONS

bne	Phosphatised bone fragment
CFA	Carbonate fluorapatite
Collophane	A term to describe amorphous, anisotropic cryptocrystalline to microcrystalline calcium phosphate (CFA)
Dahllite	A hydroxyl-rich, fluorine-poor apatite
Francolite	Francolite is generally defined as a CFA with noticeable amounts of CO_2 and crucially more than 1% fluorine (McConnell, 1938; McConnell, 1973).
ICP-MS	Inductively coupled plasma mass spectroscopy
LA-ICP-MS	Laser ablation inductively coupled plasma – mass spectroscopy
Lenses	Layers or beds of generally structureless phosphorite
NRF	National Research Foundation
PAAS	Post-Archaean average Australian shale
Pellet	A non-genetic term to describe well-rounded, ovoid phosphorite grains. The grains may contain or lack nuclei, but have no internal layering. The term should not be confused with the definition by Folk (1962). Folk (1962) defined a 'pellet' as carbonate particles smaller than 2.74phi (0.15mm).
Peloid	(See Pellet.)
Phosphate rock	A sedimentary deposit which contains less than 18% P_2O_5 apatite.
Phosphatisation	The process of replacement of carbonate material by apatite or the *in-situ* formation of phosphate/phosphorite.
Phosphogenesis	The process of authigenic and biological phosphate mineral precipitation (Trappe, 2000).
Phosphorite	A marine sedimentary deposit which contains more than 18% P_2O_5, approximately 50% apatite (Bushinsky, 1966; Tankard, 1973; Trappe, 2000)
Pph or pph	Phosphorite peloids
ppm	parts per million
PSh or psh	Phosphatised shell fragments; bioclasts
SEM	Scanning electron microscopy
UCT	University of Cape Town
XRD	X-ray diffraction

TABLE OF CONTENTS

Chapter 3: Description of study area and aims of the study

Chapter 4: Sampling localities and strategy

Chapter 5: Methodology and Analytical Techniques

Chapter 6: The petrography and mineralogy of phosphorites and phosphate rock from the studied localities

Chapter 7: Rare-earth element and trace-element geochemistry

Chapter 8: Discussion

LIST OF FIGURES

LIST OF TABLES

THESIS OVERVIEW

The usage of isotopic signatures, elemental abundances, and distribution patterns of rare-earth elements (REE) and trace-elements has become crucial in understanding marine sedimentary environments. REE have proven to be useful tracers for a variety of processes in as widely different disciplines as sedimentology, igneous petrology and cosmochemistry. REE have shown to be a remarkably coherent group of elements and are considered to be immobile. REE are known to be incorporated in phosphorite and phosphate deposits.

The present study is intended to contribute data concerning the rare-earth element and trace-element geochemical nature of the phosphatic deposits in the southwestern Cape. In this dissertation, Chapter 1 and 2 present short reviews of pertinent literature regarding the mineralogy, global distribution (of phosphate rocks and phosphorites) and the geochemistry of rare-earth elements. Chapter 2 also discusses the application of REE in the study of phosphorites and phosphatic rocks. Chapter 3 comprises a brief description of the location and a short literature review of the geological setting of the phosphorites found in the southwestern Cape. This chapter also addresses the questions, which were formulated to maintain the focus of this project.

A program of sediment and rock collection was undertaken at the Varswater Quarry, Bomgat (Hoedjiespunt), Konstabelkop and Kreefte Bay (Kreeftebaai) and this is described in Chapter 4. Chapter 5 presents the methods and methodology used. The mineralogy and petrography of the samples is presented in Chapter 6. In Chapter 7 the analysis of the abovementioned samples, with respect to rare-earth elements and trace-elements is described and the results are presented in Chapter 8 in such a form that illustrates the conclusions drawn regarding the rare-earth element and trace-element geochemistry of the phosphorites. Chapter 9 presents a short summary of the salient deduction arising from this research and recommendations are presented for future research.

CHAPTER 1
THE MINERALOGY AND GLOBAL DISTRIBUTION OF PHOSPHATE ROCKS AND PHOSPHORITES

This chapter presents a literature review of the mineralogy and global distribution of phosphate rocks and phosphorites. It provides the necessary backdrop to the subsequent chapters, which deal with various aspects of South African phosphate rock and phosphorite deposits.

1.1 INTRODUCTION

The element phosphorus is present in minor to trace amounts in most rocks (igneous, metamorphic and sedimentary). The quantities, generally expressed as % P_2O_5, range from 0.04% in most sandstones to approximately 0.4% in intermediate igneous rocks (Cook, 1984). It is only within phosphate rock (and more importantly within sedimentary, marine phosphorites) that phosphorus is significantly enriched (>18 wt% P_2O_5) to constitute an economic deposit (Bentor, 1980; Kolodny, 1981).

In the geologic record phosphate rocks and phosphorites are relatively rare, but particularly significant as an economic commodity (Figure 1.1). In particular, sedimentary phosphorites are known to contribute more than 80% of the world's production of phosphate ore and 96% of the world's total resources of phosphatic rock (Boggs, 1995). Phosphate rocks are not restricted to any specific geologic age. They have been found to occur in rocks ranging in age from Precambrian to Holocene.

1.2. MINERALOGY OF PHOSPHORITE AND PHOSPHATE DEPOSITS

Phosphorus occurs in more than 200 minerals, of which the most common occurrences are found within varieties of apatite. These varieties include the most common phosphate minerals; namely the fluorapatites [$Ca_5(PO_4)_3F$], chlorapatites [$Ca_5(PO_4)_3Cl$] and the hydroxyapatites [$Ca_5(PO_4)_3OH$]. Fluorapatites (or apatites approaching the composition of fluorapatite) are generally found within igneous and metamorphic rocks, whereas apatites that contain mixtures of the composition of hydroxyapatite and chlorapatite are particularly less abundant (McClellan and van Kauwenbergh, 1990). According to McConnell (1973) "pure" hydroxyapatite is especially rare. Apatites in sedimentary rocks (and phosphorites) are generally carbonate hydroxyl fluorapatite (Boggs, 1995) or carbonate fluorapatite (CFA). According to Altschuler (1973) carbonate fluorapatite can be represented by the approximate formula:

$Ca_{10}(PO_4)_{6-x}(CO_3)_x(F, OH)_{2+x}$.

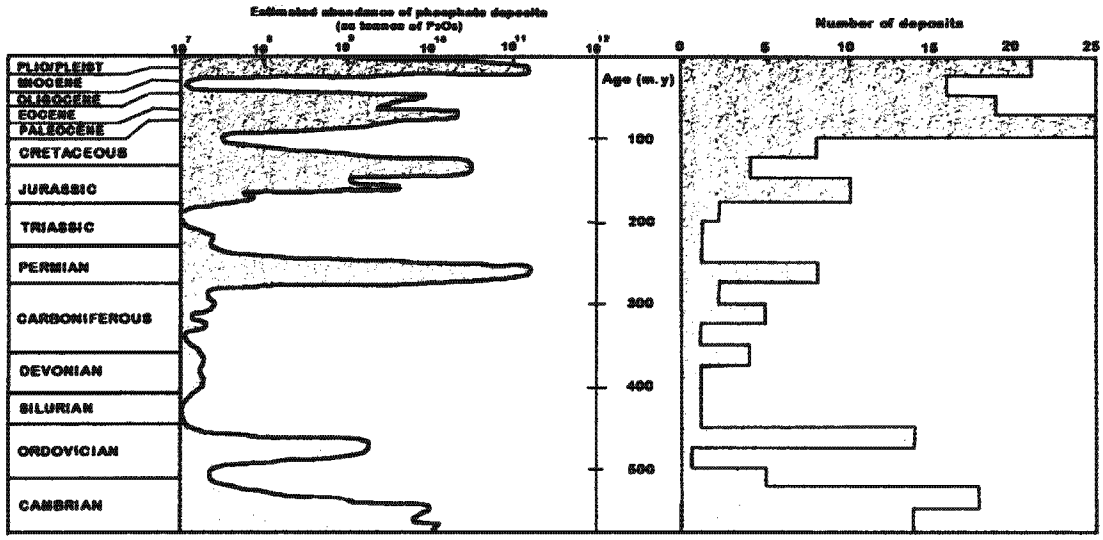

Figure 1.1. Graphical representation of the estimated global abundance of phosphate (metric tons of P_2O_5) and the number of phosphate deposits throughout the Phanerozoic (Cook and McElhinny, 1979).

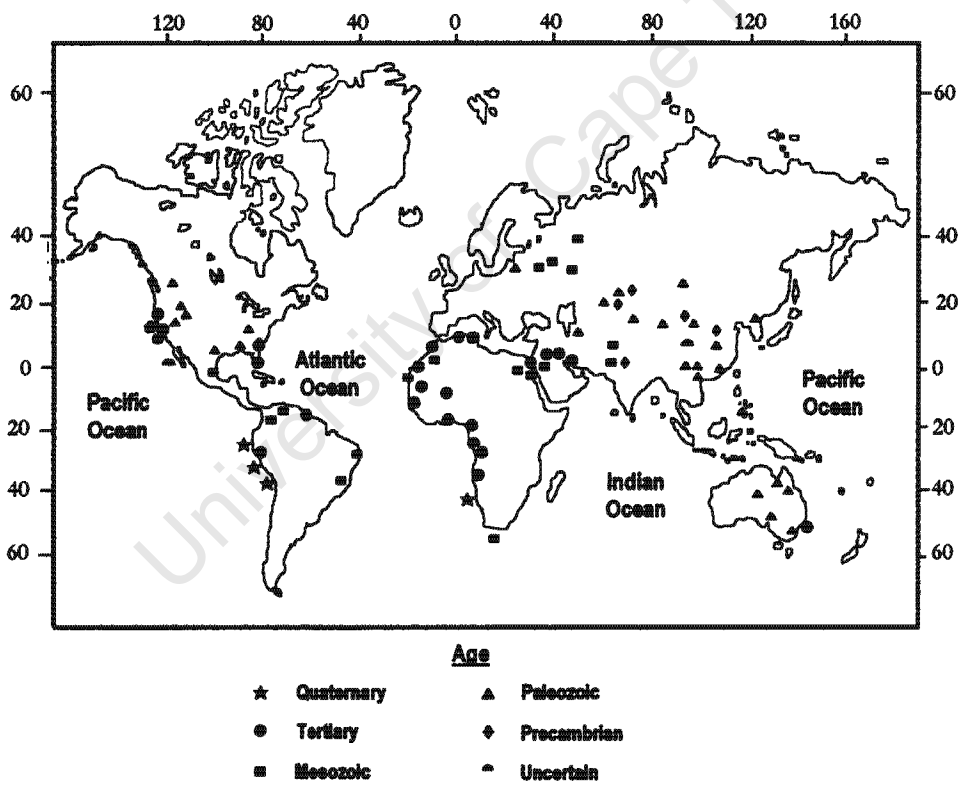

Figure 1.2. Global distribution of major phosphorite deposits (Boggs, 1995, modified after Cook, 1976).

1.2.1. Francolite

In general the most abundant variety of CFA in sedimentary rocks is the mineral francolite (Ca_{10} $[(PO_4)_{6-x}(CO_3)_x]$ F_{2+x})[1]. Francolite, in phosphorites and other sedimentary rocks is generally accepted to possess a cryptocrystalline to microcrystalline texture. It was initially believed that francolite was an amorphous fluorine-bearing calcium phosphate material called collophane[2], but on the basis of x-ray diffraction (XRD) and optical microscopy the crystallinity and pseudo-isotropic nature of the francolite was determined. Further analysis (using x-ray diffraction) showed that the x-ray diffraction patterns of francolite and fluorapatite were very similar, but that there existed distinct differences between the two minerals (McConnell, 1938; McClellan & Kauwenbergh, 1980). For instance Altschuler *et al.* (1952) noted that the unit-cell dimensions of carbonate apatite were significantly smaller than those reported for fluorapatite. Francolite is generally defined as a CFA with noticeable amounts of CO_2 and crucially more than 1% fluorine (McConnell, 1973; McConnell, 1938). In some cases as McClellan and van Kauwenbergh (1990) pointed out, francolite may contain substantially more fluorine (3.77% F) than fluorapatite. McClellan and Van Kauwenbergh (1990) also consider possible confusion arising from so-called "fluorine deficient apatites" that "contain less than 2 moles of F per unit-cell of fluorapatite". Dahllite (a different CFA mineral) is generally considered to be deficient in fluorine. According to Nathan (1984), the composition of francolite is essentially heterogeneous. In other words francolite (and many other sedimentary apatites) are naturally prone to a wide range of chemical substitutions within their structure (Table 1.1). It is believed that the substitutions within the structure of these minerals may reflect the geochemical setting or environment in which precipitation or subsequent alteration (during diagenesis or weathering) took place (Trappe, 1998). These various elements substituted into the francolite structure (such as trace-elements, REE or isotopes) can be used in understanding of the origin of phosphorites (Figure 1.3).

Table 1.1. Probable element substitutions in the francolite (apatite) structure. The elements highlighted in bold are important substitutions (Nathan, 1984).

Constituent ion	Substituting ion
Ca^{2+}	**Na^+**, K^+, Ag^+ **Mg^{2+}**, **Sr^{2+}**, Ba^{2+}, Cd^{2+}, Mn^{2+}, Zn^{2+} Bi^{3+}, Sc^{3+}, Y^{3+}, REE^{3+} $U4^+$
PO_4^{3-}	**CO_3^{2-}**, **SO_4^{2-}**, CrO_4^{2-} **CO_3**, **F^{3-}**, OH^{3-}, AsO_4^{3-}, VO_4^{3-} SiO_4^{4-}
F^-	OH^-, Cl^-, Br^- O^{2-}

[1] This is the simplified structural formula for francolite (Trappe, 1998).

[2] The term "collophane" is still used, but only when the apatite-like phase cannot be positively identified.

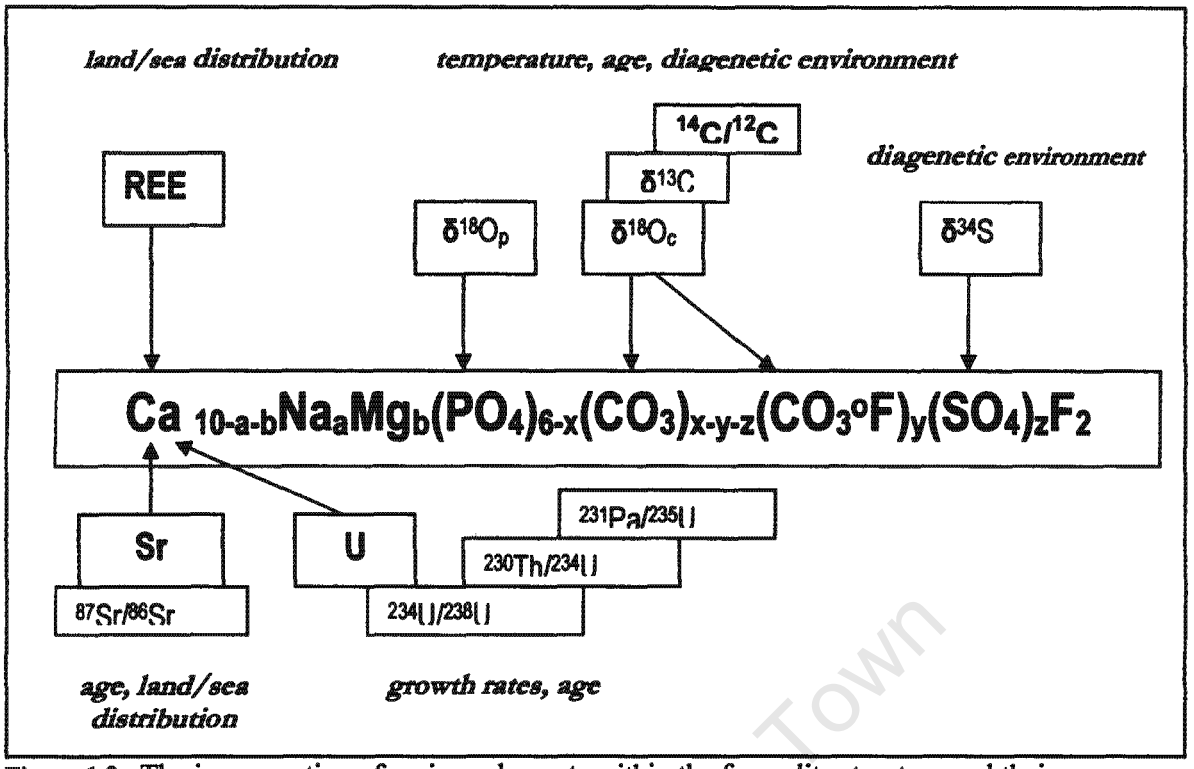

Figure 1.3. The incorporation of various elements within the francolite structure and their application for various paleoenvironmental and dating methods (modified after Trappe, 1998).

1.2.2. Other minerals found in phosphate rocks

Although francolite is the dominant mineral in unweathered marine phosphorites, other forms of CFA and phosphate minerals do exist, especially in weathered phosphorites or phosphate rocks (Nathan, 1984). It appears that a large number of other phosphate minerals are formed during the alteration of weathered material (Flicoteaux & Lucas, 1984) or during late diagenesis (Trappe, 1998). These include typical aluminium phosphate minerals (ALPO) such as crandallite [$CaAL_3(PO_4)_2(OH)_5{\cdot}H_20$], augelite [$Al_2(PO_4)_2(OH_3),$] wavellite [$Al_3(PO_4)_2(OH)_{10}{\cdot}5H_2O$] and millisite [$(Na,K)CaAl_6(PO_4)_4(OH)_6{\cdot}3H_2O$] or other forms of CFA such as whitlockite (Ca3(PO4)2), brushite ($CaHPO_4{\cdot}2H_2O$) and the more common hydroxyl-rich, fluorine poor variety of CFA, dahllite [$Ca_5(PO_4,CO_3)_3(OH,F)$]. Dahllite is easily converted to francolite through interaction with sediment pore water, during early diagenesis (Abed and Fakhouri, 1996). According to Froelich *et al.* (1983) the dahllite-francolite conversion takes place contemporaneously with direct precipitation of CFA. Other phosphate minerals are summarised in Nriagu & Moore (1984) and McConnell (1973).

1.3. GLOBAL DISTRIBUTION OF PHOSPHORITE AND PHOSPHATE DEPOSITS

Phosphate deposits can be found in sedimentary, igneous and metamorphic environments. Igneous phosphate deposits are geographically widespread. These deposits are normally associated with alkaline intrusive plutonic rocks (generally nepheline syenites, or carbonatites, or alkaline ultrabasic complexes) (Cook, 1984). In general these deposits occur within plug-like bodies or as ring complexes. Igneous phosphate deposits are generally small and non-commercial; however there are some deposits that have been very profitable. In particular the deposit at Khibiny, which is one of the largest igneous phosphate deposits found in Russia (Notholt, 1979). In South Africa the most notable igneous phosphate deposit is the Palabora deposit (Figure 1.4). The Palabora deposit is associated with a carbonatite plug which grades into the main ore zones of magnetite-olivine-apatite rock and apatite-forsterite-magnetite rock (Cook, 1988). According to Notholt (1979) a third type of igneous phosphate deposits can be identified. These are the fairly common primary apatitic carbonatites.

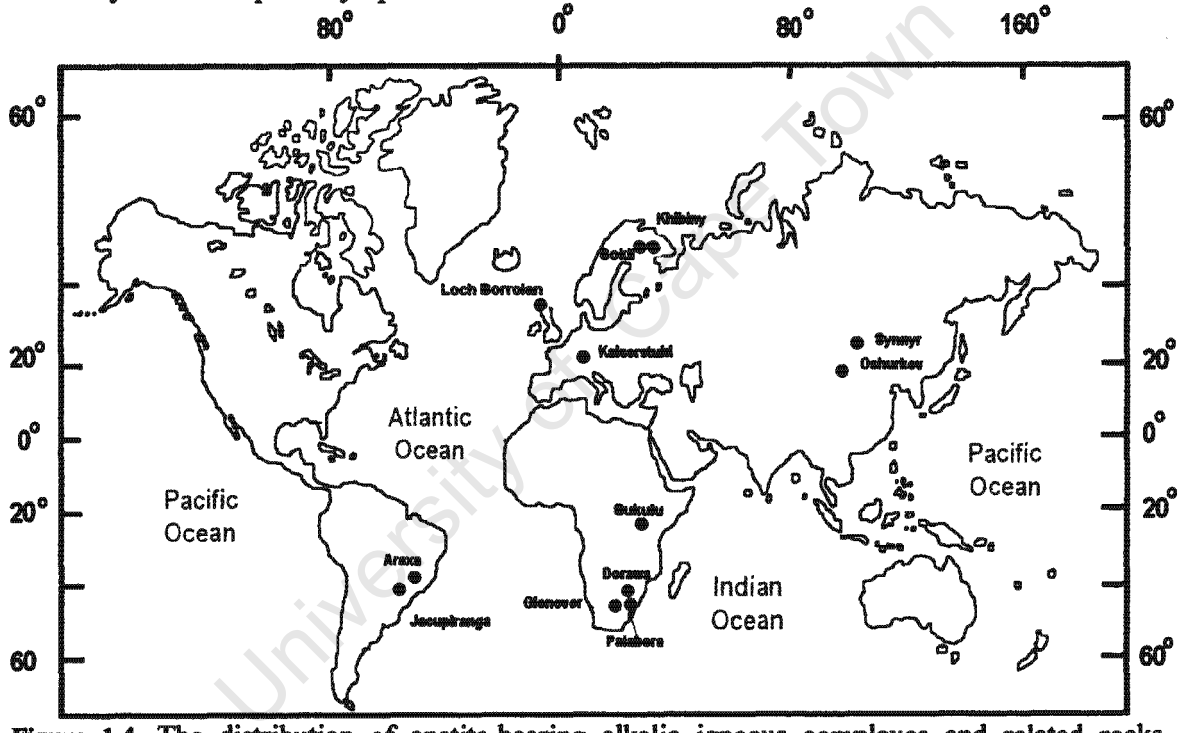

Figure 1.4. The distribution of apatite-bearing alkalic igneous complexes and related rocks (Modified after Notholt, 1979).

Sedimentary phosphate deposits or phosphorites are by far the most common type of phosphate, and have been mined extensively throughout the world. Most notable are the extensive phosphate occurrences found within Morocco (North Africa), the United States (Florida) and off the coasts of Southern Africa and Peru/Chile.

Guano deposits are another type of sedimentary phosphate deposits. These include cave deposits and insular guano (Cook, 1984). Cave deposits are phosphate deposits formed by the accumulation of bat droppings (guano), whereas insular guano deposits are formed

either directly or indirectly (chemical weathering) from the accumulation of bird droppings (Cook, 1984; Flicoteaux and Lucas, 1984). According to Flicoteaux and Lucas (1984) the weathering of limestone due to the leaching of guano (by meteoric water), may result in calcium phosphate minerals, such as brushite, whitlockite, and hydroxylapatite. Similar weathering of igneous rocks and soils may result in the formation of aluminium and iron phosphate minerals (these include minerals from the variscite-strengite isomorphous series).

In general phosphorites and certain phosphate rocks occur mostly at shallow depths on the ocean sea floor (near coastlines). Other similar deposits have also been documented on oceanic islands, seamounts, atolls and plateaus and guyots (Baturin, 1982; Burnett and Riggs, 1990; Glenn *et al.*, 1994). Marine phosphorite deposits are generally associated with organic-rich siliceous sediments or calcareous sediments hosted within a high-productivity marine environment (Birch, 1979a; Baturin and Bezrukov, 1979; Baturin, 2000). The area of high-productivity usually corresponds to the occurrence of zones of coastal upwelling (e.g. modern (concretionary) phosphorite occurrences on the Namibian continental margin and the Peru/Chile continental margin (Summerhayes *et al.*, 1973; Balson, 1990; Bremner, 1980a; Veeh *et. al.*, 1973; Baker and Burnett, 1988; Glenn and Arthur, 1988; Piper *et al.*, 1988). Intense coastal upwelling on the continental margins of Peru/Chile and southwestern Africa are caused by the Chile-Peru and Benguela currents, respectively (Price and Calvert, 1978). There are however phosphorite deposits that can form in areas of no to little upwelling (e.g. lacustrine) (Swirydczuk *et al.*, 1981). Phosphate and phosphorite deposits occur extensively along the continental shelf off the west and south coasts of southern Africa (Parker and Siesser, 1972; Parker, 1975; Birch, 1975, 1979a, 1979b, 1979c) (Figure 1.5).

In general the phosphate deposits consist of: unlithified apatite-rich clastic sands (phosphorite sand) which are composed of characteristic well rounded peloids or pellets, consolidated phosphorite rocks and concretionary phosphorite (nodules of phosphorite or phosphate) (Birch, 1979a; Bremner and Rogers, 1990). The phosphorite rock assemblage includes widespread occurrences of phosphatised limestones, conglomeratic & non-conglomeratic glauco-phosphorites, and conglomeratic & non-conglomeratic phosphorites (Parker and Siesser, 1972; Birch, 1979b; Mulabisana, 1998). The South African and Namibian phosphorites differ slightly. According to Bremner and Rogers (1990) the Namibian phosphorites are mainly of authigenic origin, whereas the South African phosphorites are generally more diagenetic. Bremner and Rogers (1990) explain that the apatite-rich (phosphorite) sands can be further subdivided into pelletal phosphorite and glauconitized pelletal phosphorite. Birch (1979c) first noted the close relationship between the two authigenic minerals of glauconite and CFA in certain phosphorite pellets from the South African continental shelf. The glauconitized pelletal phosphorite has a glauconitized outer rim, which led Bremner and Rogers (1990) to speculate on the possible origins of the pelletal phosphorite given its mineral assemblage. According to Bremner and Rogers (1990) the pelletal phosphorite was formed within a subtropical estuarine environment, as intraclasts on intertidal mudflats. The mudflats were inundated by phosphate-rich, upwelled, oceanic water. It is envisaged that the glauconitized pelletal phosphorite was formed in the upper reaches of the estuary, where

river-borne iron (provided by clay minerals) was readily available. The iron from the clay minerals is necessary for glauconitization, or the formation of glauconite.

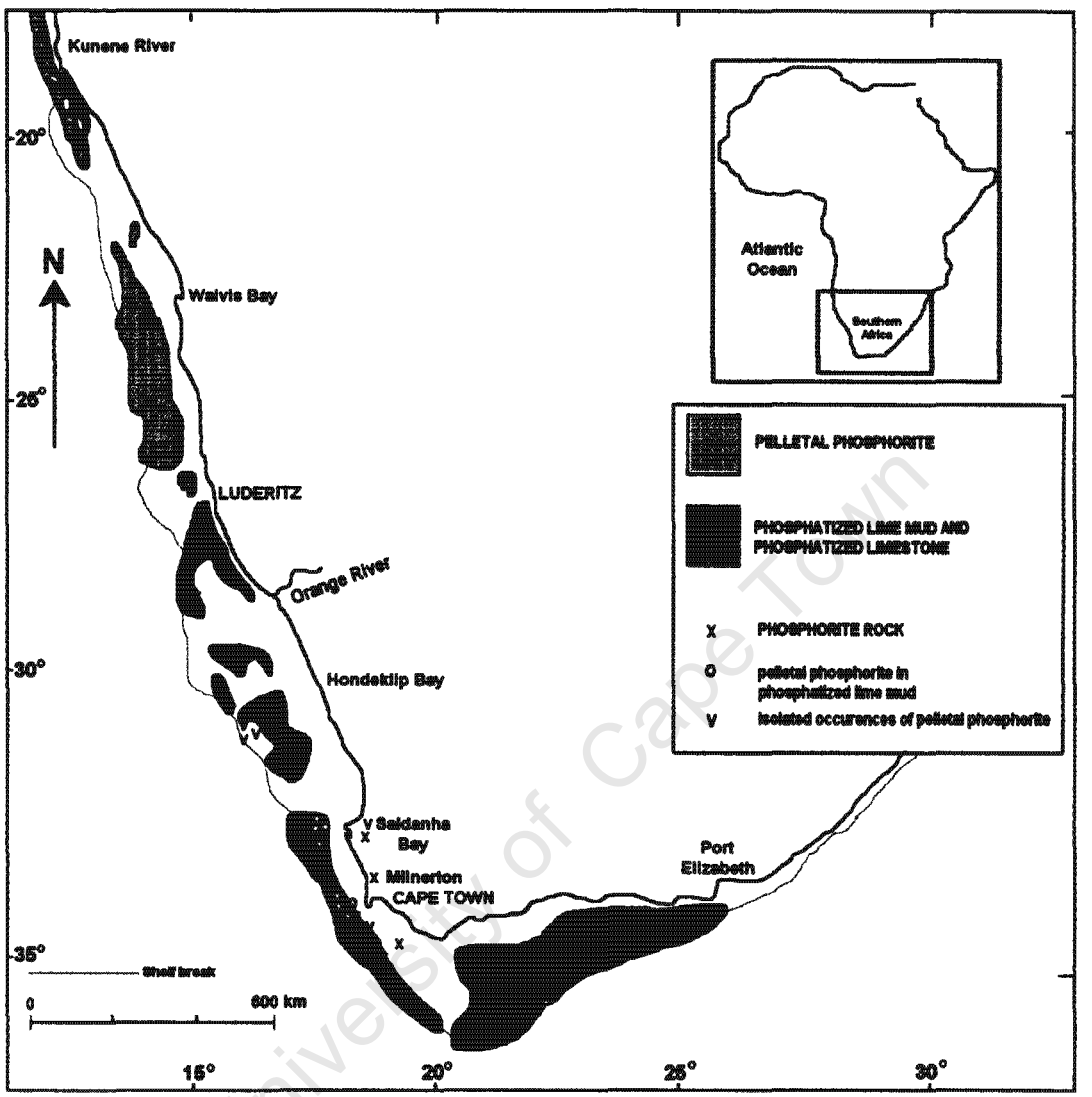

Figure 1.5. Phosphate and phosphorite distribution of the South African and Namibian Continental Shelf (modified after Birch, 1979a). Note the occurrence of phosphatised limestone and phosphatised lime mud found on the outer shelf between Luderitz and Port Elizabeth.

The Namibian shelf in particular has generated enormous recent scientific interest owing to the discovery of contemporary concretionary phosphorite, which is currently forming in the extensive postglacial Holocene diatomaceous mudbelt (Bremner, 1980a, 1980b; Bremner and Rogers, 1990). The mudbelt is located near Walvis Bay on the inner continental shelf of Namibia. Glenn *et al.* (1994) pointed out that the phosphorites on the South African margin can be described as either modern or relict (ancient). In other words, the concretionary phosphorites from the Namibian mudbelt may be described as

modern, whereas much of the other (consolidated and unconsolidated) phosphorites of southwestern Africa are typically relict.

1.4. SUMMARY

Phosphate-bearing minerals can be found in igneous, sedimentary and metamorphic rocks as varieties of apatite (fluorapatites, chlorapatites and hydroxyapatites). In sedimentary rocks the apatites are generally carbonate hydroxyl fluorapatite or carbonate fluorapatite (CFA), of which francolite is the most dominant CFA mineral. South African marine phosphorites are generally found in upwelling margins, which are characterised by high-productivity. The high productivity usually corresponds to the occurrence of zones of coastal upwelling (e.g. high productivity upwelling systems induced on the Southern African continental margin and the Peru/Chile continental margin by the Benguela and Chile-Peru currents, respectively).

Phosphorite occurrences on the southwestern coast of southern Africa include; widespread occurrences of relict phosphatised limestones, conglomeratic & non-conglomeratic glauco-phosphorites and phosphorites and widespread occurrences of phosphorite sands (pelletal phosphorite and mixed pelletal glauco-phosphorite sands). Other phosphorite deposits include modern (contemporary) concretionary (nodular) phosphorite on the Namibian continental shelf. The concretionary phosphorite deposits are currently forming in the Holocene diatomaceous ooze, located near Walvis Bay.
The following chapter lists a short literature review regarding the geochemistry and application of rare-earth elements (REE) in phosphorite research.

CHAPTER 2
RARE-EARTH ELEMENT GEOCHEMISTRY OF PHOSPHORITES

This chapter presents a short literature review regarding the geochemistry of rare-earth elements (REE) in the sedimentary environment and the uses of REE towards understanding the depositional and diagenetic history of phosphorites and phosphatic rocks. This chapter describes the use and significance of rare-earth element geochemistry to the study of authigenic phosphorites and phosphate-bearing sediments.

2.1. INTRODUCTION

Rare-earth elements include all the elements in the scandium group and all the lanthanides. The REE can be divided into the light REE (LREE) (lanthanum, cerium, praseodymium, neodymium, samarium and europium) and the heavy REE (HREE) (gadolinium, terbium, dysprosium, holmium, erbium, thulium, ytterbium and lutetium). Promethium does not occur in nature due to its radioactive instability.

In terms of their chemical properties the REE are very similar. However it is possible to distinguish between different elements on the basis of a progressive reduction in size of each element from lanthanum through to lutetium (the lanthanide contraction). Therefore due to the small, but systematic changes in chemical properties, the REE have been used successfully as tracers in unravelling the fundamental processes that govern REE cycling in the oceans (Elderfield and Greaves, 1982). For instance the HREE are predicted to be more resistant to removal from the oceans by scavenging of particulate matter. Apart from the progressive size reduction, two elements in particular; cerium (Ce) and europium (Eu) can be distinguished on the basis that they exhibit multiple oxidation states.

The possible oxidation of Ce (III) to Ce (IV) and the possible reduction of Eu (III) to Eu (II) (compared with the remaining 12 strictly trivalent elements of the REE) lead to measurable distribution anomalies of Ce and Eu. The resulting Ce (IV) in oceans tends to be easily scavenged, and subsequently seawater is typically depleted in terms of Ce (relative to neighbouring La and Pr). However in certain authigenic deposits, such as phosphorites and manganese nodules the Ce content is often enriched (De Baar *et al.*, 1985a; De Baar *et al.*, 1985b; Nath *et al.*, 1994; Kasten *et al.*, 1998). According to Wood (1990), Sm and Yb can occur as divalent species, but only under extreme reducing conditions. In the oceans, the reduction of Eu does not normally take place, however a notable Eu enrichment has been documented in hydrothermal fluids venting at the mid-oceanic ridges.

2.2. THE RARE-EARTH ELEMENT (REE) CYCLE

Rivers are generally considered by many authors to be a major input of REE into the oceans (Rasmussen *et al.*, 1998; Piper, 1974). Other possible inputs include locally significant contributions from atmospheric dust (aeolian) and hydrothermal vents (Piper *et al.*, 1975; Elderfield and Greaves, 1982; Bertram and Elderfield, 1993). The major input and outputs are illustrated in Figure 2.1.

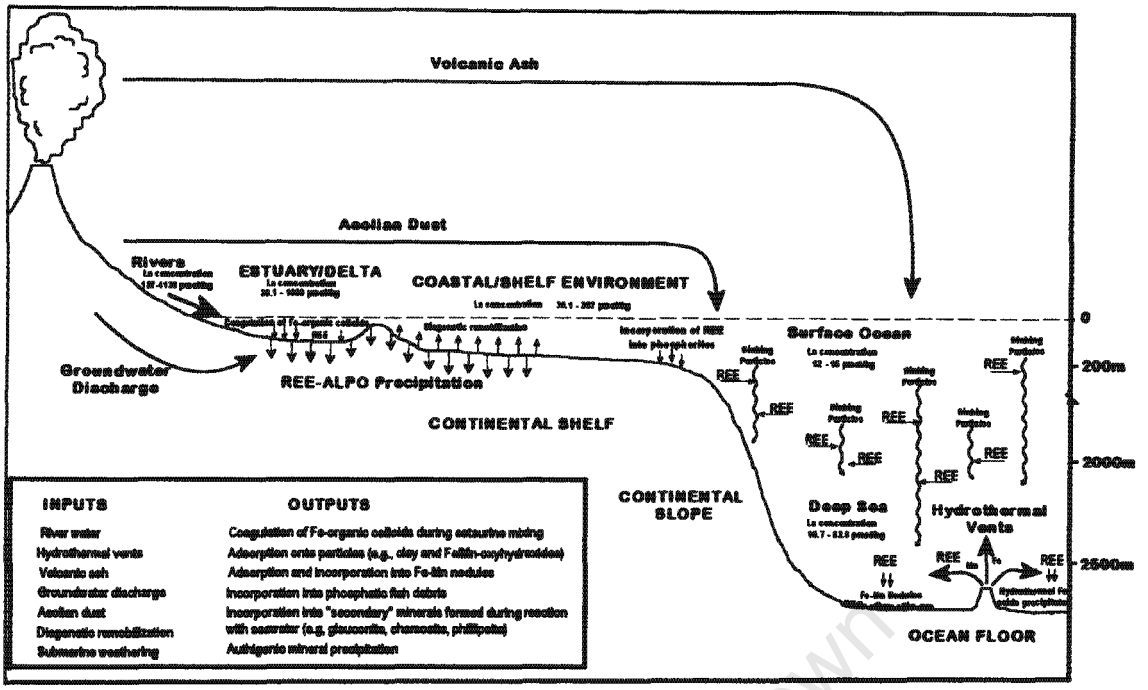

Figure 2.1. Schematic diagram depicting the major input and outputs of REE in the ocean cycle (modified from Rasmussen *et al.*,1998).

REE are derived from the weathering of continental rocks and the implication of REE fractionation during subaerial weathering has been discussed briefly by Ronov *et al.* (1967) and Aubert *et al.* (2001). According to Piper (1974) fluvial REE signatures show no pronounced fractionation of Ce (relative to the other REE). The study of Elderfield *et al.* (1990) shows a significant enrichment of HREE between La and Gd and either an enrichment or depletion of HREE between Gd and Lu in river water. However it has been shown that not all rivers show this pattern. Some rivers show shale-like patterns (of average shale), or hat patterns whereas others show LREE enriched patterns (Piper, 1974).

The REE transported by the river can either be found incorporated in suspended particulate matter or colloidal matter, or possibly in a dissolved state (Martin *et al.*, 1976; Hoyle *et al.*, 1984; Elderfield *et al.*, 1990). However, a large proportion of riverborne REE are removed in estuarine or deltaic environments (Martin *et al.*, 1976; Goldstein and Jacobsen, 1988; Elderfield *et al.*, 1990). The removal of REE (typically LREE) results in an enrichment of LREE relative to HREE in the sediments, with no or little depletion or enrichment in any particular REE (Martin *et al.*, 1976). However, according to Leleyter *et al.* (1999), REEs can undergo fractionation during river transport. Moreover, the REE do not behave as a coherent group but are preferentially linked to other matter. According to Leleyter et al. (1999) MREE are mainly bound to carbonate and organic matter, whereas LREE (except Ce) are mainly linked to organic matter. HREE and Ce are mainly associated with iron oxides. The major removal mechanisms of REE from river water have been identified as either salt-induced coagulation of riverine Fe-organic colloids or coprecipitation with iron hydroxides (Sholkovitz, 1978). In the open ocean, the remaining dissolved REE are primarily removed by a process of adsorptive scavenging, whereby REEs are bound onto suspended particle surfaces. The particle surfaces are covered by thin

coatings of organic or hydrous Fe/Mn oxides (Palmer, 1985; Sholkovitz *et al.*, 1994). REEs are also known to be incorporated through biological uptake into calcareous and opaline shells, tests or skeletons, but this process is generally viewed as being fairly insignificant given that REE concentrations of tests and shells are generally low (Palmer, 1985). The following figure serves as a conceptual model for understanding the processes by which trace-elements can bind to particle surfaces (Figure 2.2).

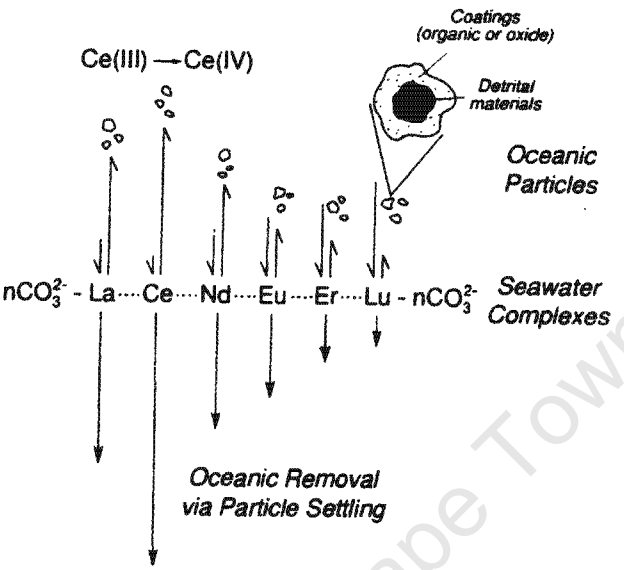

Figure 2.2. Schematic model of REE fractionation between particles and seawater. Main features include (1) the systematic variation in the relative affinity of trivalent REEs for complexation to solution carbonates and binding particles, (2) the enhanced formation of particulate Ce due to oxidation of Ce (III) to Ce (IV), and presence of surface active coatings on detrital particles. These features lead to fractionation of REE between seawater and particles and to fractionation via the settling of large particles (Sholkovitz *et al.*, 1994).

The removal of REE from the ocean leads to fractionation of the REE between particles and seawater. Numerous authors noted that seawater is typically depleted in Ce (resulting in a negative Ce-anomaly) and enriched in HREE (relative to LREE) (Figure 2.3), whereas in the detrital fraction the Ce is enriched (resulting in a positive Ce-anomaly) and the LREE are enriched (relative to the HREE). According to Moffett (1990) the negative Ce-anomaly found in seawater is dependent on microbial oxidation, followed by preferential scavenging of Ce (IV).

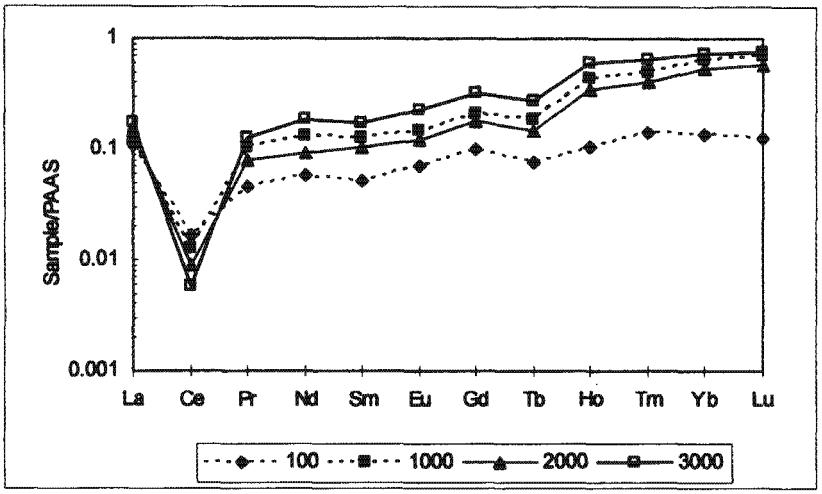

Figure 2.3. Negative Ce-anomalies in filtered sea water at selected depths in the Pacific Ocean (De Baar *et al.*, 1985a).

De Baar *et al.* (1985b) noted elevated Gd and decreased Tb concentrations in seawater, which defines Gd/Tb anomalies. According to De Baar *et al.* (1985b) the Gd anomaly and the overall trend of HREE enrichment in sea water support the idea of scavenging of REE from sea water as an important removal mechanism. According to Murphy *et al.* (1984) the adsorbed REE can be re-released during the oxidation of particles (biogenic) at the sediment-water interface or during settling through deeper water. It becomes apparent that estuaries (or deltaic environments) can play a significant role in the removal and release of dissolved REE to the ocean. The process outlined above is believed to be responsible for the notable fractionation of REE in estuaries, and the implication exists that estuaries can modify the relative abundances of dissolved REE reaching the ocean (Sholkovitz and Szymczak, 2000). REE are ultimately removed from the ocean by the burial of REE-coated particles, particularly Fe/Mn-oxides; clay minerals; REE substituted biogenic phosphates and REE-bearing authigenic minerals, particularly authigenic apatites (Piper, 1974; Dypvik and Brunfelt, 1979).

2.3. THE APPLICATION OF RARE-EARTH ELEMENT GEOCHEMISTRY TO PHOSPHORITES

One of the goals in sedimentary research is to find different methods to determine the depositional environment of sediments. In terms of marine sedimentary rocks (including phosphorites), it has been shown that petrographic and physical approaches alone cannot specify the depositional environment or illustrate the paleoenvironment. It is, however, possible to deduce the depositional environment, weathering processes and source rock geochemistry using geochemical tracers (in combination with more traditional methods such as facies analysis, petrography etc). The best geochemical tracers are typically those that are least affected by weathering processes (in other words fairly 'immobile'). Various studies have shown that REE can be employed as geochemical tracers. Altschuler (1980) employed REE to understand the depositional environments of phosphorites. It is also possible, on the basis of REE behaviour to determine sea water circulation patterns, timing of diagenesis, hydrothermal flux rates, sediment sources and redox state of the ocean and marine sediments

(Rassmussen *et al.*, 1998). Piper (1974) documented that the residence times of REE are significantly shorter than the mixing time of the oceans. It becomes apparent that REE in phosphorites (and other authigenic minerals and rocks) can be utilised as geochemical or oceanographic tracers (Piper, 1974; Nath *et al.*, 2000). According to Elderfield and Greaves (1982) REE can be used to assess the origins and depositional environments of modern sediments. It was identified that on the basis of the REE chemistry, it is possible to constrain the sources of REE (Piper, 1974; Ronov *et al.*, 1967; Dypvik and Brunfelt, 1979; Elderfield and Greaves, 1982). The ability of REE to fractionate between various marine phases, the use of Ce (and Eu) to identify redox conditions and the fact that some of the REE are weakly radioactive (^{143}Nd and ^{147}Sm) have meant that REE can be used readily in constraining sources and depositional environments. Understanding the palaeoredox is crucial to understanding the authigenesis of marine carbonate fluorapatite (e.g. francolite) in phosphorites. It is generally perceived that apatite authigenesis or phosphogenesis occurs from anoxic pore waters (in the case of francolite) or suboxic conditions at shallow burial depths particularly in sediment below areas of intense upwelling (biological productivity) (Bremner, 1980a; McArthur and Walsh, 1984; McArthur, 1985; Rao *et al.*, 2002). However, according to Ruttenberg and Berner (1993), authigenic apatite formation is not restricted to environments of active upwelling. Apatite can also precipitate in non-upwelling areas. However due to the influx of terrigenous detritus, apatite occurrences may be severely diluted (Ruttenberg and Berner, 1993). Other forms of francolite precipitation exist either by replacement of *in situ* carbonates or precipitation of francolite in phosphorus-rich bacterial cells (Parker and Siesser, 1972; McArthur and Walsh, 1984).

The behaviour of Ce has been documented to be controlled by its oxidation and reduction chemistry. Ce, unlike the other REE, except for Eu which can be reduced to Eu (II) can be altered under oxic conditions from Ce (III) to Ce (IV) by oxidation (Elderfield and Greaves, 1982). Due to the oxidation of Ce (possibly in oxygenated mid ocean waters) and the greater solubility of Ce (III), Ce is effectively removed from sea water, resulting in a negative Ce-anomaly. Fleischer and Altschuler (1969) documented that marine phosphorites can show a marked depletion in terms of Ce. Therefore, marine phosphorites can exhibit pronounced negative Ce-anomalies, very similar to "sea water patterns" (McArthur and Walsh, 1984). Toyoda and Tokonami (1990) after investigating the REE distribution in phosphatised fish debris (biogenic phosphate), reported similar negative Ce-anomalies. The negative Ce-anomaly found in some phosphorites probably indicates that the phosphorites gained their REEs under oxic conditions. In general, phosphorites that obtained their REE under anoxic conditions should not show a negative anomaly and may possibly show a positive Ce-anomaly. De Baar *et al.* (1988) concluded that the Ce-anomaly in various marine sediments can be applied to global ocean stratification and in understanding redox processes on a global scale, however Wright *et al.* (1987) and Shields & Stille (2001) propose that Ce-anomalies should rather be applied to understanding local changes in oxygen availability or oxic-anoxic conditions. In any case, the measurement of Ce-anomalies (with Th, U) provides a diagnostic trace-element indicator for differentiating between oxic-anoxic depositional environments and possibly a valuable tool to extrapolate palaeoredox conditions (Liu *et al.*, 1988; De Baar *et al.*, 1988; Wright *et al.*, 1987). Phosphorites and phosphate rocks allow for a range of possibilities of substitution and therefore enable the incorporation of various trace-elements. In general the majority of trace-elements replace Ca^{+} in the apatite structure. However, as Jarvis *et al.* (1994) documented, trace-elements are not only

located in the lattice but can be absorbed to the crystal surface or related to organic matter in phosphate particles.

2.4. REE PATTERNS IN PHOSPHORITES

When the abundances of REE in sedimentary rocks are plotted, it is common to normalize the data to a shale standard. The shale normalization not only helps to eliminate the Oddo-Harkins effect (distinctive saw-toothed pattern), but also helps to visualize fractionation. Various studies employ different shale normalization, for instance Wright *et al.* (1987) normalized their data to the North American Shale Composite Standard (NASC), whereas others like Rassmussen *et al.* (1998) normalize their data to the Post-Archaean Australian Sedimentary rocks (PAAS). Studies that involve the fractionation between different water bodies may normalize to North Pacific Deep Water (NPDW). It has been documented that the choice of shale normalization can influence interpretation; therefore caution must be paid to the type of shale standard and how anomalies (for instance the small anomalies in Gd and Tb) are interpreted. De Baar *et al.* (1985b) when investigating Gd and Tb anomalies in seawater used an arithmetic mean composite of North American, European and Russian Platform shales.

Numerous studies have utilised REE distribution patterns, for instance the studies of McArthur and Walsh (1984) on the REE geochemistry of phosphorites; Wright *et al.* (1987) on the REE geochemistry of conodonts; Granjean-Lécuyer *et al.* (1993) on REE in biogenic apatites; Watkins *et al.* (1995) on the sediments on the Namibian and South African continental shelves; Ilyin (1998) on the REE geochemistry of Russian (Vendian – Early Cambrian) phosphorites; Ogihara (1999) on the phosphorites from the Miocene Funankawa Formation (Japan); Lécuyer *et al.* (1998) on the REE contents of phosphatised brachiopods, Rao *et al.* (2000) on the Pleistocene phosphorites from the continental slope off India and Baturin (2000) on the phosphorite grains of the Namibian Shelf. From these studies it becomes apparent that different phosphorites (biogenic or authigenic) can possess distinctive pattern types. Below is a summary of the most common REE patterns found in phosphorites.

2.4.1. "Shale" patterns

"Shale" patterns are generally flat and resemble average-shale distributions (Figure 2.4). According to McArthur and Walsh (1984), the presence of "shale" patterns suggests that the REE were probably derived by diagenetic remobilisation of clastic debris. However the lack of a Ce-anomaly could indicate that the phosphorites inherited their REE in suboxic to anoxic conditions, in association with bottom or pore waters (Watkins *et al.*, 1995). The lack of a considerable negative Ce-anomaly is clearly visible from Table 2.1., given the range of Ce/Ce* values between 1.06 and 0.88. The data set also shows high europium anomaly (Eu/Eu*) values. Sample N3903 shows an enrichment of Eu relative to the neighbouring REE.

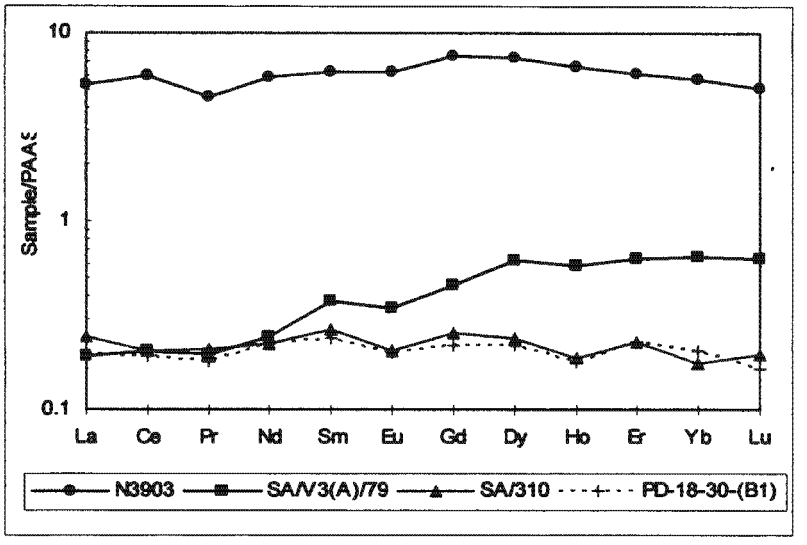

Figure 2.4. "Shale" type shale-normalized REE distribution patterns in phosphorites (from McArthur and Walsh, 1984). Locations of samples are shown in Table 2.1.

Table 2.1. Table showing summary of major REE ratios, most notably the Ce/Ce* anomaly and the Lu/La ratio for the data from McArthur and Walsh (1984). Ce-anomaly (Ce/Ce*) calculated using the formula $Ce/Ce^* = 2\ Ce/Ce_{shales}/ (La/La_{shales} + Pr/Pr_{shales})$. Eu-anomaly (Eu/Eu*) calculated using the formula $Eu/Eu^* = 2\ Eu/Eu_{shales}/ (Sm/Sm_{shales} + Gd/Gd_{shales})$.

Sample	Locality	Ce/Ce*	Eu/Eu*	LREE/HREE	(La/La)n	(Er/Nd)n	(Sm/Nd)n	ΣREE
N3903	Offshore, Namibian margin	1.06	0.90	0.62	0.95	1.06	1.08	72.55
SA/V3(A)/79	Onshore, South Africa, Varswater Quarry	0.94	0.82	0.31	3.32	2.64	1.54	5.14
SA/310	Offshore, South Africa, Agulhas Bank	0.88	0.79	0.77	0.82	1.01	1.19	2.62
PD-18-30-(B1)	Offshore, Peruvian Margin	0.93	0.86	0.73	0.84	1.04	1.09	2.44

2.4.2 "Seawater" patterns

The following features generally identify "Seawater" patterns: HREE enrichment relative to LREE, a typical convex-upward shape and negative Ce-anomaly (Figure 2.5.). The negative Ce-anomaly is also expressed by Ce/Ce* (Table 2.2.). For the data set Ce/Ce* values range between 0.23 and 0.41. The HREE enrichment relative to the LREE is also expressed by the very low LREE/HREE ratio. Values are calculated and reported as 0.23 – 0.59. HREE enrichment is also expressed by the La/Lu ratio, unsurprisingly the values calculated are fairly high, ranging between 1.59 and 1.85, with an anomalous 0.23 reported for sample Z26. Altschuler (1980) reported similar

patterns for phosphorites from Morocco. "Seawater" patterns have been used as evidence to suggest a marine authigenic origin of phosphorites.

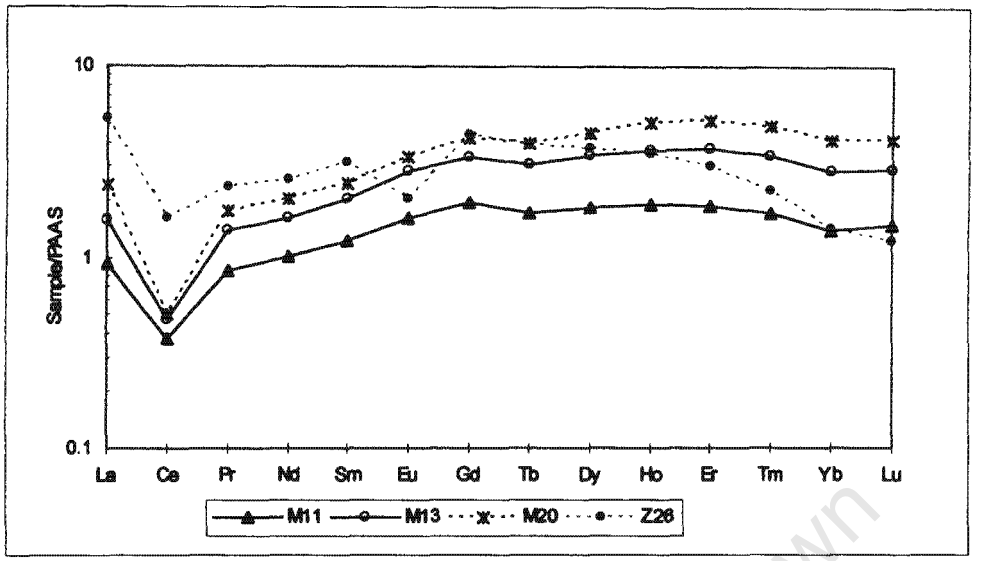

Figure 2.5. "Sea water" type shale-normalized REE distribution patterns in phosphorites (Shields and Stille, 2001). Locations of samples are shown in Table 2.2.

Table 2.2. Table showing summary of major REE ratios, most notably the Ce/Ce* anomaly and the Lu/La ratio for the data from Shields and Stille (2001). Ce-anomaly (Ce/Ce*) calculated using the formula $Ce/Ce^* = 2\ Ce/Ce_{shales}/ (La/La_{shales} + Pr/Pr_{shales})$. Eu-anomaly (Eu/Eu*) calculated using the formula $Eu/Eu^* = 2\ Eu/Eu_{shales}/ (Sm/Sm_{shales} + Gd/Gd_{shales})$.

Sample	Locality	Ce/Ce*	Eu/Eu*	LREE/HREE	(La/La)n	(Er/Nd)n	(Sm/Nd)n	ΣREE
M11	Cambrian Phosphorites from the Maidiping Section, near Chengdu, China.	0.39	1.03	0.28	1.59	1.87	1.21	19.78
M13	Maidiping Section, near Chengdu, China	0.30	1.07	0.24	1.85	2.31	1.25	36.18
M20	Maidiping Section, near Chengdu, China.	0.23	1.01	0.23	1.75	2.56	1.20	48.61
Z26	Cambrian Phosphorites from the Meishucun Section, Kunyang Mine, China,	0.41	0.54	0.59	0.23	1.19	1.24	40.42

2.4.3 MREE-enriched patterns ("Hat" patterns)

MREE-enriched patterns or "Hat" shaped (concave) distributions are very distinctive, given that the MREE (middle REE) are enriched relative to the other REE (Figure 2.6). The data set also shows negative Ce-anomalies (Table 2.3).

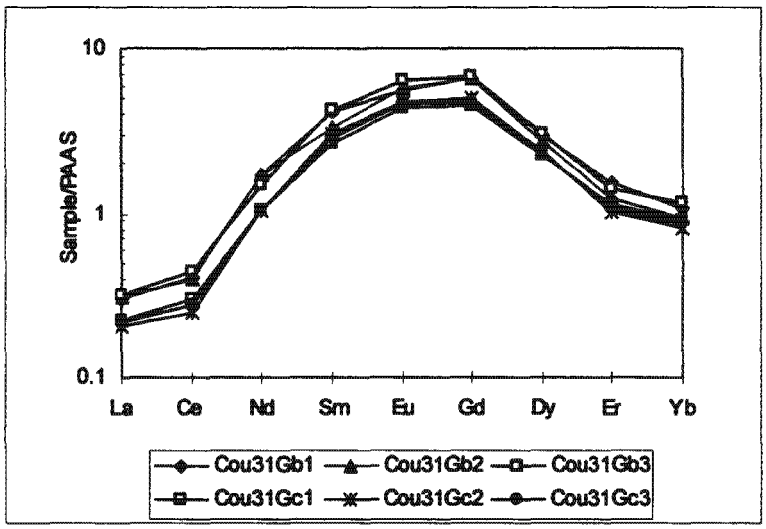

Figure 2.6. MREE-enriched patterns or "Hat" type (concave) shale-normalized REE distributions in Famennian conodonts (Granjean-Lécuyer *et al.*, 1993). The samples were taken from the Frasnian-Famennian section near Coumiac in the Montagne Noire area, southern France.

Table 2.3. Table showing summary of major REE ratios, most notably the Ce/Ce* anomaly and the Lu/La ratio for the data from Granjean-Lécuyer *et al.* (1993). Ce-anomaly (Ce/Ce*) calculated using the formula $Ce/Ce^* = 2\ Ce/Ce_{shales}/\ (La/La_{shales} + Pr/Pr_{shales})$. Eu-anomaly (Eu/Eu*) calculated using the formula $Eu/Eu^* = 2\ Eu/Eu_{shales}/\ (Sm/Sm_{shales} + Gd/Gd_{shales})$.

Sample	Ce/Ce*	Eu/Eu*	LREE/HREE	(La/La)n	(Er/Nd)n	(Sm/Nd)n	ΣREE
Cou31Gb1	0.41	1.06	0.36	N/A	0.90	2.43	24.43
Cou31Gb2	0.40	1.17	0.33	N/A	0.73	1.95	23.13
Cou31Gb3	0.49	1.16	0.34	N/A	0.96	2.84	25.24
Cou31Gc1	0.47	1.23	0.32	N/A	1.06	2.50	17.31
Cou31Gc2	0.40	1.18	0.33	N/A	0.96	2.95	18.69
Cou31Gc3	0.43	1.20	0.32	N/A	1.01	2.73	18.03

MREE-enriched patterns are very anomalous in sedimentary phosphates; however a few phosphates readily yield such patterns. Hoyle *et al.* (1984) believed that the distinctive pattern is probably caused by the gaining of the REE signature from precipitates formed in estuarine or deltaic environments. Stanley and Byrne (1990) argued that MREE are preferentially removed from water and made available to the phosphate by green algae, whereas Kidder and Eddy-Dilek (1994) suggested that both algae and bacteria may be responsible for the removal of MREE and thus the formation of MREE-enriched patterns. Elderfield *et al.* (1990) believed that another possible mechanism to remove MREE from water is through the uptake of MREE in organic rich and/or oxy-hydroxide grain coatings. It seems that the most important means of removing MREE from water is the uptake of MREE by phosphate minerals. Byrne *et al.* (1996) reported that coprecipitation of phosphate and REE compounds preferentially removed MREE from solutions. According to Kidder *et al.* (2003) phosphate selectively incorporates MREE, thus leaving pore waters depleted in

MREE. According to Hannigan and Sholkovitz (2001), the MREE enrichment found in certain river water can be explained by preferential dissolution of phosphatic minerals during weathering, which results in extensive REE fractionation between river sediment and water.

However, most researchers agree that the MREE-enriched patterns are mostly observed for skeletal or biogenic apatites and conodonts (Wright et al. 1987; Granjean-Lécuyer *et al.*, 1993). According to Shields and Stille (2001), MREE-enriched patterns can be explained by the fact that skeletal grains are more likely to be altered and less likely to retain their primary seawater REE distribution patterns. Interestingly, MREE enrichments have also been noted for certain river waters. According to Struesson (1995) MREE-enriched patterns are not only restricted to biogenic phosphate fabrics but can occur in non-skeletal phosphate material, for instance the oolitic phosphorite from the Middle Ordovician in Estonia. In general it appears that MREE-enriched patterns represent differential accumulation of MREE during phosphate lithification.

2.5. SUMMARY

The REE form a very coherent group, although Ce and Eu may develop significant anomalies. These anomalies are primarily due to changes in their oxidation states. The literature provides numerous studies, ranging from the REE geochemical cycle to examples of how REE can be applied to the study of phosphorites and phosphorite formation. In summary, REE can be applied to phosphorite research in the following ways:

- REE can be used as oceanographic or geochemical tracers;
- REE can be used to assess the origin and depositional environments of modern sediments; and
- REE can be used to indicate palaeoredox conditions using Ce-anomalies.

The shale-normalised distribution patterns of REE in phosphorites can be used to distinguish between different types of phosphorites (biogenic or diagenetic). It is also possible to use the patterns to reflect the source and mechanism of REE incorporation. However given the occurrence of untypical REE patterns in much of the literature, caution should be taken in using REE. REE can suffer from possible chemical overprint, and thus the use of REE may be severely restricted. The following chapter describes the study area and the aims of this study.

CHAPTER 3
DESCRIPTION OF THE STUDY AREA and AIMS OF THE STUDY

This chapter includes a brief description of the location and geological setting of the phosphorites found in the southwestern Cape. It also addresses the relevant questions, which were formulated to maintain the focus of this project.

3.1. INTRODUCTION

The first phosphorites recovered from modern seas were sampled from South Africa's Agulhas Bank by the 1873 – 1876 Challenger Expedition (Murray and Renard, 1891). Following this discovery, similar phosphatic deposits have been found in many areas (e.g. Peru, Chile, Australia, California, Florida, New Zealand and north-west Africa). Modern offshore deposits including the sporadic deposits on the west coast of South Africa have become the basis for comparison with similar deposits found onshore (Figure 3.1). One of the onshore sites, located near Langebaanweg has been intensively studied for at least 40 years by researchers at the South African Museum. It is regarded as one of the most fossiliferous sites in the southwestern Cape, and since 1958, when the occurrences of vertebrate fossils were first documented, intensive palaeontological studies were undertaken within the quarry (Singer and Hooijer, 1958; Hendey, 1981a). Other sites near Saldanha are also extremely rich in terms of archaeological and palaeontological material. These internationally recognised sites include the middle Pleistocene archaeological site near Hopefield, where the cranium of the Saldanha Man (an archaic *Homo sapiens*) was found, and Kraal Bay, within Langebaan Lagoon, where Upper Pleistocene fossil human footprints were discovered (Singer and Wymer, 1968; Roberts and Berger, 1997).

Langebaanweg is not the only site that features marine phosphatic sediments or phosphorites. There exist numerous sites around the southwestern Cape where similar deposits crop out such as the Bomgat phosphorites near Hoedjiespunt (Figure 3.2). Another interesting type of phosphate deposit, that is indirectly related to the phosphorites, found at Langebaanweg and Hoedjiespunt are the aluminium phosphates. These deposits have been described in some detail by Du Toit (1917), Tankard (1974a) and Visser & Schoch (1973) and are normally found on the granite hills north and south of Saldanha Bay (Tankard, 1974a).

Despite the palaeontological and geological importance of these sites very little has been published on the geology of the phosphatic deposits and especially on the geochemical nature of these deposits. The present study is intended to contribute data concerning the rare-earth element (REE) and trace-element geochemical nature of the phosphatic deposits in the southwestern Cape.

3.2. LOCATION

The sites researched are as follows, Varswater Quarry (near Langebaanweg), Bomgat (near Hoedjiespunt), Kreefte Bay (Kreeftebaai) and Konstabelkop (Constable Hill).

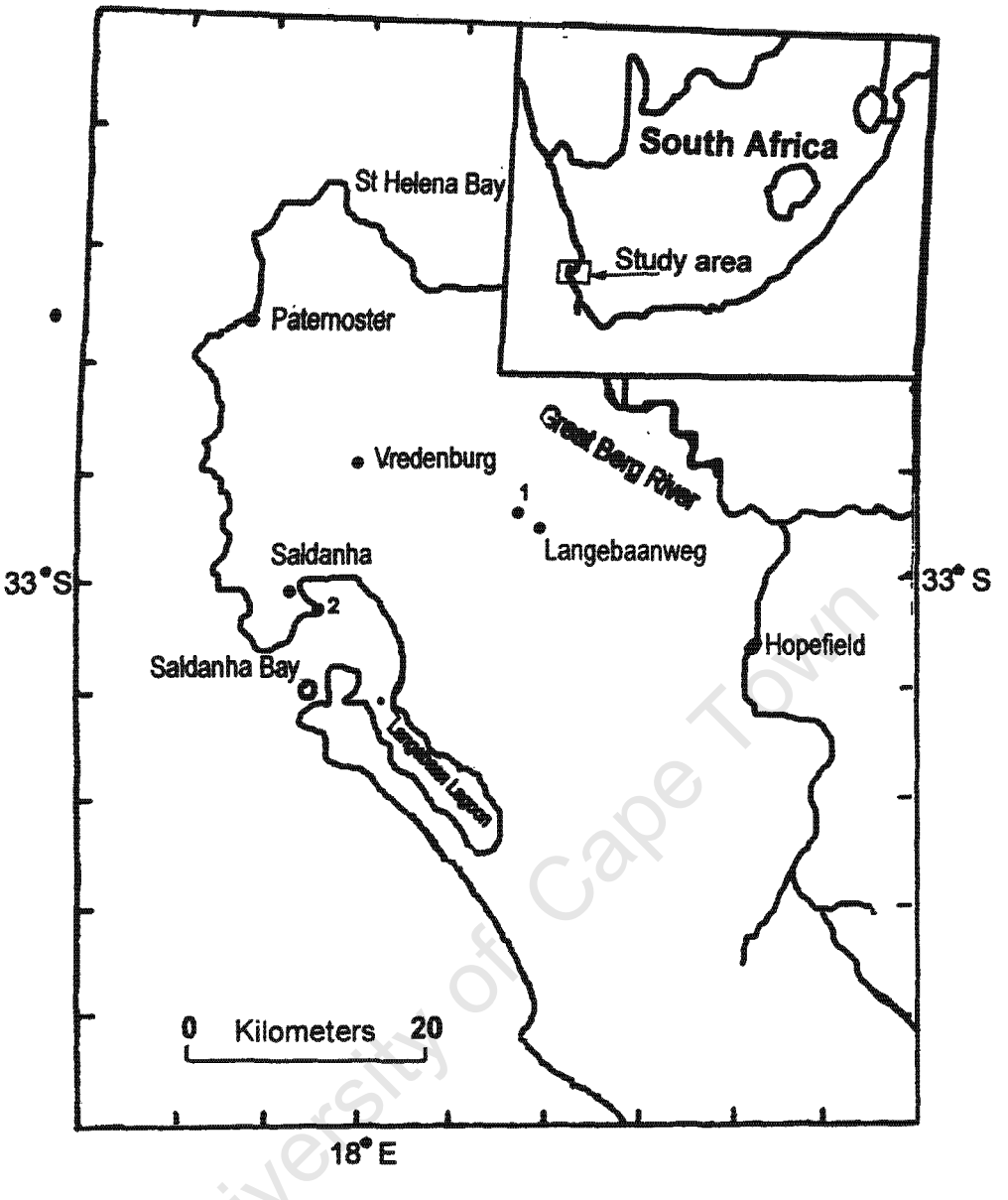

Figure 3.1. Map of the southwestern Cape (South Africa) showing the location of Varswater Quarry (1) near Langebaanweg and Bomgat (2), near Saldanha (modified after Dingle, Lord and Hendey, 1979).

Langebaanweg is situated 110 km north-north west of Cape Town in the southwestern Cape. It is roughly 13 km north-east of Saldanha Bay and 21 km south of the mouth of the Great Berg River at St Helena Bay (Hendey, 1981a). The Bomgat exposure is situated on the Hoedjiespunt Peninsula at Saldanha Bay. It is approximately 2 km south of Saldanha. The two sites containing the aluminium phosphate deposits, Konstabelkop and Kreefte Bay are located in the Posberg Reserve (on the Posberg Peninsula) (Figure 3.2). Konstabelkop is approximately 15 km south-south east of Saldanha, whereas Kreefte Bay is approximately 4 km west of Konstabelkop.

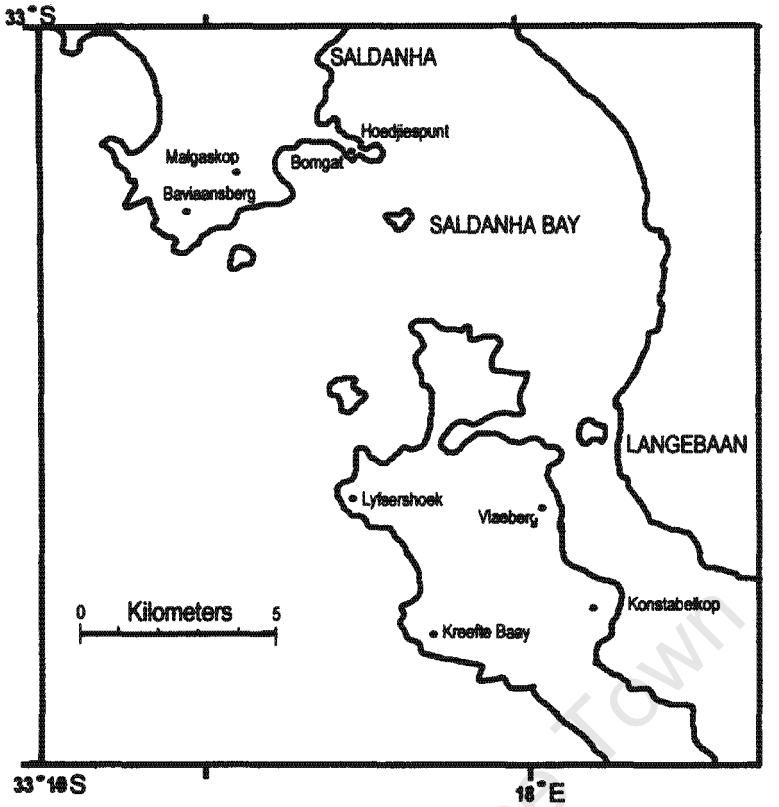

Figure 3.2. Distribution map for the aluminium phosphate deposits and Bomgat (Modified after Tankard, 1974a).

3.3. GEOLOGY

3.3.1 General coastal geology of the southwestern Cape.

The general geology of the west coast in the vicinity of Saldanha Bay consists of deeply weathered Precambrian Malmesbury Group Shales, Cape Granite suite rocks and an unconformably overlying package of Cenozoic sediments. Figure 3.3 provides a map showing the distribution of Cenozoic (Neogene and Paleogene) and Cretaceous sediments in relation to the Table Mountain Group, Cape Granite Suite and the Malmesbury Group Shales on the southwestern Cape coastal platform.

The Cenozoic sediment package consists of the Sandveld Group, which extends from Cape Hangklip (in the south east) to the Vredenburg Peninsula (in the west) (Johnson, 1994). According to Rogers (1980) it is possible to correlate the stratigraphic entities between the Vredenburg Peninsula and Cape Deseada (near Elands Bay, in the north) with the deposits of the Sandveld Group. The Sandveld Group can be subdivided into the following formations: Elandsfontyn, Saldanha, Varswater, Velddrif, Langebaan, Springfontyn and Witzand (Rogers, 1980; Tankard, 1975; Tankard, 1974b; Hendey, 1981b; Hendey and Dingle, 1983). These deposits represent a variety of sedimentary environments, including shallow marine, back-barrier, estuarine, fluvial and aeolian (Pether *et al.*, 2000).

The Elandsfontyn Formation was first recognized by Rogers (1980). It is not exposed subaerially, but has been defined on the basis of borehole and core data. The facies associations predominantly consist of upward fining sequences of angular to fine quartzose sands without phosphate or carbonate grains and indicate sedimentation within a meandering river system (Rogers, 1980, 1982). The Elandsfontyn Formation has been dated using pollen and spore assemblages and on the basis of its foraminiferal assemblage (Coetzee and Rogers, 1982; Dale and McMillan, 1999).

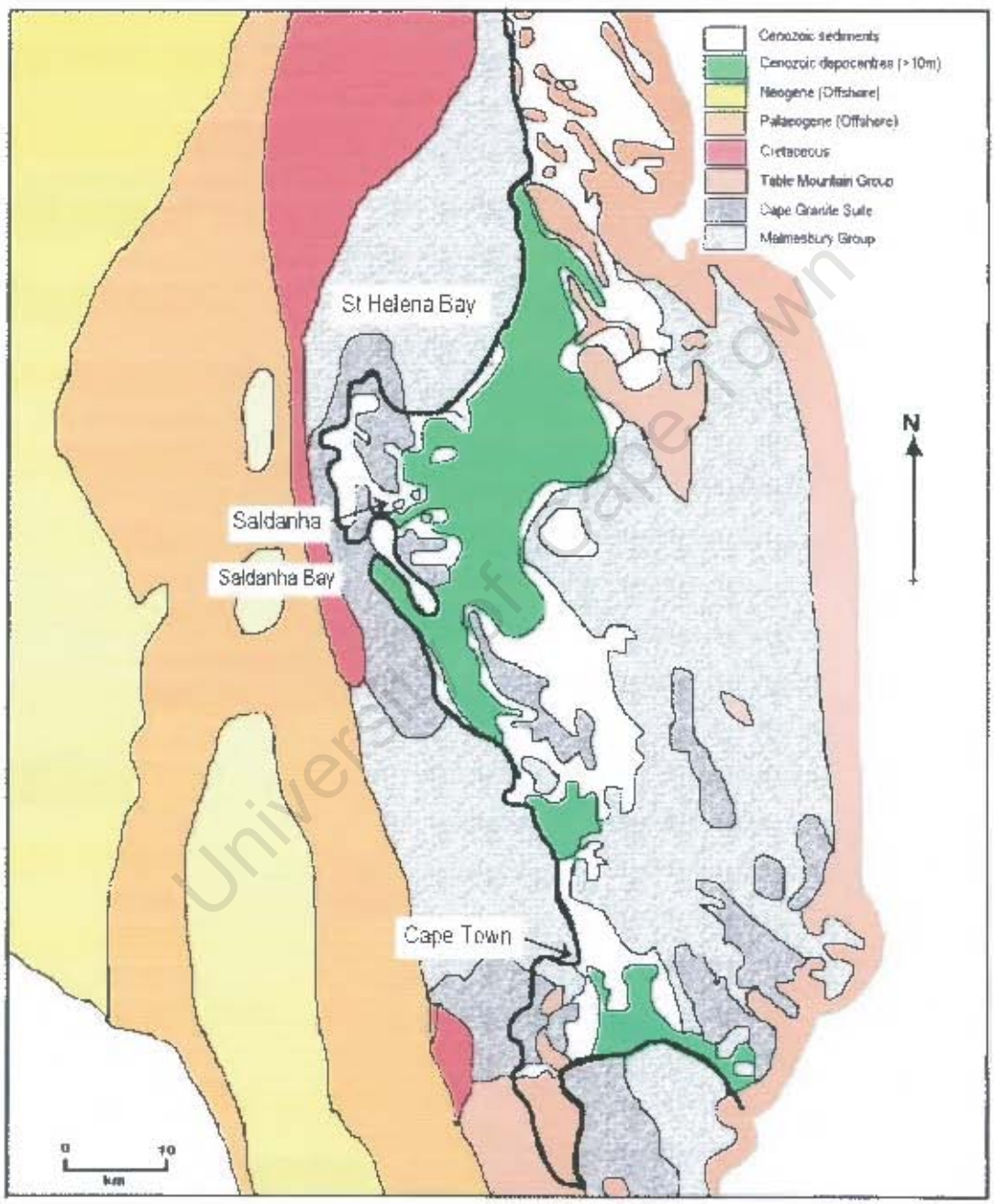

Figure 3.3. Distribution map for the Cenozoic and Cretaceous sediments of the southwestern Cape coastal platform (Modified after Rogers, 1980).

According to Coetzee and Rogers (1982) the Elandsfontyn Formation is assigned an early Miocene age, whereas Dale and McMillan (1999) ascribe a mid Cretaceous age

to the deposit. Overlying the Elandsfontyn Formation is the phosphate-rich Varswater Formation (Hendey, 1974). The Varswater Formation is especially well preserved in the Varswater Quarry, near Langebaanweg and generally the deposit is unconformably overlain by the Quaternary Springfontyn, Velddrif and Langebaan Formations (Rogers, 1980). The Springfontyn and Langebaan Formations are primarily aeolian deposits, whereas the Velddrif Formation is generally considered to be a littoral deposit (foreshore environment), composing of coarse-grained shelly sands and shell-coquina (cold water fauna). The Velddrif Formation is overlain by the Langebaan Formation (Tankard, 1976; Rogers, 1980). The Saldanha Formation and the Varswater Formation contain the key onshore phosphate occurrences, particularly from the phosphorites at Bomgat and Langebaanweg.

3.3.2 The Varswater Formation: The geology of Varswater Quarry

The phosphate deposits at the Varswater Quarry are well exposed due mainly to a period of commercial phosphate mining, which commenced in 1943 (Hendey, 1981a) and ceased in 1995. The mine is currently being managed as the West Coast Fossil Park, under the South African Museum. Owing to the discovery of Cenozoic fossil remains within the mine area, the site has been very well researched; however the stratigraphy at the Varswater Quarry remains controversial. Changes to the nomenclature of the subdivisions have caused confusion, although the lithostratigraphy recognized in various studies has remained unchanged (Rogers, 1980). The stratigraphy of the mine has been described by various authors (Hendey, 1973, 1974, 1976, 1980; Tankard 1974a, 1974b, 1975; Smith, 1971; Dingle *et al.*, 1979; Rogers, 1980 and Middleton, 2000). The exposed geologic succession at Langebaanweg can be subdivided into the phosphate-bearing Varswater Formation and the Langebaan Formation. The Langebaan Formation (or Calcareous Sand member or Anyskop member aeolianites) overlies the Varswater Formation (Hendey, 1981a; Dale and McMillan, 1999). A south-easterly panoramic view showing the stratigraphic relationship between the Varswater Formation and the Langebaan Formation at the Varswater Quarry (West Coast Fossil Park) is shown in Figure 3.4.

Figure 3.4. South-easterly panoramic view across the Mine Floor area (modified after Middleton, 2000).

The Varswater Formation is informally divided into three main units; the basal Gravel member (*or Konings Vlei member*), Quartzose Sand member and Pelletal Phosphorite member (*or Muishonds Fontein member*) (Roberts, pers. comm. 2000; Rogers, 1980; Hendey, 1981a; Hendey and Dingle, 1983) (Figure 3.5). Some authors prefer to

The Quartzose Sand member and the Pelletal Phosphorite member unconformably overlie the Gravel member, owing to a possible late Miocene hiatus between the overlying sediments and the Gravel member (Pether *et al.*, 2000). The Quartzose Sand member is a moderately sorted, fine to coarse grained quartzose sand that generally lacks phosphate grains (Rogers, 1980). According to Hendey and Deacon (1977), the Quartzose Sand member is derived from a variety of depositional environments, including fluvial, estuarine, floodplain, marsh, tidal mud flat and pond. Hendey (1981a) proposed that the unit was deposited by the proto-Berg river during an early period of the early Pliocene transgression.

The Quartzose Sand member is highly fossiliferous and contains abundant invertebrate and vertebrate fossils. These include tortoises (*Chersina sp.*), rhinoceroses (*Ceratotherium praecos*), seals (*Homiphoca capensis*), giraffids (*Sivatherium*) and pigs (*Nyanzachoerus cf. pattersoni*) (Hendey, 1981a). Kensley (1977) also noted that the invertebrate fossils suggested deposition under calm conditions within an estuarine area. This supports Tankard's (1975) view that the Quartzose Sand member contains a fluvial and estuarine facies. In terms of its micropalaeontological assemblage, the Quartzose Sand member appears to have a complete absence of foraminifera (Dale and McMillan, 1999). Dale and McMillan (1999) ascribe the lack of foraminifera to decalcification processes by meteoric/groundwater leaching. The Quartzose Sand member appears to be partially contemporaneous with the Pelletal Phosphorite member with indications that the unit passes laterally and vertically into the latter (Pether *et al.*, 2000; Middleton, 2000).

Tankard (1974a) proposed that the Pelletal Phosphorite member is derived by erosion from the Miocene basal bed (or Gravel member). The Pelletal Phosphorite member consists of moderately sorted, fine to medium grained phosphatic-quartzose sand and ~1 to 0.5 m thick lenses or "phosphate rock layers" of cemented Pelletal Phosphorite (Tankard, 1974a; Rogers, 1980; Middleton, 2000) (Figure 3.6). The locally highly fossiliferous Pelletal Phosphorite member was once commercially exploited. Smith (1971) and Middleton (2000) documented the different grain types within the Pelletal phosphorite member and, most notably, the occurrence of phosphatised shell fragments and pelletal (peloidal) phosphorite. Tankard (1974a), Dingle et al. (1979) and Middleton (2000) maintain that the phosphorite lenses were formed due to *in situ* lithification or precipitation of the pelletal phosphorite.

Hendey (1981a, 1981b) assigned an Early Pliocene age to the Pelletal Phosphorite member on the basis of the vertebrate fossil assemblage, indicating that the unit might have been deposited during the Early Pliocene transgression. Pickford (1997 quoted in Dale and McMillan, 1999), however maintains that the vertebrate fossils are in fact Miocene in age, based on a revision of the East African vertebrate stratigraphy. Dale and McMillan (1999) assigned an early Pleistocene age (possibly Waalian to earliest Menapian) to the deposit on the basis of the microfossil assemblage which contains distinctive *Uvigerina sp.* and *Discorbis "algoaensis"*.. Strontium isotope ratios ($^{87}Sr/^{86}Sr$) of the phosphorite peloids indicate an Early Pleistocene age (Franscerschini, 2003). Notwithstanding the dating controversy, the fossil assemblage does however indicate that by approximately 5 Ma, cold-seawater conditions already existed on the west coast. The different dates can be ascribed to possible reworking of the Early Pliocene fossils during the Pleistocene (Middleton, 2000).

include the overlying uppermost Calcareous Sand member or Anyskop member aeolianites as a unit within the Varswater Formation (Hendey, 1981; Dale and McMillan, 1999). The decision is largely based on the presence of marine benthic foraminifera and the occasional phosphorite pellet/peloid (or phosphatised grain) within the unit; however the general palaeontology (i.e. the presence of the pulmonate dune gastropod, *Trigonephrus globulus*), lithology and sedimentary structures are identical to the aeolian Langebaan Formation.

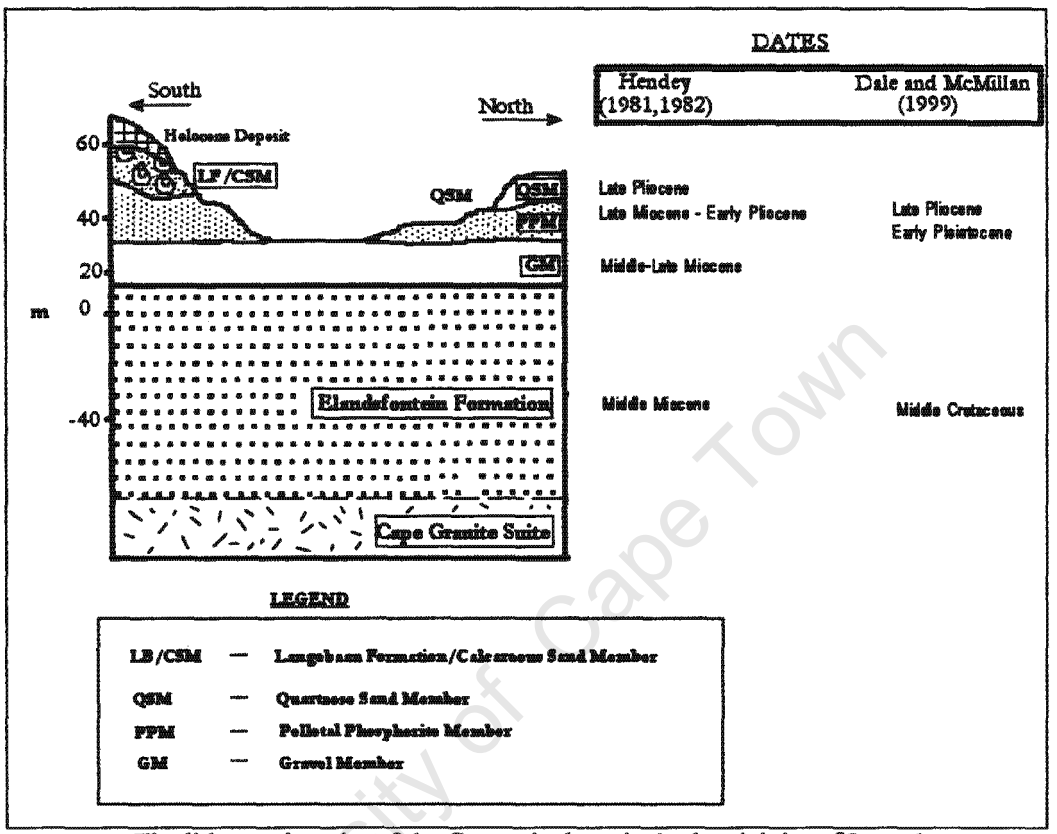

Figure 3.5. The lithostratigraphy of the Cenozoic deposits in the vicinity of Langebaanweg (modified after Hendey, 1982).

The basal Gravel member accounts for the lowest unit within the Varswater Formation. It consists of unconsolidated, well rounded to subrounded phosphatic cobbles, pebbles and silty sand, as well as up to 1 m thick consolidated lenses comprised of older, eroded clasts of phosphorite (Tankard, 1975; Dingle *et al.* 1979; Rogers, 1980; Middleton, 2000). The basal Gravel member and Pelletal Phosphorite member are the principal phosphate-bearing units. The presence of a marine invertebrate fossil assemblage indicates the marine origin of the unit (Kensley, 1977). Other fossils are also present; including shark teeth, molluscs and the teeth of the late Miocene horse *Hipparion primigenium* (Hendey, 1981a, 1981b; Dingle *et al.*, 1979; Hendey and Dingle, 1983). The vertebrate and invertebrate fossil assemblage is indicative of warm water conditions, which are believed to be typical sea conditions during the Miocene (Hendey, 1981b). In contrast, the marine fauna (seal and molluscs) of the Quartzose Sand member and the Pelletal Phosphorite member indicates cold-water conditions (Hendey, 1981b). Therefore, the Gravel member is proposed to have been deposited during the Miocene transgression and eroded during a +30 m stillstand of the late Miocene regression (Hendey, 1981a, 1981b).

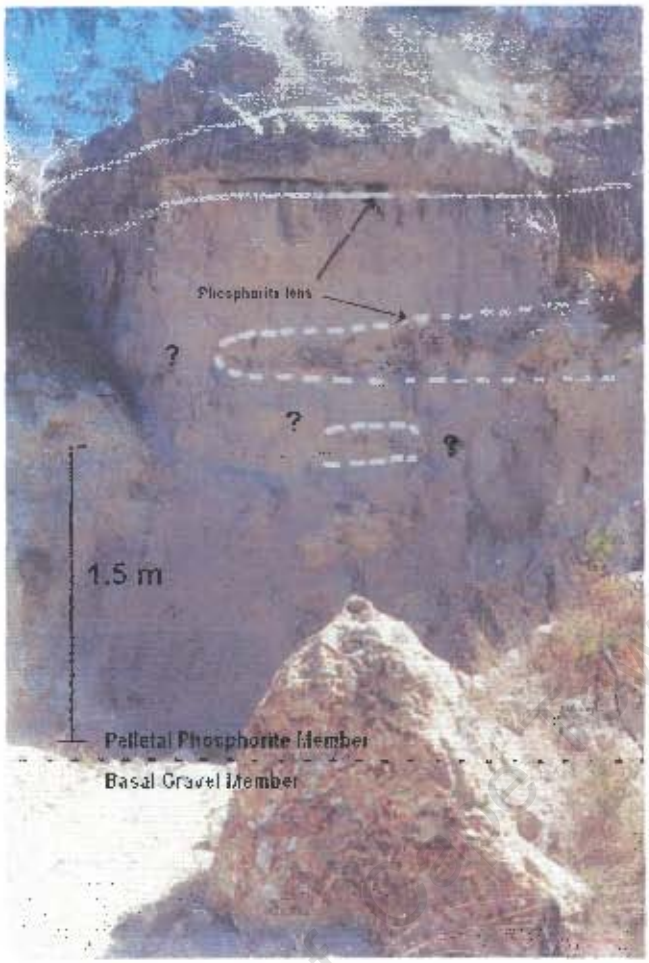

Figure 3.6. 0.5 to 1m thick phosphorite lenses underlain and overlain by unconsolidated Pelletal Phosphorite member sediments. The outcrop is found within the Mine Floor area and east of the Western High Wall

3.3.3. The geology of Bomgat (Hoedjiespunt)

The stratotype for the Saldanha Formation proposed by Tankard (1975) is found within the Bomgat in the Hoedjiespunt Peninsula (Figure 3.7). It is described as the occurrence of thin layers of resinous cryptocrystalline and reworked microsphorite (shell-rich apatite) that rests on the Saldanha quartz porphyry (Tankard, 1975). Tankard (1975) also describes shell fragments, bryozoa and foraminifera set within a collophane (dahllite)/micrite groundmass. The thin (<1m) phosphorite lenses (beds) nonconformably overlie the 600 Ma Hoedjiespunt granite and are overlain itself by calcarenites and aeolianites from the Velddrif Formation and Langebaan Formation. The phosphorite that characterises the Bomgat deposit can be divided into (a) a thinly bedded amber-coloured basal layer and (b) a layer of reworked phosphorite, found in association with granite boulders and cobbles.

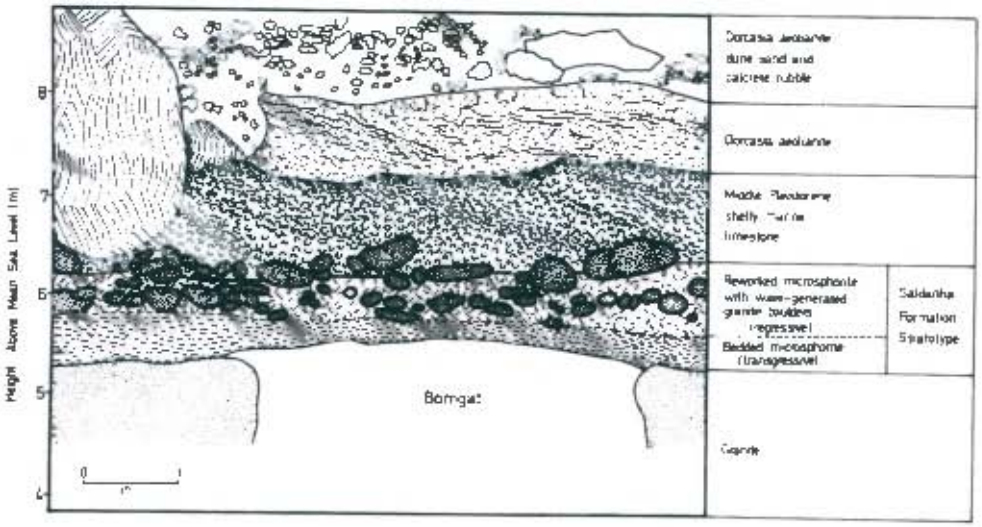

Figure 3.7. Detailed section of the Saldanha Formation stratotype at Hoedjiespunt, Saldanha (Tankard, 1975).

Tankard (1975) proposed that the deposits underlying the Varswater Formation, should be incorporated into the Saldanha Formation, however, Dingle *et al.* (1979) believed that it is not possible to correlate the stratotype of the Saldanha Formation with any of the horizons within Langebaanweg.

3.3.4. The geology of the deposits at Konstabelkop and Kreefte Bay

The aluminium phosphate deposits of the quartz porphyry hills near Saldanha and the Posberg Peninsula have generally been overlooked and are understudied. The deposits have been briefly documented by Du Toit (1917), Visser & Schoch (1973) and Tankard (1974b). The aluminium phosphate deposits at Konstabelkop and Kreefte Bay are restricted to the slopes of the quartz porphyry hills of the Saldanha Quartz Porphyry. In general the outcrops are poor, and occur sporadically about the quartz porphyry hills (Visser & Schoch, 1973). According to Visser and Schoch (1973) the phosphate deposits owe their existence to the phosphatisation of weathered bedrock (grit, rubble and sand) mixed with guano. It is proposed that organic, phosphate-rich solutions percolated from guano deposits into the underlying and surrounding sediments and granitic bedrock, whereafter the material became phosphatised (Visser & Schoch, 1973).

3.4. AIMS AND OBJECTIVES

The objectives of this study were to review the pertinent literature on the geochemical behaviour of rare-earth elements and trace-elements (U, Th etc) in phosphorites, and to conduct an investigation into the rare-earth element geochemistry of the phosphate-bearing sediments of the Varswater Formation (exposed within the Varswater Quarry, near Langebaanweg), the phosphatised limestones from the Saldanha Formation (exposed within the Bomgat cave, near Hoedjiespunt), and the aluminium phosphate deposits found on the Posberg Peninsula.

The specific aims of this study were as follows:

- Document the petrography and stratigraphy of the phosphorite deposits at Langebaanweg, Bomgat and the deposits on the Posberg Peninsula.
- Determine the geochemistry of the different phosphorite grain types, using rare-earth elements and trace-elements and propose possible depositional environments and diagenetic histories.

3.5. LIMITATIONS AND CONSTRAINTS

The major limitations and constraints of this study are:

- Owing to extensive mining at Langebaanweg and Konstabelkop, most of the primary structures and sediments that would have improved our understanding of the geology have been mined out (Middleton, 2000).
- The mining at Langebaanweg has also increased the risk of contamination between the different lithologies (Middleton, 2000).
- The outcrops of the aluminium phosphates on the Posberg Peninsula are extremely sporadic and access to most of the aluminium phosphate sites was restricted, therefore sampling of the other 'known' aluminium phosphates sites (at Vlaeberg, Lyfserhoek, Baviaansberg and Malgaskop) was not possible.

The following chapter presents a brief discussion on the localities investigated, the sampling techniques used and the sampling convention utilised.

CHAPTER 4
SAMPLING LOCALITIES AND STRATEGY

This chapter includes a brief description on the sampling techniques used, the localities investigated and the sampling convention utilised.

4.1 SAMPLING RATIONALE AND NAMING CONVENTION

Sample names are derived from the abbreviations of the site name and each sample is assigned a sample number. An example is **VW46**. In this example **VW** refers to the sampling site from which the sample was collected, i.e. VW = Varswater Quarry. The last two numbers differentiate between samples from the same type taken at different locations in the same site, for example **VW46** and **VW12**. Selected samples were also collected from various exposed mine/quarry faces. These samples can be identified by the "@" symbol. For example, VW1@1.79m indicates that the sample is from the Varswater Quarry, at Site 1, and taken from a height of 1.79m (above the base of the outcrop). For the purpose of this research only samples with appreciable amounts of phosphorite were further analysed. Additional offshore samples (i.e. Mjm samples Mulabisana (1998)) were also analysed and are used for comparison to the onshore samples.

4.2 SEDIMENT/ROCK SAMPLES

A total of 71 sediment and 23 rock samples were obtained during January 2000 and October 2002. The sediment samples were acquired from selected exposed faces, which were first cleaned using a trench shovel to obtain an uncontaminated sample. Approximately 1 kg of sediment sample was collected using a trench shovel, stored in a plastic sampling bag and labelled. Sediment colours were documented according to the Munsell soil colour charts. Rock samples were taken using a geological hammer, with care taken to ensure that the samples were unweathered. This is particularly important for samples taken from Konstabelkop and Kreefte Bay. The samples were also labelled and stored in plastic sampling bags.

4.3 SAMPLING LOCALITIES

Samples were collected principally from the Varswater Quarry near Langebaanweg. Other sample localities include Bomgat, Kreefte Bay and Konstabelkop.

4.3.1 Varswater Quarry

Phosphorite rocks and phosphatic sands are well exposed on cut faces within the mine area. This can be attributed to the period of commercial phosphate mining of the quarry before 1995. Mining has also increased the risk of contamination of the underlying phosphate rich sediments of the Varswater Formation by the overlying calcareous sand of the Langebaan Formation (Calcareous Sand member) (Middleton, 2000). Several sampling points were identified within the mine area (Figure 4.1).

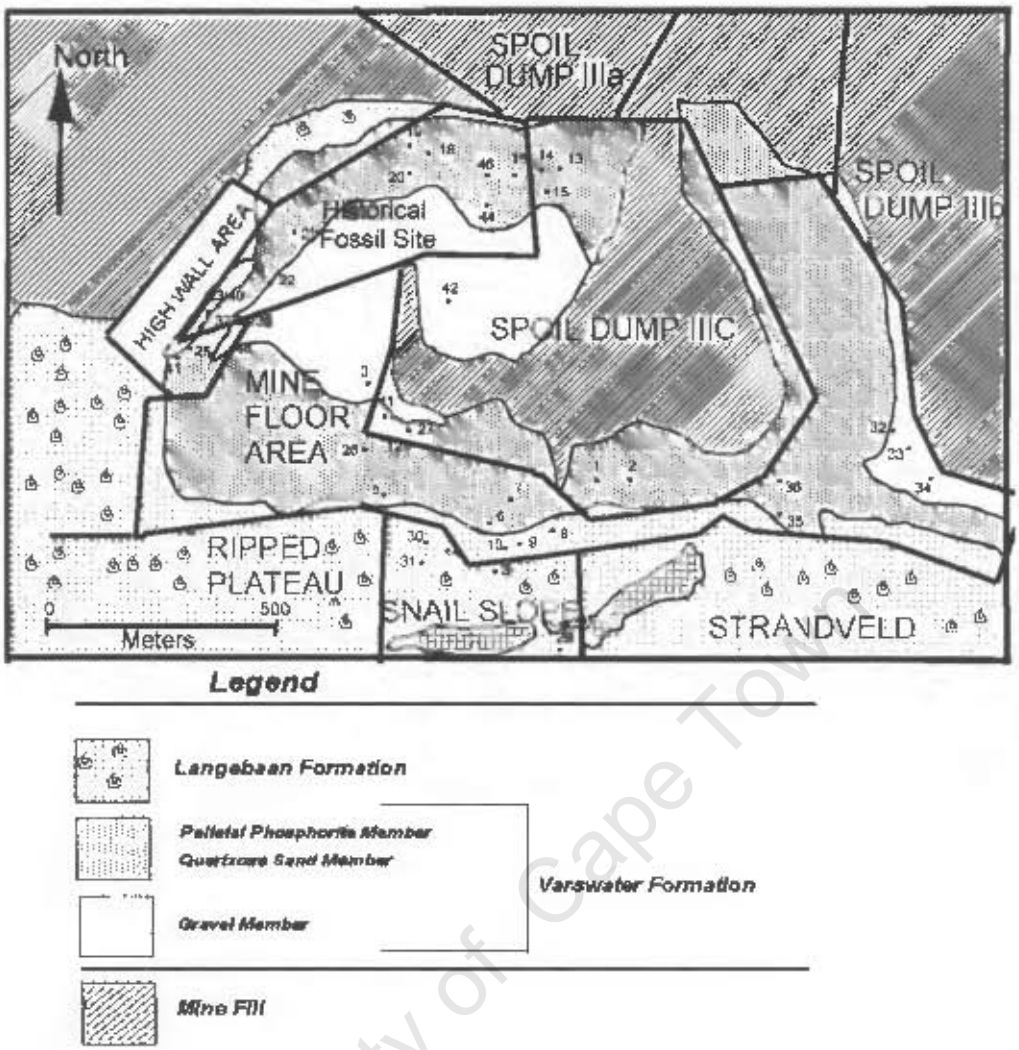

Figure 4.1. Map showing a general overview of the surface geology of Varswater Quarry, near Langebaanweg and the distribution of sampling sites.

The exposed sections within the mine are not always ideal, given lack of primary sedimentary structures and ambiguous contacts. The mine area does offer good sections such as VW1/BirdHide near the southern margin of the Dam, within the Spoil Dump IIIc (Figure 4.1). The Bird Hide section exhibits variations within the Pelletal Phosphorite member (Middleton, 2000). The Bird Hide section has been subdivided into 4 layers, on the basis of the presence or absence of primary sedimentary structures and colour differences (Figure 4.2).

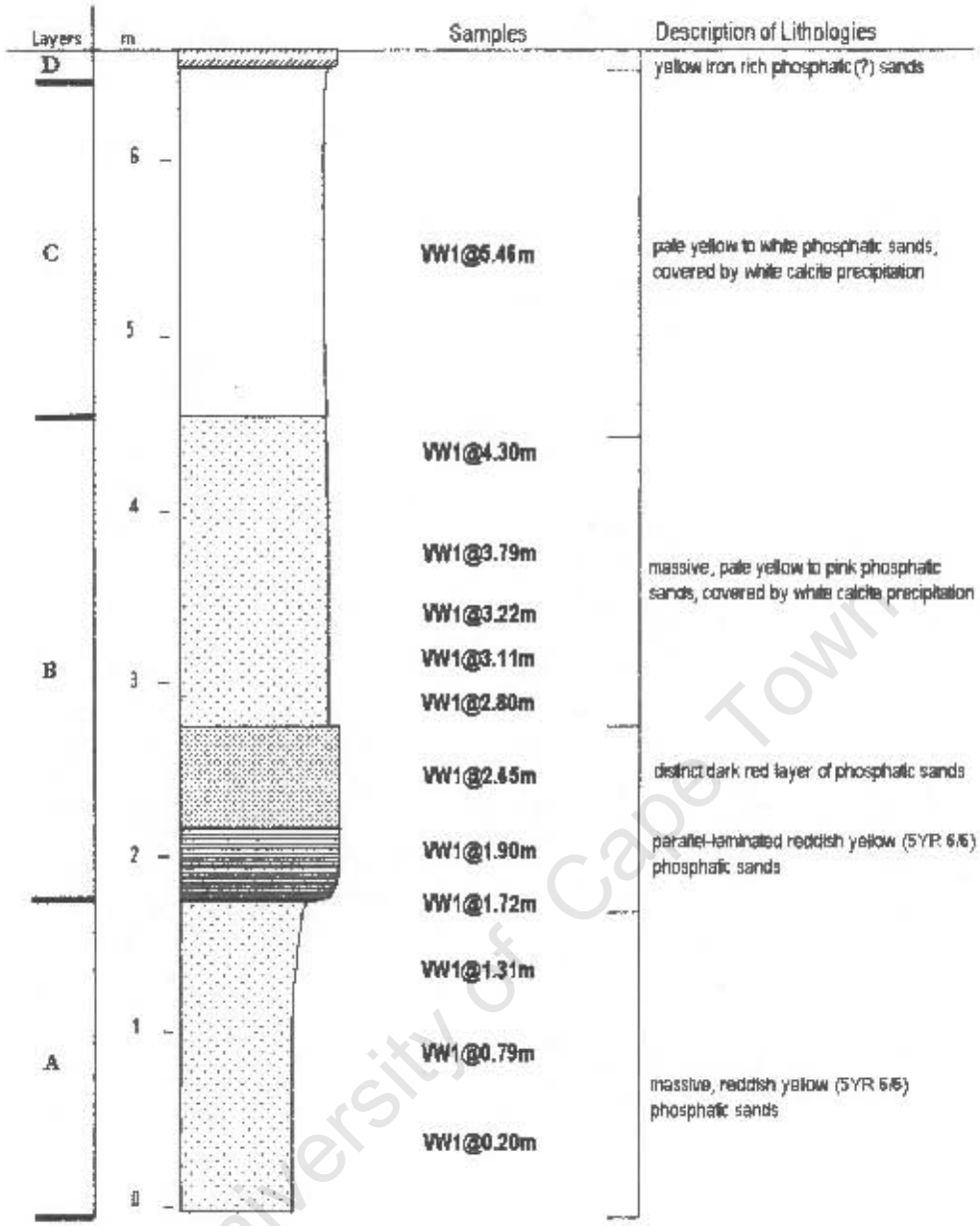

Figure 4.2. Stratigraphic column for samples from the Bird Hide (Site VW1) Varswater Quarry, Langebaanweg (modified after Middleton, 2000).

Layer A represents the lowermost unit, which is a 1.79 m thick, massive unconsolidated, reddish yellow (5YR 6/6) phosphatic sand. Layer B is 3 m thick and in the lowermost 0.20 m has horizontal laminations (Figure 4.3). Overlying the laminated unit is the laterally persistent and distinctive 0.3 m thick, dark red coloured unit. Overlying Layer B is a 2.30 m thick massive pale yellow to white phosphatic sand. The Bird Hide section is capped by Layer D, a 10 m thick layer that exhibits a mottled surface texture (yellow (10YR 8/8) sediments with frequent dark red (10YR 3/8) patches).

Figure 4.3. Laminated phosphatic quartzose sand within the Pelletal Phosphorite member at the Bird Hide section (VW1) (Geological hammer for scale).

At site VW46 in the Historic Fill site on the north side of the mine, there is a 0.4 m to 0.6 m thick consolidated phosphorite bed associated with highly fossiliferous medium grained iron-stained white (10YR 8/1) to pale yellow sediments (Figure 4.4.). The sediments contain phosphatised bone fragments (predominantly *Sivathere*, a short-neck giraffid) (Hendey, 1982).

(a) (b)

Figure 4.4. Some features of sampling Site VW46. (a) Phosphatised *Sivathere* jaw bone. (b) *Sivathere* bone fragments within the southern limb of the excavation.

Figure 4.5 provides a schematic diagram indicating the location of samples relative to the phosphorite bed Figure 4.6 indicates the general outcrop of the phosphorite bed and the relative positions at which samples were taken. For the purpose of this research the phosphorite bed will be referred to as VW16.

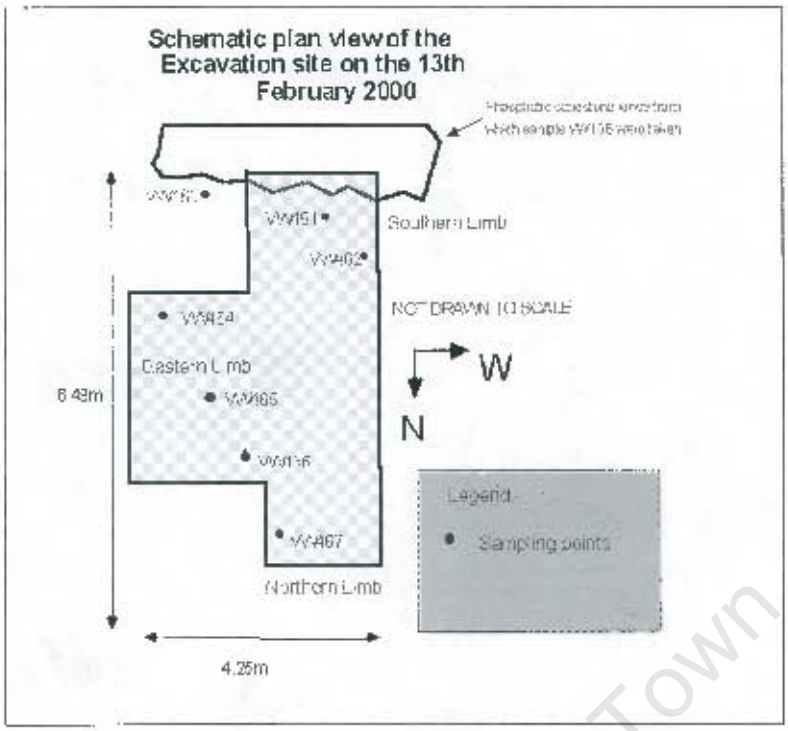

Figure 4.5 Schematic plan view of the excavation at Site VW46 (Middleton, 2000).

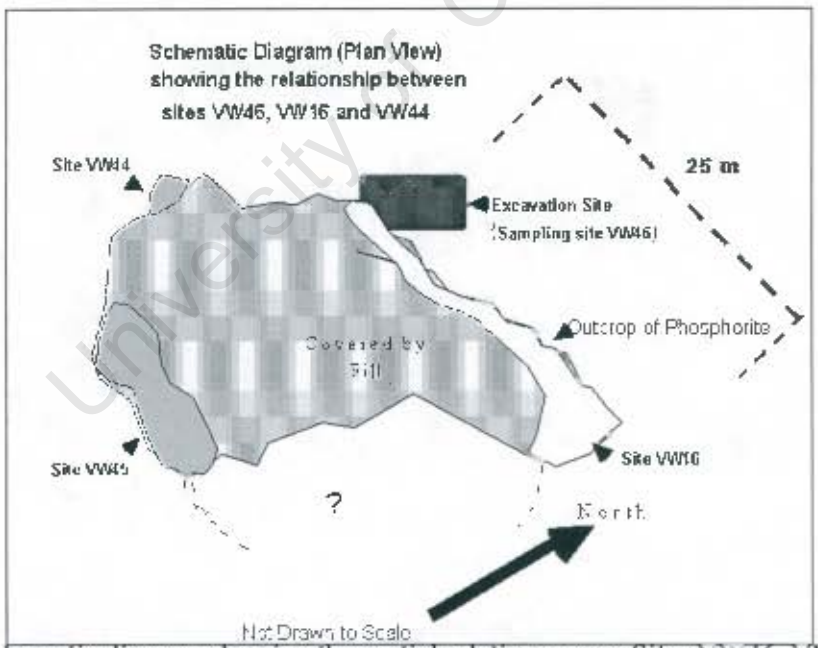

Figure 4.6. Schematic diagram showing the spatial relation among Sites VW46, VW16 and VW44 (Middleton, 2000).

4.3.2 Bomgat (near Hoedjiespunt)

The Bomgat cave, situated on the Hoedjiespunt Peninsula, provides an excellent opportunity to study and sample the Hoedjiespunt phosphorites. Samples collected from the Bomgat cave were taken from the basal phosphorite layer and a few rounded pebbles from the overlying reworked phosphorite (Figure. 4.7).

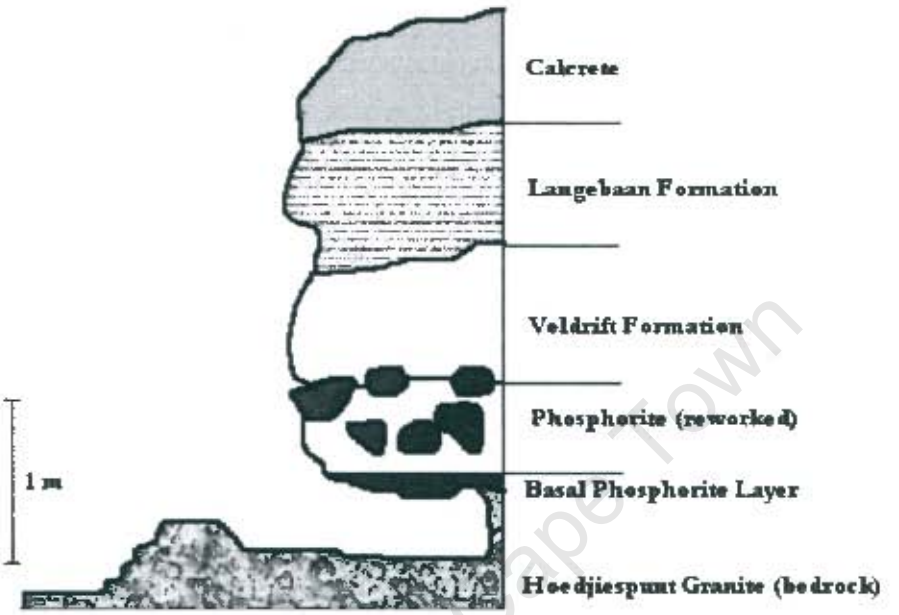

Figure 4.7. Stratigraphic section of the sediments and rocks exposed at the Bomgat Cave on the Hoedjiespunt Peninsula, Saldana Bay (Modified after Tankard, 1976).

4.3.3 Kreefte Bay and Konstabelkop

The aluminium phosphate deposits found on the Quartz Porphyry hills of the Posberg Peninsula are poorly preserved and extremely rare (Visser and Schoch, 1973)(Figure 3.2). In many places the deposits are partly to entirely covered by a thick layer of black organic-rich soil. The layer of soil also supports a very dense growth of vegetation which, in addition to the black soil layer, covers the phosphate deposits. The phosphate from Kreefte Bay was difficult to sample given the dense undergrowth and the layer of black soil; however *in situ* samples were obtained from a few well exposed outcrops. The phosphate from Konstabelkop was easier to sample, because the Konstabelkop deposit was once mined and as a result adequate outcrop exists. According to Visser and Schoch (1973), the reason why the deposit was mined was because of two, well-developed joint systems within the Quartz Porphyry that controlled the distribution of the deposit. The samples from Konstabelkop and Kreefte Bay are given the sample labels **Ko** and **KR**, respectively. Kreefte Bay samples were taken from two adjacent hills near Kreefte Bay with samples from hill 1 designated **KR10x** and samples from the second hill designated **KR20x**.

Table 4.1. List of samples taken from Konstabelkop (Ko) and Kreefte Bay (Kr). The asterisks (*) indicates sample analysed.

Sample	Locality	Description
KR201*	Kreefte Bay	Weathered, yellowish brown, brittle aluminium phosphate (*in situ*)
KR202	Kreefte Bay	Weathered, brittle greyish aluminium phosphate (not *in situ*)
KR203	Kreefte Bay	Replaced quartz porphyry
KR103	Kreefte Bay	Not *in situ* greyish consolidated phosphate
KR207*	Kreefte Bay	Replaced quartz porphyry
Ko1	Konstabelkop	Weathered, yellowish brown aluminium phosphate
Ko2	Konstabelkop	Replaced quartz porphyry
Ko3	Konstabelkop	Replaced quartz porphyry

CHAPTER 5
METHODOLOGY AND ANALYTICAL TECHNIQUES

The following chapter includes a brief discussion on the methodology and analytical techniques used. It presents the necessary background to the subsequent chapters which deal with the results, discussion and conclusions of the study.

5.1. INTRODUCTION

The primary objectives and aims of the study, as outlined in Chapter 3, are to document the petrography, mineralogy and rare-earth and trace-element geochemistry of the various phosphorite and phosphate deposits in the vicinity of Saldanha Bay. In order to accomplish this task, several analytical techniques were used. The techniques used included:

- optical microscopy (binocular and polarised microscopes),
- photomicroscopy,
- scanning electron microscopy (SEM),
- X-ray diffraction (XRD),
- Inductively Coupled Plasma – Mass Spectroscopy (ICP-MS) and
- Laser ablation Inductively Coupled Plasma – Mass Spectroscopy (LA-ICP-MS).

All of the analytical facilities were used at the University of Cape Town (UCT). The relationship between the various techniques and the methodology used are described in Figures 5.1 a and b.

5.2. METHODS

The following section discusses the various techniques used and briefly discusses the principles behind the methods. Results are shown in the Appendices.

5.2.1. X- ray diffraction (XRD)

In order to determine the mineralogy, samples were analyzed using the XRD (X-ray diffraction) facility, within the Department of Geological Sciences at UCT .

Sample preparation

For the purpose of this research, phosphatic sand sub-samples were separated into several main groups based on the different grain types, such as phosphatised shell fragments (PSh), phosphorite pellets/peloids (Pph) and phosphatised bone fragments (Bne). The procedure for separating the different grain types required a binocular microscope, a thin-tipped paintbrush and sample holders. Identified grains were picked using the wetted tip of the paintbrush, and separated into labelled sample holders. Care was taken to ensure that only the relevant grains were picked and stored in their respective labelled sample holders. A typical label would show the sampling locality and grain type (e.g. vw1@1.90m Pph).

In the XRD lab the different grain types were crushed using a hand-held, agate mortar and pestle and placed on a zero-background quartz slide. The zero-background quartz slide is normally used to reduce the amorphous overprint/pattern that can result from using very small amounts of a sample on a conventional glass slide (Figure 5.2).

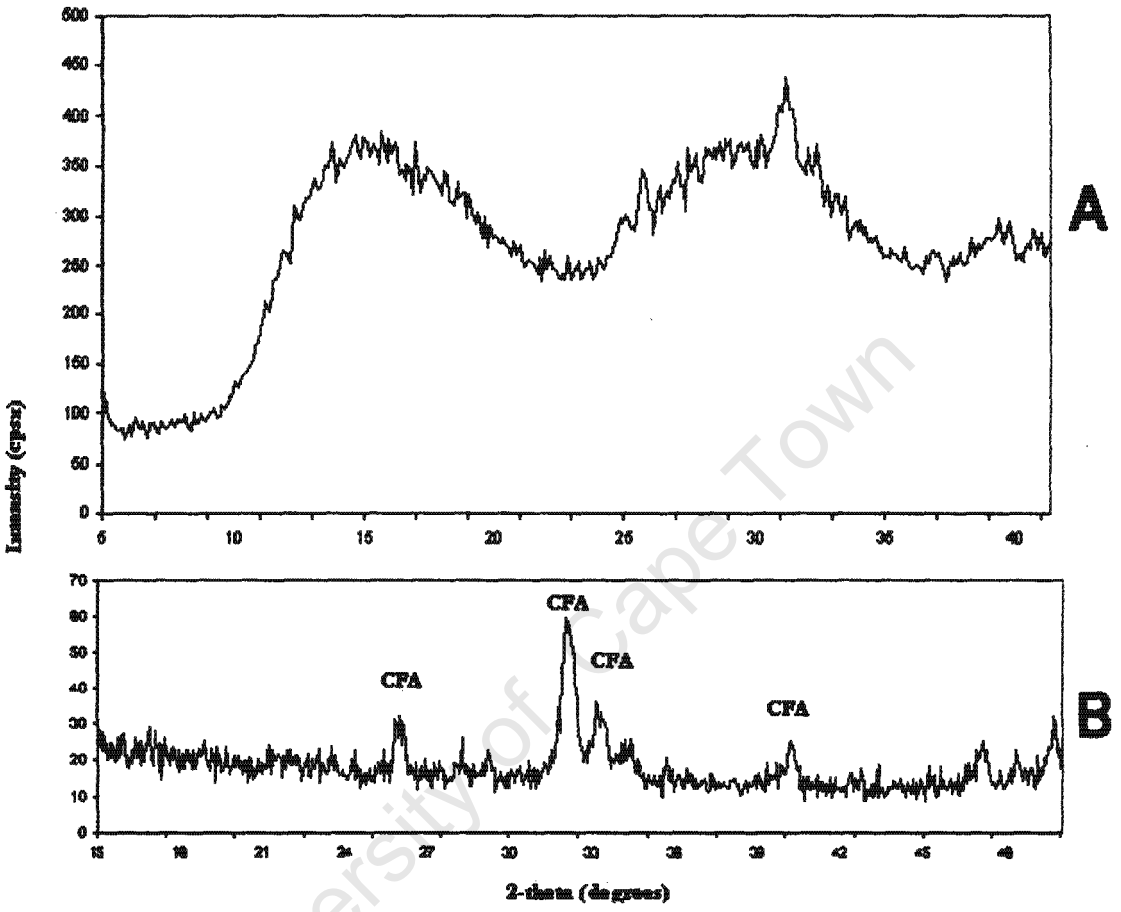

Figure 5.2. Diffractogram A was obtained from the analysis of a sample using a conventional glass slide. The diffractogram shows an amorphous overprint, which makes interpretation difficult. Diffractogram B was obtained using the zero-background quartz slide. The sample used in both analyses is the same. The peaks identified are of the carbonate fluorapatite mineral (CFA) francolite.

Rock samples were prepared for XRD by first being crushed and milled into a powder form. Using a hand-held press, the powder was pressed into a XRD sample holder. A Philips PW1050/80 X-ray Diffractometer was used to determine the mineralogy of the sub-samples and to test for the presence of calcite. A copper target X-ray tube (Cu K_D) was used at a current of 20 mA and a voltage setting of 40 kV. The zero-background quartz slide (or XRD sample holder) was inserted into the diffractometer sample chamber and scanned over a theta range of 15 - 50 degrees (in some cases the sample was scanned over a theta range of 5 – 80 degrees). The resultant diffractograms were analysed using the Philips X-ray diffraction software, supplied with the X-ray diffractometer to identify

the main minerals in the samples and sub-samples. Minerals were identified using search-match routines. The search-match routines, although easy to use, can result in erroneous identification. Therefore, when necessary, a search manual was used. Afterwards the files were exported to Windows Excel 2000. Results are shown in Appendix A3.

5.2.2. Scanning electron microscope (SEM)

In order to document the surface textures and features of specific phosphorite grain-types (PSh, Pph, and Bne) and selected phosphorite/phosphate rock samples, the UCT Electron Microscope Unit's scanning electron microscope (SEM) facility housed within the R.W. James Building (departments of Physics, Astronomy and Oceanography) was used.

Sample preparation

The sample or specimen is glued to a sample holder or "post". Given that samples examined by the SEM must be able to endure the strong electric currents produced by the electron beam, the samples must first be coated with a thin layer of conductive material of gold or carbon. The gold acts as a conductor thus preventing any charge build up at the point of analysis. After the initial preparation the sample is placed in the SEM vacuum chamber and the electron gun is switched on. The high-resolution images are obtained from the emission of secondary electrons. Results are shown in Appendix A5.

5.2.3. Photomicro/macroscopy

Phosphorite and phosphate rock thin sections were examined and photographed using the photomicroscope facility housed within the Department of Geological Sciences. Selected sediment samples were photographed using the photomacroscope facility housed within the Department of Archaeology (UCT). Results are given in Chapter 6 and Appendix A4.

5.2.4. Inductively Coupled Plasma – Mass Spectroscopy (ICP-MS)

Samples were analysed using the Perkin Elmer/Sciex Elan 6000 inductively coupled plasma mass spectrometer housed within the Department of Geological Sciences.

Sample Preparation

In order to analyse samples using inductively coupled plasma mass spectrometry (ICP-MS) the samples must be in solution (Table 5.1). Given the sensitivity of the ICP-MS method, great care was taken to ensure that contamination did not occur during preparation or analysis.

Table 5.1. Table showing the procedure used for bulk-rock preparation for ICP-MS analysis. The following procedure is listed on the UCT ICP-MS Short course website at http://www.uct.ac.za/depts/geolsci/icpms/procedrs/bulkrock.html

1. Samples were weighed into clean, 5ml Savillex beakers, using the microbalance (a Mettler Toledo AG245 balance) in the IC-PMS preparation lab (on the first floor of the Department of Geological Sciences). Approximately 50 mg were needed. Sample weights were recorded on a weighing sheet and the beakers labelled and closed.
2. In the wet chemistry lab on the 3rd floor of the Department of Geological Sciences, 4ml of a HF/HNO_3 solution was added using a 1-10 ml pipette to each sample.
3. The beakers (with their lids closed tightly) were placed on clean aluminium trays on the hotplates. The samples were left for approximately 48 hours to be digested at a temperature of 50-60°C.
4. Once dried the samples were taken off the hotplates and using the 100-1000 microliter pipette, 2 ml of concentrated 2-bottled HNO_3 was added to each sample.
5. The beakers (with their lids closed tightly) were placed on the hotplates until the samples were completely dissolved.
6. Once dissolved the beakers were removed from the hotplates and allowed to cool. The beakers, once cooled were returned to the hotplates (with their lids removed) and allowed to evaporate to complete dryness at a temperature of ~75°C.
7. Steps 5 and 6 were repeated.
8. The beakers were taken off the hotplates and allowed to cool down.
9. In the 1st floor preparation lab, 4 ml of internal standard stock solution was added using a 1-10 ml pipette to each sample beaker. The samples were allowed to dissolve.
10. The dissolved samples were than quantitatively transferred on the microbalance using a labeled and dried 50 ml centrifuge tube.
11. The sample beakers were washed with the 2 ml internal standard stock solution and droplets on the beaker walls were transferred to the centrifuge tubes on the microbalance.
12. In order to create a 1000-fold dilution of the original solid sample, dissolved samples were made up to 50 mg using the internal standard stock solution. 4 drops of concentrated HF were added to each sample.
13. The samples were prepared and ready to be run on the IC-PMS.

In principle, samples in the ICP-MS are aspirated in an argon (Ar) stream through high-energy radio frequency coils to form a plasma. The ions within the plasma are analysed, with a quadrupole mass spectrometer. Within the mass spectrometer the ions are sorted according to mass and detected using a scanning electron multiplier. The results are then displayed on the computer monitor. The results were exported to Windows Excel 2000 and StatSoft's Statistica 6 for further statistical analysis and will be discussed in Chapter 7. Results are shown in the Appendix A1.

5.2.5. Laser ablation Inductively Coupled Plasma – Mass Spectroscopy (LA-ICP-MS)

The Elan 6000 inductively coupled plasma mass spectrometer can be connected to the laser ablation setup/extension. The laser ablation setup consists of a Cetac lSX-200 laser ablation module that uses a frequence-quadrupled Nd-YAG laser. The laser is connected to a high-resolution colour video camera, colour monitor and 54 mm sample chamber. Petrographic thin-sections were analysed using the laser ablation setup that can be connected to the Elan 6000.

Sample Preparation

Polished thin sections ("thick sections") were cut from rock samples. The polished thin sections were first viewed under a polarising light microscope where specific grain types (PSh, Pph), textures, cement etc. were identified. The identified areas were marked or encircled using a colour or black marker, with care being taken to ensure that the grain/cement to be ablated would not be contaminated with ink. The markings also served as a means to navigate, given that the sample chamber is mounted on a stage. The stage allows the sample to be moved relative to the laser (useful for focussing and positioning). Once the sample was placed into the sample chamber, the ablation process was observed using the colour monitor, which showed a direct video stream captured from the video camera. A pulsed laser beam is used to ablate the surface of the sample and the resultant material is transported into the Ar plasma of the ICP-MS. The results were exported to Windows Excel 2000 and StatSoft's Statistica 6 for further statistical analysis (Chapter 7). Results are shown in Appendix A2.

5.3. DISCUSSION OF METHODOLOGY

Given the existence of two different primary sample types (consolidated and unconsolidated) two different methodologies were created. The output of the methodologies was the same, but the methods were different. For instance, consolidated samples were cut and crushed prior to analyses whereas unconsolidated samples were first split, and using a binocular microscope selected grain-types were picked and then crushed (using a hand-held mortar). The crushed samples (consolidated and unconsolidated) were then analysed using XRD. In addition to mineralogy, XRD scans allowed the detection of minerals other than CFA such as calcite. Determining whether calcite was present was crucial for the unconsolidated phosphatic samples from the Varswater Formation because analyses of these samples was predominantly grain specific and carbonate contamination from the overlying calcareous Langebaan Formation into the sediment samples from the Varswater Formation was a possibility. Samples that contained calcite were first treated with acetic acid. Calcite-free and "treated" samples were completely digested for ICP-MS analysis. Consolidated or rock samples were either analysed using LA-ICP-MS (to analyse individual grain types) or ICP-MS (for bulk rock rare earth element composition). Therefore, it is possible to compare the LA-ICP-MS data from the rock samples and the ICP-MS data from the sediment samples.

CHAPTER 6
THE PETROGRAPHY AND MINERALOGY OF PHOSPHORITES AND PHOSPHATIC ROCKS FROM THE STUDIED LOCALITIES

This chapter presents the mineralogy and petrography of the phosphorites and phosphate rocks from the studied localities. The petrography of the samples was determined using binocular, scanning electron and petrographic microscopes. X-ray diffraction patterns (XRD) were used to determine mineralogy and to complement the petrography.

6.1. PETROGRAPHY AND MINERALOGY OF THE VARSWATER FORMATION, LANGEBAANWEG

6.1.1. The basal Gravel member

Gravel member samples are pale brown (10 YR 8/3) to yellowish brown (10 YR 5/4), but weathered surfaces are dark grey (2.5 YR 4/0). Gravel member clasts are generally well to sub rounded and pebble to cobble sized (Figure 6.1). Evidence for periodic reworking and re-phosphatisation includes the presence of notably different phosphatic intraclasts and phosphatic cement within the sample. The intraclasts range between rounded to angular. Samples are generally composed of predominantly (80%) subrounded to rounded quartz grains (Qtz) and occasional phosphorite peloids (Pph) (<15%). Platy phosphatised shell fragments (PSh) are also present but rare (<1%). The phosphorite peloids are generally structureless; however they can contain quartz grain nuclei (Figure 6.2).

Figure 6.1. An outcrop of the basal Gravel member, showing rounded cobbles and pebble-size phosphorite from the Varswater Quarry, Langebaanweg. The field of view is towards the southwest. A 0.30 m geological hammer is for scale.

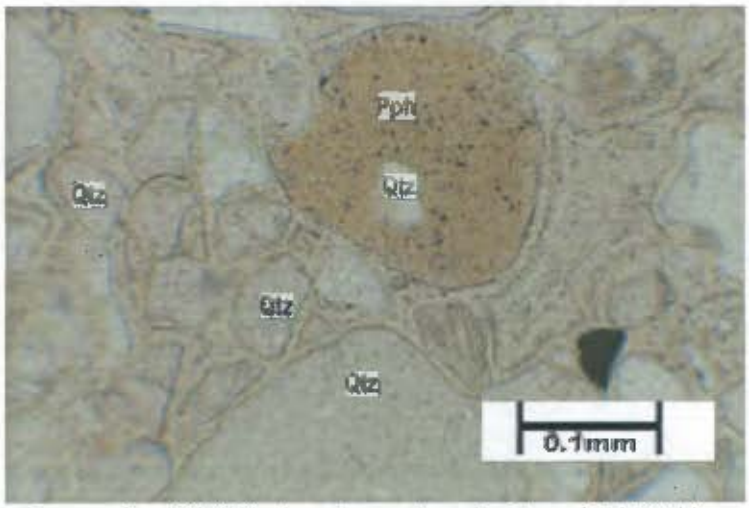

Figure 6.2. Photomicrograph of VW01 showing a phosphorite peloid (Pph) containing silt-sized quartz particles and quartz grains cemented by CFA. A 0.1 mm bar is for scale (photomicrograph taken in plane-polarised light).

The quartz grains are bimodal. There is a population of coarse, well to sub rounded quartz grains (<2.0 phi) and a population of fine (>3 phi) angular quartz grains (Figure 6.3). The different grain types (Pph, PSh, Qtz etc) are set within a cement of cryptocrystalline carbonate fluorapatite (CFA). The CFA cement is brown to light brown under plane-polarised light and pseudoisotropic under cross polarised light.

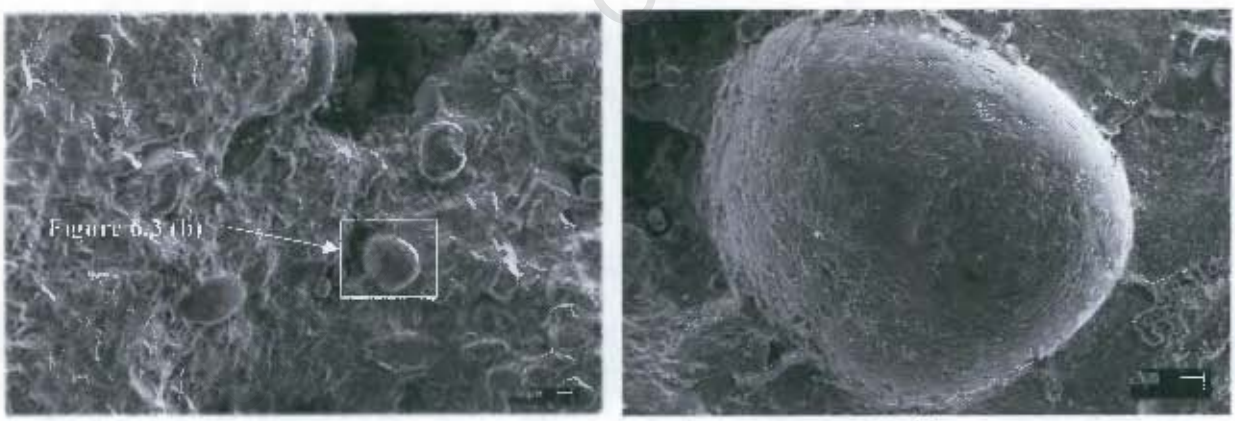

(a) (b)

Figure 6.3. SEM photograph of the interior of a Gravel member phosphorite rock sample (VW43), showing (a) an overview and (b) an enlargement of a well-rounded, spherical and pitted quartz grain. The phosphorite sample (a & b) is characterised by being poorly sorted and composed of medium to fine grained, rounded to well rounded quartz grains set within a fine CFA cement. Peloids are not present. The scale bar for (a) reads 100 microns and for (b) 20 microns.

The Gravel member samples range between medium-grained quartzose phosphatic packstones and wackestones. The Gravel member specimens are comprised of different intraclasts that suggest numerous episodes of phosphatisation and subsequent reworking (Figure 6.4.).

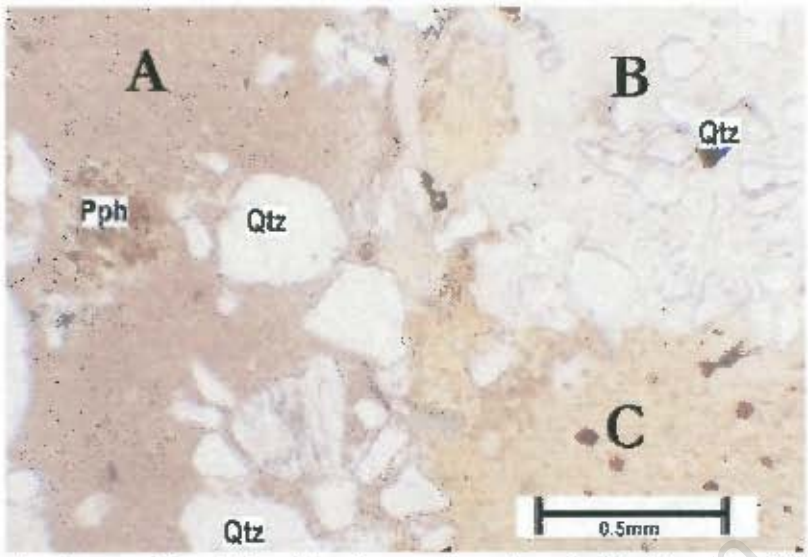

Figure 6.4. Photomicrograph of the Gravel member phosphorite (Sample VW422) showing dissimilar CFA cement (labelled A, B, C). Cement A is darker in colour, and contains medium grained quartz grains and the occasional phosphorite pellet. Cement B and C are devoid of phosphatic grains, but contains very fine angular grains of quartz (photomicrograph taken in plane-polarised light).

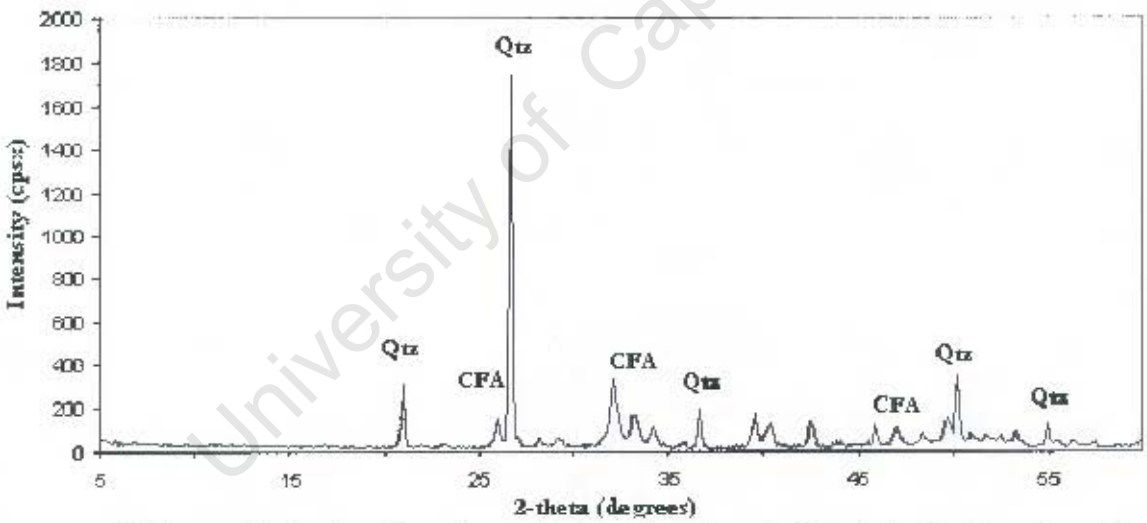

Figure 6.5. XRD profile obtained from the preferred orientation of minerals in the Gravel member sample VW43.

Quartz and francolite (CFA) are the two major minerals identified from a typical Gravel member XRD diffractogram (XRD profile) (Figure 6.5).

6.1.2. The Pelletal Phosphorite member

The Pelletal Phosphorite member is composed of unconsolidated-phosphatic sands and occasional lenses of consolidated quartzose phosphorites. The consolidated quartzose phosphorites are generally overlain and underlain by unconsolidated-phosphate-rich sands (Figure 6.6). The phosphorite lenses are light yellowish brown (2.5Y 6/4) to light brownish grey (2.5Y 6/2) in colour and the mean size of the grains is medium sand.

Figure 6.6. Unconsolidated phosphate-rich sediments overlain by a consolidated quartzose phosphorite bed (lens) at Site VW16 (field compass for scale).

Unconsolidated phosphatic sediment samples of the Pelletal Phosphorite member are moderately sorted to moderately well sorted, fine to medium sands, and range in colour from dark red (10YR 3/8) to pale yellow (5Y 8/3), but in general can be described as pink (7.5YR 8/4). The major components of these sediments are quartz grains (Qtz), peloidal phosphorite (Pph), phosphatised shell fragments (PSh) and occasionally phosphatised echinoid spines (PEch) (Figure 6.7). Occasional calcareous grains and opaque heavy minerals are also present. The quartz grains appear in a variety of different forms, ranging from well rounded and polished to angular and frosted.

The peloidal phosphorite (Pph) grains are generally medium sands, ovoid in shape, becoming more rounded with decreasing grain size, which is opposite to the trend seen for the quartz grains. Coarse peloidal phosphorite (<2.0 phi) are less rounded, occasionally pitted and exhibit a variety of different forms, i.e. prolate grains and oblate grains (Figure 6.8). The peloidal phosphorite grains are generally reddish brown in colour, opaque, and have polished surfaces. The amber to red coloured phosphatised shell fragments (PSh) are generally translucent and platy in shape, with rounded rims (Figure 6.9). The morphology and surface texture of the phosphatised shell fragments reflects the original shell morphology. Another biogenic component within the samples

is phosphatised echinoid spines (PEch). In terms of the proportion of components, the peloidal phosphorite and quartz grains are very abundant, whereas the phosphatised shell fragments are subordinate. Occasionally phosphatised and partially dissolved benthic foraminifera (typically *Elphidium* sp.) are present, although extremely rare. Similar to the Gravel member samples, the very fine quartz grains are generally much more angular than the medium quartz grains. The medium quartz grains are generally well rounded to rounded. In general these well-rounded grains are fractured, indicating that they have been reworked prior to deposition.

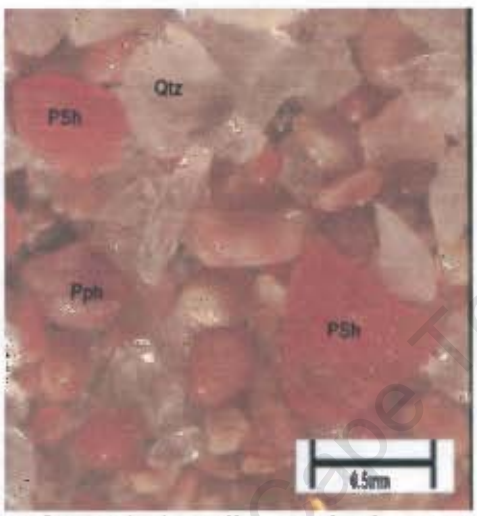

Figure 6.7. Photomacrograph of a typical medium grained, unconsolidated sediment from the Pelletal Phosphorite member (Site VW1) showing amber-coloured phosphatised bivalve shell fragments (PSh), phosphorite peloids (Pph) and quartz. The phosphatised shell fragments have well rounded edges and a distinctive platy shape. The quartz grains are generally well rounded to sub rounded, however fractured grains are also present (x10 magnification).

The consolidated phosphorite lenses (beds) consist of fine to medium sand with medium to fine, rounded to angular quartz grains (Qtz) (50-70%), ovoidal phosphorite peloids (or peloids) (Pph) (20-30%), platy phosphatised bivalve fragments (PSh) (15 - 20%) and trace amounts of opaque heavy minerals (Op) set within a cryptocrystalline cement of CFA (Figure 6.10). Occasionally, minor amounts of rounded to subrounded feldspar grains, phosphorite peloids containing benthic foraminifera and lithic fragments are also present. The quartz grains are bimodal, with angular very fine to fine sand size (~0.1mm) quartz grains and rounded coarse to very coarse sand quartz grains (~0.5mm).

In thin section, the phosphorite peloids, phosphatised shell fragments (PSh) and cement are pseudo-isotropic, but under plane-polarised light they are generally yellowish brown to brown in colour. The phosphorite peloids are structureless, but can contain disseminated silt-size angular quartz grains. According to Middleton (2000) one phosphorite peloid contained a benthic foraminifera (possibly *Ammonia* sp. or *Elphidium* sp.), whereas another contained a very coarse particle of what appears to be a shell fragment (Figure 6.11). This gives the impression that the phosphorite peloids have nuclei.

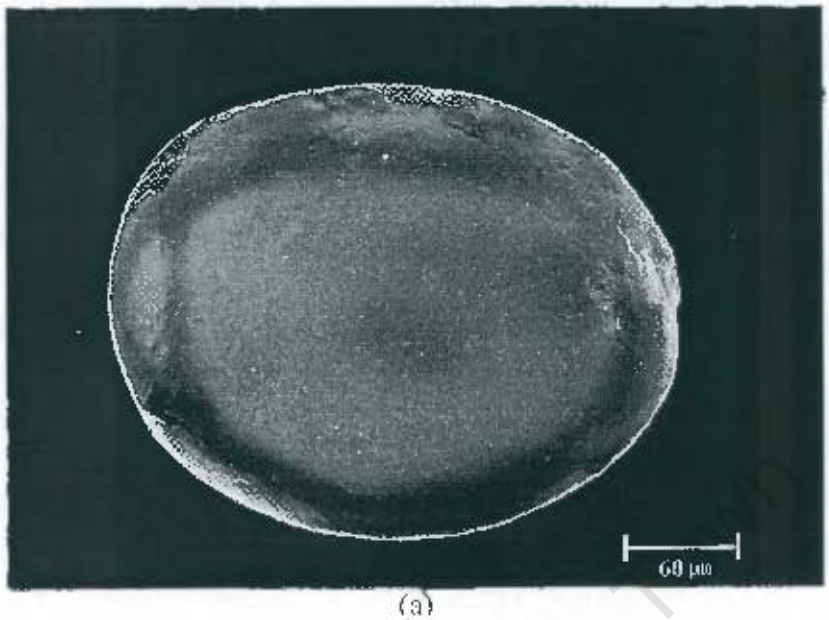

(a)

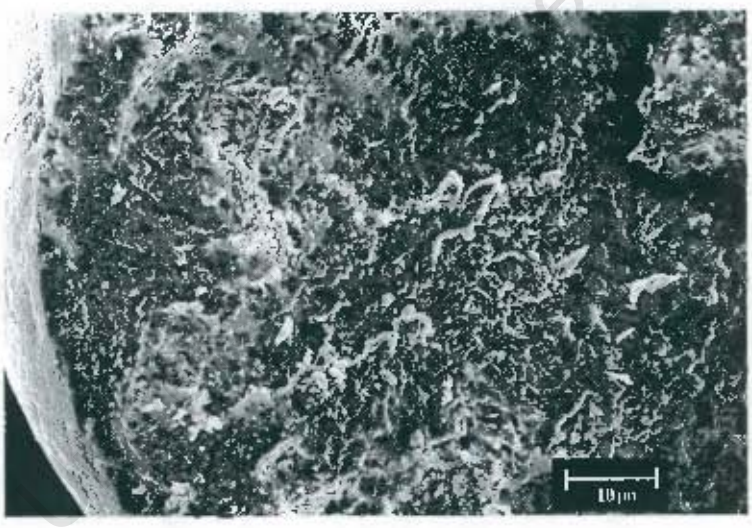

(b)

Figure 6.8. SEM photographs of sample VW1A3, (a) showing a well-rounded subspherical peloid and (b) close-up image of the smooth rim and extremely fine grained, but extremely irregular fractured interior of a broken surface. The surface of the grain is distinctively smooth, with occasional micropits. The grain is composed predominantly of microscopic anhedral crystals of francolite (CFA).

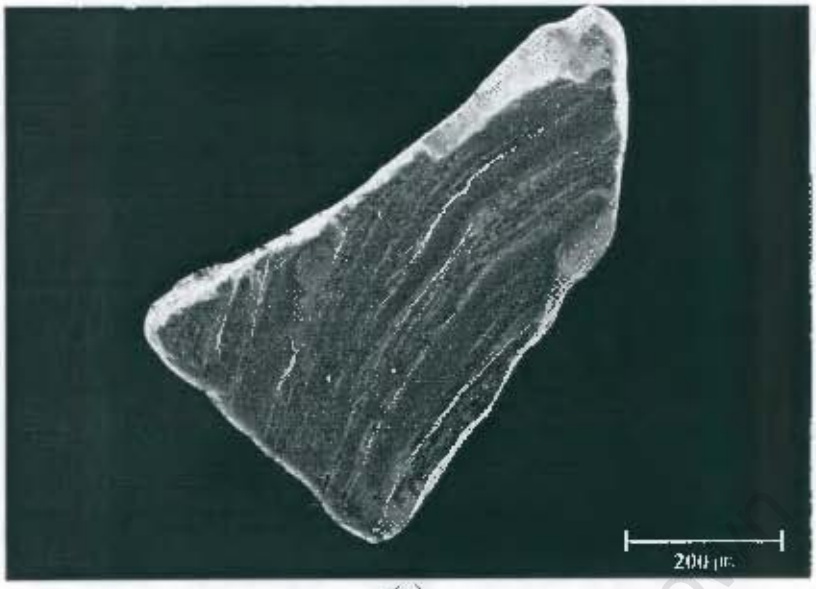

(a)

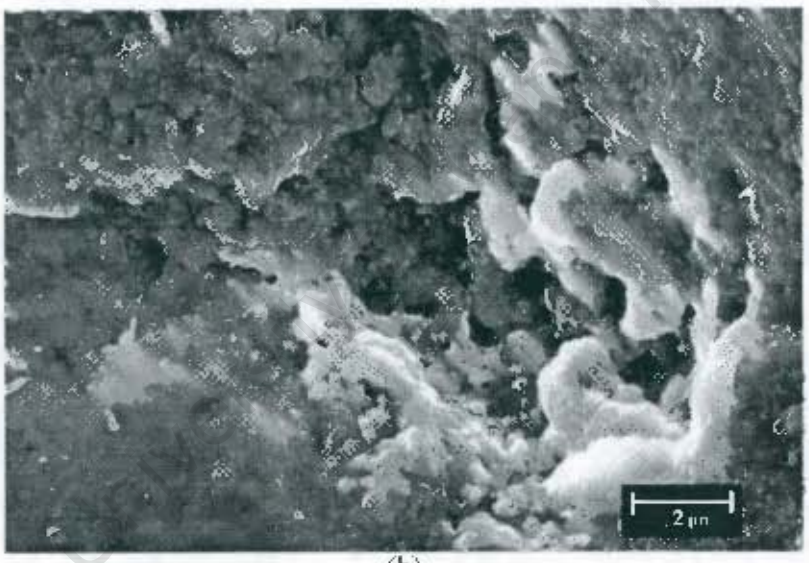

(b)

Figure 6.9. SEM photographs of sample VW1A3, showing (a) a phosphatised shell fragment (PSh), with distinctive well rounded edges and (b) a close-up image of the pitted, fine grained surface with anhedral to subhedral francolite crystals.

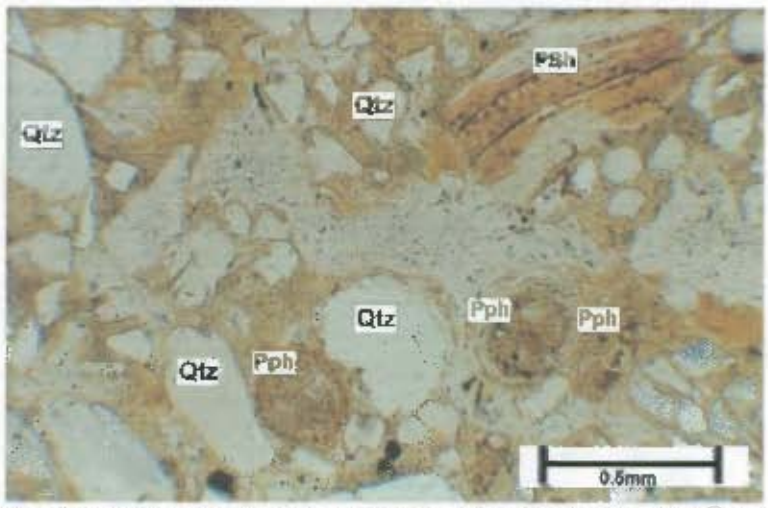

Figure 6.10. Photomicrograph of a typical medium grained, consolidated Pelletal Phosphorite member sample showing laths of phosphatised bivalve shell fragments (PSh), ovoidal phosphorite peloids (Pph) and abundant fractured subrounded to angular quartz grains (Qtz) set within a fine cement of CFA. Middleton (2000) described the phosphorites as a medium-grained phosphorite packstone (photomicrograph taken in plane-polarised light).

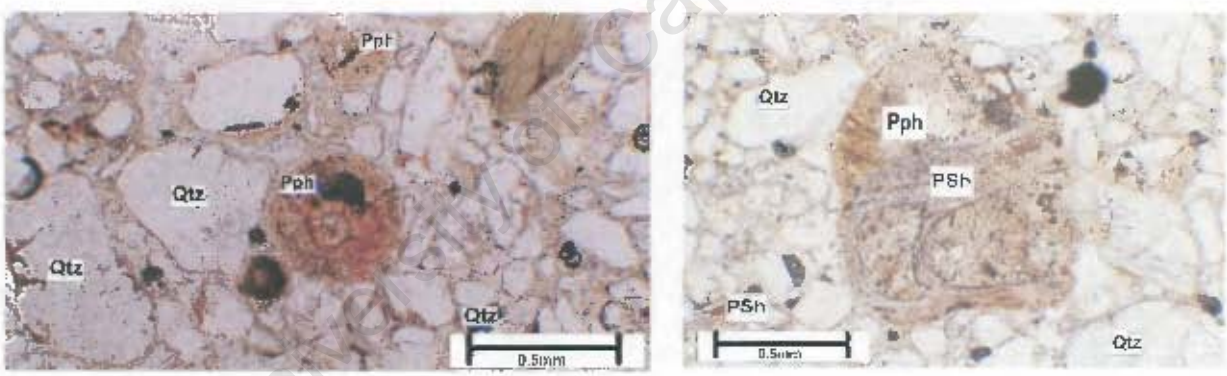

(a) (b)

Figure 6.11. Photomicrographs of typical medium grained, consolidated Pelletal Phosphorite member (VW16) showing (a) ovoidal phosphorite peloids (Pph) containing a benthic foraminifer and (b) a coarser phosphorite peloid containing a shell fragment (photomicrograph taken in plane-polarised light).

Some of the samples show a distinctive light-coloured pellicle surrounding the peloidal phosphorite and occasionally the quartz grains. Typically, within the ferruginous phoscretes, the quartz grains are rimmed by a brownish coloured material that could be an iron oxide. This rim is isotropic. The packing of the phosphorites is grain-supported, although some samples are matrix-supported. Therefore, packstones are more common than wackestones.

6.2. PETROGRAPHY AND MINERALOGY OF PHOSPHORITE FROM THE SALDANHA FORMATION, BOMGAT, HOEDJIESPUNT PENINSULA

The Bomgat phosphorites are made up of various well to poorly preserved phosphatised bioclasts (allochems). The bioclasts are set within a very fine grained phosphatised micrite/CFA groundmass. It is possible to identify some of the bioclasts present. These include well preserved bryozoan fragments, echinoid fragments (mostly ossicles), mollusc shell fragments (typically gastropods and bivalves) and occasional benthic foraminifers (Figure 6.12 a and b).

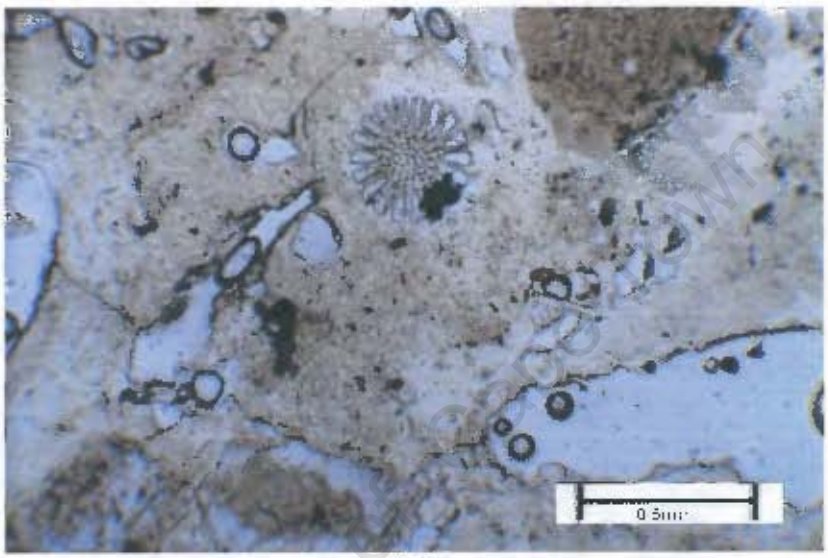

(a)

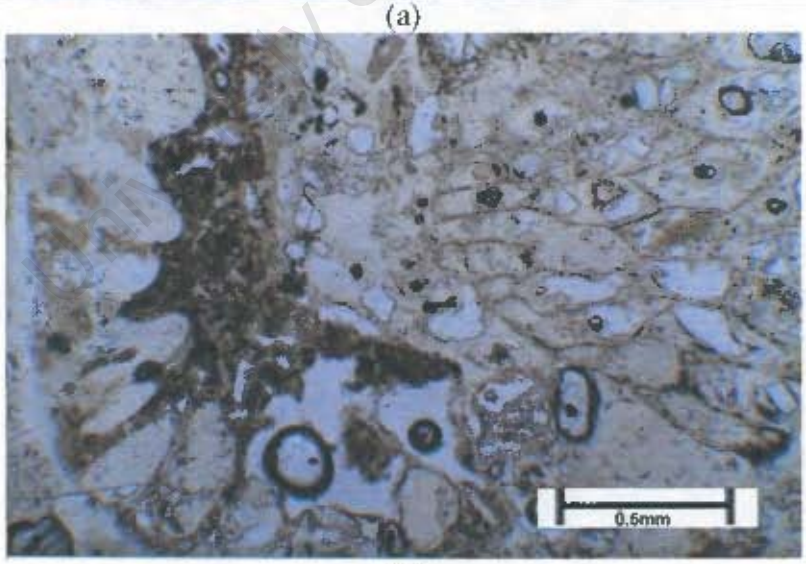

(b)

Figure 6.12. Photomicrographs of the Hoedjiespunt phosphorite (B1) showing a (a) cross section of an echinoid ossicle and (b) a bifurcating bryozoa set within a fine grained CFA groundmass (photomicrographs taken in plane-polarised light).

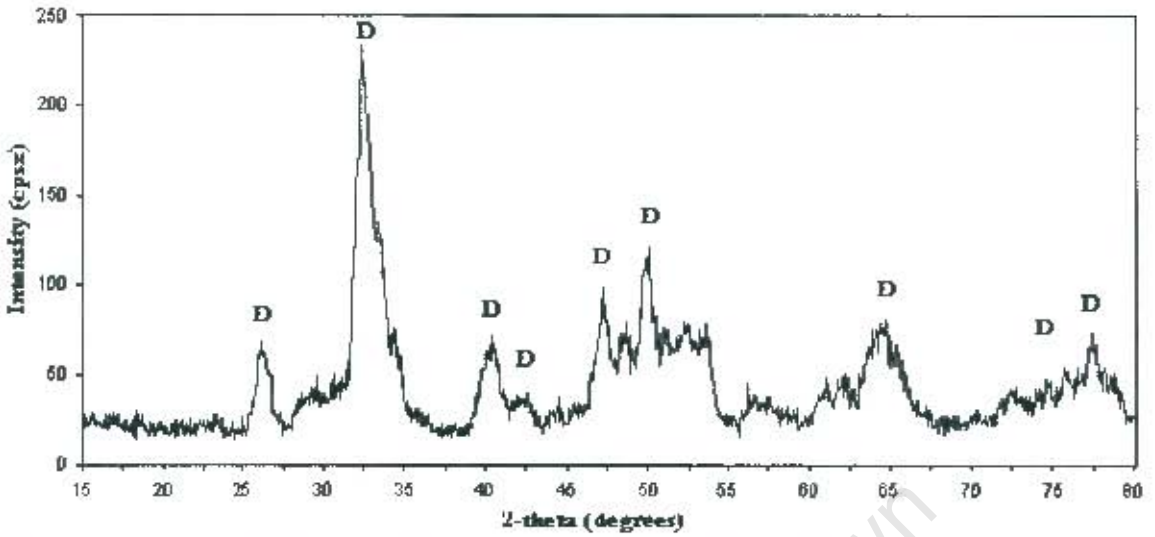

Figure 6.13.. XRD profile of sample B1 from Bomgat. The identified peaks indicate that the sample is dominated by the mineral Dahllite (*D*).

XRD analysis of phosphorite from the Bomgat, Hoedjiespunt Peninsula indicates that it is predominantly composed of the mineral dahllite, a fluorine-poor carbonate apatite (Figure 6.13). It also appears that there is no detectable clay or carbonate minerals, indicating that all of the biogenic carbonate has been phosphatised. According to Tankard (1973), some of the Bomgat phosphorites are partially phosphatised and retain some of the precursor carbonate.

6.3. PETROGRAPHY AND MINERALOGY OF THE ALUMINIUM PHOSPHATE FROM THE POSBERG PENINSULA.

The aluminium phosphates from the Posberg Peninsula are a diverse group of phosphates. The deposits are found in association with the quartz porphyry (Cape Granite Suite) of the Posberg Peninsula and in the immediate vicinity of Saldanha. The quartz porphyry consists of K-feldspar, plagioclase feldspar, quartz, biotite and accessory grains of zircon and hornblende. The aluminium phosphate is discernible as a weathered brown, hard phosphatic crust on the quartz porphyry (as found at Konstabelkop and Kreeftebay) or as an unconsolidated, friable, brown, phosphatic, weathered soil (Kreeftebay). In general altered feldspar grains are commonly partially phosphatised. The phosphate is generally found within cracks or fractures.

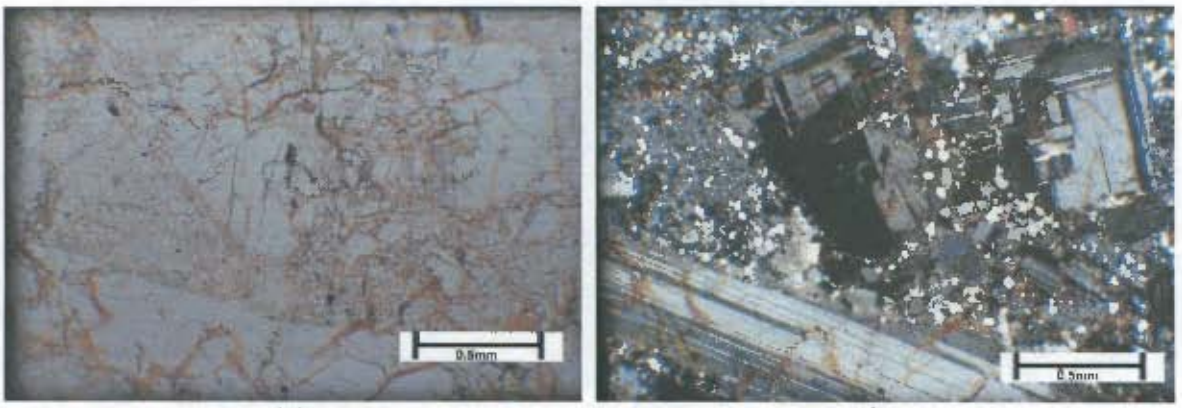

(a) (b)

Figure 6.14. KR203 is a sample of the weathered, replaced quartz porphyry. The sample shows anhedral to subhedral parallel twinned phenocrysts of feldspar set within a groundmass of anhedral quartz. The aluminium phosphate (orange) is found within small cracks. (a) Sample KR203 under plane-polarised light (PPL) (b) Sample KR203 under cross polarised light (XPL).

The following diffractograms were obtained from the analysis of typical aluminium phosphate from Kreefte Bay and Konstabelkop. XRD analysis of the aluminium phosphates from the Posberg Peninsula indicates that the phosphate mineral from Kreefte Bay is varsicite, whereas the aluminium phosphate of the Konstabelkop samples is crandallite (Figure 6.15).

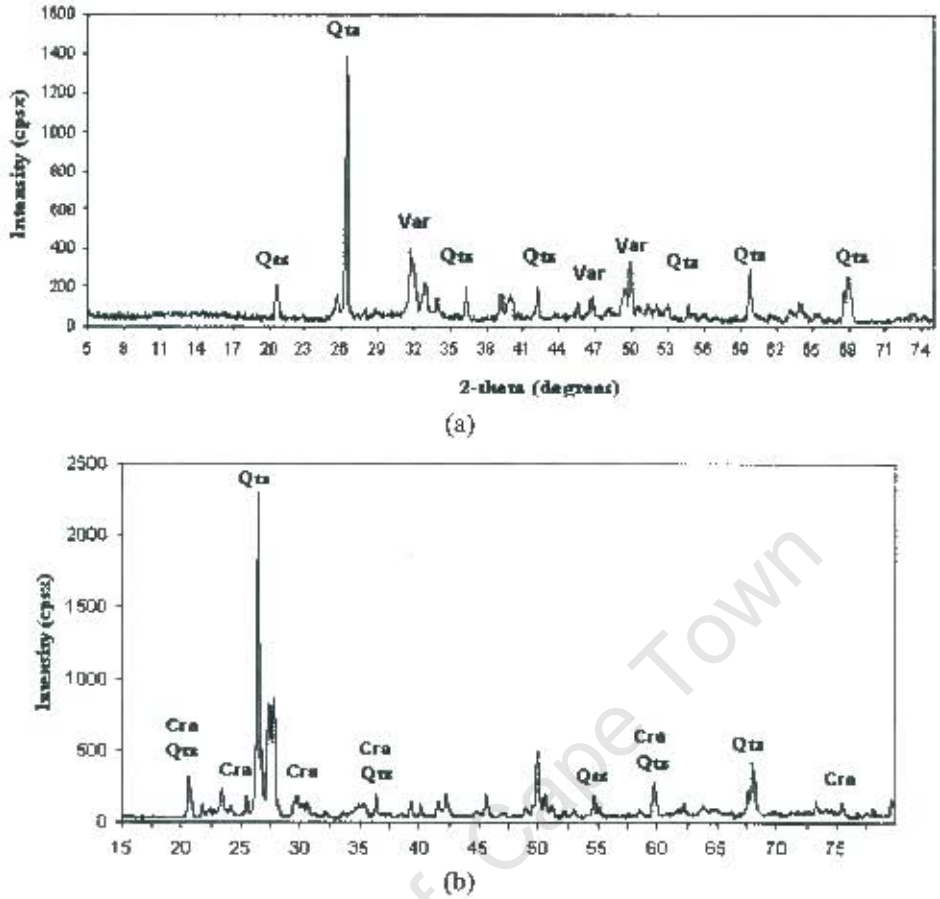

Figure 6.15. XRD profiles of the aluminium phosphates from Posberg Peninsula, showing (a) the XRD profile of sample KR201 and (b) the XRD profile of sample Ko1. The identified peaks indicate the following minerals: Var = Varsicite, Cra = Crandallite and Qtz = quartz.

CHAPTER 7
RARE-EARTH AND TRACE-ELEMENT GEOCHEMISTRY

7.1. ANALYTICAL RESULTS

This chapter presents the results obtained from the inductively coupled plasma – mass spectroscopy (ICP-MS) and laser ablation inductively coupled plasma – mass spectroscopy (LA-ICP-MS). The method of processing of the results is explained. All REE concentrations are reported in ppm (parts per million). Ce-anomalies are calculated as $Ce/Ce^* = 2\ Ce/Ce_{shales}/\ (La/La_{shales} + Nd/Nd_{shales})$. Europium anomalies are calculated as $Eu/Eu^* = 2\ Eu/Eu_{shales}/\ (Sm/Sm_{shales} + Gd/Gd_{shales})$. Eu/Eu* values less than 0.95 indicate depletion, whereas values greater than 1.05 indicate an enrichment relative to the neighbouring REE. In both formulae, X/X_{shale} (X= Ce, La, Nd, Eu, etc.) are ratios to average shale (i.e. PAAS). Results (raw and normalised) obtained by ICP-MS are presented in Appendix **A1**, whereas results obtained by LA-ICP-MS are presented in Appendix **A2**. The REE values of similar grain types from the same sample are averaged for plotting (usually 2 to 4 analyses). REE data are normalised to the Post-Archaean average Australian shale (PAAS) (Table 7.1). In some cases, samples were normalized to both PAAS and chondritic meteorites. The REE distributions were plotted using Microsoft Excel 2000/XP. Statistical analysis and scatterplots/binary plots were obtained using Statsoft's Statistica 6.

Table 7.1. The Post-Archaean average Australian shale (PAAS) and chondritic meteorites were used to normalize the raw data (Taylor and McLennan, 1985).

	La	Ce	Pr	Nd	Sm	Eu	Gd	Tb	Dy	Ho	Er	Tm	Yb	Lu	Y
PAAS	38.2	79.6	8.8	33.9	5.6	1.1	4.7	0.8	4.7	1	2.9	0.4	2.8	0.4	22
Chondrite	0.37	0.96	0.14	0.71	0.23	0.09	0.31	0.06	0.38	0.09	0.25	0.04	0.25	0.04	2.1

7.2. RARE-EARTH ELEMENT GEOCHEMISTRY

7.2.1. Gravel member, Varswater Formation

The salient features of the REE patterns of the Gravel member are the heavy REE (HREE) enrichment and the fairly flat middle and heavy REE patterns (the patterns are flat from europium to lutetium). This type of REE pattern is widely shown by the peloidal phosphorite fraction (Pph) (Figure 7.1). There is some variation amongst the phosclast allochems (Pph), especially peloids from sample gm-03 (the average of the REE distribution taken from these grains is gm-03-pph). The result is a steep pattern, with pronounced HREE enrichment and high REE abundances relative to PAAS.

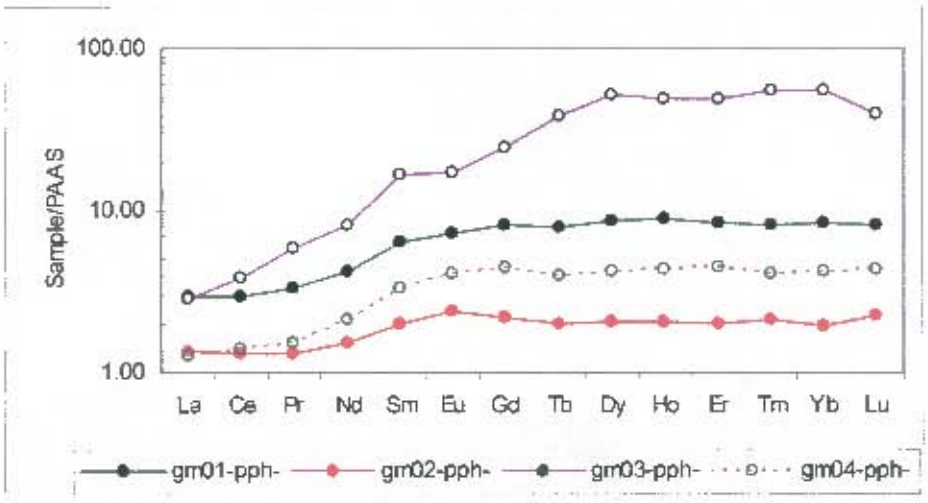

Figure 7.1. PAAS-normalized REE diagram of the averages of LA-ICP-MS measurements taken from specific grain types within the Gravel member from the Varswater Formation (Site VW01).

Biogenic allochems (phosphatised shell fragments) are rare in the Gravel member. The REE pattern is similar, but the REE content is lower than associated peloidal phosphorite grains from the same sample (Figure 7.2).

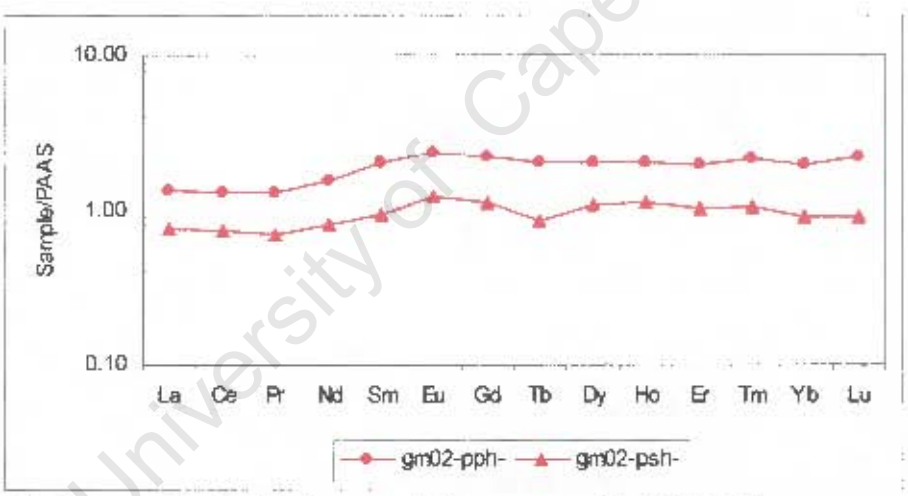

Figure 7.2. PAAS-normalized REE diagram of the averages of LA-ICP-MS measurements taken from specific grain types within the Gravel member from the Varswater Formation.

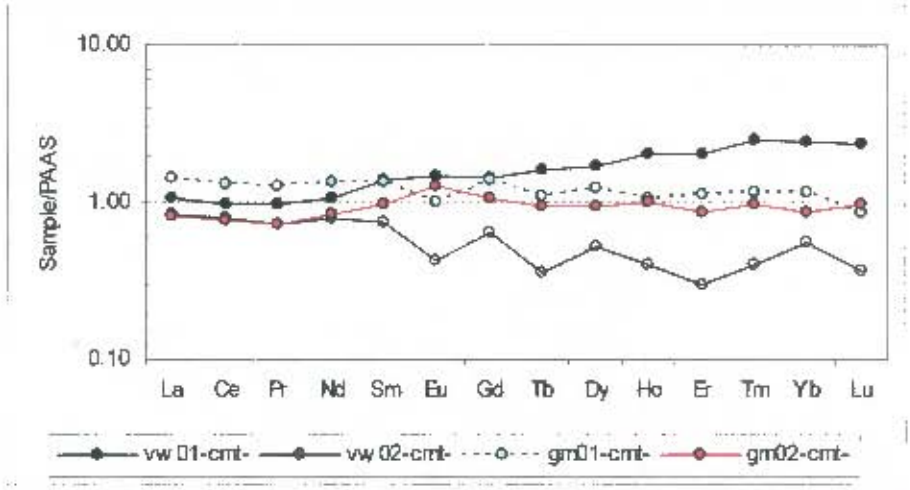

Figure 7.3. PAAS-normalized REE diagram of the averages of LA-IC-PMS measurements taken from specific CFA cement within the Gravel member from the Varswater Formation.

The REE patterns of the CFA cement (cmt) are different from the peloidal and biogenic Gravel member components. The REE patterns are generally flat and show slight LREE enrichment relative to HREE in several cement samples (gm01-cmt, gm02-cmt and vw02-cmt) (Figure 7.3). Vw01-cmt shows a slight HREE enrichment relative to LREE. The REE content of the cement is generally less than that of the phosphorite peloidal grains. Variations in the REE patterns are best expressed using the Lu/La, LREE/HREE and Er/Nd ratios. For instance, the Lu/La and LREE/HREE ratios show the amount of fractionation between the LREE and the HREE, whereas Er/Nd ratios provide a measure of the fractionation within the MREE. The Lu/La ratios calculated for the various grain types from the Gravel member are highly variable with a mean of 1.64 for peloids and a value of 0.98 for the ablated CFA cement (Table 7.2).

Table 7.2. A summary of Lu/La values for the Gravel member samples. The table shows median, mean, standard deviation, minimum and maximum values.

Grain Type	Median	Mean	Standard deviation	Minimum	Maximum
Pph	2.04	1.64	1.86	0.02	8.11
PSh	N/A	1.2	N/A	N/A	N/A
Cement (CMT)	0.88	0.98	0.72	0.04	2.87

Peloids have a mean value of 0.53 for LREE/HREE, whereas the CFA cement has a mean value of 0.70 (Table 7.3). The Lu/La and LREE/HREE ratios for the phosphatised shell grain are 1.2 and 0.42, respectively. The Lu/La and LREE/HREE ratios for the Gravel member peloids and shell fragment imply significant HREE enrichment relative to the LREE. The CFA cement (on average) tends to show a slight LREE enrichment relative to the HREE.

Table 7.3. A summary of LREE/HREE values for the Gravel member samples. The table shows median, mean, standard deviation, minimum and maximum values.

Grain Type	Median	Mean	Standard deviation	Minimum	Maximum
Pph	0.40	0.53	0.43	0.17	1.93
PSh	N/A	0.42	N/A	N/A	N/A
Cement	0.5	0.70	0.26	0.35	1.33

In terms of the Er/Nd ratios, a mean of 1.51 with a standard deviation of 0.82 was calculated for Gravel member peloids (Table 7.4). However, some grains do show anomalously high values (such as sample gm03-pph- with an average Er/Nd value of 5.98) (Table 7.5). In terms of Er/Nd values, the Gravel member peloids and phosphatised shell fragment are slightly enriched in heavy MREE as compared to the lighter MREE. The CFA cement shows a slight light MREE enrichment relative to the heavier MREE with a mean Er/Nd of 0.91.

Table 7.4. A summary of Er/Nd values for the Gravel member samples. The table shows median, mean, standard deviation, minimum and maximum values.

Grain Type	Median	Mean	Standard deviation	Minimum	Maximum
Pph	1.50	1.51	0.82	0.11	3.13
PSh	N/A	1.29	N/A	N/A	N/A
Cement	1	0.91	0.54	0.20	2.26

Table 7.5. Averaged samples showing the indices Ce/Ce*, Eu/Eu*, Lu/La, Er/Nd, Sm/Nd and LREE/HREE.

Averages	Ce/Ce*	Eu/Eu*	(Lu/La)n	(Er/Nd)n	(Sm/Nd)n	LREE/HREE
vw01-pph-	0.94	0.77	1.67	1.61	1.2	0.4
vw02-pph-	1.01	0.38	0.3	0.4	0.82	1.27
gm01-pph-	0.95	0.98	2.75	2.12	1.54	0.27
gm02-pph-	0.98	1.14	1.65	1.34	1.31	0.4
gm03-pph-	0.89	0.83	13.89	5.98	2	0.1
gm04-pph-	0.99	1.05	3.4	2.07	1.59	0.25
gm02-psh-	1.01	1.21	1.2	1.38	1.16	0.42
vw01-cmt-	0.96	1.06	2.2	1.92	1.3	0.31
vw02-cmt-	1.01	0.61	0.43	0.51	0.95	0.98
gm01-cmt-	0.97	0.74	0.6	0.79	1.01	0.67
gm02-cmt-	1	1.24	1.17	1.21	1.17	0.47
gm03-cmt-	1	1.15	1.63	1.17	1.24	0.42
gm04-cmt-	0.24	3.4	0.68	0.58	1.14	0.72

The Ce- and Eu-anomalies vary with grain type (Table 7.6 and Table 7.7). Ce/Ce* values for the peloids range between 0.85 and 1.08, whereas the Eu/Eu* values show a substantial range between 0.01 and 1.72. The CFA cement has similar Ce/Ce* and Eu/Eu* values to the peloids.

Table 7.6. A summary of Ce/Ce* values for the Gravel member samples. The table shows median, mean, standard deviation, minimum and maximum values.

Grain Type	Median	Mean	Standard deviation	Minimum	Maximum
Pph	0.96	0.96	0.05	0.85	1.08
PSh	N/A	1.01	N/A	N/A	N/A
Cement	0.93	0.90	0.16	0.26	1.06

Table 7.7. A summary of Eu/Eu* values for the Gravel member samples. The table shows median, mean, standard deviation, minimum and maximum values.

Grain Type	Median	Mean	Standard deviation	Minimum	Maximum
Pph	0.96	0.89	0.34	0.01	1.72
PSh	N/A	1.21	N/A	N/A	N/A
Cement	0.96	1.04	0.93	0.3	4.83

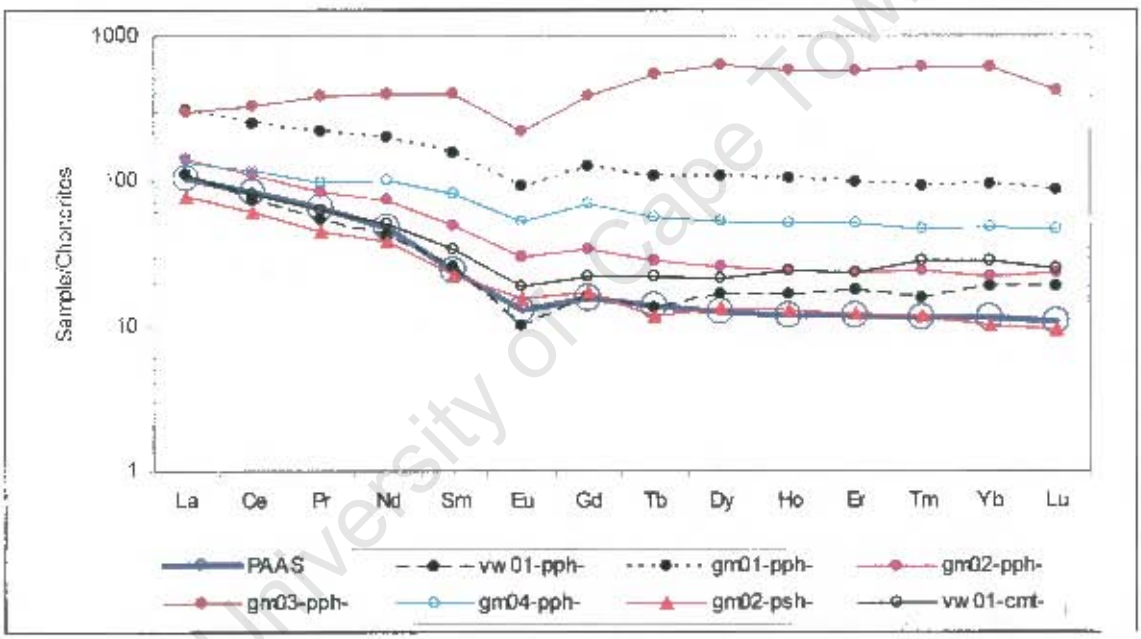

Figure 7.4. Chondrite-normalized REE diagram of the phosphorite allochems of the Gravel member. The patterns show fairly flat heavy REE patterns with pronounced light REE enrichment, relative to chondritic meteorites. The patterns also show a significant Eu-anomaly. The Gravel member has a much higher REE abundance than PAAS. The shape of the patterns (including the Eu-anomaly) is similar to that of PAAS.

In terms of a chondrite-normalized REE diagram, the REE data of the Gravel member resemble that of PAAS (Figure 7.4). The absolute abundances are slightly higher as in the case of vw01-pph, gm04-pph and gm02-pph; however gm03-pph shows a different pattern, with HREE enrichment relative to chondritic meteorites.

7.2.2. Pelletal Phosphorite member, Varswater Formation

The REE patterns for the Pelletal Phosphorite member are generally flat with a slight convex-upwards shape (Figure 7.5). The REE distributions for the grain types are generally uniform amongst the peloids (Pph) and the cement (cmt). The LREE are depleted relative to the MREE and HREE. REE abundances tend to be lower in the Pelletal Phosphorite member than the Gravel member. The peloids and cement also show fairly flat middle and heavy REE patterns, similar to the Gravel member patterns. The phosphatised shell fragments (PSh) and phosphatised bone fragments (bnc) have similar REE patterns to phosphorite peloids and cement, but the LREE depletion is accentuated (Figure 7.6). The REE patterns for the shell fragments and phosphatised bone fragments show an inclined flat shape, with pronounced HREE enrichment, relative to the LREE.

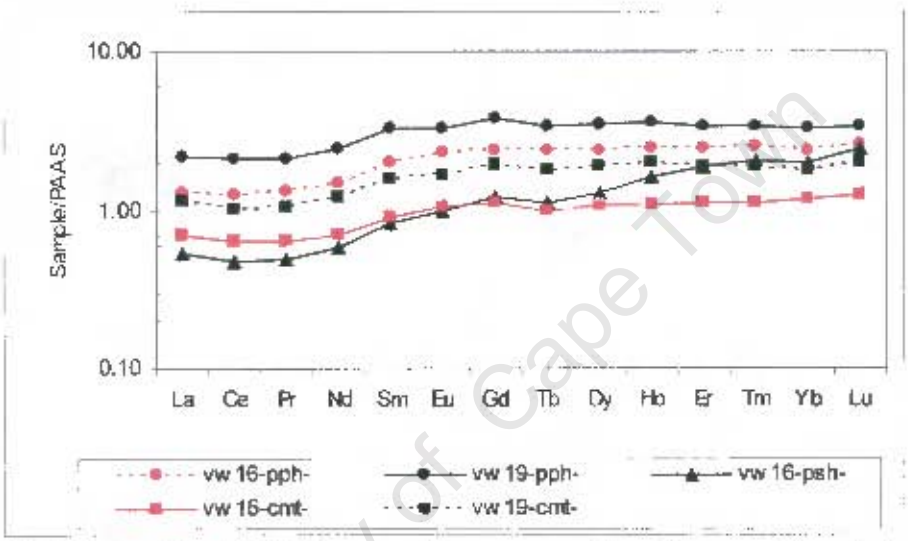

Figure 7.5. PAAS-normalized REE diagram of the averages taken from specific grain types (Pph, PSh, cmt) within the Pelletal Phosphorite member from the Varswater Formation.

In terms of the Lu/La ratios, the peloids show a range of values between 1.15 and 2.92, with a median and mean of 1.7 and 1.76 (standard deviation of 0.45), respectively (Table 7.9). The values reported for the cement is very similar with a range of values between 1 and 2.75, and a median and mean of 1.68 and 1.67 (standard deviation of 0.52), respectively. The bone fragments and shell fragments show slightly higher Lu/La values. The bone fragments show a mean of 18.02 (standard deviation of 10.18), whereas the shell fragments show a range of Lu/La values between 1.7 and 30.77, with a median and mean of 2.13 and 5.27 (standard deviation of 9.60) respectively.

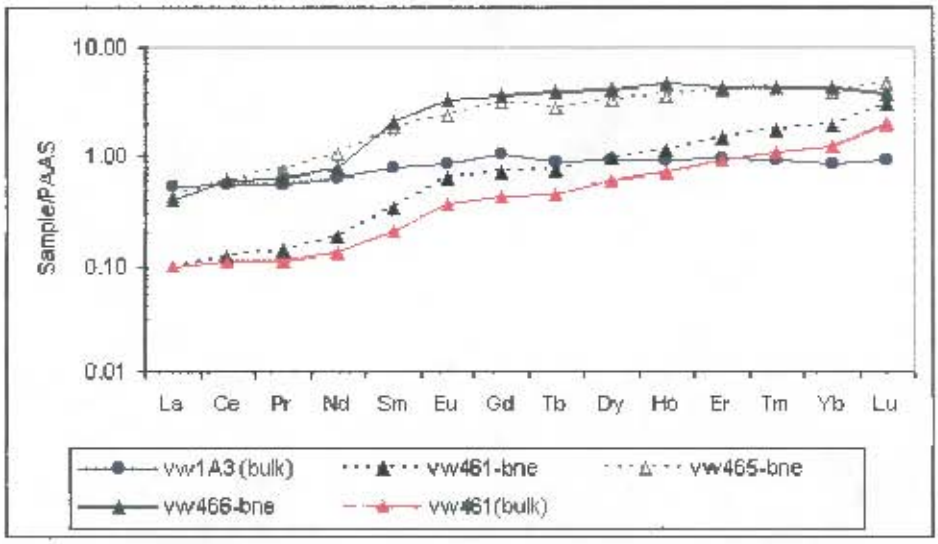

Figure 7.6. PAAS-normalized REE diagram of phosphatised bone fragments (bne) found within the Pelletal Phosphorite member from the Varswater Formation. Vw1A3 and vw465 are bulk sediment samples run on the ICP-MS.

Table 7.8. Pelletal Phosphorite member averaged samples showing the indices Ce/Ce*, Eu/Eu*, Lu/La, Er/Nd, Sm/Nd and LREE/HREE.

Averages	Ce/Ce*	Eu/Eu*	(Lu/La)n	(Er/Nd)n	(Sm/Nd)n	LREE/HREE
vw16-pph-	0.97	1.04	2.02	1.67	1.36	0.34
vw19-pph-	1	0.94	1.56	1.45	1.35	0.39
vw16-psh-	0.93	0.96	4.63	2.84	1.44	0.2
vw16-cmt-	0.94	1.05	1.84	1.53	1.3	0.36
vw19-cmt-	0.93	0.96	1.77	1.65	1.3	0.35

Table 7.9. A summary of Lu/La values for the Pelletal Phosphorite member samples. The table shows median, mean, standard deviation, minimum and maximum values.

Grain Type	Median	Mean	Standard deviation	Minimum	Maximum
Pph	1.70	1.76	0.45	1.15	2.92
PSh	2.13	5.27	9.60	1.7	30.77
Bne	15.50	18.02	10.18	9.6	31.49
Cement	1.68	1.67	0.52	1.0	2.75

The LREE/HREE values are also similar between the peloids and the cement. The LREE/HREE ratio for the peloids ranges between 0.29 and 0.5, with a median and mean of 0.38 (standard deviation is 0.06) whereas the LREE/HREE ratio for the cement ranges between 0.29 and 0.53, with a median and mean of 0.41 and 0.40 (standard deviation of 0.07), respectively (Table 7.10). The shell fragments show a LREE/HREE ratio of between 0.05 and 0.73. The median and mean are 0.34 and 0.36 (standard deviation

0.19), respectively. The bone fragments show a mean of 0.11 (standard deviation of 0.04).

Table 7.10. A summary of LREE/HREE values for the Pelletal Phosphorite member samples. The table shows median, mean, standard deviation, minimum and maximum values.

Grain Type	Median	Mean	Standard deviation	Minimum	Maximum
Pph	0.38	0.38	0.06	0.29	0.5
PSh	0.34	0.36	0.19	0.05	0.73
Bne	0.10	0.11	0.04	0.07	0.15
Cement	0.41	0.40	0.07	0.29	0.53

The similarity in terms of the MREE distribution of the peloids and cement are shown by the Er/Nd ratio (Table 7.11.). The bone fragments show much higher values than the other grain types. The LREE/HREE, Er/Nd and Lu/La values support the similarity between the cements and peloids.

Table 7.11. A summary of Er/Nd values for the Pelletal Phosphorite member samples. The table shows median, mean, standard deviation, minimum and maximum values.

Grain Type	Median	Mean	Standard deviation	Minimum	Maximum
Pph	1.59	1.55	0.26	1.09	1.92
PSh	1.81	2.93	3.9	0.77	13.35
Bne	6.38	6.19	1.94	3.83	8.17
Cement	1.47	1.42	0.29	0.8	1.87

The values reported for the Ce/Ce* ratio are similar amongst the peloids, shell fragments, bone fragments and the cements (Table 7.12). In general the Ce/Ce* values for peloids range between 0.84 and 1.05, whereas the values for the cement range between 0.84 and 1.0. The shell fragments show a range in Ce/Ce* values between 0.87 and 1.02. The bone fragments show a range of values between 1.03 and 1.16. The bone fragments appear to have a slight positive Ce-anomaly.

Table 7.12. A summary of Ce/Ce* values for the Pelletal Phosphorite member samples. The table shows median, mean, standard deviation, minimum and maximum values.

Grain Type	Median	Mean	Standard deviation	Minimum	Maximum
Pph	0.96	0.96	0.05	0.84	1.05
PSh	0.92	0.94	0.05	0.87	1.02
Bne	1.03	1.06	0.07	1.03	1.16
Cement	0.94	0.93	0.04	0.84	1.0

The Eu/Eu* are similar for the CFA cement, shell fragments and peloids (Figure 7.13). Typical Eu/Eu* values range between 0.92 and 1.53 for cement and between 0.9 and 1.13 for peloids, with means of 1.07 and 0.99, respectively. Eu/Eu* values for the shell fragments show a similar range. The shell fragments show a mean of 1.03 and a range in values between 0.86 and 1.26. The bone fragments show a mean of 1.11 (standard

deviation 0.12). In terms of the Eu/Eu and Ce/Ce indices, there exist significant coherence and similarity in the pelletal phosphorite member data, amongst peloids, cement, bone and shell fragments. The bone fragments (and some shell fragments) possess appreciably different REE signatures from the other grain types.

Table 7.13. A summary of Eu/Eu* values for the Pelletal Phosphorite member samples. The table shows median, mean, standard deviation, minimum and maximum values.

Grain Type	Median	Mean	Standard deviation	Minimum	Maximum
Pph	0.97	0.99	0.07	0.9	1.13
PSh	1.05	1.03	0.12	0.86	1.26
Bne	1.15	1.11	0.12	0.93	1.19
Cement	1.02	1.07	0.18	0.92	1.53

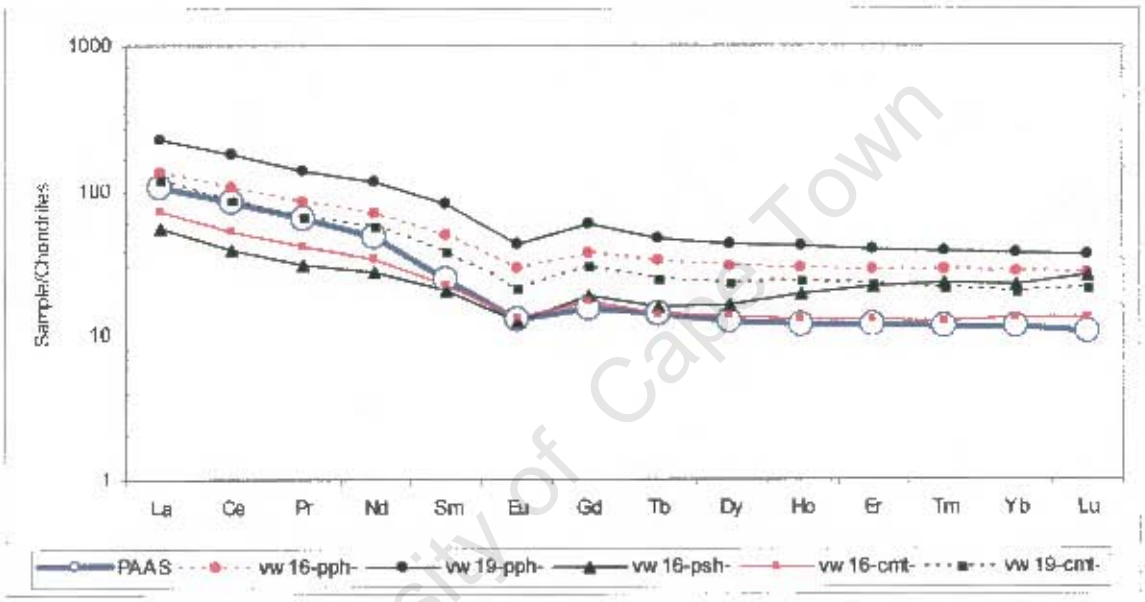

Figure 7.7. Chondrite-normalized REE diagram of the phosphorite allochems of the Pelletal phosphorite member. The patterns show fairly flat heavy REE patterns with pronounced light REE enrichment, relative to chondritic meteorites. The patterns also show a significant Eu-anomaly. The Pelletal Phosphorite member phosphorites show much higher abundances of REE than PAAS. The shape of the patterns (including the Eu-anomaly) is similar to that of PAAS; however vw16-psh and vw16-cmt have lower LREE, but higher HREE abundances than PAAS. Sample vw16-psh is particularly HREE enriched compared to the other REE patterns.

In terms of a chondrite-normalized REE diagram, the REE data of the Pelletal Phosphorite member resemble that of PAAS (Figure 7.7). The absolute abundances are slightly higher, as in the case of vw16-pph, vw19-pph and vw19-cmt. Vw16-psh and Vw16-cmt show much lower LREE abundances than PAAS, but in terms of the HREE the abundances for these averaged samples are higher.

7.2.3. Phosphorite deposit at Bomgat (Hoedjiespunt)

The REE patterns of the Bomgat phosphorites are flat, with slight HREE enrichment relative to LREE (Figure 7.8). Ce-anomalies are not evident. However, a negative Ce-anomaly can be assigned to these samples as the Ce/Ce* ratio ranges between 0.71 and 0.95 (Table 7.14). The HREE enrichment is also expressed by the Lu/La and LREE/HREE ratios. The Lu/La and LREE/HREE values range between 1.02 and 3.18 and 0.28 and 0.65, respectively. B1, b3-cmt and b3-bio have roughly the same REE pattern, whereas b2-cmt and b1-cmt are distinctly different. For example, B2-cmt shows a positive Eu-anomaly, whereas the other samples show a lack of or slightly negative Eu-anomalies.

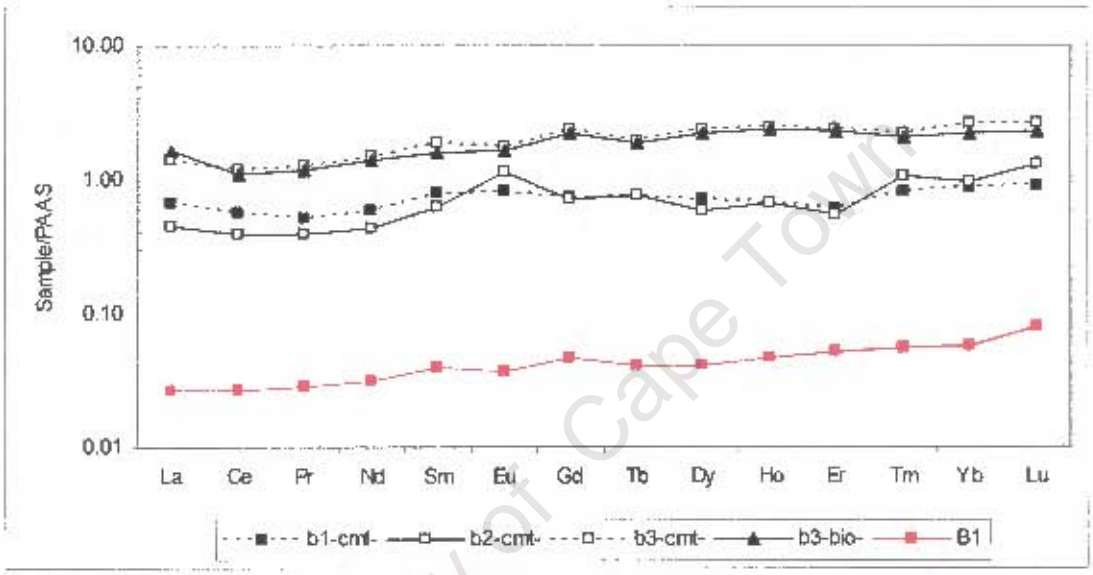

Figure 7.8. PAAS-normalized REE diagram of the averages taken from specific grain types within the Bomgat phosphorite. Sample B1 is a "whole rock" sample, the abundance of REE in B1 is significantly less than for cement and bioclasts. This implies enrichment of REE in some parts of the rock or perhaps dilution of the sample by quartz.

Table 7.14. Samples from Bomgat (Hoedjiespunt) showing the indices Ce/Ce*, Eu/Eu*, Lu/La, Er/Nd, Sm/Nd and LREE/HREE.

Sample	Ce/Ce*	Eu/Eu*	(Lu/La)n	(Er/Nd)n	(Sm/Nd)n	LREE/HREE
b1-cmt-1	0.83	1.10	1.03	0.77	1.62	0.51
b1-cmt-2	0.94	1.12	1.11	0.98	1.23	0.45
b1-cmt-3	0.88	0.98	3.00	1.83	1.38	0.29
b1-cmt-4	0.95	1.12	0.66	0.78	1.20	0.65
b2-cmt-1cfa	0.89	1.72	3.04	1.21	1.45	0.28
b2-cmt-2cfa	0.93	2.13	3.18	1.23	1.48	0.31
b2-cmt-3cfa	0.89	1.35	2.30	1.43	1.45	0.34
b3-cmt-1	0.68	0.72	1.02	2.00	0.80	0.43
b3-cmt-2	0.71	0.49	1.12	1.42	1.18	0.44
b3-cmt-4	0.83	0.92	2.83	1.83	1.40	0.29
b3-bio-3	0.76	0.57	0.94	1.19	0.90	0.52

Table 7.14. continues.

Sample	Ce/Ce*	Eu/Eu*	(Lu/La)n	(Er/Nd)n	(Sm/Nd)n	LREE/HREE
b3-bio-5	0.89	0.50	0.43	1.02	0.96	0.65
b3-bio-6	0.73	0.92	1.53	1.72	1.18	0.34
B1 (bulk)	0.95	0.81	3.00	1.68	1.21	0.34

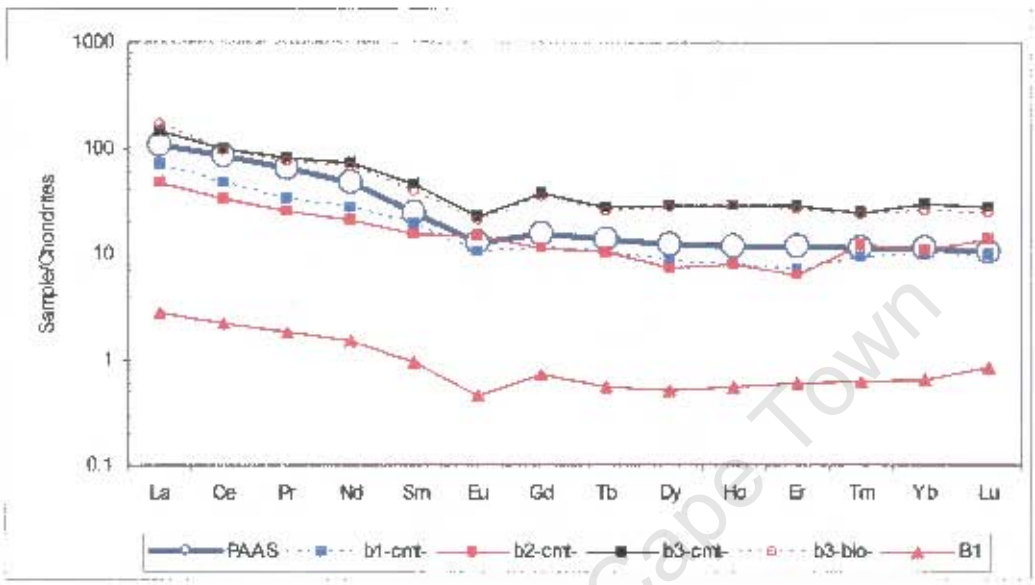

Figure 7.9. Chondrite-normalized REE diagram of the phosphatic components of the Bomgat phosphorites. The patterns show fairly flat heavy REE patterns with pronounced light REE enrichment, relative to chondritic meteorites. The patterns also show a significant Eu-anomaly. The B1 sample shows significantly less REE abundances than PAAS. The shape of the patterns (including the Eu-anomaly) is similar to that of PAAS; however b2-cmt is the exception and shows a positive Eu-anomaly.

In terms of a chondrite-normalized REE diagram, the REE data of the Bomgat (Hoedjiespunt) phosphorite resemble that of PAAS (Figure 7.9). The absolute abundances are slightly higher as in the case of vw16-pph, vw19-pph and vw19-cmt. B1, b1-cmt and b2-cmt show much lower LREE abundances than PAAS. B2-cmt also shows a positive Eu-anomaly.

7.2.4. Aluminium phosphate deposits at Kreefte Bay (Kreeftebaai)

The REE patterns of the Kreefte Bay aluminium phosphates show a significant HREE enrichment relative to LREE, and a notable positive Eu-anomaly (Figure 7.10). The prominent positive Eu-anomaly is also expressed by the Eu/Eu* ratio, Eu/Eu* values for the Kreefte Bay samples range between 1.36 and 1.81 (Table 7.15). The REE diagrams indicate that the samples show prominent HREE enrichment from Ho to Lu (Figure 7.11 (a)). The Lu/La and LREE/HREE ratios also reflect HREE enrichment. Typical values range from 1.55 to 5.85 for the Lu/La ratio, whereas the LREE/HREE shows a range of

values from 0.21 to 0.41. MREE enrichment is expressed by the Er/Nd ratio, with a range in values between 1.22 and 2.51. Unlike the flat REE patterns of the Varswater Formation and Bomgat phosphorites, the Kreefte Bay REE patterns are exceptionally jagged.

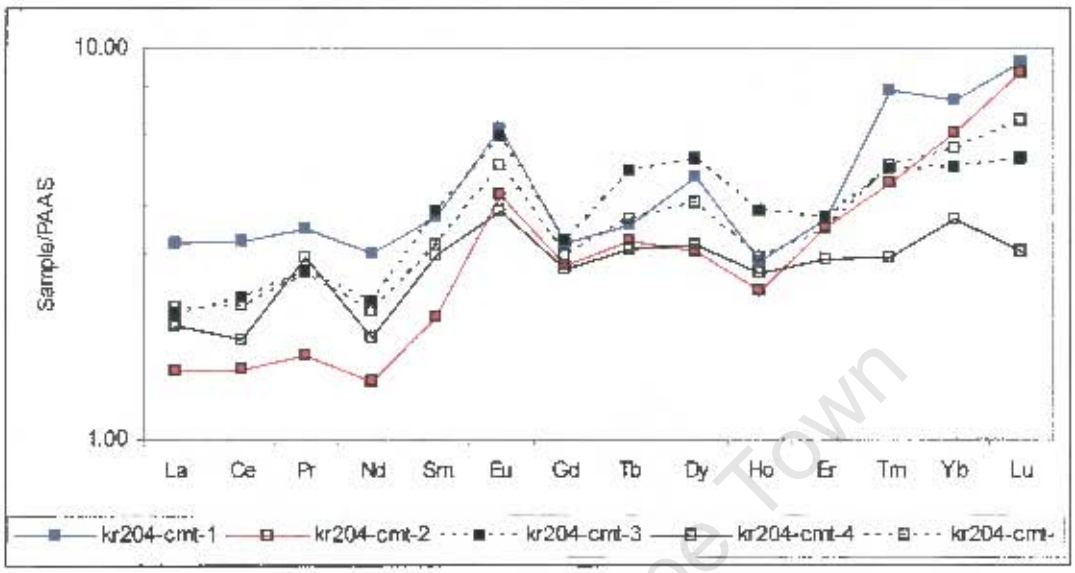

(a)

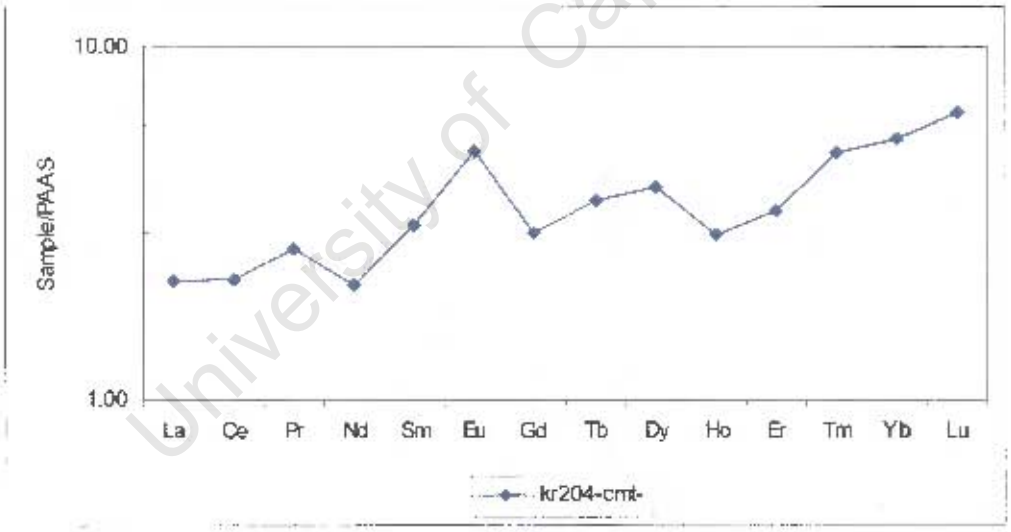

(b)

Figure 7.10. PAAS-normalized REE diagrams of the (a) aluminium phosphates and (b) average from Kreefte Bay.

Table 7.15. Samples from Kreefte Bay showing the indices Ce/Ce*, Eu/Eu*, Lu/La, Er/Nd, Sm/Nd and LREE/HREE.

Sample	Ce/Ce*	Eu/Eu*	(Lu/La)n	(Er/Nd)n	(Sm/Nd)n	LREE/HREE
kr204-cmt-1	1.04	1.81	2.87	1.22	1.23	0.34
kr204-cmt-2	1.04	1.75	5.85	2.51	1.47	0.21

Table 7.15. continues.

Sample	Ce/Ce*	Eu/Eu*	(Lu/La)n	(Er/Nd)n	(Sm/Nd)n	LREE/HREE
kr204-cmt-3	1.06	1.68	2.49	1.65	1.70	0.32
kr204-cmt-4	0.95	1.36	1.55	1.57	1.61	0.41

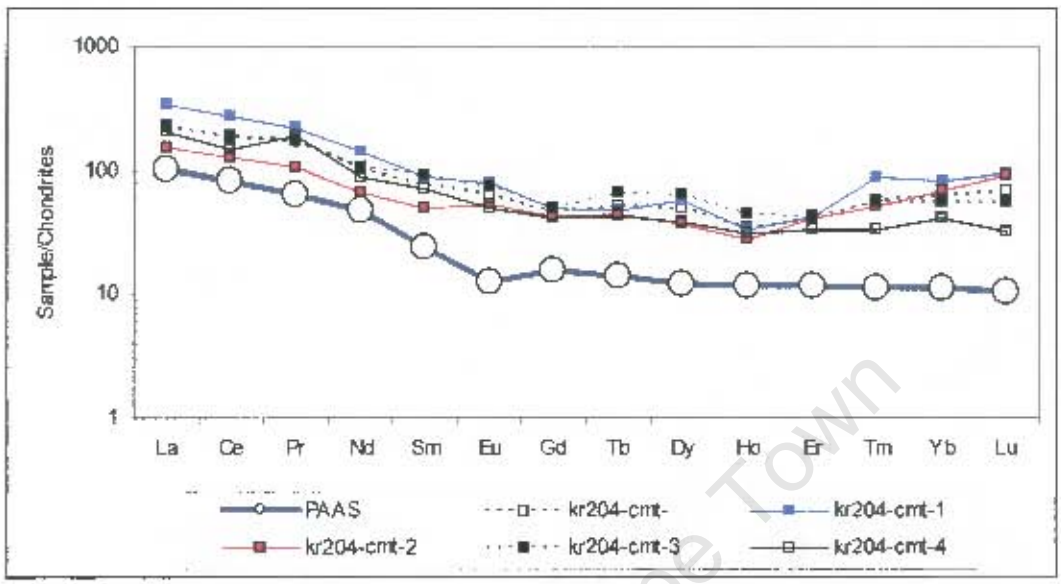

(a)

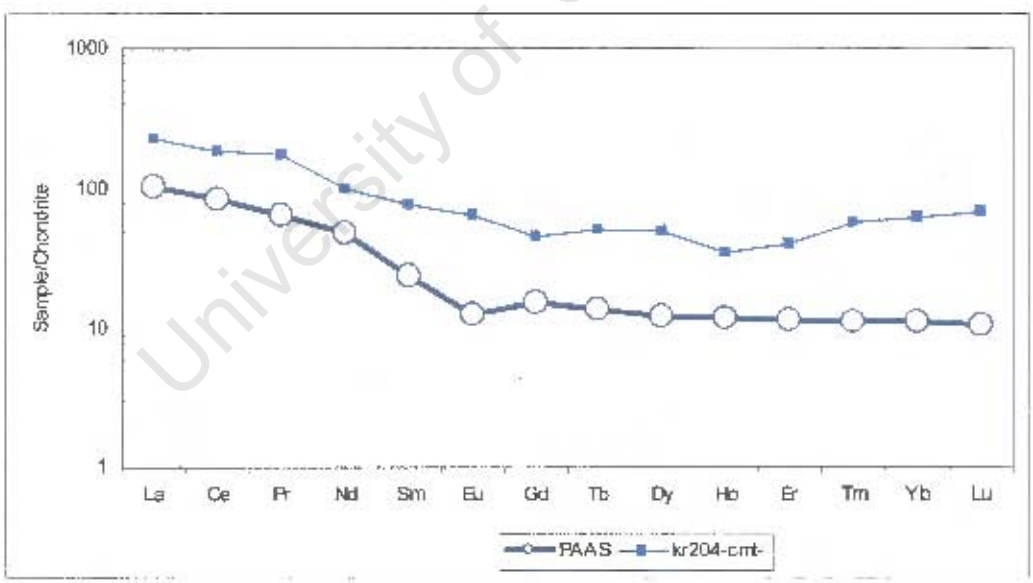

(b)

Figure 7.11. Chondrite-normalized REE diagrams of (a) the aluminium phosphates and (b) average of cement from Kreefte Bay. The Kreefte Bay patterns differ from the PAAS pattern. The patterns show a positive Eu-anomaly and an enrichment of HREE (between Ho and Lu).

The chondrite-normalized REE diagrams of the Kreefte Bay phosphates do not resemble PAAS (Figure 7.11). The absolute abundances of the REE are slightly higher than for PAAS. The patterns show a positive Eu-anomaly, and an enrichment of HREE (between Ho and Lu).

7.2.5. Selected offshore phosphorite samples

The REE patterns of the offshore phosphorite samples show considerable variability, nonetheless the REE patterns are generally flat with some HREE enrichment relative to the LREE (Figure.7.12). The REE content varies by an order of magnitude.

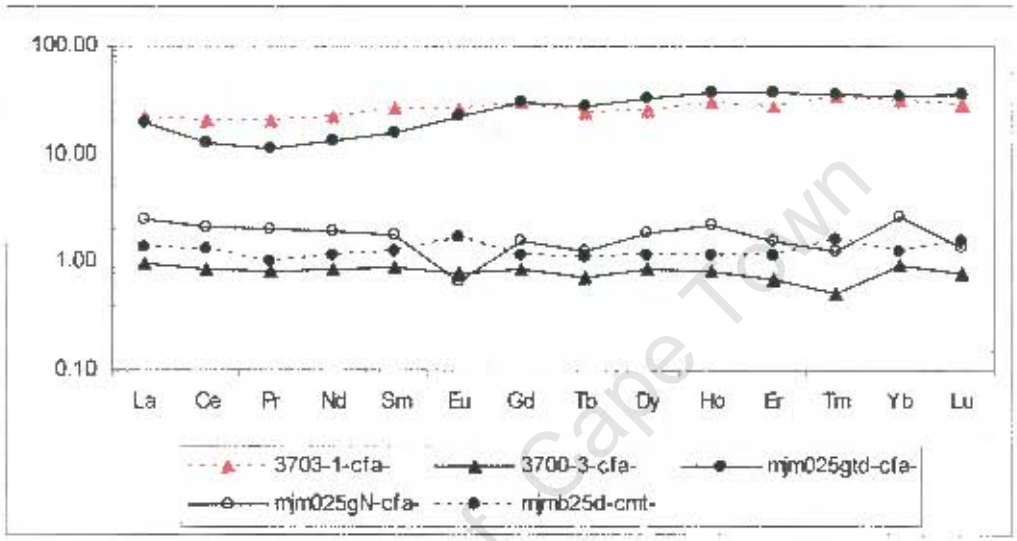

Figure 7.12. PAAS-normalized REE diagrams of selected offshore phosphorites.

In terms of the Ce-anomaly there exists a range in values; however the results are consistent per sample (Table. 7.16). REE abundances are similar to PAAS except for 2 types where REE abundances are greater than PAAS.

Table 7.16. Offshore samples showing the indices Ce/Ce*, Eu/Eu*, Lu/La, Er/Nd, Sm/Nd and LREE/HREE.

Misc.	Ce/Ce*	Eu/Eu*	(Lu/La)n	(Er/Nd)n	(Sm/Nd)n	LREE/HREE
3703-1-cfa-1	0.93	0.94	1.38	1.23	1.2	0.43
3703-1-cfa-3	0.93	1.33	0.61	0.97	1.27	0.58
3703-1-cfa-4	0.9	0.72	1.96	2.04	1.45	0.26
3700-3-cfa-1	0.9	1.07	0.56	0.8	0.89	0.65
3700-3-cfa-2	0.93	0.72	0.92	0.76	1.16	0.64
3700-3-cfa-3	0.91	1.01	0.9	0.84	1.02	0.62
mjm025gtd-cfa-1	0.78	1.03	2.09	3.32	1.25	0.22
mjm025gtd-cfa-2	0.77	0.96	1.63	2.62	1.19	0.27
mjm025gtd-cfa-3	0.78	0.96	1.77	2.71	1.12	0.26
mjm025gtd-cfa-4	0.82	1.02	1.99	2.64	1.25	0.25
mjm025gN-cfa-1	0.85	0.68	1.45	2.29	1.12	0.32
mjmb25d-cmt-1	0.95	1.53	1.27	1.04	1.05	0.51

Table 7.16. continues.

Misc.	Ce/Ce*	Eu/Eu*	(Lu/La)n	(Er/Nd)n	(Sm/Nd)n	LREE/HREE
mjmb25d-cmt-2	0.99	1.29	1.09	1.09	1	0.5
mjmb25d-cmt-3	1.05	1.37	0.92	0.83	1.2	0.55
mjmb25d-cmt-4	1.2	1.32	1.19	1	1.06	0.51

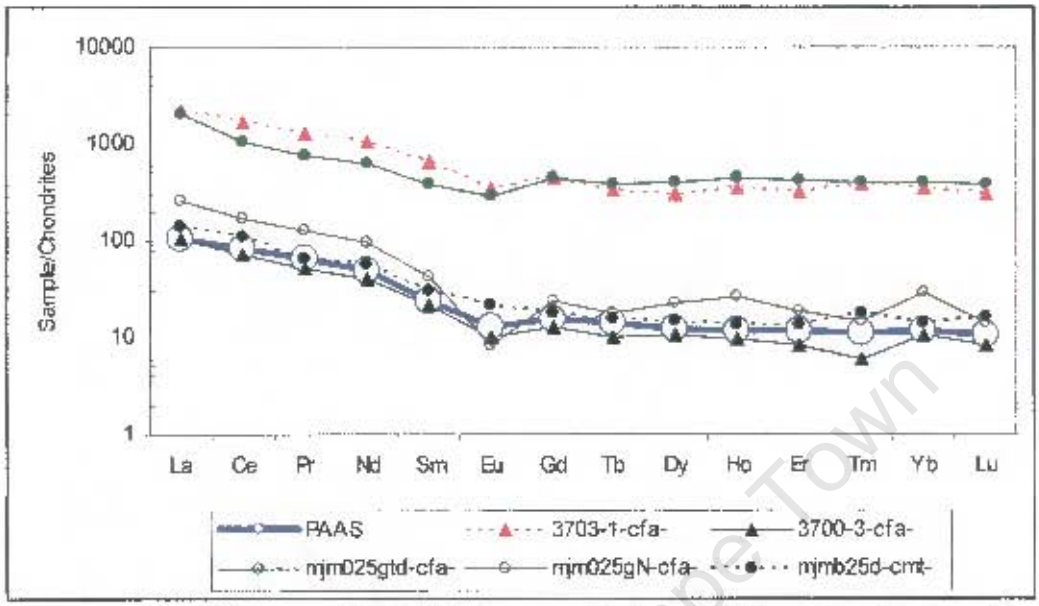

Figure 7.13. Chondrite-normalized REE diagram of selected offshore phosphorites. The patterns show fairly flat heavy REE patterns with pronounced light REE enrichment, relative to chondritic meteorites. The majority of the patterns show a significant negative Eu-anomaly except for sample mjmb25d.

In terms of a chondrite-normalized REE diagrams the REE data of the offshore phosphorites resembles that of PAAS (Figure 7.13). The absolute abundances of the REE are slightly higher than for PAAS; however the REE abundances for 3700-3-cfa are marginally less than PAAS.

7.3 TRACE-ELEMENT COMPOSITION

7.3.1. Gravel member (Varswater Formation)

Trace-element data for the phosphorites, phosphate sands and phosphate rocks are given in appendices A1 and A2. This section discusses the chemical variability amongst Gravel member components. The Gravel member is enriched in terms of strontium (Figure. 7.14). This is not surprising considering that phosphorites are known to contain the highest contents of strontium of all rock types. Sr is generally accepted to substitute for calcium in the apatite mineral lattice. The Sr content in the Gravel member ranges between 808 ppm and 5524 ppm[1]. Another element that phosphorites are known to be distinctly enriched in is uranium. U is believed to be incorporated primarily during the

[1] According to Gulbrandsen (1966) "average phosphorite" from the Phosphoria Formation contains 1000 ppm Sr

initial phase of phosphorite formation; therefore the U was most likely complexed to organic matter (pre-phosphorite formation) and incorporated into the apatite lattice. The plots for the components (Pph, PSh and cmt) of the Gravel member show similar scatter, however no clear trend is present. There is a positive correlation between Sr and U (Figure 7.15). Plots of the REE elements and Sr are roughly the same. A plot of Lu/La vs. Sr shows a slight difference between the CFA cement and the peloids (Figure 7.16).

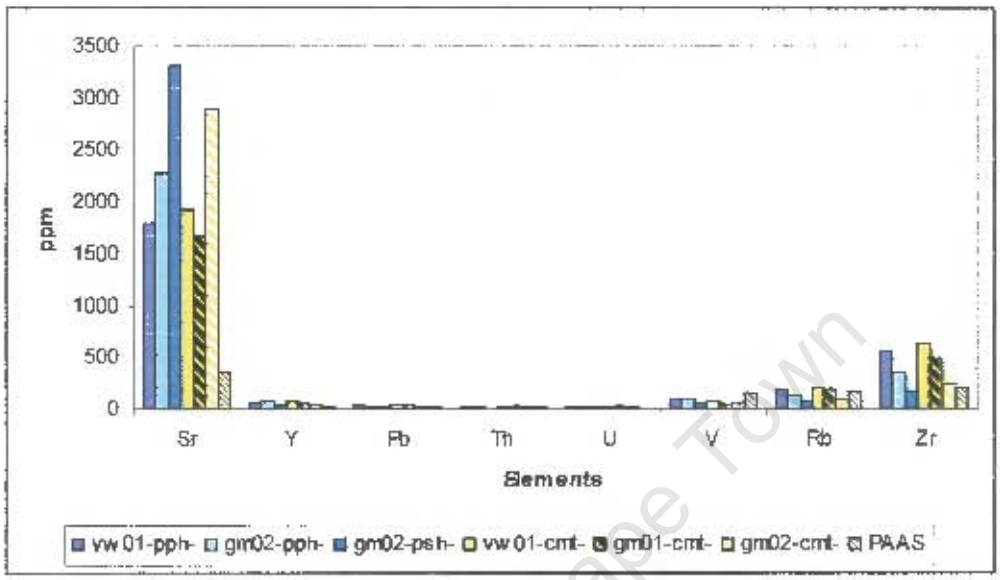

(a)

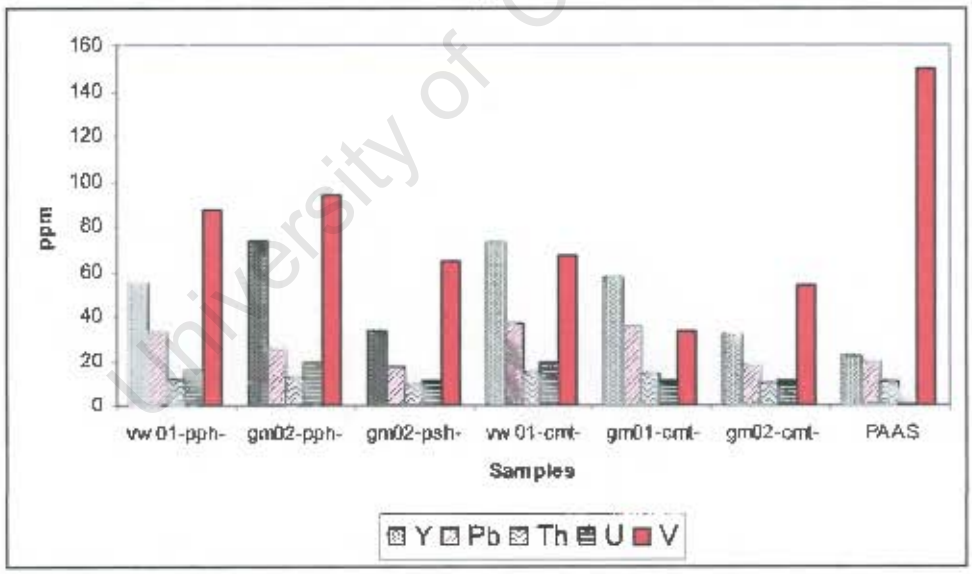

(b)

Figure 7.14. Trace-element concentrations in comparison with PAAS for the phosphorite allochems (Pph), bioclasts (PSh) and CFA cement (CMT) from the Gravel member, Varswater Formation. The graphs show that (a) Sr , (b) U and Y are notably enriched, whereas V is depleted relative to PAAS. Pb and Th show normal abundances.

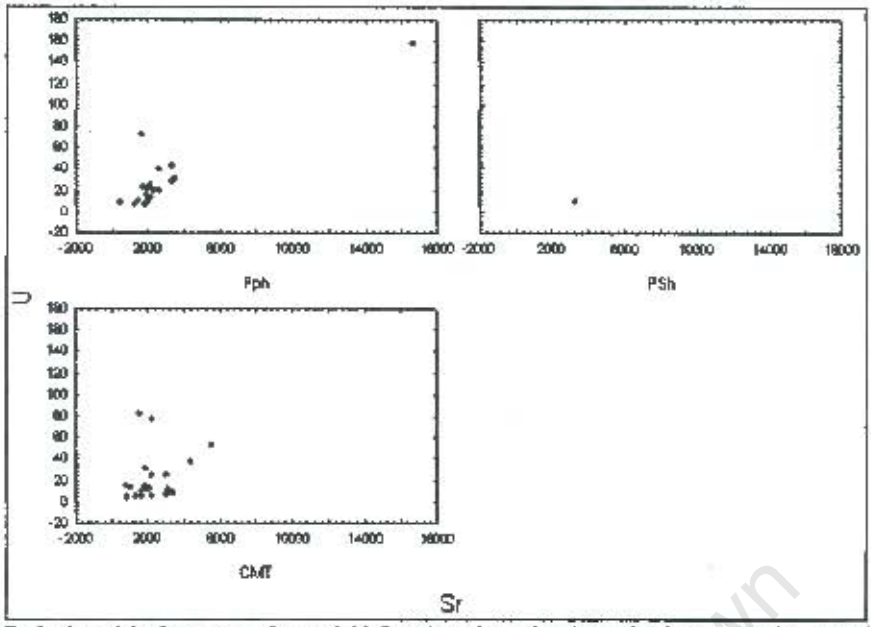

Figure 7.15. Relationship between Sr and U for the phosphorite allochems (Pph), bioclasts (PSh) and CFA cement (CMT) from the Gravel member, Varswater Formation.

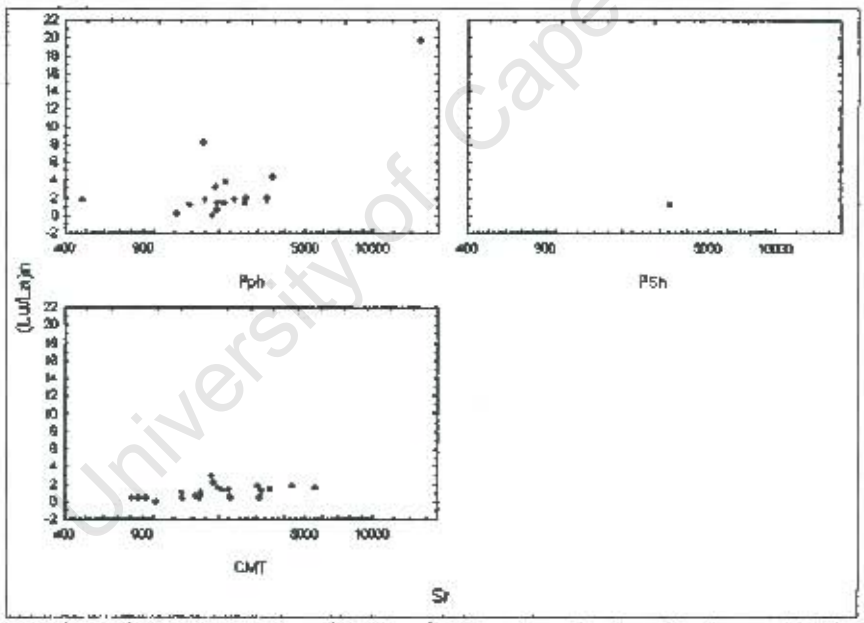

Figure 7.16. Relationship between Sr and Lu/La for the phosphorite allochems (Pph), bioclasts (PSh) and CFA cement (CMT) from the Gravel member, Varswater Formation. The horizontal axis shows a logarithmic scale. All values in ppm.

On the basis of the trace-elements, the Gravel member components (Pph, PSh and CMT) are remarkably homogenous. The scatter plots show no clear distinction between the various components.

7.3.2. Pelletal Phosphorite member (Varswater Formation)

This section discusses the trace-element composition of Pelletal Phosphorite member components. Similar to the Gravel member, the Pelletal Phosphorite member is enriched in strontium and uranium (Figure 7.17). Sr values range between 800 ppm and 3000 ppm. The trace-element scatterplots are distinct for the different components of the Pelletal Phosphorite member. The relationships between Nb, Rb and Sr, show distinct grain-specific clusters (Figure 7.18). The peloids appear to be enriched in terms of Nb and Rb, relative to the bioclasts (phosphatised shell fragments).

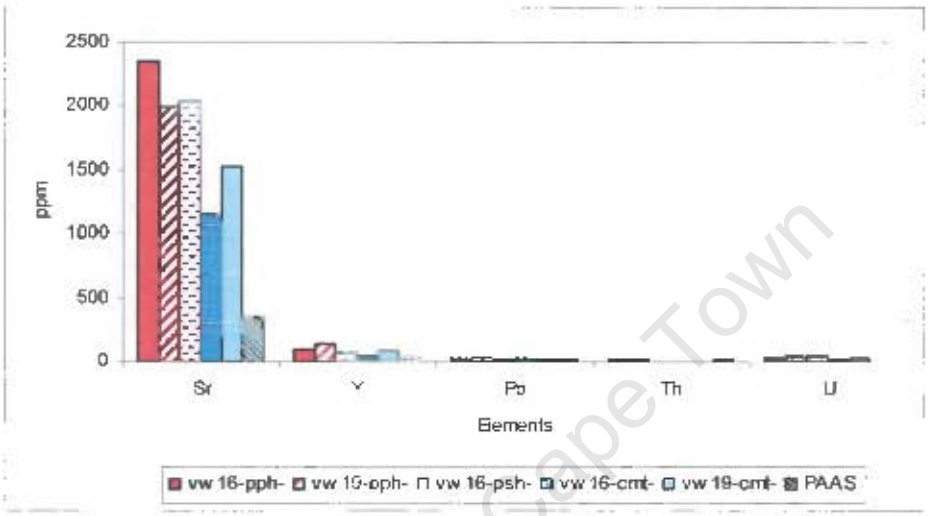

(a)

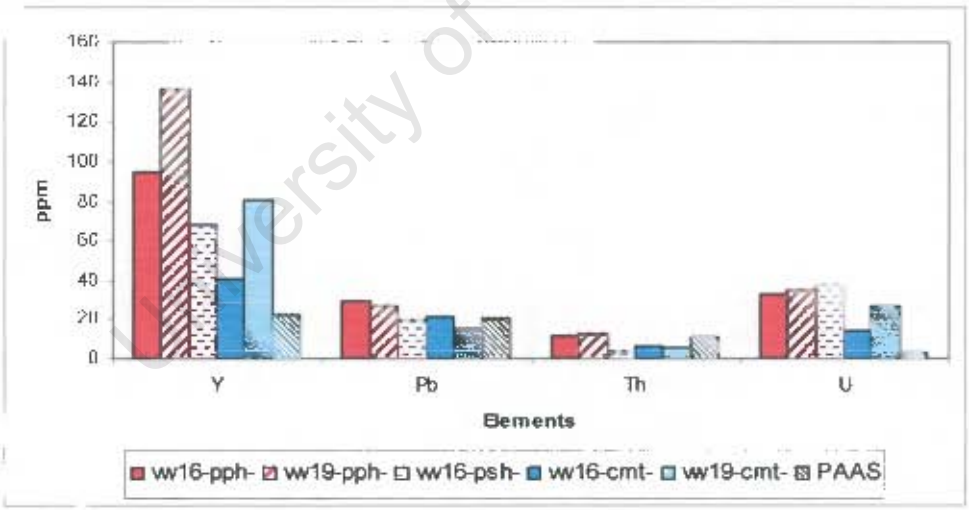

(b)

Figure 7.17. Trace-element concentrations in comparison with Post-Archaean average Australian shale (PAAS) for the phosphorite allochems (Pph), bioclasts (PSh) and CFA cement (CMT) from the Pelletal Phosphorite member, Varswater Formation. The graphs show that (a) Sr, (b) U and Y are notably enriched relative to PAAS. Pb and Th show normal abundances.

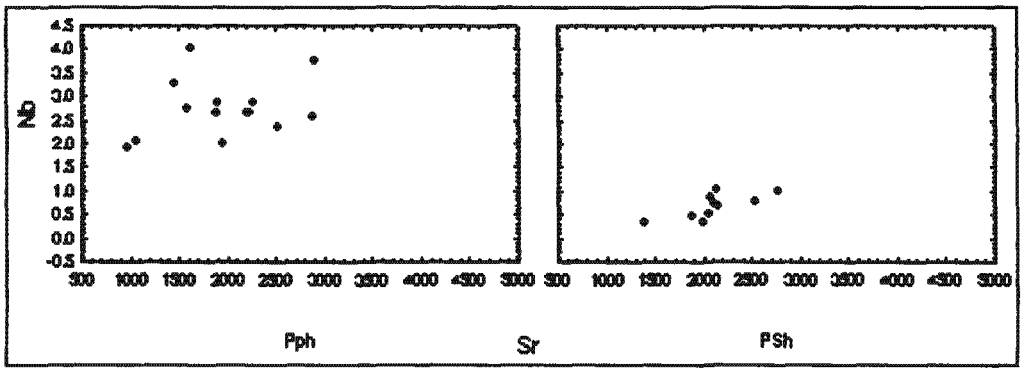

(a)

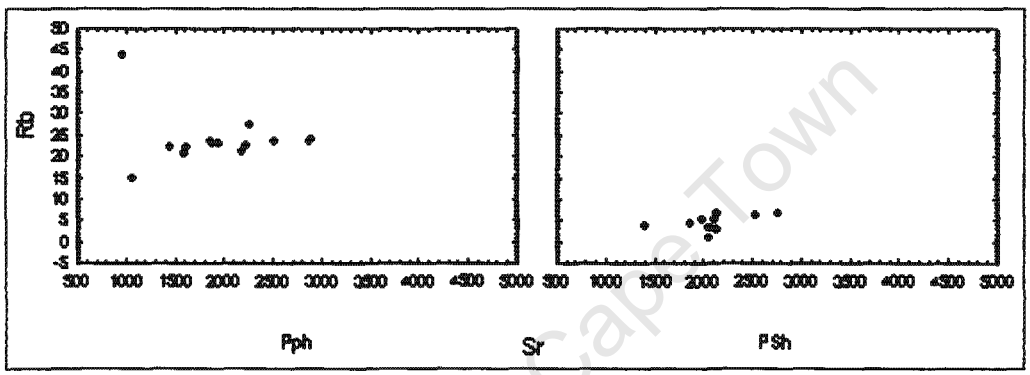

(b)

Figure 7.18. Relationship between (a) Nb and Sr and (b) Rb and Sr for the phosphorite allochems (Pph) and bioclasts (PSh) from the phosphatic sands from the Pelletal Phosphorite member, Varswater Formation. All values in ppm.

The scatterplot of Sr and Th/U indicates that, although there is some overlap, the various components show dissimilar scatter (Figure 7.19). This is also true for the scatterplot of La vs. Sr (Figure 7.20). The phosphatised shell fragments (PSh) appear to have a fairly constant La content with increasing Sr. The components of the Pelletal Phosphorite member show some heterogeneity in terms of their trace-elements abundances. The scatterplots are successful in distinguishing between the various components, most notably between the peloids and the phosphatised shell fragments. The CFA cement and peloidal phosphorite grains show the greatest amount of variability and scatter. The phosphatised shell fragments appear to show more compact and defined clusters. The clusters however are not very distinct, as they show significant overlap.

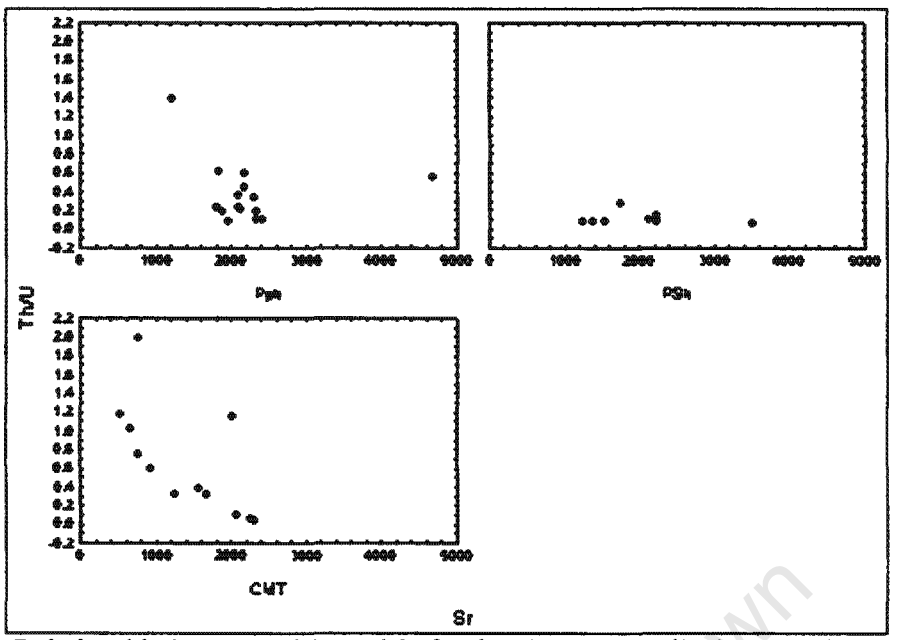

Figure 7.19. Relationship between Th/U and Sr for the phosphorite allochems (Pph) bioclasts (PSh) and CFA cement from the consolidated phosphorite from the Pelletal Phosphorite member, Varswater Formation. All values in ppm.

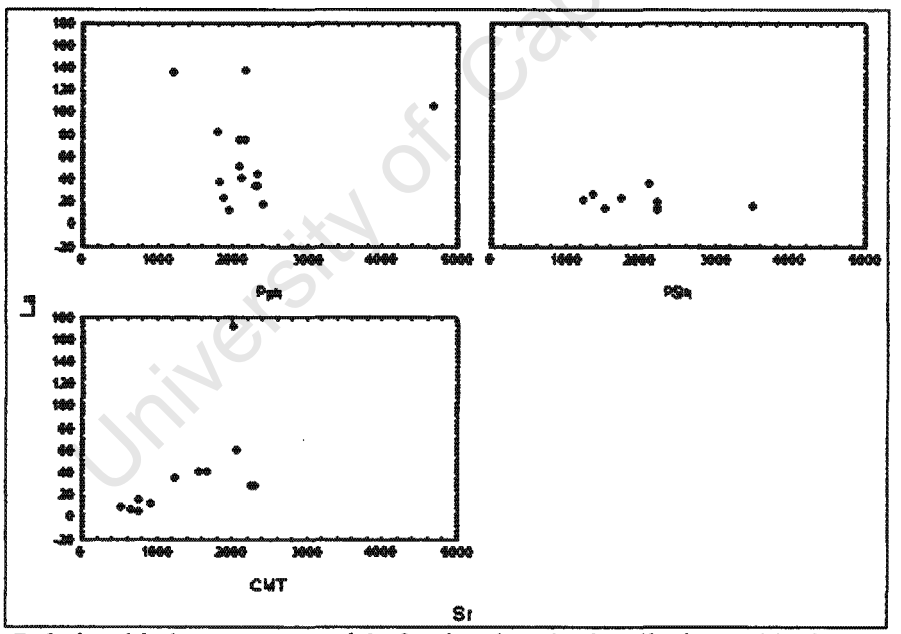

Figure 7.20. Relationship between La and Sr for the phosphorite allochems, bioclasts and CFA cement from the Pelletal Phosphorite member, Varswater Formation. All values in ppm.

7.3.3 Bomgat phosphorites, aluminium phosphates and the offshore phosphorites.

The Bomgat and offshore phosphorites are enriched in strontium and uranium (Table 7.17). The Sr values for the offshore phosphorites reach 6000 ppm. U values for the offshore phosphorites reach 300 ppm. Sr values for the Bomgat phosphorites and aluminium phosphates range between 800 ppm and 4000 ppm, whereas U values range between 8 – 60 ppm and 35 – 150 ppm, respectively. In contrast to the Bomgat and offshore phosphorites, the aluminium phosphates are also enriched in Zr, Pb, Th, V and Rb (Figure 7.21). The offshore phosphorites show significant enrichment in one of the samples for Zr V, Th, Pb and Y (Figure 7.22), however the offshore phosphorites are enriched in Zr with normal abundances shown for Rb and V.

Table 7.17. Trace-element abundances of the Bomgat phosphorites, aluminium phosphates and offshore phosphorites. Post-Archaean average Australian shale (PAAS) is included for comparison. All values reported in ppm.

1. BOMGAT, HOEDJIESPUNT

Sample	Sr	Y	Pb	Th	U	V	Rb	Zr
			Biogenic grains					
B1-cmt-1	3250	16.2	31.4	7.41	58.9	31.8	154	381
B1-cmt-2	3958	14.0	17.8	5.63	13.8	34.4	97.1	303
B1-cmt-3	3502	14.4	22.5	6.81	11.5	23.9	101	337
B1-cmt-4	5943	19.7	29.9	8.72	11.1	28.7	154	455
B2-cmt-1cfa	7278	21.2	29.8	9.22	7.4	26.4	148	444
B2-cmt-2cfa	2176	8.73	11.1	3.26	10.4	24.4	49.6	227
B2-cmt-3cfa	3936	9.09	20.1	3.69	8.27	26.1	65.8	187
B3-cmt-1	2170	66.3	6.77	1.77	68.3	29.8	12.2	62.5
B3-cmt-2	2600	29.7	4.96	0.72	25.3	19.4	6.21	26.5
B3-cmt-3	889	23.0	25.7	9.63	26.6	7.64	184	462
B3-cmt-4	2731	320	24.1	16.8	35.8	23.8	5.85	82.1
			Biogenic grains					
B3-bio-1	2517	3.85	7.8	0.91	20.0	50.7	14.7	53.5
B3-bio-2	2450	3.44	4.96	0.77	15.0	37.0	11.7	40.3
B3-bio-3	2853	30.9	12.3	1.97	45.3	63.2	31.1	99.5
B3-bio-5	1642	15	11.3	1.82	11.0	93.3	16.4	47.7
B3-bio-6	2274	528	12.5	4.86	93.9	40.9	16.1	74.9

2. ALIMINIUM PHOSPHATES

Sample	Sr	Y	Pb	Th	U	V	Rb	Zr
kr204-cmt-1	724	96.6	2235	907	129	1196	348	1456
kr204-cmt-2	911	82.6	2689	1671	145	1231	302	2287
kr204-cmt-3	2436	94.3	803	595	71.9	377	304	1331
kr204-cmt-4	2268	66.2	292	173	35.3	117	324	933

3. OFFSHORE PHOSPHORITES/PHOSPHATES

Sample	Sr	Y	Pb	Th	U	V	Rb	Zr
3703-1-cfa-1	25792	2624	2296	906	229	11742	7630	7739

Table 7.17. continues.

Sample	Sr	Y	Pb	Th	U	V	Rb	Zr
3703-1-cfa-3	5612	215	146	82	18	1003	736	841
3703-1-cfa-4	3943	94.4	37.2	18.7	42.8	198	186	325
3700-3-cfa-1	1819	28.3	36.7	11.0	310	56.8	192	469
3700-3-cfa-2	1922	25.0	29.6	10.3	175	50.9	186	436
3700-3-cfa-3	1671	23.2	31.0	10.6	169	50.7	197	457
mjm025gtd-cfa-1	6572	1488	111	18	212	171	208	870
mjm025gtd-cfa-2	6060	1079	41.9	16.5	262	168	203	813
mjm025gtd-cfa-3	7956	1494	43.1	18.6	281	207	192	1332
mjm025gtd-cfa-4	6640	1526	47.5	15.7	264	141	182	827
mjm025gN-cfa-1	1441	185	40.1	13.5	26.1	82.2	214	628
mjm025gN-cfa-2	432	49.8	74.7	27.5	7.8	14.7	438	1335
mjm025gN-cfa-3	494	57.1	72.9	26.7	21.1	26.6	442	1297
mjmb25d-cmt-1	431	31.9	45.0	15.8	37.0	33.4	321	775
mjmb25d-cmt-2	527	33.0	37.9	15.3	62.5	26.2	299	730
mjmb25d-cmt-3	516	31.2	41.5	14.9	82.2	29.5	305	742
mjmb25d-cmt-4	473	31.7	66.4	16.1	70.4	30.6	332	764

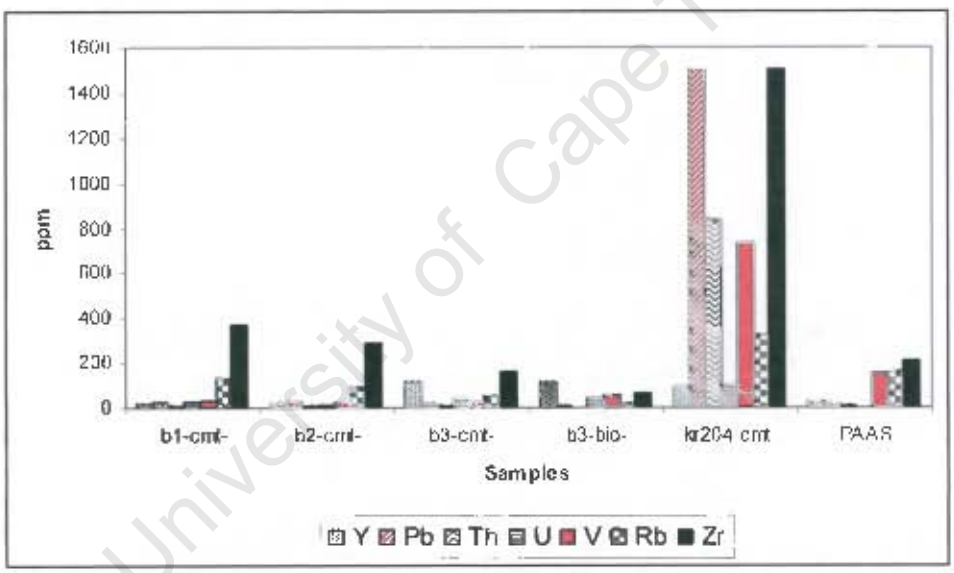

Figure 7.21. Trace-element concentrations in comparison with Post-Archaean average Australian shale (PAAS) for the Bomgat phosphorites and the aluminium phosphates from Posberg Peninsula. The graph shows that the aluminium phosphates are enriched in Zr, V, Th, Pb and possibly Y.

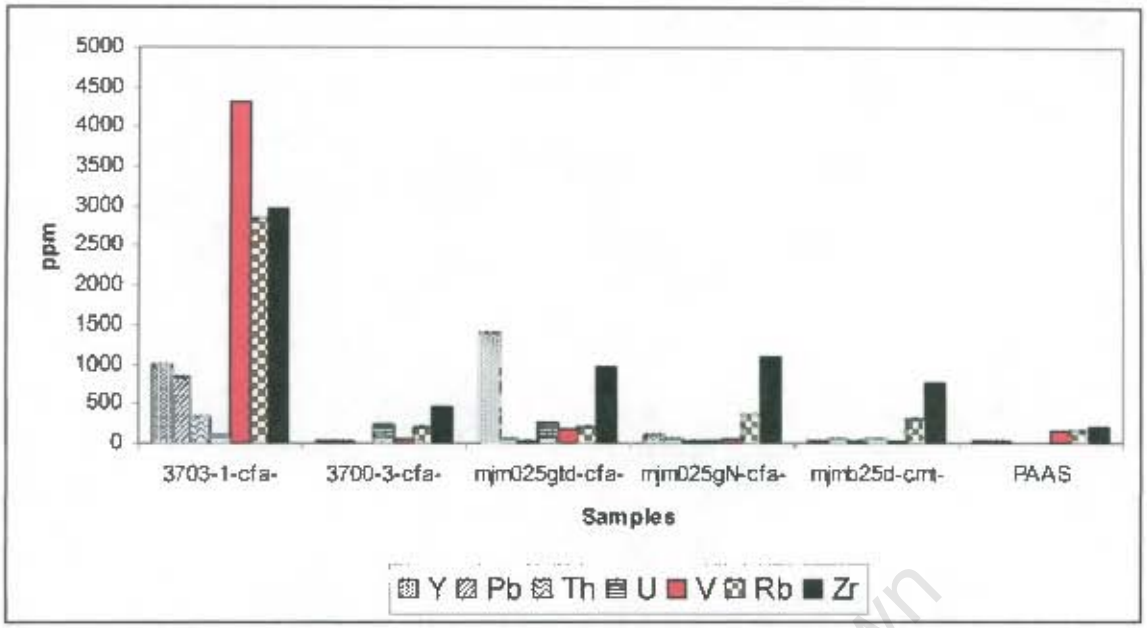

Figure 7.22. Trace-element concentrations in comparison with Post-Archaean average Australian shale (PAAS) for the offshore phosphorites. The graph shows that the offshore phosphorites are generally enriched in Zr and U, however 3703-1-cfa is enriched in Zr, V, Th, Pb and Y.

7.4. CHEMICAL VARIABILITY AMONG THE PHOSPHORITE DEPOSITS

The trace-element abundances of the various phosphorite deposits are compared in the following figures. The relationship between La and Sr shows similar clusters among the Varswater Formation phosphorite grain types (Figure 7.23). The abundances of La is similar for both the Gravel member and the Pelletal Phosphorite member, however the Gravel member shows higher concentrations of Sr. The relationship is comparable to the clusters for the Varswater Formation shown by Sr and U (Figure 7.24). There is some overlap between Pb and Sr, however the Gravel member has higher abundances of Pb compared to the Pelletal Phosphorite member (Figure 7.25). The Bomgat phosphorites show similar Sr, Pb, U and La relationships, with La, U, Pb and Sr values similar to the Varswater Formation phosphorites. In terms of the Th/U and Sr relationship, the Bomgat phosphorites show different trends to the Varswater Formation (Figure 7.26). In general, the individual tight clusters shown by the Varswater Formation and the Bomgat phosphorites show that the phosphorite grain types are generally homogenous. The scatter between the Gravel member and the Pelletal Phosphorite member is similar; and the minute differences can be ascribed to the presence of phosphatised shell fragments. The lack of coherence amongst the offshore phosphorites indicates that the group is geochemically heterogeneous.

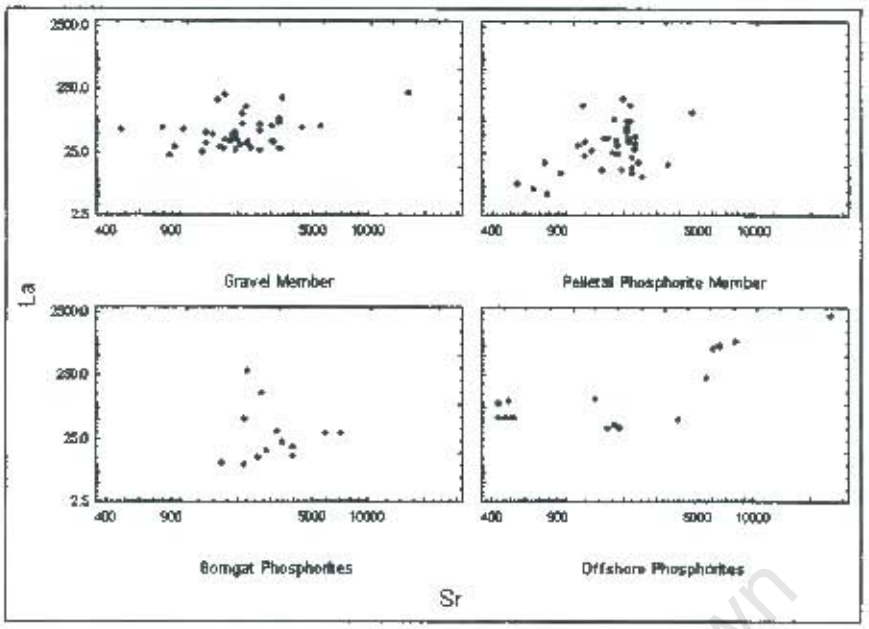

Figure 7.23. Relationship between La vs. Sr for the various phosphorite deposits. The phosphorites compared are from the Varswater Formation, Bomgat (Hoedjiespunt) and selected offshore phosphorites. The horizontal and vertical axes show logarithmic scales. All values in ppm.

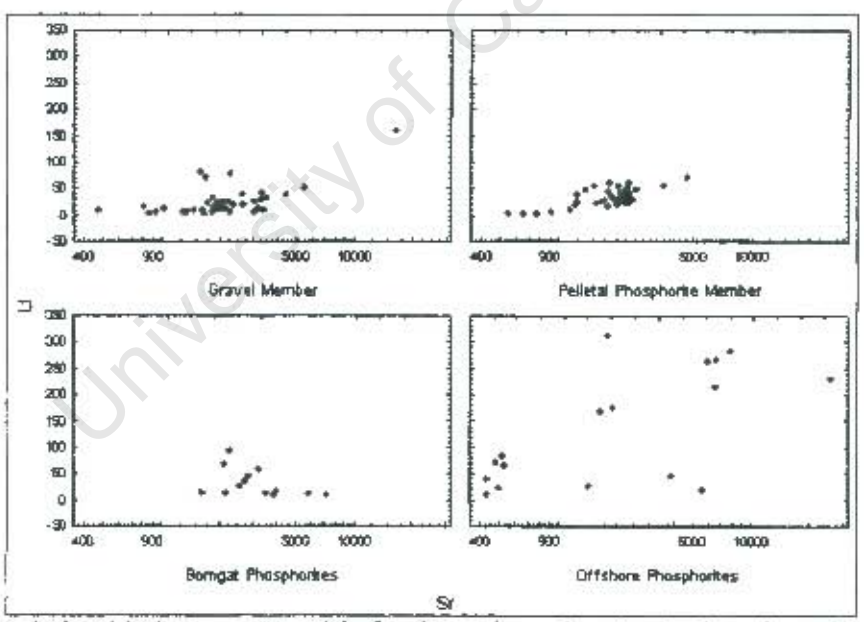

Figure 7.24. Relationship between U and Sr for the various phosphorite deposits. The phosphorites compared are from the Varswater Formation, Bomgat (Hoedjiespunt) and selected offshore phosphorites. The horizontal axis shows a logarithmic scale. All values in ppm.

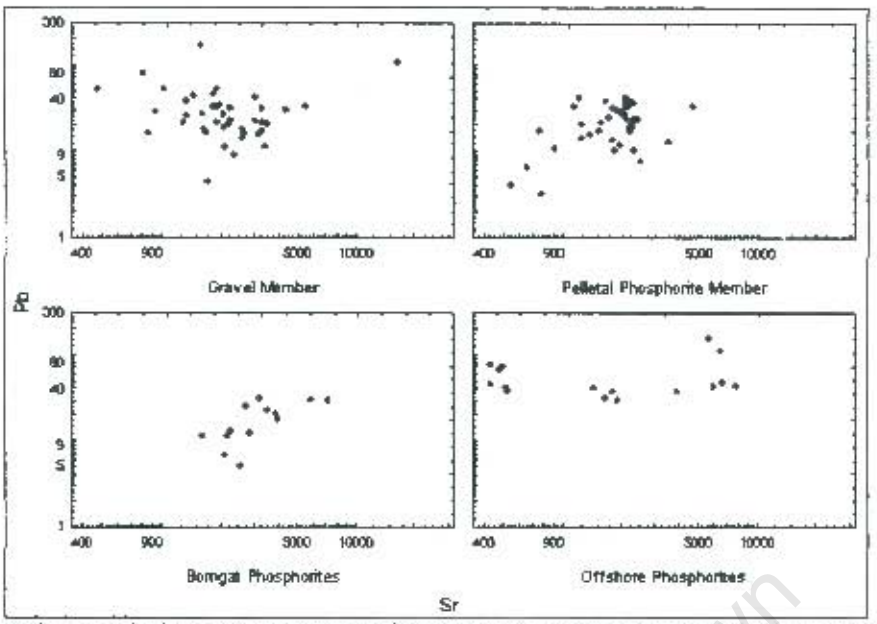

Figure 7.25. Relationship between Pb and Sr for the various phosphorite deposits. The phosphorites compared are from the Varswater Formation, Bomgat (Hoedjiespunt) and selected offshore phosphorites. The horizontal and vertical axes show logarithmic scales. All values in ppm.

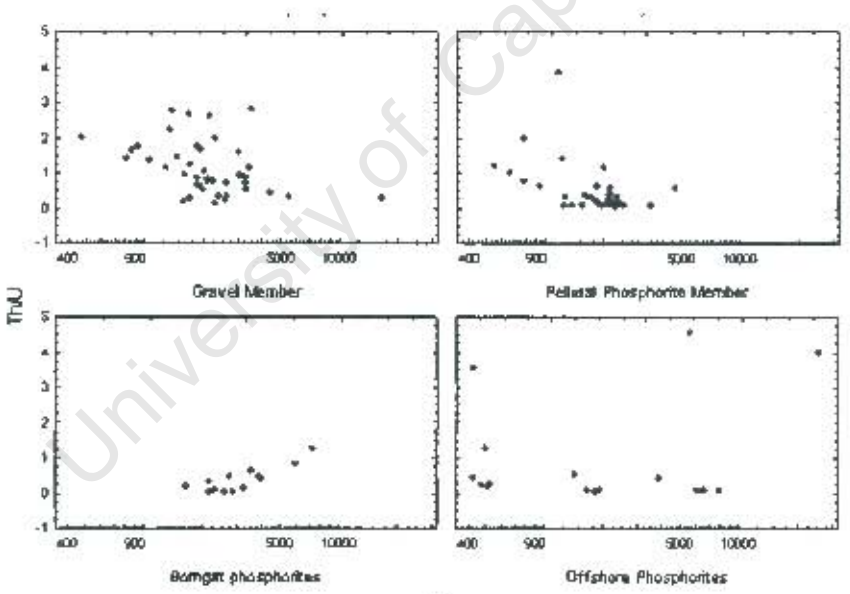

Figure 7.26. Relationship between Th/U and Sr for the various phosphorite deposits. The phosphorites compared are from the Varswater Formation, Bomgat (Hoedjiespunt) and selected offshore phosphorites. The horizontal axis shows a logarithmic scale. All values in ppm.

CHAPTER 8
DISCUSSION

This chapter discusses the results of this study. A short summary of the conclusions from this research as well as future research directions are given in Chapter 9.

8.1 INTRODUCTION

The objective of this study, as outlined in Chapter 3 was to determine and document the rare-earth and trace-element geochemistry of the phosphorites and phosphate rocks from selected sites around the southwestern Cape. The specific aims of the study are:

- to document the petrography and stratigraphy of phosphorite deposits at Langebaanweg, Bomgat and Posberg Peninsula, and
- to determine the rare-earth and trace-element geochemistry of the different phosphorite grain types, and propose possible depositional environments and diagenetic histories for the phosphorite deposits.

This chapter will interpret the results and attempt to answer the questions posed in Chapter 3. An attempt will be made to provide models for the formation of the phosphorites and phosphates at the various localities.

8.2. PHOSPHORITE TEXTURES

8.2.1 Varswater Formation

The Gravel member accounts for the lowest unit within the Varswater Formation. It consists of unconsolidated, well rounded to subrounded phosphatic cobbles, pebbles and silty sand, in addition to thin consolidated lenses comprised of older, eroded clasts of phosphorite (Tankard, 1975; Dingle *et al.* 1979; Rogers, 1980; Middleton, 2000). Individual phosphorite pebbles or cobbles contain rounded to angular phosphatic intraclasts set within a fine CFA cement. The intraclasts are composed of predominantly subrounded to rounded quartz grains (Qtz) and occasional phosphorite peloids (Pph). The modal proportions of the components are dependent on the intraclasts, with proportions varying considerably. In general the intraclasts contain at least 80% quartz and 15 – 20% ovoidal phosphorite peloids. Platy phosphatised shell fragments (PSh) are also present but rare (<1%). The different intraclasts are apparent on the basis of varying CFA cements and proportions of phosphatic constituents (Figure 8.1). The presence of the various CFA cements and intraclasts indicates that the Gravel member has been reworked extensively, and provides evidence of reworking and multiple episodes of phosphatisation.

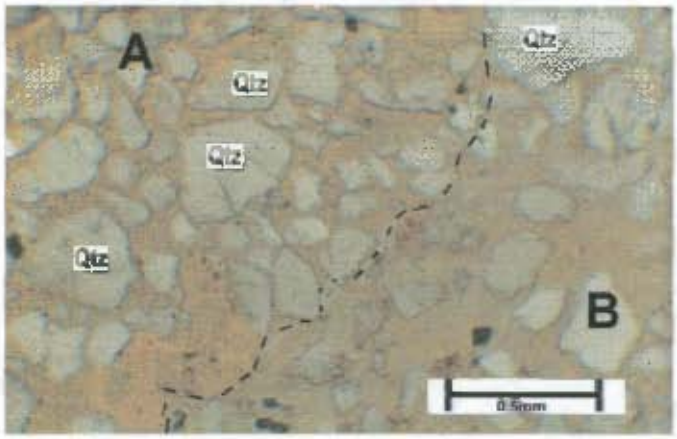

Figure 8.1. Photomicrograph of the Gravel member phosphorite (Sample VW48) showing dissimilar intraclasts and cement (labelled A, B). Intraclast A shows darker-coloured CFA cement and tightly packed medium quartz grains. Intraclast B shows lighter-coloured CFA cement with loosely packed medium quartz grains (photomicrograph taken in plane-polarised light).

The Pelletal Phosphorite member consists of unconsolidated phosphatic sands and occasional beds of consolidated quartzose phosphorite. The consolidated quartzose phosphorites are generally overlain and underlain by unconsolidated-phosphate-rich sands. The consolidated phosphorite beds were formed by precipitation of authigenic apatite within the pore spaces of the phosphate-rich sediments (Dingle *et al.*, 1979; Tankard, 1974a). The consolidated phosphorites and the unconsolidated phosphatic sands are texturally similar; however the grains of the consolidated phosphorites are cemented by CFA (Figure 8.2). The Pelletal Phosphorite member phosphorites are texturally different from the underlying Gravel member phosphorites. For instance the Pelletal Phosphorite member contains considerable phosphatised shell fragments (PSh) (15 – 20%) and peloids (Pph) (20 -30%). Unlike the Gravel member the Pelletal Phosphorite member does not contain characteristic phosphatic intraclasts, comprised of older, eroded clasts of phosphorite.

The presence of well-rounded, sand-sized peloidal phosphorite grains, in association with fractured but rounded quartz grains suggests multiple reworking and CFA precipitation in the Gravel and Pelletal Phosphorite members. The origin of the peloidal grains is unclear. The peloidal grains may represent phosphatised faecal pellets, rounded phosphatised pore fillings (or rip-up clasts) or phosphate-coated quartz grains. According to Tankard (1974a) the Pelletal Phosphorite member is derived from the Miocene basal bed and the Gravel member, through continual reworking within a high-energy environment. The presence of laminated sand layers within the Pelletal Phosphorite member does support deposition and reworking in a high-energy upper-flow environment (Middleton, 2000). One possibility is that phosphorite peloids form as intraclasts on eroded intertidal mudflats (Bremner and Rogers, 1990; Middleton, 2000). The smaller intraclasts are subsequently modified through accretion resulting in pseudo-oolitic textures and the larger intraclasts are rounded through erosion, resulting in completely

unstructured peloids (Bremner and Rogers, 1990). The Varswater Formation peloids are essentially unstructured. A significant number of peloids do contain silt-size particles and even biogenic particles such as foraminifera or shell fragments, which may indicate that a number of the peloids may have been phosphatised faecal pellets.

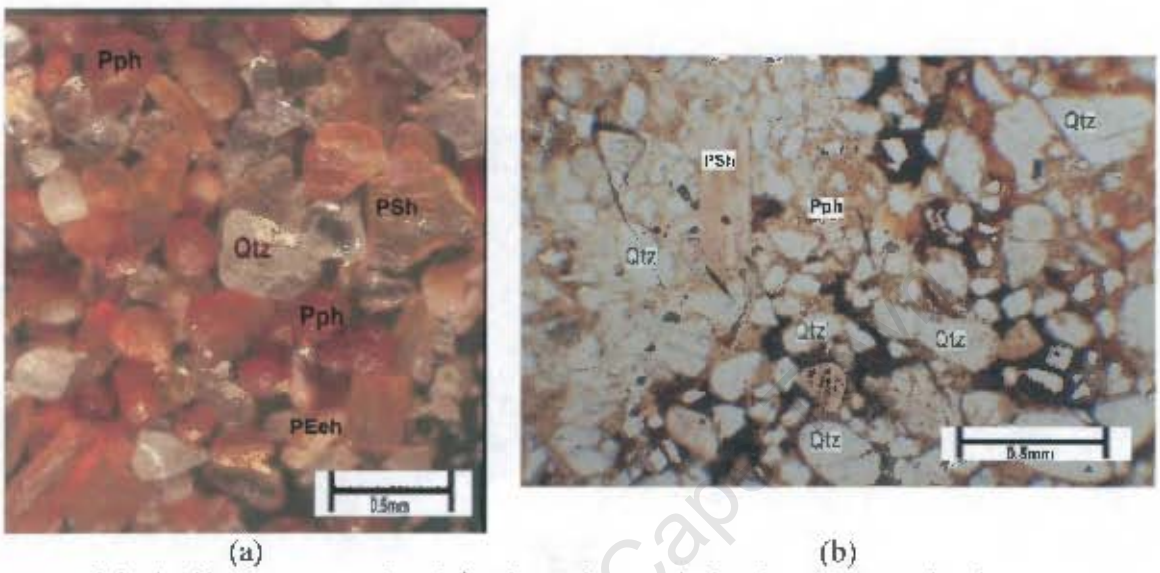

(a) (b)

Figure 8.2. (a) Photomacrograph and (b) photomicrograph showing the textural and component similarity between the unconsolidated (Sample VW1a3) and consolidated phosphorites (VW16) from the Pelletal Phosphorite member, Varswater Formation. The photomicro/macrographs show peloidal phosphorite (Pph), phosphatised shell fragments (PSh) and quartz (Qtz).

The presence of phosphatised bivalve shell fragments (PSh), echinoid spines (PEch) and the occasional benthic foraminifera (*Elphidium* sp.) indicate that the Pelletal Phosphorite member is marine. Middleton (2000) pointed out that the phosphorite beds are generally associated with yellow iron-stained sediments. The iron-stained sediments indicate that the sediments were later subaerially exposed, whereas the presence of burrows within the consolidated phosphorite beds indicates relatively shallow, well-oxygenated waters during deposition.

In summary the Gravel member is a much older deposit than the Pelletal Phosphorite member and it is clear from petrographic evidence that the Gravel member shows a more complex history of phosphatisation and reworking than the Pelletal Phosphorite member.

8.2.2. Bomgat phosphorites (Hoedjiespunt)

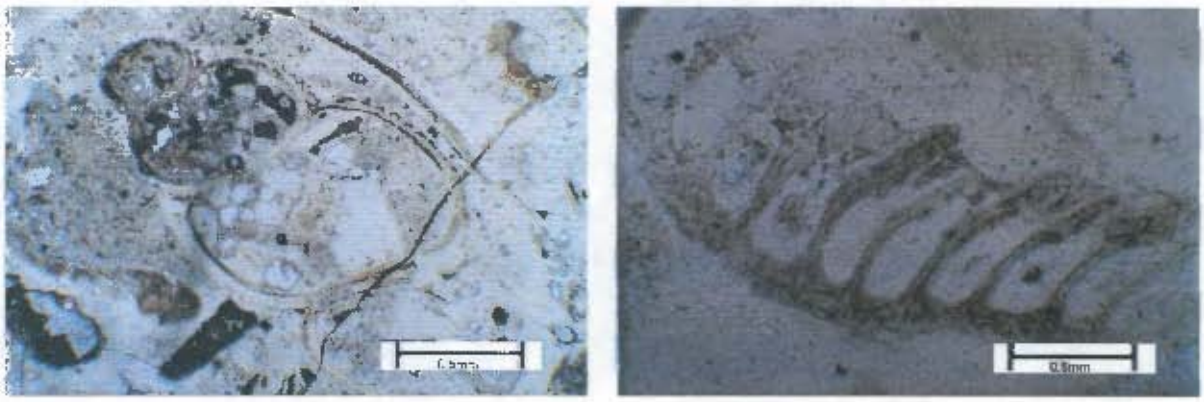

(a) (b)

Figure 8.3. Sample B1 is characterised by an extremely fine-grained homogenous, light brown CFA matrix. The sample shows biogenic grains, (a) gastropod (b) bivalve shell fragment (photomicrograph taken in plane-polarised light).

The Bomgat phosphorites include well-preserved bryozoa, echinoid ossicles, mollusc shell fragments and occasional benthic foraminifera (Figure 8.3.). The phosphatised bioclasts and in particular the presence of abundant bryozoa, indicate that the carbonate precursor was deposited in a shallow-marine environment, within the photic zone. The bioclasts are well preserved and show little evidence of re-deposition or erosion. The relative abundance of the phosphatised micrite/CFA cement and the nature of the bioclasts indicate that the carbonate precursor was deposited in a low-energy environment.

The timing of phosphogenesis is not known, but would have been between deposition of the phosphatised limestone and deposition of the overlying units. The presence of the phosphate indicates that the depositional environment must have been rich in organic matter, although the deposit currently has only minor amounts of organic material based on the petrography. The Bomgat phosphorite deposit is different in a number of respects. Firstly, the apatite mineral is dahllite rather than CFA (francolite), the phosphorite is highly resinous in texture and has clearly replaced a carbonate-rich precursor sediment.

8.2.3. Offshore phosphorites

Mulabisana (1998) examined the petrography of selected offshore phosphorites and classified the phosphorites according to six groups (Table 8.1). The phosphorites are typically fine-grained to medium-grained, composed of predominantly quartz, glauconite, CFA and authigenic pyrite. These phosphorite samples were recovered from the shelf on the Orange River Prodelta, but phosphorite samples from the continental margin off Cape Columbine are similar in texture and age (Miocene) (Compton *et al.*, 2002). The offshore phosphorite textures are far more variable than and are distinctly different from the onshore phosphorites. In addition to quartz, the offshore phosphorites commonly contain glauconite and pyrite (Compton *et al.*, 2002). They are typically tan to orange to brown or

grey in colour and often have polished black exterior surfaces, but are never as resinous in texture as the onshore samples. Although transparent amber-coloured CFA-replaced shell fragments are observed in places. The offshore phosphorites are often internal casts of bivalves or gastropods and contain more evidence of marine bioclastic material. The offshore phosphorite is commonly concentrated in reworked, condensed gravel to sandy deposits and lack pure resinous CFA cements.

Table 8.1. Classification of phosphorite samples of the western continental shelf of South Africa based on texture and mineralogy (modified after Mulabisana, 1998). The samples analysed in this study are indicated.

Brief Description	Group (Mulabisana, 1998)	Phosphorites	offshore phosphorite samples analysed
Extremely fine, no glauconite	A	Phosphorite (Watkins *et al.*,1995)	
Contains glauconite, coarser quartz grains	B	Glauco-phosphorites (Birch, 1975; 1979b, Parker, 1975)	3700-3 3703-1
Glauconite in semi circular structures	C	Conglomeratic phosphorites (Bremner, 1980a)	
Clastic, shell moulds	D	-	Mjmb25d
Layered, contains more organic matter	E	-	
Bone material (phosphatised bone material e.g. fish etc.)	F	Fish debris	

8.3. REE CONTENT OF PHOSPHORITES

According to McArthur and Walsh (1984), Recent phosphorites have low REE concentrations. Piper *et al.* (1988), while documenting phosphorites (Recent) from the continental shelf of Peru showed similar low REE concentrations. The concentrations were especially low within the biogenic fraction (fish debris). Watkins *et al.* (1995) concluded that "francolite characteristically forms with extremely low REE content". The REE concentrations for the South African onshore and offshore phosphorites discussed in this study have similar low REE concentrations (Table 8.2).

Table 8.2. Rare-earth element composition (in ppm) of offshore and onshore phosphorites and phosphate samples from Peru, Namibia and South Africa. The data are from Piper *et al.* (1988), Watkins *et al.* (1995) and this study.

Sample	Number	Locality	Description
GC-1	1.	Offshore, Peruvian continental shelf	Glauconite
BX-2 (8-10)	2.	Offshore, Peruvian continental shelf	Apatite pellets
BX-2(18-20)	3.	Offshore, Peruvian continental shelf	Apatite pellets
Fish Debris	4.	Offshore, Peruvian continental shelf	Fish debris
Phos1	5.	Offshore, Namibian continental shelf	Phosphatised glauconitic sediment
Phos2	6.	Offshore, Namibian continental shelf	Phosphatised glauconitic sediment
Yn-1	7.	Offshore, Namibian continental shelf	Phosphorite
Yn-2	8.	Onshore, Bomgat sea cave, South Africa	Phosphorite
Yn-3	9.	Onshore, Varswater Formation, South Africa	Phosphorite
A-13393	10.	Offshore, Agulhas Bank, South Africa	Phosphorite
VW1A3 (Bulk)	11.	Onshore, Varswater Formation, South Africa	Phosphate-rich sediments
B1	12.	Onshore, Bomgat, South Africa	Phosphorite

	Piper *et al.*(1988)				Watkins *et al.*, (1995)						This Study	
Sample No.	1.	2.	3.	4.	5.	6.	7.	8.	9.	10.	11.	12.
La	5.1	35	44	4.8	67.3	67.5	44.3	0.51	27.5	44.7	20.6	1.01
Ce	7.7	41	52	9.1	162	145	96.1	0.97	60.6	93.8	45.5	2.09
Pr	2	7.8	10	1.2	19.1	16.4	11.1	0.13	7.23	10.4	5	0.25
Nd	4.9	34	43	3.8	77.8	70.2	45.3	0.51	28.8	43.6	21.9	1.07
Sm	1.1	8.1	11	1.7	18.5	16.4	10.2	0.11	6.76	9.47	4.46	0.22
Eu	0.23	2.2	2.8	0.18	4.12	3.8	2.07	0.03	1.28	1.92	0.95	0.04
Gd	3.4	10.4	14	7	19.3	17.7	10.5	0.1	7.03	9.4	4.97	0.22
Tb	-	-	-	-	2.8	2.53	1.52	0.02	1.03	1.31	0.7	0.03
Dy	-	-	-	-	15.8	14.6	9.57	0.1	6.44	7.66	4.44	0.19
Ho	0.24	2.6	3.2	0.15	-	-	-	-	-	-	0.93	0.05
Er	1	8.4	10	0.8	7.46	6.88	5.55	0.06	3.83	4.06	2.77	0.15
Tm	-	-	-	-	-	-	-	-	-	-	0.37	0.02
Yb	0.82	8.4	10	1.1	5.38	4.54	4.77	0.06	3.38	2.83	2.4	0.16
Lu	0.14	1.4	1.7	0.11	-	-	-	-	-	-	0.37	0.03
∑REE	26.63	159.3	201.7	29.94	399.56	365.55	240.98	2.6	153.88	229.15	115.36	5.53

8.4. CE-ANOMALY AS A PALAEOREDOX INDICATOR

The majority of the phosphorites show flat, "shale" REE patterns, including the offshore phosphorites. Flat REE patterns indicate that the phosphorites incorporated their REEs under non-oxidising conditions (Watkins *et al.* 1995). According to McArthur and Walsh (1984) flat patterns can be interpreted to reflect significant detrital influence. However, Cruse *et al.* (2000) suggest that the flat patterns are produced from non-phosphate phases that form during diagenesis of organic-rich muds. The non-phosphate phases are generally formed after phosphogenesis. As the shape of the REE pattern is not always a

reliable palaeoredox indicator, Ce-anomalies were determined. The Ce-anomalies determined for the various phosphorite deposits are similar and rarely pronounced. The typical range of values is between 0.74 and 1.06. The Ce-anomaly documented for the various deposits are generally slightly negative to negligible with strong negative Ce-anomalies shown only by some of the offshore phosphorites. McArthur and Walsh (1984) and Kidder *et al.* (2003) attribute negative Ce-anomalies to the oxidizing effect of seawater or oxygenated water. Marine minerals directly precipitated from seawater have negative Ce anomalies reflecting that of seawater (refer to figure in literature review chapter). Significant exposure of the phosphate to oxygenated water is believed to occur during early diagenetic winnowing of phosphate concretions in unconsolidated organic-rich muds (Kidder and Eddy-Dilek, 1994; Cruse *et al.*, 2000).

The phosphorites and phosphate rocks show significant dissimilarity in terms of their Eu-anomalies. The Gravel member and the offshore phosphorites show a wide range of Eu-anomalies from strongly negative to strongly positive (0.01-4.83) and from strongly negative to slightly positive (0.1-1.53), respectively.

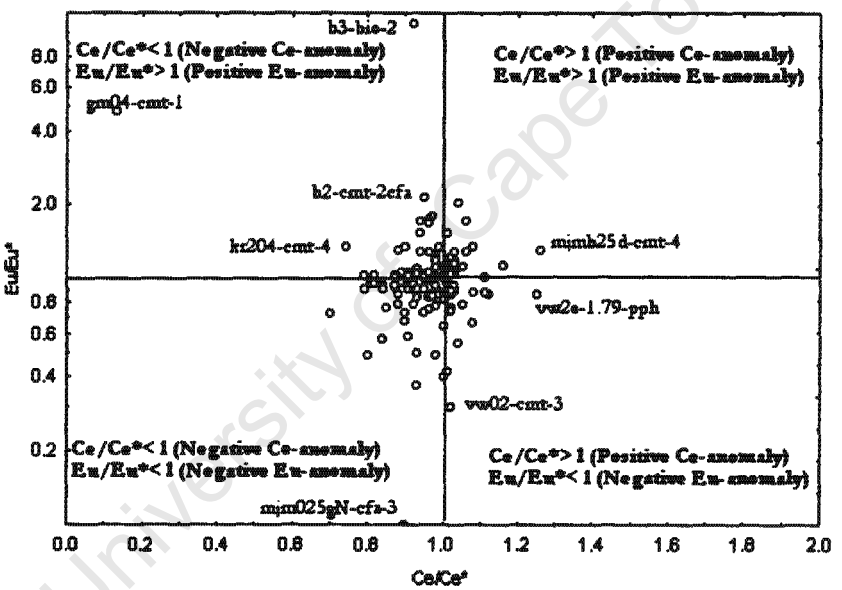

Figure 8.4. Relationship between Ce/Ce* and Eu/Eu* for the phosphorites and phosphate rocks. In general the phosphates and phosphorites show negligible to small negative and positive Ce-anomalies, however large positive and negative Eu-anomalies are noticeable. Anomalies defined relative to PAAS.

The Pelletal Phosphorite member and the Bomgat phosphorites show more conservative ranges, with Eu/Eu* values between 0.86 and 2.06 and 0.4 to 2.13, respectively (Figure 8.4). According to Ogihara (1999) and Kidder *et al.* (2003), positive Eu-anomalies indicate extreme reducing conditions, whereas negative Eu-anomalies, as reported by Elderfield and Sholkovitz (1987) for the reducing sediments of Buzzard's Bay Massachusetts, indicate much lower levels of reduction. Kidder *et al.* (2003) propose that within a closed reducing system the decay of organic matter would quickly use up available oxygen and therefore favour the reduction of Eu^{3+} to Eu^{2+}, resulting in positive

Eu-anomalies. The presence of glauconite and pyrite within the offshore phosphorites indicate reducing environments, or at least reducing micro-environments, within a general oxidising, low sedimentation environment (Birch, 1975; Parker, 1975; Deer *et al.*, 1992; Mulabisana, 1998). Authigenic glauconite and pyrite are not present in the onshore phosphorites. The lack of pyrite and glauconite in the onshore phosphorites may be related to oxidation during reworking. This appears to be plausible for the Varswater Formation; however the explanation is not sufficient for the Bomgat phosphorites. According to Compton *et al.* (2002), the occurrence and inclusion of Fe-rich diagenetic minerals (glauconite, pyrite and siderite) indicate formation of these minerals penecontemporaneously with the phosphorite in Fe-rich terrigenous muds. Petrographic evidence suggests that the Bomgat deposit (predominantly carbonate bioclasts) was deposited in a low-energy environment, and subsequently phosphatised, however the lack of terrigenous material offers a more likely explanation for the lack of glauconite and pyrite in the Bomgat phosphorites. In other words a lack of Fe limited the formation of glauconite and pyrite. The presence of burrows within the consolidated phosphorite lenses indicates that the deposit was well oxygenated. According to Kidder *et al.* (2003) biogenic oxygenation through bioturbation can import or alter Ce-anomalies. However, burrows were not observed in the Gravel member which also has slightly negative Ce-anomalies. A possible explanation may lie in REE mobilisation during diagenesis. The Bomgat phosphorites show relatively small negative Ce-anomalies, however there is a possibility that the Bomgat phosphorites inherited some REE from the carbonate precursor. In any case, less negative to positive Ce-anomalies are generally considered to represent suboxic conditions (Table 8.3.).

Other uses for the Ce/Ce* ratio also became apparent, when used in conjunction with another REE index, the Lu/La ratio. The relationship between Ce/Ce* and Lu/La shows a means for distinguishing between biogenic clasts and the phosphorite allochems (Figure 8.5). Biogenic clasts including the phosphatised shell fragments and bone fragments have relatively high Lu/La values. The dissimilarity is probably also a result of the mineralogy of the biogenic clasts being converted from dahllite to francolite. The conversion of dahllite to francolite is probably due to replacement rather than dissolution/precipitation, because of the conservation of biogenic shell/bone microstructures.

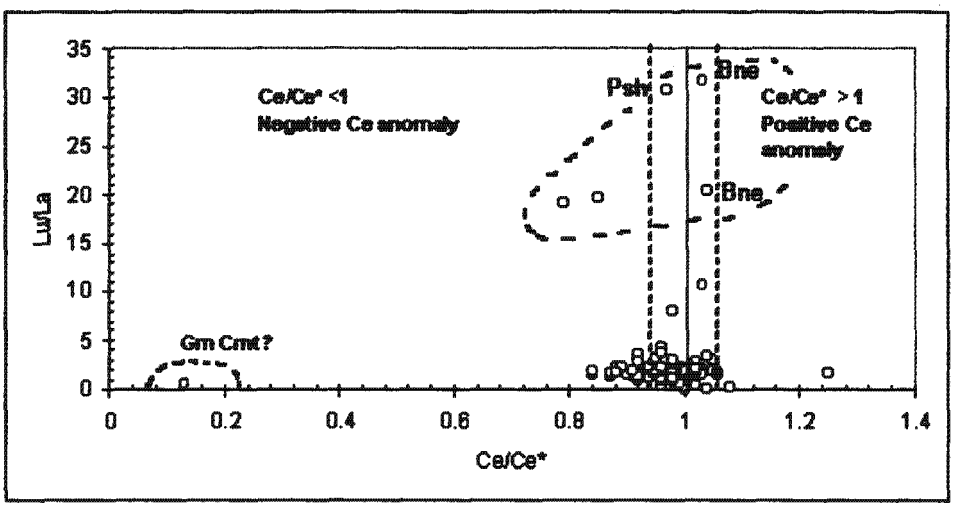

Figure 8.5. Relationship between Ce/Ce* and Lu/La for the phosphorite allochems, bioclasts and CFA cement from the Varswater Formation.

Table 8.3. A summary of the behaviour of Ce (Ce-anomaly) under different redox conditions and within different media.

MEDIUM	OXIC	SUBOXIC	ANOXIC
Seawater	Ce less readily dissolved in seawater: therefore Ce is depleted in oxic sea water.	During suboxic conditions Ce within sediments is mobilized resulting in Ce being released in to the water column (De Baar *et al.*, 1985a, 1985b, 1988).	
	NEGATIVE CE-ANOMALY	LESS NEGATIVE to POSITIVE CE-ANOMALY	POSITIVE CE-ANOMALY
Sediments	Oxic sediments are enhanced with respect to Ce. Fe-oxide-rich oxic sediments are enriched with Ce (Thomson *et al.* 1994).		During anoxic conditions, sediments are typically depleted with respect to Ce.
	POSITIVE CE-ANOMALY		NEGATIVE CE-ANOMALY
Phosphate & Phosphorite	Organisms responsible for extracting phosphate from oxic seawater show negative ce anomaly (Wright et al., 1987).		Phosphates/phosphorites from predominantly anoxic waters are typically enriched in Ce (Wright *et al.*, 1987; Grandjean-Lécuyer *et al.*, 1993).
	NEGATIVE CE-ANOMALY	LESS NEGATIVE to POSITIVE CE - ANOMALY	POSITIVE CE-ANOMALY

8.5. REE PATTERNS OF PHOSPHORITE

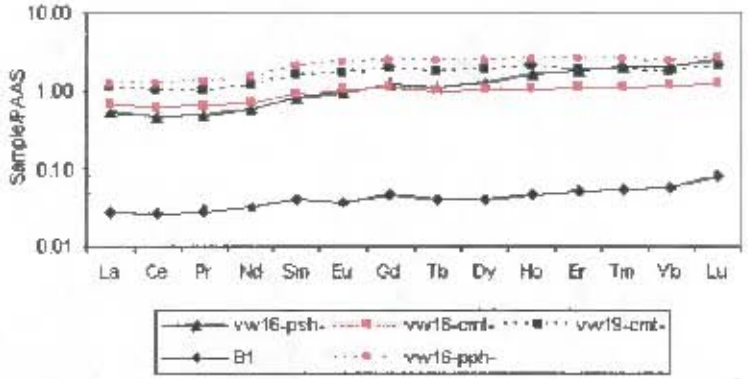

Figure 8.6. PAAS-normalized REE diagram of the averages of LA-IC-PMS and IC-PMS measurements taken from the Pelletal Phosphorite member (vw16 – 19) and Bomgat (B1) samples, respectively. The Pelletal Phosphorite member show specific grain types. These include peloidal phosphorite (pph), phosphatised shell fragments (psh) and CFA cement (cmt).

The majority of the onshore phosphorites show "shale" type REE patterns with no to small Ce-anomalies, but the patterns do show fractionation between LREE and HREE (Figure 8.6). The samples are HREE enriched, relative to LREE in contrast to typical river-borne detrital sediments, which are generally LREE enriched. The enrichment of LREE in detrital sediments is due to the removal of REE from the river water column (Martin *et al.*, 1976). According to Leleyter *et al.* (1999), LREE (except Ce) are removed from the water column by being bound to organic matter, whereas MREE are mainly bound to carbonate and organic matter. HREE and Ce are believed to be mainly associated with Fe-oxides (Leleyter *et al.*, 1999). However other studies have shown that LREE can be associated with Fe-oxides (e.g., Koeppenkastrop and DeCarlo, 1993). Elderfield *et al.* (1990) recognized MREE enrichments in a variety of natural waters, including lake waters, groundwaters and river waters. The enrichment of MREE in river water can be explained by preferential dissolution of phosphatic minerals during weathering (Hannigan and Sholkovitz, 2001). However, according to Johannesson *et al.* (1996) MREE enrichment is controlled by solid-liquid exchange reactions or dissolution of surface coatings and/or secondary phases or sulfate complexation in natural acidic water. Pronounced MREE enrichments are commonly found in skeletal or biogenic apatites and conodonts (Wright *et al.* 1987; Grandjean-Lécuyer *et al.*, 1993). MREE are preferentially removed from the water column by coprecipitation of phosphate and REE compounds or by uptake from organic-rich oxy-hydroxide grain coatings (Elderfield *et al.*, 1990; Byrne *et al.*, 1996).

The weathering of soils can result in REE remobilisation. According to Compton *et al.* (in press) the behaviour of REE during weathering is affected by hydrology, precipitation and climate regime. For example in temperate climates HREE are readily removed from the weathered soil profile (Aubert *et al.* 2001), whereas in arid to semi-arid climates the removal of HREE is greatly diminished. Compton *et al.* (in press) shows that HREE are more mobile than LREE in carbonate-free soils and sediments. In the open ocean, the

removal of REE leads to fractionation of the REE between particles (detrital fraction) and seawater. The detrital fraction is enriched in terms of Ce and LREE, whereas seawater is enriched in HREE. HREE are known to be associated with carbonate ions. The enrichment of HREE and depletion in Ce results in typical "sea water patterns". These patterns are typically convex-upward, HREE enriched and show pronounced negative Ce-anomalies. The phosphorites from Varswater Formation, in particular the peloids (Pph) and CFA cement show mid-to-HREE enrichment relative to LREE. The phosphatised shell fragments (PSh) also show HREE enrichment however the patterns are generally inclined, with pronounced HREE enrichment. The Bomgat phosphorites show similar flat HREE enriched patterns to the Varswater peloids and CFA cement. However the Bomgat phosphorites do not show the distinctive MREE-HREE enrichment. The Bomgat REE patterns are similar to some of the offshore phosphorites, however the offshore REE patterns are variable. None of the phosphorites (onshore and offshore) show pronounced negative Ce-anomalies. Phosphorites are formed at shallow depths on the ocean sea floor (near coastlines) due to the precipitation of CFA in phosphorus supersaturated interstitial fluids within sediments or diatomaceous muds (Bremner, 1980a). Phosphorites should therefore contain the REE signature of seawater, however diagenetic remobilization of associated clastic debris, may be responsible for the shale patterns. However, the REE patterns for the Varswater Formation with the MREE-HREE enrichment relative to LREE are consistent with precipitation in seawater or groundwater.

8.6. TRACE-ELEMENT GEOCHEMISTRY OF PHOSPHORITES

Geochemical investigations of marine phosphorites have shown that phosphorite deposits are enriched with a wide range of elements (trace-elements) relative to average sedimentary rocks (Lucas *et al.*, 1990; Soudry *et al.*, 2002). Phosphorites are also known to be notably depleted (or show normal abundances) in other trace-elements (Table 8.4). From the literature it appears that Ag, Cd, Cr, Sr, U and Y are most likely to be enriched within phosphorites. According to Thomson *et al.* (1984), Sr and U are present in high concentrations in phosphates of all ages. Other elements that can have significant enrichment include Zn, Cu, V and Pb, whereas the elements Zr, B and Ba are likely to be depleted. The ability of phosphorites to incorporate trace-elements by substitution is believed to be due to the nature of the apatite lattice (Soudry *et al.*, 2002). However, according to Jarvis *et al.* (1994), the elements may not necessarily occur in the lattice, but be absorbed to crystal surfaces, organic matter, or other constituents of phosphorite. Lucas *et al.* (1990) provide a model that explains the enrichment of trace-elements in phosphorites by

- adsorption onto particle surfaces,
- coprecipitation into distinct minor mineral phases,
- association with organic matter and
- substitution for major elements in the mineral lattice .

Table 8.4. Concentration of trace-elements (ppm) of "Average Marine Phosphorite" (Altschuler, 1980), "Modal abundances in Phosphorite" (Gulbrandsen, 1966), "Average Shale"[1] (Turekian and Wedepohl, 1961) and PAAS (Taylor and McLennan, 1985).

	Phosphorites		Shale	
Element	Altschuler (1980)	Gulbrandsen (1966)	Average Shale[1]	PAAS
Ag	2	3	0.07	-
As	23	40	13	-
B	16	-	100	100
Ba	350	100	580	650
Be	2.6	-	3	-
Cd	18	-	0.3	-
Co	7	-	19	23
Cr	125	1000	90	110
Cu	75	100	45	50
Ga	4	-	19	20
Hg	0.06	-	0.4	-
La	147	300	40	38
Li	5	-	66	75
Mo	9	30	2.6	1.0
Ni	53	100	68	55
Pb	50	-	20	20
Sc	11	10	13	16
Se	4.6	10	0.6	-
Sn	3	-	6	4.0
Sr	750	1000	300	200
U	120	90	3.7	3.1
V	100	300	130	150
Y	260	300	26	27
Yb	14	10	2.6	2.8
Zn	195	300	95	85
Zr	70	30	160	210

Table 8.5. Comparison of the trace-element abundances of the phosphorites and phosphates from this study with the Post-Archaean average Australian shale (PAAS) (Taylor and McLennan, 1985). All values reported in ppm.

1. GRAVEL MEMBER, LANGEBAANWEG

Sample	Sr	Y	Pb	Th	U	V	Rb	Zr
PAAS	**200**	**27**	**20**	**14.6**	**3.1**	**150**	**160**	**210**
			Peloidal grains					
vw01-pph-1	1476	41.6	43.9	14.2	9.82	128	239	769
vw01-pph-2	1950	56.7	21.6	8.72	14.5	78.6	126	384
vw01-pph-3	1985	65.6	32.2	10.7	21	55.9	181	505
vw02-pph-1	1955	29.0	50.7	13.8	8.52	34.0	238	636
vw02-pph-2	1299	18.5	21.5	6.95	6.02	63.7	113	282
vw02-pph-3	1860	22.0	32.5	9.95	5.68	33.6	171	446
gm01-pph-1	3492	753	20.2	87.6	31.0	68.5	49.5	218
gm01-pph-2	2657	106	18.1	12.9	39.0	62.3	50.7	157
gm01-pph-3	2122	152	18.3	17.9	23.9	68.9	90.0	247
gm02-pph-1	3338	127	21.0	13.7	27.6	61.9	71.9	174
gm02-pph-2	2672	91.5	16.2	13.8	19.4	168	58.7	251
gm02-pph-3	2619	39.2	13.9	4.06	19.4	99.8	48.4	133
gm02-pph-4	478	36.1	50.6	17.4	8.61	44.9	327	855
gm03-pph-2	3344	167	31.5	29.1	42.4	37.8	190	502
gm03-pph-3	1719	274	16.5	19.2	71.5	30.1	88.4	268
gm04-pph-1	2382	48.4	8.89	6.43	19.7	59.5	30.2	96.1
gm04-pph-2	1735	360	4.37	27.7	22.5	44.1	6.65	55.5
gm04-pph-3	2145	229	11	33.4	12.8	69.5	48.4	189
			Biogenic grains					
gm02-psh-1	3311	33.7	16.9	8.61	10.2	64.6	67.1	173
			CFA cement					
vw01-cmt-1	1866	116	44.2	19.8	30.4	50.5	215	662
vw01-cmt-2	1884	52.4	32.1	12.2	14.3	106	184	592
vw01-cmt-3	2023	50.6	34.2	13.2	12.6	43.8	208	652
vw02-cmt-1	2282	33.0	31.5	11.2	77.0	62.4	161	426
vw02-cmt-2	943	19.8	28.1	9.27	5.41	34.9	152	417
vw02-cmt-3	1638	23	27.4	9.37	10.0	55.3	138	371
gm01-cmt-1	2278	31.6	22.9	11	5.48	58.1	112	314
gm01-cmt-2	3073	33.5	22.5	11.2	7.0	42.8	119	325
gm01-cmt-3	2244	206	20.6	18.3	24.3	31.8	68.2	212
gm01-cmt-4	1375	32.1	36.6	14.6	5.30	3.03	224	621
gm01-cmt-5	866	15.4	15.8	6.30	3.80	49.2	94.1	258
gm01-cmt-6-darkrim	809	38.6	76.6	19.3	13.8	33.7	376	908
gm01-cmt-7-darkrim	1046	39.7	51.2	16.5	12.2	14.5	356	772
gm02-cmt-1	2098	26.7	27.4	9.38	11.8	60.5	147	348
gm02-cmt-2	3432	33.8	11.0	9.44	8.11	46.9	60.68	169
gm02-cmt-3	3148	34.7	15.4	10.3	10.8	54.5	68.89	199
gm03-cmt-4	4386	86.8	29.3	15.6	37.5	53.1	203	537
gm03-cmt-5	5525	112	32.3	15.9	51.4	56.6	191	497

Table 8.5 continues.

Sample	Sr	Y	Pb	Th	U	V	Rb	Zr
gm03-cmt-6	3059	67.6	40.3	22.3	24.0	45.1	254	697
gm04-cmt-1	1596	35.9	161	15.8	80.9	396	210	274
gm04-cmt-2	1686	32.4	17.8	10.1	3.83	77.2	63.5	181
gm04-cmt-3	1361	35.8	25.5	11.3	5.03	58.4	107.7	349
gm02-cmt-7	243	-	949	2.5	20.6	217	1051	82.2

2. PELLETAL PHOSPHORITE MEMBER, LANGEBAANWEG

Sample	Sr	Y	Pb	Th	U	V	Rb	Zr
				Peloidal grains				
vw16a-pph-1	2324	37.4	36.2	7.36	21.4	-	-	-
vw16a-pph-2	1966	20.8	11.7	2.34	26.6	-	-	-
vw16a-pph-3	1884	25.8	30.2	6.08	34.6	-	-	-
vw16a-pph-4	2335	60.7	22.1	6.2	33.9	-	-	-
vw16a-pph-5	2180	95.2	38.3	14.1	24.2	-	-	-
vw16a-pph-6	2097	96.4	41.4	9.75	42.6	-	-	-
vw16a-pph-7	1831	36.4	30.3	9.83	15.8	-	-	-
vw16a-pph-8	4679	328	33.1	38.8	71.1	-	-	-
vw19b-pph-1	2426	23.4	23.5	3.17	29.3	-	-	-
vw19a-pph-1	1226	200	41.8	27.5	19.7	-	-	-
vw19a-pph-2	2180	236	31.9	17.4	39.9	-	-	-
vw19a-pph-3	2348	66.9	23.9	3.92	39.8	-	-	-
vw19a-pph-4	1808	156	13.4	10.3	43.1	-	-	-
vw16b-pph-1	2112	152	26.5	10.6	29.7	-	-	-
vw16b-pph-2	2141	93.3	23.8	5.49	26.3	-	-	-
				Biogenic grains				
vw16a-psh-1	2123	78.3	35.8	3.41	32.8	-	-	-
vw16a-psh-2	2242	17.7	16.6	2.55	28.3	-	-	-
vw16a-psh-3	1248	56.1	14.2	3.28	39.4	-	-	-
vw16a-psh-4	1381	72.1	15.6	3.79	46.6	-	-	-
vw16a-psh-5	1544	9.91	17.2	4.42	54.3	-	-	-
vw16a-psh-6	1762	13.0	24.2	7.72	28.7	-	-	-
vw16b-psh-1	2248	34.3	17.6	3.43	30.4	-	-	-
vw16b-psh-2	2249	19.5	19.6	2.94	21.3	-	-	-
vw16b-psh-3	3509	315	13.0	3.57	53.9	-	-	-
				CFA cement				
vw16a-cmt-1	773	10.3	17	5.34	2.68	-	-	-
vw16a-cmt-2	1263	80.1	20.6	7.6	23.4	-	-	-
vw16a-cmt-3	1671	63.1	36.7	7.32	23.3	-	-	-
vw16a-cmt-4	932	8.5	10.7	3.48	5.78	-	-	-
vw19b-cmt-1	2009	367	27.4	21.2	18.3	-	-	-
vw19b-cmt-2	664	5.5	6.45	1.68	1.65	-	-	-
vw19b-cmt-3	2076	104	30.2	5.62	53.3	-	-	-
vw19a-cmt-1	2318	53.9	10.4	1.69	59.4	-	-	-
vw19a-cmt-2	2269	41.2	18.4	2.98	52.0	-	-	-
vw19a-cmt-3	1575	60.1	21.0	8.01	21.0	-	-	-
vw19a-cmt-4	780	5.29	3.15	1.74	2.34	-	-	-
vw19a-cmt-5	546	8	4.01	2.99	2.54	-	-	-

Table 8.5 continues.

Sample	Sr	Y	Pb	Th	U	V	Rb	Zr
				Misc.				
vw16b-S1	1873	72.1	10.2	7.91	60.3	-	-	-
vw16b-S2	2523	169	7.69	3.44	49.1	-	-	-
vw19b-test	1160	30.7	32.1	35.5	9.24	-	-	-

3. BOMGAT, HOEDJIESPUNT

Sample	Sr	Y	Pb	Th	U	V	Rb	Zr
				Biogenic grains				
b1-cmt-1	3250	16.2	31.4	7.41	58.9	31.8	154	381
b1-cmt-2	3958	14.0	17.8	5.63	13.8	34.4	97.1	303
b1-cmt-3	3502	14.4	22.5	6.81	11.5	23.9	101	337
b1-cmt-4	5943	19.7	29.9	8.72	11.1	28.7	154	455
b2-cmt-1cfa	7278	21.2	29.8	9.22	7.35	26.4	148	444
b2-cmt-2cfa	2176	8.73	11.1	3.26	10.4	24.4	49.6	227
b2-cmt-3cfa	3936	9.09	20.1	3.69	8.3	26.1	65.8	187
b3-cmt-1	2170	66.3	6.77	1.77	68.3	29.8	12.2	62.5
b3-cmt-2	2600	29.7	4.96	0.72	25.3	19.4	6.21	26.5
b3-cmt-3	889	23	25.7	9.63	26.6	7.64	184	462
b3-cmt-4	2731	320	24.1	16.8	35.8	23.8	5.85	82.1
				Biogenic grains				
b3-bio-1	2517	3.85	7.8	0.91	20	50.7	14.7	53.5
b3-bio-2	2450	3.44	4.96	0.77	15	37	11.7	40.3
b3-bio-3	2853	30.9	12.3	1.97	45.3	63.2	31.1	99.5
b3-bio-5	1642	15	11.3	1.82	11	93.3	16.4	47.7
b3-bio-6	2274	528	12.5	4.86	93.9	40.9	16.1	74.9

4. ALUMINIUM PHOSPHATES

Sample	Sr	Y	Pb	Th	U	V	Rb	Zr
kr204-cmt-1	724	96.6	2235	907	129	1196	348	1456
kr204-cmt-2	911	82.6	2689	1671	145	1231	302	2287
kr204-cmt-3	2436	94.3	803	595	71.9	377	304	1331
kr204-cmt-4	2268	66.2	292	173	35.3	117	324	933

5. OFFSHORE PHOSPHORITES/PHOSPHATES

Sample	Sr	Y	Pb	Th	U	V	Rb	Zr
3703-1-cfa-3	5612	215	146	82.2	18.0	1003	736	841
3703-1-cfa-4	3943	94.4	37.2	18.7	42.8	198	186	325
3700-3-cfa-1	1819	28.3	36.7	11.0	310	56.8	192	469
3700-3-cfa-2	1922	25.0	29.6	10.3	175	50.9	186	436
3700-3-cfa-3	1671	23.2	31.0	10.6	169	50.7	197	457
mjm025gtd-cfa-1	6572	1488	111	17.6	212	171	208	870
mjm025gtd-cfa-2	6060	1079	41.9	16.5	262	168	203	813
mjm025gtd-cfa-3	7956	1494	43.1	18.6	281	207	192	1332
mjm025gtd-cfa-4	6640	1526	47.5	15.7	264	141	182	827
mjm025gN-cfa-1	1441	184.7	40.1	13.5	26.1	82.2	214	628
mjm025gN-cfa-2	432	49.8	74.7	27.5	7.77	14.7	438	1335

Table 8.5 continues.

Sample	Sr	Y	Pb	Th	U	V	Rb	Zr
mjm025gN-cfa-3	494	57.1	72.9	26.7	21.1	26.6	442	1297
mjmb25d-cmt-1	431	31.9	45.0	15.8	37.0	33.4	321	775
mjmb25d-cmt-2	527	33.0	37.9	15.3	62.5	26.2	299	730
mjmb25d-cmt-3	516	31.2	41.5	14.9	82.2	29.5	305	742
mjmb25d-cmt-4	473	31.7	66.4	16.1	70.4	30.6	332	764

Compared to shale (PAAS and "Average Shale") the onshore and offshore phosphorite samples from this study are markedly enriched in Sr, U, Zr, Rb and Y. In contrast, the aluminium phosphate deposits from the Posberg Peninsula are notably enriched in Zr, Pb, Th, V and Rb (Table. 8.5). The Gravel member and Bomgat phosphorite components are notably enriched with Sr, and reach values of more than 3000 ppm. High Sr values are also found in the Pelletal Phosphorite member; however the Sr abundances are generally lower, with values for the Pelletal Phosphorite member reaching 2000 ppm, with some grains as high as 3000 to 4000 ppm. Sr is generally found to be enriched within phosphorites, with Sr accepted to substitute for calcium in the apatite mineral lattice (Altschuler, 1980; Price and Calvert, 1978). According to Price and Calvert (1978) Ba, Ce, La, Mo, Ni, U, Y, Zn and Zr are all able to substitute for Ca in the apatite lattice.

U is also notably enriched in the phosphorites from this study. The U content for the onshore phosphorites (Varswater Formation and Bomgat) are not as high as values found in the offshore phosphorites. The offshore phosphorites have U values that reach 280 ppm. The offshore phosphorite values are comparable with the values obtained by Veeh *et al.* (1973) and Thomson *et al.* (1984) for marine phosphorites from the Namibian shelf (Table. 8.7). However, the onshore and offshore phosphorites of this study show higher Th values than those from the Namibian shelf (Veeh *et al.* 1973; Thomson *et al.* 1984). The abundances of the trace-elements are comparable to the phosphorite averages given by Altschuler (1980) and Gulbrandsen (1966) (Table 8.6).

Table 8.6. U and Th contents (ppm) in marine phosphorites and sediments from the Namibian shelf.

Study A: Veeh *et al.* (1973)
Locality of samples: Namibian Shelf

Sample	U (ppm)	Th (ppm)	U/Th
Sediment			
CIR 175 (0-10 cm)	10.2	1.1	9.27
CIR 175 (70-75 cm)	25.5	2.4	10.63
CIR 177B (0-10 cm)	13.7	2.0	6.85
CIR 177B (70-75 cm)	21.8	1.3	16.77
CIR 179B (0-10 cm)	15.7	-	-
CIR 179B (70 -75 cm)	29.6	1.4	21.14
CIR 189 B (0-10 cm)	38.7	2.2	17.59
CIR 189 B (70-75 cm)	54.6	8.1	6.74
Phosphorites/Phosphates			
CIR 162 (surface)	120	18	6.67
CIR 175P (40-50 cm)	158	3	52.67
CIR 175P (90-100 cm)	117	1	117

Table 8.6 continues.

Sample	U (ppm)	Th (ppm)	U/Th
CIR 186A/188A (20– 30 cm)	78.6	1	78.60
CIR 175P (30-40 cm)	139	22	6.32

Study B: Thomson *et al.* (1984)*
Locality of samples: Namibian Shelf

Sample (brief description)	U (ppm)	Th (ppm)	U/Th
3424 (friable concretion)	18.3 ± 0.4	0.38 ± 0.05	48 ± 6
3429 (pelletal phosphorite)	130 ± 2	25.5 ± 1.1	5.1 ± 0.2
3903 (glauconitized pelletal phosphorite)	95.1 ± 2.6	20.1 ± 0.5	4.7 ± 0l2
5798C (?coprolite/concretion)	107 ± 2	0.96 ± 0.06	111 ± 7
5798G (phosphatised fish scales)	333 ± 12	1.00 ± 0.17	333 ± 58
5799 (lithified concretion)	75.8 ± 2.2	0.52 ± 0.12	146 ± 34
5799B (coprolite)	81.8 ± 2.0	1.5 ± 0.4	55 ± 15
5799D (lithified concretion)	48.6 ± 1.4	0.32 ± 0.10	152 ± 48
5800 (lithified concretion)	57.6 ± 1.6	0.33 ± 0.05	175 ± 27
5801 (lithified concretion)	60.7 ± 1.4	2.6 ± 0.3	23 ± 3
5801A (coprolite)	34.5 ± 0.9	0.65 ± 0.06	53 ± 5

*Institute of Oceanographic Research (I.O.S) sample set reported.

The Gravel member is remarkably homogenous in terms of its trace-element geochemistry. The Gravel member components (Pph, PSh and CMT) analysed had similar trace-element contents. The homogeneity can be explained by the fact that the Gravel member has been reworked and re-phosphatised, therefore the re-phosphatisation of the Gravel member may have had a homogenizing effect on the trace-element abundances. In contrast to the Gravel member, the Pelletal Phosphorite member shows some heterogeneity in terms of its trace-elements abundances. Differences in trace-element content make it possible to distinguish various grain types, most notably the peloids and the phosphatised shell fragments. According to the trace-element abundances of the various phosphorite deposits, the Gravel member and the Pelletal Phosphorite member are similar. The trace-element abundances of the Pelletal Phosphorite member peloids are similar to the Gravel member peloids and Gravel member CFA cement. Notable differences can be ascribed to the presence of the geochemically distinct phosphatised shell fragments in the Pelletal Phosphorite member. This similarity indicates that the peloids from the Pelletal Phosphorite member are likely to be derived from the Gravel member in accordance with Tankard (1974a). Peloids from the Pelletal Phosphorite member may have been derived from the erosion of the underlying Gravel member.

The Bomgat phosphorites show similar trace-element abundances to the Varswater Formation phosphorites. The similarity can be interpreted to indicate similar environments of phosphatisation. The offshore phosphorites are a heterogeneous group and unrelated to the onshore phosphorites in terms of their mineralogy and trace-element geochemistry, however they are typical of other offshore phosphorites analysed in previous studies.

8.7. ORIGIN OF THE PHOSPHORITE

In order to understand the geochemical nature of the phosphorites, an attempt must be made to understand conceptual models of phosphogenesis (Figure.8.7). The upwelling of nutrient-rich deep ocean water onto continental shelves is widely cited as the prerequisite to the formation of phosphorite deposits (Birch, 1979a, 1979b, 1980; Bremner, 1980a; Balson, 1990). The upwelling replenishes the nutrient (and phosphorus) supply in the surface waters and results in enhanced productivity and ultimately phosphogenesis. Phosphorus accumulated in phytoplankton is deposited on the sea floor upon death of the phytoplankton. Bacterial degradation of relatively fresh organic matter buried on the shelf results in the release of the organic phosphorus as phosphate ion. Elevated phosphate ion concentrations in the interstitial fluids within the pore spaces of marine sediments, diatomaceous muds or organic-rich muds can then lead to supersaturation and precipitation of CFA (Bremner, 1980a). Precipitation of CFA can occur as a pore-filling cement or by replacement of precursor biogenic carbonate (bioclasts). According to Garrison and Kastner (1990), the CFA precipitate will gradually form CFA-cemented phosphorite nodules and ultimately transform the sediment into a hard, lithified phosphorite rock. CFA is generally considered to be the stable form of apatite in seawater (Nathan and Sass, 1981).

According to Trappe (1998) the steps towards phosphogenesis can be summarised as follows;

- The supply of phosphorus and degradation of organic matter (High bio-productivity). This stage occurs dominantly in suboxic to occasionally oxic to anoxic environments.
- Removal of phosphorus from biologic recycling.
- Concentration of phosphorus in porewater or sediment/water interface. This stage is characterised by dominantly suboxic to anoxic conditions.
- And the formation and precipitation of solid-phase phosphate, possible phosphatisation (or impregnation) of carbonate rocks and phosphatisation of bone.

Marine phosphorites are generally associated with glauconite, dolomite and pyrite (Glenn and Arthur, 1988). The minerals are believed to form within the same diagenetic environment as the phosphorite. The presence of pyrite indicates formation during the late stages of organic matter degradation or early diagenesis, under anoxic conditions (Trappe, 1998; Compton *et al.*, 2002). Pyrite is generally precipitated within the microbial sulphate-reduction zone, whereas glauconite is formed relatively early by the partial reduction of ferric iron (Glenn and Arthur, 1988; Compton *et al.*, 2002). Therefore the occurrence of pyrite (and glauconite) indicates the development of oxygen-deficient micro-environments. The occurrence and inclusion of Fe-rich diagenetic minerals (glauconite, pyrite and siderite) indicate formation of these minerals penecontemporaneously with the phosphorite in Fe-rich terrigenous muds (Compton *et al.*, 2002).

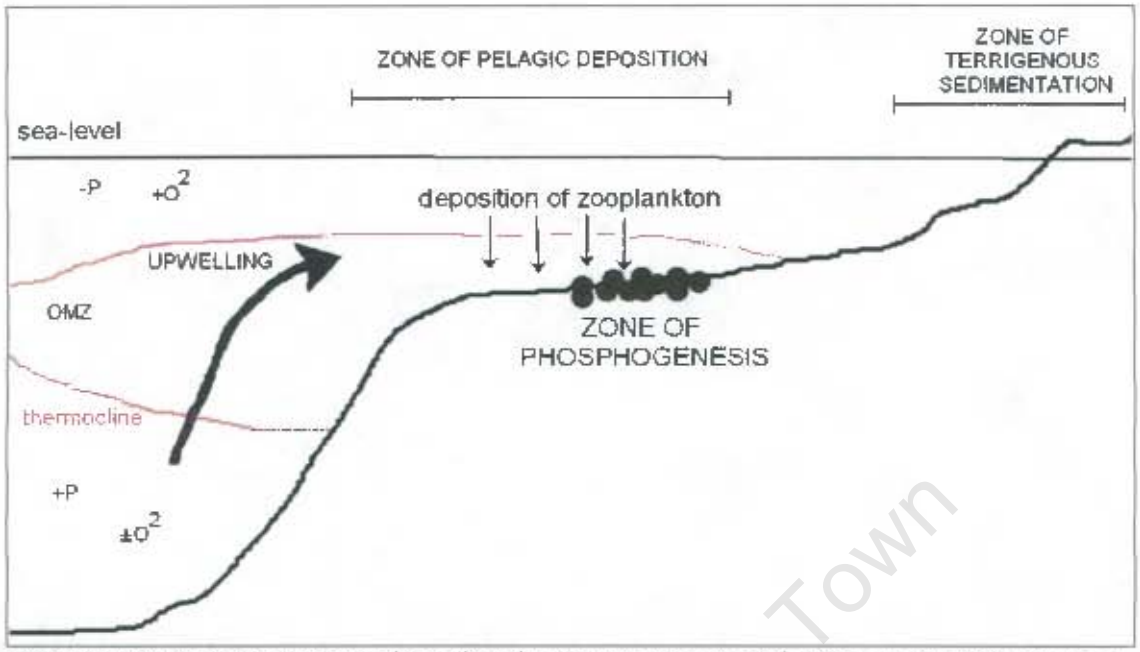

Figure 8.7. Schematic diagram of the phosphorite-upwelling model. The oxygen minimum zone (OMZ) can increase in size resulting in anoxic to suboxic conditions on the outer shelf (modified after Birch, 1979a; Trappe, 1998).

Extensive reworking of the Pelletal Phosphorite member resulted in the removal of pyrite (and noticeable organic matter) by oxidation. Owing to extensive reworking the original sediment composition or depositional environment of the phosphate sediment are uncertain. The deposit is no longer associated with the host sediment but has been reworked into younger sediments. This assumption holds true for the Gravel member as well. The Gravel member shows evidence of episodic sediment-reworking and subsequent re-phosphatisation. According to Glenn and Arthur (1988), periodic erosion, bioturbation and winnowing of organic-rich sediments may in fact promote peloidal grain concentration and nodule growth. Glenn and Arthur (1988) argue that below certain sediment depths, excessive carbonate ion concentrations and diminished reactive Fe and sulfate concentrations can favour the precipitation of dolomite instead of CFA during diagenesis.

A reworking/re-phosphatisation model is envisioned for the phosphorites from the Varswater Formation. The exact nature of the early diagenesis is not known, however the assumption is made that the process is similar to that outlined by Trappe (1998). On the basis of the Ce-anomalies, the phosphorites were formed in suboxic to anoxic conditions. This is consistent with traditional views on phosphogenesis, however due to the lack of stable isotope (C, Sr, O, and S) data the hypothesis cannot be tested. The components (peloids, cement etc.) of the Gravel member and the peloids from the Pelletal Phosphorite member are similar in terms of their trace-element and rare-earth element geochemistry. The phosphatised shell fragments and bone fragments from the Pelletal Phosphorite member are geochemically different and may represent other phosphatisation events, unrelated to the phosphatisation event that created the Gravel member. The difference

may also be related to a different geochemical signature that has been imparted by the precursor shell and bone material onto the phosphatised bioclast.

In contrast to the Varswater Formation phosphorites, the Bomgat phosphorites show little evidence of re-deposition or erosion. The relative abundance of the phosphatised micrite/CFA cement and the nature of the bioclasts indicate that the carbonate precursor was deposited in a low-energy depositional environment. The precursor carbonate was subsequently replaced by CFA. Similar to the Varswater Formation the original organic-rich sediments that hosted or facilitated the phosphatisation have been removed. The aluminium phosphate deposits are very different from the marine phosphorites (onshore and offshore). The deposits on the Posberg peninsula are believed to be leached guano deposits.

8.8 DIAGENETIC ALTERATION OF THE PHOSPHORITE DEPOSITS

The offshore phosphorite samples contain glauconite and pyrite. Many of the glauconite grains are rounded and may have been reworked prior to cementation by CFA. The pyrite occurs distributed in the CFA cement. The onshore phosphorites do not contain pyrite or glauconite. The absence of glauconite and pyrite from the onshore phosphorites may indicate that it was not present originally or that the glauconite and pyrite have since been removed by alteration of the phosphorite. Alteration most likely included subaerial to supergene weathering of the phosphorites, as the area was subaerially exposed over much of the Tertiary during lowering of sea level as well as tectonic uplift. Francolite is known to be vulnerable to chemical alteration during weathering, diagenesis and metamorphism (Flicateaux and Lucas, 1984; McArthur, 1985; McArthur *et al.*, 1987; McArthur and Herczeg, 1990). Francolite is generally protected by associated carbonates which increases its field of stability and buffers it from corrosive acidic pore waters (Nathan and Sass, 1981). According to Van Kauwenbergh *et al.* (1990) the removal of carbonates by dissolution results in the alteration of highly carbonate substituted francolites to low carbonate varieties. In other words the weathering of francolite results in the loss of carbonate and possibly F from the structure and the mineral evolves to a fluorapatite. McArthur and Herczeg (1990) provide isotopic evidence that the phosphorite from the Varswater Quarry may have been altered by meteoric diagenesis. Extreme chemical alteration of marine CFA may result in the formation of aluminium phosphates (Parron and Nahon, 1980). These aluminium phosphates include the following minerals: augelite, beraunite, cacoxenite, crandallite, goyazite, Ca-millisite, turquoise, varsicite, vivianite, wardite and wavellite (Nriagu and Moore, 1984). According to Dill (2001) the alteration of CFA to aluminium phosphate is expressed by a depletion in Sr, Ca, Na and F. During intensive weathering (when the lithology is depleted in Ca) meteoric waters become more acidic which results in various APS (aluminium-phosphate-sulphate) minerals being formed (Dill, 2001). According to Nriagu (1976) crandallite and wavellite forms under low phosphate concentrations whereas montgomeryite form under higher concentrations. However the amount of amorphous $Al(OH)_3$ available in the weathering system determines the type of APS mineral (Dill, 2001).

Aluminium phosphates are also found in association with guano deposits. Bird guano is generally composed of urine and faecal matter. Both are generally phosphate-rich and

related to the metabolic cycle of the bird and the phosphate content of the food supply (Ayliffe *et al.,* 1992). Guano deposits are formed either directly or indirectly from the accumulation of bird droppings (Cook, 1984; Flicoteaux and Lucas, 1984). The leaching of guano deposits by meteoric waters results in chemical weathering of most rocks (igneous, sedimentary etc.). In particular the leaching and weathering of limestone may result in calcium phosphate minerals, such as brushite, whitlockite, and hydroxylapatite (Flicoteaux and Lucas, 1984). Similar weathering of igneous rocks and soils may result in the formation of aluminium and iron phosphate minerals (e.g. varsicite). The mineralogy of the Posberg Peninsula aluminium phosphates is generally crandallite (calcium aluminium phosphate) and varsicite. The crandallite appears within the phosphatic soils from Kreeftebay, whereas varsicite appears readily in the Konstabelkop and Kreeftebay weathered quartz porphyry samples. Crandallite may have been formed within the phosphatic soils due to the weathering of CFA (within the soils) by meteoric waters. The occurrence of varsicite in the weathered phosphate crusts from the Konstabelkop and Kreeftebay quartz porphyry is consistent with the leaching of guano by meteoric water and subsequent chemical weathering of the quartz porphyry.

CHAPTER 9
CONCLUSIONS AND RECOMMENDATIONS

9.1 CONCLUSIONS

The preceding chapters outlined the mineralogy, rare-earth and trace-element geochemistry of the phosphorites and phosphate rocks from selected sites around the southwestern cape. The following is a summary of the main conclusions drawn in the preceding chapters.

9.1.1 Mineralogy

The phosphorites from Varswater Quarry are shown to have a mineralogy of primarily quartz and francolite (CFA), whereas the phosphorite from Bomgat is composed of predominantly dahllite. Occasional calcite is also present. The offshore phosphorites are composed of predominantly glauconite, francolite (CFA) and quartz with occasional pyrite. The mineralogy for the various phosphorites is consistent with the literature on marine phosphorites. The aluminium phosphate deposits show a vastly different mineralogy to the marine phosphorites (onshore and offshore). The mineralogy of the aluminium phosphates is determined to be either crandallite or varsicite. The mineralogy is consistent with the weathering of igneous rocks and CFA by the leaching of guano by meteoric water, resulting in the aluminium phosphates.

9.1.2. Geochemistry

The PAAS-normalised REE patterns of the offshore and onshore marine phosphorites show generally flat, heavy REE (HREE) enriched, relative to light REE (LREE) patterns, with no to slight Ce-anomalies. The various deposits are distinguishable on the basis of their REE patterns. For example the phosphorites from Varswater Formation show mid-to-HREE enrichment relative to LREE. The Bomgat phosphorites and offshore phosphorites show similar flat HREE enriched patterns, however the Bomgat phosphorites do not show the distinctive MREE-HREE enrichment. The offshore phosphorites show variable patterns. None of the phosphorites (onshore and offshore) show pronounced negative Ce-anomalies, however Eu-anomalies are found on some of the offshore phosphorites. The REE patterns of the aluminium phosphate deposits from Kreefte Bay are "toothed" and reflect the aluminium phosphates dissimilar chemical composition. The REE patterns for the Gravel member components (peloids, cement and biogenic) are generally similar, however the REE patterns for the Pelletal Phosphorite member components are different. It is possible to distinguish between peloids and phosphatised shell fragments (and phosphatised bone) of the Pelletal Phosphorite member using the REE patterns. The REE patterns for the shell fragments and phosphatised bone fragments show an inclined flat shape, with pronounced HREE enrichment, relative to the LREE. The phosphatised shell fragments and bone fragments also show slightly higher La/Lu ratios. The REE patterns for the Gravel member peloids and cement are similar to the Pelletal Phosphorite member peloids and cement, however the REE abundances for

the Gravel member are generally higher than the Pelletal Phosphorite member. Ce-anomalies (Ce/Ce*), determined for the various phosphorite and phosphate rocks show that the phosphorite and phosphate rocks have slightly negative to positive Ce-anomalies, therefore implying that the deposits gained their REE under suboxic oxygenation. The MREE-HREE enrichment found within the Varswater Formation is consistent with precipitation in seawater or groundwater.

The phosphorites are enriched in Sr, U, Zr, Rb and Y, whereas the aluminium phosphate deposits are notably enriched in Zr, Pb, Th, V and Rb. In terms of the trace-elements it is possible to make a geochemical distinction between the peloids and the phosphatised shell fragments of the Pelletal Phosphorite member.

9.1.3. General

The Gravel member phosphorite shows evidence of subsequent reworking and re-phosphatisation. On the basis of the geochemical and petrographic investigation phosphatisation occurred in a marine setting, however post-phosphogenesis groundwater-induced phosphatisation or alteration cannot be excluded. The consolidated phosphorites and the unconsolidated phosphate-rich sands are texturally similar, however the consolidated phosphorite grains are cemented by CFA. The lithification of the consolidated phosphorites occurred due to the precipitation of authigenic apatite within the pore spaces of the phosphate-rich sediments (Dingle *et al.*, 1979; Tankard, 1974a), however whether the setting was marine is debatable. An alternative hypothesis would be CFA precipitation between the grains (peloids, quartz and phosphatised shell fragments) from P-rich groundwater. The consolidated phosphorite is texturally very different from the marine offshore phosphorites. The geochemical similarity between the Gravel member peloids, cement and the Pelletal Phosphorite member peloids indicates that the peloids from the Pelletal Phosphorite member are in fact erosional remnants from the Gravel member. In contrast to the Varswater Formation phosphorites the Bomgat phosphorites show little evidence of re-deposition or erosion. The relative abundance of the phosphatised micrite/CFA cement and the nature of the bioclasts indicate that the carbonate precursor was deposited in a low-energy depositional environment. The precursor carbonate was subsequently replaced by CFA.

9.2. RECOMMENDATIONS

A number of problems remain unresolved, including the following:

- The exact setting of phosphatisation of the onshore phosphorites is unclear (marine or groundwater?)

- The extent of onshore phosphorite alteration by weathering (meteoric and groundwater?)

Further work should be carried out using stable isotopes (e.g. C, O, S, and Sr). Carbon and sulphur isotopes can be used to determine (or differentiate) the phosphogenesis among oxic, suboxic or anoxic (sulphate-reducing) environments. In this regard rare-earth elements should by no means be seen as an alternative to isotope studies. The dating of the deposits (using $^{87}Sr/^{86}Sr$) is possible, however due to unanticipated technical difficulties (instrument failure), isotope and age determination using Sr-isotopes were unfortunately not attempted in this study. Further research should expand the REE and trace-element data set and possibly attempt comparisons of other offshore phosphorite deposits (i.e. the concretionary phosphorites from Walvis Bay) with onshore sedimentary phosphate deposits. The extent of phosphorite alteration needs to be addressed; preferably using stable isotopes (C and O). Additional research needs to be done on the aluminium phosphate deposits of the Posberg peninsula, concerning major oxides, and trace-elements.

REFERENCES

Abed, A.M. and Fakhouri, K. (1996) On the chemical variability of phosphatic particles from the Jordanian phosphorite deposits. *Chem. Geol*, **131**: 1 - 13.

Altschuler, Z.S., Cisney, E.A. & Barlow, I.H. (1952) X-ray evidence of the nature of carbonate apatite. *Bulletin Geological Society of America*, **63**: 1230 – 1231.

Altschuler, Z.S., 1973. The weathering of phosphate deposits — geochemical and environmental aspects. In: Griffith, E., Beeton, Al., Spencer, J. and Mitchell, D., (Eds.). *Environmental Phosphorous Handbook*, Wiley, New York, pp. 33–96.

Altschuler, Z.S. (1980) The geochemistry of trace elements in marine phosphorites. Part 1. Characteristic abundance and enrichment. In: Bentor, Y.K. (Ed.). Marine Phosphorites. *Soc. Econ. Paleontol. Mineral. Spec. Publ.*, **29**: 19 - 30.

Aubert, D., Stille, P. and Probst, A. (2001) REE fractionation during granite weathering and removal by waters and suspended loads: Sr and Nd isotopic evidence, *Geochim. Cosmochim. Acta.*, **65**: 387 - 406.

Ayliffe, L.K., Veeh, H.H. and Chivas, A.R. (1992) Oxygen isotopes of phosphate and the origin of island apatite deposits, *Earth Planet. Sci. Lett.*, **108**: 119 - 129.

Baker, K.B. and Burnett, W.C. (1988) Distribution, texture and composition of modern phosphate pellets in Peru shelf muds. *Mar Geol.*, **80**: 195 – 213.

Balson, P. (1990) Episodes of phosphogenesis and phosphorite concretion formation in the North Sea Tertiary, In: Northolt, A.J.G. & Jarvis, I. (Eds.). Phosphorite Research and Development. *Geological Society Special Publication.*, **52**: 125 - 137.

Banfield, J.P. and Eggleton, R.A. (1989) Apatite replacement and rare earth mobilization, fractionation and fixation during weathering. *Clays Clay Miner.*, **37**: 113 - 127.

Baturin, G.N. (1982) Phosphorites on the Sea Floor: Origin, Composition, and Distribution. Elsevier, Amsterdam. *Developments in Sedimentology.*, **33**: 343.

Baturin, G. N. (2000) Formation and evolution of phosphorite grains and nodules on the Namibian shelf, from recent to Pleistocene, In: Glen, G. R., Prevot-Lucas, L and Lucas, J. (Eds.). Marine Authigenesis from Global to Microbial: Tulsa, *Society of Sedimentary Geology, (SEPM) Special Publication*, **66**: 185 – 199.

Baturin, G.N. and Bezrukov, P.L. (1979) Phosphorites on the sea floor and their origins. *Mar Geol.*, **31**: 317 – 332.

Bentor, Y.K. (1980) Phosphorites – the unresolved problems. *Soc. Econ. Paleontol. Mineral. Spec. Pub.*, **29**: 3-18.

Bertram, C.J and Elderfield, H. (1993) The geochemical balance of the rare earth elements and neodymium isotopes in the oceans. *Geochim. Cosmochim. Acta.*, **57**: 1957 - 1986.

Birch, G.F. (1975) *Sediments on the Continental Margin off the West Coast of South Africa.* Unpubl.PhD Project, Dept Geol. Sciences, Univ. Cape Town, 210pp

Birch, G.F. (1979a) Phosphorite pellets and rock from the western continental margin and adjacent coastal terrace of South Africa. *Mar Geol.*, **33**: 91 – 116.

Birch, G.F. (1979b) Phosphatic rocks on the western margin of South Africa. *J. Sed. Petrol.*, **49**: 93 – 110.

Birch, C.F. (1979c) The nature and origin of mixed apatite/glauconite pellets from the continental shelf off South Africa. *Mar Geol.*, **29**: 313 – 334.

Birch, C.F. (1980) A model of penecontemporaneous phosphatisation by diagenetic and authigenic mechanisms from the western margin of southern Africa. In: Bentor, Y.K. (Ed.), Marine Phosphorites: Geochemistry, Occurrence, Genesis. *Soc. Econ. Paleontol. Mineral. Spec. Publ.*, **29**: 3 – 18.

Boggs. S, 1995, *Principles of Sedimentology and Stratigraphy*, 2nd ed.: Prentice Hall, New Jersey, 773pp.

Bremner, J.M. (1980a) Concretionary phosphorite from southwest Africa. J. *Geol, Soc. London.*, **137**: 773 - 786.

Bremner, J.M. (1980b) Physical parameters of the diatomaceous mud belt off south west Africa. *Mar Geol.*, **34**: M67 – M76.

Bremner, J.M. and Rogers, J. (1990) Phosphorite deposits on the Namibian continental shelf, In: Burnett, W.C. and Riggs, S.R. (eds.) *Phosphate Deposits of the World, v3: Neogene to Modern Phosphorites*: Cambridge University Press, **4**: 143 – 152.

Burnett, W.C. and Riggs, S.R. (eds.) (1990) *Phosphate Deposits of the World, v3: Neogene to Modern Phosphorites:* Cambridge University Press, 464 pp.

Byrne, R.H., Liu, X. and Schuf, J. (1996) The influence of phosphatic coprecipitation on rare-earth distribution in natural waters, *Geochim. Cosmochim. Acta.*, **60**: 3341 - 3346.

Coetzee, J.A. & Rogers, J. (1982) Palynological and lithological evidence for the Miocene Paleoenviroment in the Saldanha Region (South Africa), *Paleogeography, Paleoclimatology, Paleoecology*, **39**: 71 – 85.

Compton, J.S., Mulabisana, J. and McMillan, I.K. (2002) Origin and age of phosphorite from the Last Glacial Maximum to Holocene transgressive succession off the Orange River, South Africa. *Mar Geol.*, **186**: 243 – 261.

Compton, J.S. White, R.A. and Smith, M. (in press) Rare earth element behaviour in soils and salt pan sediments of a semi-arid granitic terrain in the Western Cape, South Africa.

Cook, P.J. and McElhinny, M.W. (1979) A re-evaluation of the spatial and temporal distribution of sedimentary phosphate deposits in the light of plate tectonics. *Econ. Geol.*, **74**: 315 – 330.

Cook, P.J. (1984) Spatial and temporal controls on the formation of phosphate deposits – A review. In: Nriagu, J.O and Moore, P.H (eds.) *Phosphate Minerals*, Springer Verlag: 243 – 274.

Cruse, A.M., Lyons, T.W. and Kidder, D.L. (2000) Rare-earth element behaviour in phosphates and organic-rich host shales: an example from the Upper Carboniferous of mid-continent North America, In: Glen, G. R., Prevot-Lucas, L and Lucas, J. (Eds). Marine Authigenesis from Global to Microbial: Tulsa, *Society of Sedimentary Geology (SEPM) Special Publication*, **66**: 445 – 453.

Dale, D.C. and McMillan, I.K (1999) *On the Beach, A field guide to the Late Cainozoic micropalaeontological history, Saldanha region*, South Africa, De Beers Marine, Cape Town, 127pp

De Baar, H.J.W., Bacon, M.P. and Brewer, P.G. (1985a) Rare earth elements in the Pacific and Atlantic Oceans. *Geochim. Cosmochim. Acta.*, **49**: 1943 - 1959.

De Baar, H.J.W., Brewer, P.G. and Bacon, M.P. (1985b) Anomalies in rare earth distributions in sea water; Gd and Tb. *Geochim. Cosmochim. Acta.*, **49**: 1961 - 1969.

De Baar, H.J.W., German, C.R., Elderfield, H., van Gaans, P. (1988) Rare earth element distributions in anoxic waters of the Cariaco Trench. *Geochim. Cosmochim. Acta.*, **52**: 1203 - 1219.

Deer, W.A., Howie, R.A. and Zussman, J. (1992) *An Introduction to the Rock Forming Minerals*, 2nd ed. Longman Scientific and Technical, Essex, England, 696pp.

Dill, H.G. (2001) The geology of aluminium phosphates and sulphates of the alunite group: a review. *Earth Science Reviews.*, **53**: 35 -93.

Dingle, R.V., Lord, A.R. and Hendey, Q.B. (1979) New sections in the Varswater Formation (Neogene) of the Langebaan Road, south-western Cape, South Africa. *Ann.S.Afr.Mus.*, **78**: 81 – 92.

Du Toit, A.L. (1917) Report on the phosphates of Saldanha Bay. *Mem. geol. Surv. S. Afr*, **10**: 1- 38.

Dypvik, H., and Brunfelt, A.O. (1979) Distribution of rare earth elements in some North Atlantic Kimmeridgian black shales. *Nature*, **278**: 339 - 341.

Elderfield, H. and Greaves, M. (1982) The rare earth elements in sea water. *Nature*, **296**: 214 - 219.

Elderfield, H. and Sholkovitz, E.R. (1987) Rare earth elements in the pore waters of reducing nearshore sediments. *Earth Planet. Sci. Lett.*, **82**: 280 - 288.

Elderfield, H., Upstill-Goddard, R. and Sholkovitz, E.R. (1990) The rare earth elements in rivers, estuaries, and coastal areas and their significance to the composition of ocean waters. *Geochim. Cosmochim. Acta.*, **54**: 971 - 991.

Fleischer, M. and Altschuler, Z.S. (1969) The relationship of the rare-earth composition of minerals to geological environment. *Geochim. Cosmochim. Acta.*, **33**: 725 - 732.

Flicoteaux, R. and Lucas, J. (1984) Weathering of phosphate minerals. In: Nriagu, J.O and Moore, P.H (eds.) *Phosphate Minerals*, Springer Verlag: 292 – 317.

Franceschini, G. (2003) *Geology of Aeolian and Marine Deposits in the Saldanha Bay region, Western Cape, South Africa.* Unpubl.PhD Project, Dept Geol. Sciences, Univ. Cape Town, 276pp.

Froelich, P.N., Kim, K.H., Jahnke, R., Burnett, W.C., Soutar, A. and Deakin, M. (1983) Pore water fluoride in Peru continental margin sediments: uptake from sea water, *Geochim. Cosmochim. Acta.*, **47**: 1905 - 1912.

Garrison, R.E. and Kastner, M. (1990) Phosphatic sediments and rocks recovered from the Peru margin during ODP Leg 112. *Proc. ODP Sci. Results.*, **112**: 111 – 134.

Glenn, C.R. and Arthur, M.A. (1988) Petrology and major element geochemistry of Peru margin phosphorites and associated diagenetic minerals: Authigenesis in modern organic-rich sediments. *Mar Geol.*, **80**: 231 – 267.

Glenn, C.R., Follmi, K.B., Riggs, S.R., Baturin, G.N., Grimm, K.A., Trappe, J., Abed, A.M., Galli-Olivier, C., Garrison, R.E., Ilyin, A.V., Jehl, C., Rohrlich, V., Sadaqah, R.M.Y., Schidlowski, M., Sheldon, R.E. and Siegmund, H. (1994) Phosphorus and phosphorite: Sedimentology and environments of formation. *Eclogae Geol. Helv.*, **87**: 747 – 788.

Goldstein, S.L. and Jacobsen, S.B. (1988) REE in the Great Whale River estuary, northwest Quebec. *Earth Planet. Sci. Lett.*, **88**: 241 - 252.

Grandjean-Lécuyer, P., Feist, R. and Albarede, F. (1993) Rare earth elements in old biogenic apatites. *Geochim. Cosmoschim. Acta.*, **57**: 2507 – 2514.

Gulbrandsen, R.A. (1966) Chemical composition of phosphorites of the Phosphoria Formation. *Geochim. Cosmoschim. Acta.*, **30**: 769 – 778.

Hannigan, R.E. and Sholkovitz, E.R. (2001) The development of middle rare earth element enrichments in freshwaters: weathering of phosphate minerals. *Chem. Geol*, **175**: 495 - 508.

Hendey, Q.B. (1973) Fossil occurrences at Langebaanweg, Cape Province. *Nature*, **244**:13-14

Hendey, Q.B. (1974) The late Cenozoic Carnivora of the south-western Cape Province. *An.S.Afr.Mus.*, **63**: 1-369.

Hendey, Q.B. (1976) The Pliocene fossil occurrences in 'E' Quarry, Langebaanweg, South Africa. *Ann.S.Afr.Mus.*, **69**: 215-247.

Hendey, Q.B. (1980) *Agriotherium* (Mamalia, Ursidae) from Langebaanweg, South Africa, and relationships of the genus. *Ann. S.Afr.Mus.*,**81**: 53-63.

Hendey, Q.B. (1981a) Paleoecology of the Late Tertiary fossil occurrences in 'E' Quarry, Langebaanweg, South Africa, and a reinterpretation their geological context. *Ann. S. Afr. Mus.*, **84**: 1 – 89.

Hendey, Q.B. (1981b) A geological succession at Langebaanweg, Cape Province, and global events of the Late Tertiary. *S. Afr. J. Sci.*, 77: 33 –38

Hendey, Q.B. (1982) *Langebaanweg, a Record of Past Life*, South African Museum, Cape Town, Rustica Press (Pty) Ltd, Wynberg, 71pp.

Hendey, Q.B. and Dingle, R.V. (1983) *Technical Rep. Joint Geol.Surv/University of Cape Town Marine Geoscience Unit,* 14, 27.

Hendey, Q.B. and Deacon, H.J. (1977) Studies in palaeontology and archaeology in the Saldanha region, *Trans. Roy. Soc. Afr.*, **42**: 371 – 381.

Hoyle, J., Elderfield, H., Gledhill, A. and Greaves, M. (1984) The behaviour of the rare earth elements during the mixing of river and sea waters. *Geochim. Cosmochim. Acta.*, **48**: 143 - 149.

Ilyin, A. V. (1998) Rare-earth geochemistry of "old" phosphorites and probability of syngenetic precipitation and accumulation of phosphate. *Chem. Geol.,* **144**: 243 – 256.

Jarvis, I., Burnett, W.C., Nathan, Y., Almbaydin, F.S.M., Attia, A.K.M., Castro, L.N., Flicoteaux, R., Hilmy, M.E., Husain, V., Qutawnah, A.A., Serjani, A. and Zanin, Y.N. (1994) Phosphorite geochemistry: state-of-the-art and environmental concerns, *Eclogae. geol. Helv.,* **87**: 643-700.

Johannesson, K.H., Berry Lyons, W., Yelken, M.A., Gaudette, H.E. and Stetzenbach, K.J. (1996) Geochemistry of the rare-earth elements in hypersaline and dilute acidic natural terrestrial waters: Complexation behavior and middle rare-earth element enrichments, *Chem. Geol.,* **133**: 125-144.

Johnson, M.R. (1994) *Lexicon of South African Stratigraphy. Part One: Phanerozoic Units. S. Afr. Counc. Geosci.,* Pretoria.

Kasten, S., Glasby, G.P. Schultz, H.D., Friedrich, G. and Andreev, S.I. (1998) Rare earth elements in manganese nodules from the South Atlantic Ocean as indicators of oceanic bottom water flow. *Mar. Geol.*, **146**: 33 – 52.

Kensley, B. (1977) A second assemblage of Pliocene invertebrate fossils from Langebaanweg, Cape. *Ann. S. Afr. Mus.,* **72**: 189 - 210

Kidder, D.L. and Eddy-Dilek, C.A. (1994) Rare-earth element variation in phosphate nodules from mid-continent Pennsylanian cyclothems, *J. Sed. Res.*, **A64**: 584 - 592.

Kidder, D.L., Krishnaswamy, R. and Mapes R.H. (2003) Elemental mobility in phosphatic shales during concretion growth and implications for provenance analysis, *Chem. Geol.*,**198**: 335-353.

Koeppenkastrop, D. and De Carlo, E.H. (1993) Uptake of rare earth elements from solution by metal oxides, *Environ. Sci. Techn.,* **27**: 1796 - 1802

Kolodny, Y. (1981) Phosphorites. In: Emiliani, C. (ed.) *The Sea.* John Wiley and Sons, New York, 981 -1083.

Lécuyer, C., Grandjean, P., Barrat, J., Nolvak, J., Emig, C., Paris, F. and Robardet, M. (1998) d18O and REE contents of phosphatic brachiopods: A comparison between modern and lower Palaeozoic populations. *Geochim. Cosmoschim. Acta.*, **62**: 2429 – 2436.

Leleyter, L., Probst, J., Depetris, P., Haida, S., Mortatti, J., Rouault, R. and Samuel, J. (1999) REE distribution pattern in river sediments: partitioning into residual and labile fractions. *Earth Planet. Sci.*, **329**: 45 – 52.

Hendey, Q.B. and Dingle, R.V. (1983) *Technical Rep. Joint Geol.Surv/University of Cape Town Marine Geoscience Unit,* 14, 27.

Hendey, Q.B. and Deacon, H.J. (1977) Studies in palaeontology and archaeology in the Saldanha region, *Trans. Roy. Soc. Afr.*, **42**: 371 – 381.

Hoyle, J., Elderfield, H., Gledhill, A. and Greaves, M. (1984) The behaviour of the rare earth elements during the mixing of river and sea waters. *Geochim. Cosmochim. Acta.*, **48**: 143 - 149.

Ilyin, A. V. (1998) Rare-earth geochemistry of "old" phosphorites and probability of syngenetic precipitation and accumulation of phosphate. *Chem. Geol.*, **144**: 243 – 256.

Jarvis, I., Burnett, W.C., Nathan, Y., Almbaydin, F.S.M., Attia, A.K.M., Castro, L.N., Flicoteaux, R., Hilmy, M.E., Husain, V., Qutawnah, A.A., Serjani, A. and Zanin, Y.N. (1994) Phosphorite geochemistry: state-of-the-art and environmental concerns, *Eclogae. geol. Helv.*, **87**: 643-700.

Johannesson, K.H., Berry Lyons, W., Yelken, M.A., Gaudette, H.E. and Stetzenbach, K.J. (1996) Geochemistry of the rare-earth elements in hypersaline and dilute acidic natural terrestrial waters: Complexation behavior and middle rare-earth element enrichments, *Chem. Geol.*, **133**: 125-144.

Johnson, M.R. (1994) *Lexicon of South African Stratigraphy. Part One: Phanerozoic Units. S. Afr. Counc. Geosci.*, Pretoria.

Kasten, S., Glasby, G.P. Schultz, H.D., Friedrich, G. and Andreev, S.I. (1998) Rare earth elements in manganese nodules from the South Atlantic Ocean as indicators of oceanic bottom water flow. *Mar. Geol.*, **146**: 33 – 52.

Kensley, B. (1977) A second assemblage of Pliocene invertebrate fossils from Langebaanweg, Cape. *Ann. S. Afr. Mus.*, **72**: 189 - 210

Kidder, D.L. and Eddy-Dilek, C.A. (1994) Rare-earth element variation in phosphate nodules from mid-continent Pennsylanian cyclothems, *J. Sed. Res.*, **A64**: 584 - 592.

Kidder, D.L., Krishnaswamy, R. and Mapes R.H. (2003) Elemental mobility in phosphatic shales during concretion growth and implications for provenance analysis, *Chem. Geol.*,**198**: 335-353.

Koeppenkastrop, D. and De Carlo, E.H. (1993) Uptake of rare earth elements from solution by metal oxides, *Environ. Sci. Techn.*, **27**: 1796 - 1802

Kolodny, Y. (1981) Phosphorites. In: Emiliani, C. (ed.) *The Sea.* John Wiley and Sons, New York, 981 -1083.

Lécuyer, C., Grandjean, P., Barrat, J., Nolvak, J., Emig, C., Paris, F. and Robardet, M. (1998) d18O and REE contents of phosphatic brachiopods: A comparison between modern and lower Palaeozoic populations. *Geochim. Cosmoschim. Acta.*, **62**: 2429 – 2436.

Leleyter, L., Probst, J., Depetris, P., Haida, S., Mortatti, J., Rouault, R. and Samuel, J. (1999) REE distribution pattern in river sediments: partitioning into residual and labile fractions. *Earth Planet. Sci.*, **329**: 45 – 52.

Liu, Y.G., Miah, M.RU. and Schmitt., R.A. (1988) Cerium: a chemical tracer for paleo-oceanic redox conditions. *Geochim. Cosmochim. Acta.*, **52**: 1361 - 1371.

Lucas, J., El Faleh, E. and Prevot, L. (1990) Experimental study of the substitution of Ca by Sr and Ba in synthetic apatites, In: Northolt, A.J.G. & Jarvis, I. (eds.). Phosphorite Research and Development. *Geological Society Special Publication,* **52**: 33 - 47.

Martin, J.M., Hogdahl, O. and Philipott, S.C. (1976) Rare earth element supply to the ocean. *J. Geophys. Res.*, **81**: 3119 - 3124.

McArthur, J.M. (1985) Francolite geochemistry - compositional controls during formation, diagenesis, metamorphism and weathering. *Geochim. Cosmochim. Acta.*, **49**: 23 - 35.

McArthur, J.M., Hamilton, P.J., Greensmith. J.T., Walsh. J.N., Boyce, A.B., Fallick, A.E., Birch, G., Benmore, R.A. and Coleman, M.L. (1987) Francolite geochemistry – meteoric alteration on a local scale. *Chem. Geol.* **65**: 415 -425.

McArthur, J.M., and Herczeg, A. (1990) Diagenetic stability of the isotopic composition of phosphate-oxygen: Palaeoenvironmental implications. In: Northolt, A.J.G. & Jarvis, I. (eds.). Phosphorite Research and Development. *Geological Society Special Publication,* **52**: 119 - 124.

McArthur, J.M., and Walsh, J.N. (1984) Rare-earth geochemistry of phosphorites. *Chem. Geol.*, **47**: 191-220.

McClellan, G.H. and van Kauwenbergh, S.J. (1990) Mineralogy of sedimentary apatites. In: Northolt, A.J.G. & Jarvis, I. (eds.). Phosphorite Research and Development. *Geological Society Special Publication,* **52**: 23 - 31.

McConnell, D. (1938) A structural investigation of the isomorphism of the apatite group. *Amer. Mineral*, **23**: 1 – 19.

McConnell, D. (1973) *Apatite – Its Crystal Chemistry, Mineralogy, Utilization and Geologic and Biologic Occurrences,* Springer Verlag, Vienna-Heidelberg. 111pp.

Middleton, X. N. (2000) *The Sedimentology and Stratigraphy of Varswater Quarry, Langebaanweg*, Unpubl.Honours Project, Dept Geol. Sciences, Univ. Cape Town, 78pp

Moffett, J.W. (1990) Microbially mediated cerium oxidation in sea water. *Nature*, **345**: 421 - 423.

Mulabisana, M.J. (1998) *Petrographic Evidence for the Origin of Phosphorite Nodules from the Western Continental Shelf of South Africa.* Unpubl.Honours Project, Dept Geol. Sciences, Univ. Cape Town, 34pp

Murphy, K. and Dymond, J. (1984) Rare earth element fluxes and geochemical budget in the eastern equatorial Pacific. *Nature*, **307**: 444 - 447.

Murray, J. and Renard, A.F. (1891) Report on deep-sea deposits based on the specimens collected during the voyage of HMS Challenger. *Rep. Voy. Challenger 1873 – 1876* (Deep-sea deposits): 391-400.

Nath, B. N., Rao, B. R., Rao, K. M. and Rao, C. M. (2000) Rare-earth elements and uranium in phosphatic nodules from the continental margins of India, In: Glen, G. R., Prevot-Lucas, L and Lucas, J. (Eds). Marine Authigenesis from Global to Microbial: Tulsa, *Society of Sedimentary Geology (SEPM) Special Publication*, **66**: 222 – 232.

Nath, N.B., Roelandts, I., Sudhakar, M., Pluger, W.L. and Balaram., V. (1994) Cerium anomaly variations in ferromanganese nodules and crusts from the Indian Ocean. *Mar. Geol.*, **120**: 385 – 400.

Nathan, Y. (1984) The mineralogy and geochemistry of phosphorites. In: Nriagu, J.O and Moore, P.H (eds.) *Phosphate Minerals*, Springer Verlag: 275 – 291.

Nathan, Y. and Sass, E. (1981) Stability relations of apatites and calcium carbonates. *Chem. Geol.*, **34**: 103 -111.

Notholt, A.J.G. (1979) The economic geology and development of igneous phosphate deposits in Europe and the USSR. *Econ. Geol.*, **74**: 339 – 350.

Nriagu, J.O. (1976) Phosphate-clay mineral relations in soils and sediments. *Canadian Journal of Earth Science.*, **13**: 717 – 736.

Nriagu, J.O and Moore, P.H (1984) *Phosphate Minerals*, Springer Verlag, Berlin Heidelberg, 442pp.

Ogihara, S. (1999) Geochemical characteristics of phosphorite and carbonate nodules from the Miocene Funakawa Formation, western margin of the Yokote Basin, northeast Japan. *Sediment. Geol.*, **125**: 69 – 82.

Palmer, M.R. (1985) Rare earth elements in foraminifera tests. *Earth Planet. Sci. Lett.*, **73**: 285 - 298.

Parker, R.J. (1975) The petrology and origin of some glauconitic and glauco-conglomeratic phosphorites from the South African continental margin. *J. Sed. Petrol.*, **45**: 230 – 242.

Parker, R.J. and Siesser, W.G. (1972) Petrology and origin of some phosphorites from the south African continental margin. *J. Sed. Petrol.*, **42**: 434 – 440.

Parron, C. and Nahon, D. (1980) Red bed genesis by laterite weathering of glauconitic sediments. *J. Geol. Soc. Lon.*, **137**: 689 – 693.

Pether, J., Roberts, D.L. and Ward, J.D. (2000) Deposits of the West Coast, Chapter 3, In: Partridge, T.C. and Maud, R.R. (eds.) *The Cenozoic of South Africa*, Oxford University Press: 33 – 54.

Piper, D. (1974) Rare earth elements in the sedimentary cycle: a summary. *Chem. Geol.*, **14**: 285 -304.

Piper, D. Z., Veeh, H.H., Betrand, W. and Chase, R.L. (1975) An iron-rich deposit from the northeast Pacific. *Earth Planet. Sci. Lett.*, **26**: 114 – 120.

Piper, D.Z., Baedecker, P.A., Crock, J.G., Burnett, W.C. and Loebner, B.J. (1988) Rare earth elements in the phosphatic-enriched sediment of the Peru shelf. *Mar. Geol.*, **80**: 269 – 285.

Price, N.B. and Calvert, S.E. (1978) The geochemistry of phosphorites from the Namibian Shelf. *Chem. Geol.*, **23**: 151 – 170.

Rao, V. P., Michard, A., Naqvi, S.W.A., Bottcher, M.E., Krishnaswamy, R., Thamban, M., Natarajan, R. and Borole, D.V. (2002) Quaternary phosphorites off the southeast coast of India. *Chem. Geol.*, **182**: 483 - 502.

Rao, V. P., Naqvi, S. W. A., Kumar, M. D., Cardinal, D., Michard, A., Borole, D. V., Jacobs. E. and Natarajan, R. (2000) A comparative study of Pleistocene phosphorites from the continental slope of western India. *Sedimentology.*, **47**: 945 – 960.

Rasmussen, B., Buick, R. and Taylor, W.R. (1998) Removal of oceanic REE by authigenic precipitation of phosphatic minerals. *Earth Planet. Sci. Lett.*, **164**: 135 - 149.

Roberts, D.L. and Berger, L. (1997) Last interglacial (c. 117 kyr) human footprints from South Africa. *S.Afr.J.Sci*, .**93**, 349 -350.

Ronov, A.B., Balashov, Y.A. and Migdisov, A.A., (1967). Geochemistry of the rare earths in the sedimentary cycle. *Geochem. Int.*, **4**: 1 - 17.

Rogers, J. (1980) First report on the Cenozoic sediments between Cape Town and Eland's Bay. *Rep. geol. Surv. S.Afr.***165**:1-64.

Rogers, J. (1982) Lithostratigraphy of Cenozoic sediments between Cape Town and Bay. *Palaeoecology of Africa*, 15: 121 -137.

Ruttenberg, K.C. and Berner, R.A. (1993) Authigenic apatite formation and burial in sediments from non-upwelling, continental margin environments. *Geochim. Cosmochim. Acta.*, **57**: 991 - 1007.

Singer, R. and Hooijer, D.A. (1958) A Stegolophodon from South Africa, *Nature*. **182**: 101-102.

Singer, R. and Wymer, J. (1968) Archaeological investigations at the Saldanha skull site in South Africa. *S.Afr.Archaeol. Bull.*, 23, 63 - 75.

Shields, G. and Stille, P. (2001) Diagenetic constraints on the use of cerium anomalies as palaeoseawater redox proxies: an isotopic and REE study of Cambrian phosphorites. *Chem. Geol.*, **175**: 29 - 48.

Sholkovitz, E.R. (1978) The flocculation of dissolved Fe, Mn, Al, Cu, Ni, Co and Cd during estuarine mixing. *Geochim. Cosmochim. Acta.*, **41**: 77 - 86.

Sholkovitz, E.R., Landing, W.M., and Lewis, B.L. (1994) Ocean particle chemistry: The fractionation of rare earth elements between suspended particles and seawater. *Geochim. Cosmochim. Acta.*, **58**: 1567 - 1579.

Sholkovitz, E. and Szymczak, R. (2000) The estuarine chemistry of rare earth elements: comparison of the Amazon, Fly, Sepik and the Gulf of Papua systems. *Earth Planet. Sci. Lett.*, **179**: 299 - 309.

Smith, P.J.R. (1971) *Langebaan Phosphate Deposits.* Unpubl.Honours Project, Dept Geol. Sciences, Univ. Cape Town, 38pp.

Soudry, D., Ehrlich, S., Olga, Y. and Nathan, Y. (2002) Uranium oxidation state and related variations in geochemistry of phosphorites from Negev (southern Israel). *Chem. Geol.*, **189**: 213 – 230.

Stanley Jr, J.K. and Byrne, R.H. (1990) The influence of solution chemistry on REE uptake by *Ulva lactuca* L. in seawater. *Geochim. Cosmochim. Acta.*, **54**: 1587 - 1595.

Streusson, U. (1995) Llanvirnian (Ord.) iron ooids in Baltoscandia: element mobility, REE distribution patterns, and origin of the REE. *Chem. Geol.*, **125**: 45 – 60.

Summerhayes, C.P., Birch, G.F., Rogers, J. and Dingle, R.V. (1973) Phosphate in sediments off south-western Africa. *Nature*, **243**: 509 -511.

Swirydczuk, K., Wilkinson, B.H. and Smith, G.R. (1981) Synsedimentary lacustrine phosphorites from the Pliocene Glenns Ferry Formation of southwestern Idaho. *J. Sed. Petrol.*, **51**: 1205 – 1214.

Tankard, A.J. (1974a) Petrology and origin of the phosphorite and aluminium phosphate rock of the Langebaanweg-Saldanha area, south-western Cape Province. *Ann. S.Afr.Mus.*, **65**: 217-249.

Tankard, A.J. (1974b) Varswater Formation of the Langebaanweg-Saldanha area, Cape Province. *Trans.geol.Soc.S.Afr.*, **77**: 265 – 283.

Tankard, A.J. (1975) The Marine Neogene Saldanha Formation. *Trans.Geol.Soc.Afr.*, **78**: 257 –264.

Tankard, A.J. (1976) Pleistocene history and coastal morphology of the Ysterfontein-Eilands Bay area. *Ann. S.Afr.Mus.*, **69**: 73 - 119.

Taylor, S.R., and McLennan, S.M. (1985) *The Continental Crust, Its Composition and Evolution*, London, Blackwell, 312pp.

Thomson, J., Calvert, S.E., Mukherjee, S., Burnett, W.C. and Bremner, J.M. (1984) Further studies of the nature, composition and ages of contemporary phosphorite from the Namibian Shelf. *Earth Planet. Sci. Lett.*, **69**: 341 - 353.

Toyoda, K. and Tokonami, M. (1990) Diffusion of rare-earth elements in fish teeth from deep-sea sediments. *Nature*, **345**: 607 - 609.

Trappe, J. (1998) *Phanerozoic Phosphorite Depositional Systems, a Dynamic Model of Sedimentary Resource Systems*, Springer, Berlin Heidelberg, 316pp.

Turekian, K.K. and Wedepohl, K.H. (1961) Distribution of some major elements of the Earth's crust. *Bull. Geol. Soc. America.*, **72**: 172 – 195.

Van Kauwenbergh, S.J., Cathcart, J.B. and McClellan, G.H. (1990) Mineralogy and alteration of the phosphate deposits of Florida, *Bull. U.S. Geologic. Survey.* **1914**: 1 – 46.

Veeh, H.H., Burnett, W.C. and Soutar, A. (1973) Contemporary phosphorites on the continental margin of Peru. *Science*, **181**: 844 – 845.

Visser, H.N., and Schoch, A. E. (1973) The geology and mineral resources of the Saldanha Bay area. *Mem.Geol.Surv.S.Afr.*, **63**, i - iv: 1 –50

Watkins, R. T., Nathan, Y., Bremner, J. M. (1995) Rare-earth elements in phosphorite and associated sediment from the Namibian and South African continental shelves. *Mar. Geol.*, **129**: 111 – 128.

Wood, S.A. (1990) The aqueous geochemistry of the rare-earth elements and yttrium, 1. Review of available low temperature data for inorganic complexes and the inorganic REE speciation of natural waters. *Chem. Geol.*, **82**: 159 - 186.

Wright, J., Schrader, H. and Holser, W.T. (1987) Paleoredox variations in ancient oceans recorded by rare earth elements in fossil apatite. *Geochim. Cosmochim. Acta.*, **51**: 631 - 644.

Internet References

http://www.uct.ac.za/depts/geolsci/icpms/procedrs/bulkrock.html

A1. Inductively Coupled Plasma – Mass Spectroscopy (ICP-MS)

Table A1.1. Abundances of trace elements in the Varswater Formation phosphatic sands and Bomgat phosphorite (B1). All values in ppm (pph = peloidal phosphorite, psh = phosphatised shell fragments and bne=bone fragments).

Sample	Sr	Y	Pb	Th	U	V	Rb	Zr	Ta	Sc
vw1A3 (bulk)	958	37.1	14.7	4.1	18.5	19.7	43.8	20.1	0.1	2.9
vw1A3-pph-	2190	34.4	23.5	5.9	54	43	21.12	50.5	0.3	3.1
vw1A3-psh-	2110	37.8	33.9	1.8	28.1	38.4	4.99	29	0.5	2.5
vw1-0.2-pph-	2870	42.8	19.7	4.4	54.5	44	23.4	60.9	0.4	4.6
vw1-0.2-psh-	2067	37.6	34	1.9	34	33.7	3.19	28.3	0.3	2.4
vw1-1.31-pph	2270	44.2	25.9	4.7	23	34	27.6	62.2	0.3	4.9
vw1-1.31-psh	2532	45.3	22.3	2.2	33.4	46	5.89	33.6	0.6	3.1
vw1-1.72-pph	2892	39.8	22.1	7.6	57.1	57	24.2	50.8	0.3	4.4
vw1-1.72-psh	2151	65.3	29.3	2.6	32.5	42.4	2.93	22.3	0.3	4.1
vw1-1.90-pph-	1892	36.8	19.1	6.6	54.1	47	23.2	51.8	0.2	4
vw-1-1.90-psh-	2051	64.3	22.3	1.9	31.5	32.4	0.93	15.3	0.2	3.1
vw1-2.65-pph-	1950	56.7	21.6	6.7	44.4	38.6	22.8	51.3	0.3	4.2
vw1-2.65-psh-	2077	41.9	29.5	2.2	33.3	30.6	3.19	34.6	0.6	4.6
vw1-3.22-pph	2227	62.8	20.8	6.1	47.5	38.1	22.5	50.2	0.3	6.1
vw1-3.22-psh	2132	77.3	36.7	3.4	33.6	38.2	6.78	28.6	0.2	5.4
vw2a-0.5-pph-	1870	42.8	17.7	4.4	53.5	42	23.4	70.9	0.4	4.8
vw2a-0.5-psh	1991	65.3	27.3	3.9	37.5	42.4	4.93	12.3	0.3	3.2
vw2e-1.79-pph	1589	40.1	36.5	4.5	41.8	42.3	20.8	69.1	0.4	4.9
vw2e-1.79-psh	1395	45.5	19.4	2.7	27.5	30.5	3.4	9.78	0.2	2.6
vw2e-2.80-pph	2520	53.9	19.7	3.4	61.7	42.8	23.6	58.2	0.3	4.5
vw2e-2.80-psh	1876	56.4	24.4	3.5	37.8	39.9	4.37	12.3	0.3	3.3
vw36a2-0.98-pph	1624	34	38.1	7.8	58	60.9	21.9	65.8	0.3	4.7
vw36a2-0.98-psh	2765	56.3	45.5	3.5	45.6	53.5	6.7	38.8	0.7	3.4
VW13A-pph	1453	43.8	22.4	4.7	33.3	53.1	22.2	55.7	0.6	4.2
VW23C-pph	1059	127	26.3	8.0	12.8	52.7	14.7	65.5	0.2	5.5
vw461-bne	552	44.6	6.4	1	80.3	83.1	2.7	34.1	0.4	4.5
vw465-bne	1006	150	16.2	6.8	71.1	41.9	12.7	47.1	0.1	9.8
vw466-bne	789	56.6	11.3	5.6	65.1	51.3	6.3	27.1	0.3	9.6
vw461 (bulk)	379	27.6	4.6	0.9	56.5	59.4	4.3	26.4	0.1	3.4
B1	9080	1.47	1.8	0.4	15.9	26.9	2.7	54.5	0.1	0.3

Table A1.1. continues.

Sample	Cr	Co	Ni	Cu	Hf	Nb	Cs	Ba
vw1A3 (bulk)	75.7	1.5	7.0	5.9	0.5	1.9	1.2	169
vw1A3-pph-	120	16	22.1	30.9	1.2	2.6	1.3	78
vw1A3-psh-	82.6	8.5	20.6	23.9	0.5	0.7	0.7	79.3
vw1-0.2-pph-	133	16.8	15.2	24.2	1.5	2.5	1.8	115
vw1-0.2-psh-	86.5	9.1	9.3	24.7	0.6	0.8	0.5	75
vw1-1.31-pph	87.5	16.9	19.4	24	1.3	2.8	1.9	90.3
vw1-1.31-psh	87.6	11.5	11.5	24.5	0.6	0.7	0.7	78.3
vw1-1.72-pph	143	13.9	18.1	24	1.5	3.7	1.5	102
vw1-1.72-psh	83.9	11.3	12.9	14.3	0.2	0.6	0.6	68.6
vw1-1.90-pph-	153	14	16.1	14	1.2	2.8	1.6	99.1
vw-1-1.90-psh-	87.9	12.3	11.9	11.3	0.2	0.5	0.1	58.7
vw1-2.65-pph-	124	13.8	17.4	24	0.3	1.9	0.4	144
vw1-2.65-psh-	81.6	7.45	12.8	19.4	0.6	0.8	0.3	78.2
vw1-3.22-pph	136	4.87	12.2	14.6	1.1	2.6	1.6	111
vw1-3.22-psh	90.4	16.9	14.5	24.5	0.4	1	0.6	123
vw2a-0.5-pph-	143	11.8	15.2	20.2	1.5	2.6	1.5	135
vw2a-0.5-psh	88.9	13.3	12.9	17.3	0.4	0.3	0.2	68.9
vw2e-1.79-pph	274	5.2	70.4	74	1.5	2.7	1.4	180
vw2e-1.79-psh	78.4	9.3	9.2	12.3	0.2	0.3	0.1	69.5
vw2e-2.80-pph	149	9.6	14.5	20.5	1.2	2.3	1.8	115
vw2e-2.80-psh	98.4	11.6	12.6	15.6	0.3	0.4	0.2	89.4
vw36a2-0.98-pph	164	399	22.1	30.9	1.5	4	1.7	86.2
vw36a2-0.98-psh	112.4	11.4	27.8	32.6	0.7	0.9	0.7	104.5
VW13A-pph	129	10.5	21.4	17.8	1.2	3.2	1.5	105
VW23C-pph	62	14.1	15.2	18.6	1.3	2	0.8	108
vw461-bne	52.5	176	12.9	20.9	0.6	0.7	0.2	63.3
vw465-bne	102	18.4	23.7	27	1	0.7	0.4	176
vw466-bne	62.8	19.4	23.5	27	1	0.7	0.4	176
vw461 (bulk)	30.4	3.5	7.4	10.8	0.5	1.3	0.2	46.7
B1	35.7	1.8	9.72	48.7	1.1	1	0.2	110

Table A1.2. Samples from Langebaanweg and Bomgat (Hoedjiespunt) showing the indices La/Th, Th/U, La/Yb, La/Sc, Th/Sc, Cu/Cr, Ni/Co and V/Cr (pph = peloidal phosphorite, psh = phosphatised shell fragments and bne=bone fragments).

Sample	La/Th	Th/U	La/Yb	La/Sc	La/Sr	Th/Sc	Cu/Cr	Ni/Co	V/Cr
vw1A3 (bulk)	5.06	0.22	8.58	6.98	0.02	1.38	0.08	4.69	0.26
vw1A3-pph-	2.86	0.11	6.79	5.42	0.01	1.89	0.26	1.38	0.36
vw1A3-psh-	8.88	0.07	7.17	6.57	0.01	0.74	0.29	2.44	0.46
vw1-0.2-pph-	5.75	0.08	9.44	5.42	0.01	0.94	0.18	0.90	0.33
vw1-0.2-psh-	13.21	0.06	10.37	10.37	0.01	0.79	0.29	1.03	0.39
vw1-1.31-pph	6.77	0.21	11.39	6.49	0.01	0.96	0.27	1.15	0.39
vw1-1.31-psh	8.97	0.07	7.12	6.42	0.01	0.72	0.28	1.00	0.53
vw1-1.72-pph	3.54	0.13	9.89	6.05	0.01	1.71	0.17	1.30	0.40
vw1-1.72-psh	10.23	0.08	7.49	6.34	0.01	0.62	0.17	1.14	0.51
vw1-1.90-pph-	4.16	0.12	11.33	6.77	0.01	1.63	0.09	1.15	0.31
vw-1-1.90-psh-	13.62	0.06	7.25	8.52	0.01	0.63	0.13	0.97	0.37
vw1-2.65-pph-	3.90	0.15	4.79	6.17	0.01	1.58	0.19	1.25	0.31
vw1-2.65-psh-	8.49	0.07	7.67	4.15	0.01	0.49	0.24	1.72	0.38
vw1-3.22-pph	5.30	0.13	7.98	5.28	0.01	1.00	0.11	2.51	0.28
vw1-3.22-psh	10	0.10	7.06	6.43	0.02	0.64	0.27	0.86	0.42
vw2a-0.5-pph-	5.77	0.08	9.14	5.22	0.01	0.90	0.14	1.29	0.29
vw2a-0.5-psh	6.29	0.11	6.54	7.65	0.01	1.22	0.19	0.97	0.48
vw2e-1.79-pph	5.34	0.11	8.96	4.86	0.02	0.91	0.27	13.36	0.15
vw2e-1.79-psh	6.33	0.10	6.55	6.67	0.01	1.05	0.16	0.99	0.39
vw2e-2.80-pph	7.12	0.06	6.98	5.42	0.01	0.76	0.14	1.50	0.29
vw2e-2.80-psh	6.71	0.09	6.95	7.08	0.01	1.05	0.16	1.08	0.41
vw36a2-0.98-pph	3.12	0.14	10.52	5.13	0.02	1.64	0.19	0.06	0.37
vw36a2-0.98-psh	6.26	0.08	6.85	6.55	0.01	1.05	0.29	2.42	0.48
VW13A-pph	4.42	0.14	7.24	5.06	0.01	1.14	0.14	2.04	0.41
VW23C-pph	5.03	0.63	5.14	7.40	0.04	1.47	0.30	1.08	0.85
vw461-bne	3.66	0.01	0.68	0.82	0.01	0.23	0.40	0.07	1.58
vw465-bne	2.42	0.10	1.48	1.68	0.02	0.69	0.26	1.29	0.41
vw466-bne	2.72	0.09	1.26	1.60	0.02	0.59	0.43	1.21	0.82
vw461 (bulk)	3.85	0.02	1.08	1.12	0.01	0.29	0.36	2.09	1.95

Table A1.2. continues.

Sample	La/Th	Th/U	La/Yb	La/Sc	La/Sr	Th/Sc	Cu/Cr	Ni/Co	V/Cr
B1	2.53	0.03	6.31	3.48	0.00	1.38	1.36	5.17	0.75

Table A1.3. Abundances of rare-earth elements in the Varswater Formation phosphatic sands and Bomgat Phosphorite (B1). PAAS is included for comparison. All values given in ppm (pph = peloidal phosphorite, psh = phosphatised shell fragments and bne=bone fragments).

Sample	La	Ce	Pr	Nd	Sm	Eu	Gd	Tb	Dy	Ho	Er	Tm	Yb	Lu
PAAS	38.2	79.6	8.8	33.9	5.6	1.1	4.7	0.8	4.7	1.0	2.9	0.4	2.8	0.4
vw1A3 (bulk)	20.6	45.5	5.0	21.9	4.5	1.0	5.0	0.7	4.4	0.9	2.8	0.4	2.4	0.4
vw1A3-pph-	16.9	34.8	3.9	16.4	4.5	0.9	5.0	0.7	4.5	0.8	3.0	0.4	2.5	0.5
vw1A3-psh-	16.7	33.3	3.6	16.1	3.2	0.7	4.0	0.6	3.7	0.9	2.6	0.4	2.3	0.4
vw1-0.2-pph-	25.3	63.7	6.8	24.0	5.1	1.0	5.8	0.8	5.0	1.1	4.2	0.5	2.7	0.4
vw1-0.2-psh-	25.1	56.4	5.5	22.0	4.9	1.0	4.3	0.7	3.9	0.8	2.7	0.4	2.4	0.4
vw1-1.31-pph	32.3	68.5	7.4	31.4	6.0	1.0	6.5	0.8	5.5	1.1	3.2	0.5	2.8	0.5
vw1-1.31-psh	20.0	39.5	4.3	20.2	4.0	0.8	4.8	0.7	4.5	1.0	3.1	0.5	2.8	0.5
vw1-1.72-pph	26.8	56.6	6.3	25.4	5.2	0.8	5.6	0.8	4.9	0.9	2.8	0.4	2.7	0.4
vw1-1.72-psh	26.5	50.3	5.6	25.3	4.7	1.1	6.3	0.8	5.8	1.5	4.1	0.7	3.5	0.7
vw1-1.90-pph-	27.3	57.2	6.1	26.0	5.1	0.9	5.4	0.7	4.5	0.9	2.8	0.4	2.4	0.4
vw-1-1.90-psh-	27.1	49.3	5.4	24.1	4.9	1.0	6.2	0.9	5.8	1.3	4.2	0.6	3.7	0.6
vw1-2.65-pph-	26.1	48.3	5.2	21.4	4.2	0.9	4.0	0.7	6.4	1.3	4.3	0.6	5.5	0.8
vw1-2.65-psh-	19.1	38.5	4.1	18.5	3.8	0.8	4.8	0.7	4.3	0.9	2.9	0.4	2.5	0.4
vw1-3.22-pph	32.3	76.3	8.7	38.5	8.2	1.5	9.0	1.3	7.9	1.6	4.8	0.6	4.1	0.6
vw1-3.22-psh	34.9	56.7	6.4	27.6	6.2	1.3	6.7	1.1	6.5	1.8	4.7	0.7	4.9	0.7
vw2a-0.5-pph-	25.4	53.7	5.8	25.0	5.0	1.0	5.7	0.8	5.0	1.1	3.2	0.4	2.8	0.4
vw2a-0.5-psh	25.1	51.1	4.3	24.5	4.8	1.1	6.3	0.9	5.9	1.4	4.3	0.7	3.8	0.7
vw2e-1.79-pph	24.1	62.3	5.5	23.5	4.8	1.0	5.5	0.8	4.9	1.0	3.1	0.4	2.7	0.4
vw2e-1.79-psh	17.6	35.6	3.0	17.1	3.3	0.7	4.4	0.7	4.2	1.0	3.2	0.5	2.7	0.5
vw2e-2.80-pph	24.7	51.1	5.5	24.9	5.0	1.1	6.2	0.9	5.7	1.3	3.9	0.5	3.5	0.6
vw2e-2.80-psh	23.5	44.9	3.8	21.7	4.2	0.9	5.6	0.8	5.3	1.3	4.0	0.6	3.4	0.6
vw36a2-0.98-pph	24.4	52.2	5.7	23.8	4.6	0.8	5.0	0.7	4.2	0.9	2.6	0.4	2.3	0.4
vw36a2-0.98-psh	22.3	44.7	4.8	22.6	4.6	0.9	5.2	0.7	5.0	1.2	3.8	0.4	3.3	0.5
VW13A-pph	21.0	46.6	5.1	23.2	4.8	1.0	5.7	0.8	5.3	1.1	3.4	0.5	2.9	0.5

Table A1.3. continues.

Sample	La	Ce	Pr	Nd	Sm	Eu	Gd	Tb	Dy	Ho	Er	Tm	Yb	Lu
VW23C-pph	40.5	100.0	12.4	58.3	12.8	2.7	15.3	2.2	14.1	3.1	9.3	1.3	7.9	1.2
vw461-bne	3.7	9.6	1.2	6.3	1.9	0.7	3.4	0.6	4.6	1.2	4.4	0.7	5.5	1.2
vw465-bne	16.4	48.1	6.6	36.3	10.3	2.6	15.1	2.2	15.5	3.7	11.9	1.7	11.1	1.8
vw466-bne	15.3	48.3	5.7	26.4	11.6	3.6	17.2	3.1	19.3	4.7	12.3	1.7	12.1	1.5
vw461 (bulk)	3.8	8.7	1.0	4.4	1.2	0.4	2.0	0.4	2.9	0.7	2.8	0.5	3.5	0.8
B1	1.0	2.1	0.3	1.1	0.2	0.0	0.2	0.0	0.2	0.0	0.2	0.0	0.2	0.0

Table A1.4. Abundances of PAAS-normalised rare-earth elements for the phosphatic sands and Bomgat phosphorites. All values in ppm (pph = peloidal phosphorite, psh = phosphatised shell fragments and bne=bone fragments).

Sample	La	Ce	Pr	Nd	Sm	Eu	Gd	Tb	Dy	Ho	Er	Tm	Yb	Lu
vw1A3 (bulk)	0.54	0.57	0.57	0.65	0.80	0.86	1.06	0.88	0.94	0.93	0.96	0.93	0.86	0.93
vw1A3-pph-	0.44	0.44	0.44	0.48	0.80	0.78	1.07	0.83	0.95	0.75	1.04	1.10	0.89	1.13
vw1A3-psh-	0.44	0.42	0.41	0.47	0.57	0.62	0.86	0.70	0.80	0.87	0.90	0.90	0.83	0.93
vw1-0.2-pph-	0.66	0.80	0.77	0.71	0.91	0.94	1.23	0.99	1.06	1.07	1.44	1.20	0.96	1.00
vw1-0.2-psh-	0.66	0.71	0.62	0.65	0.87	0.92	0.92	0.83	0.83	0.78	0.92	0.93	0.86	0.98
vw1-1.31-pph	0.85	0.86	0.84	0.93	1.08	0.95	1.37	1.04	1.16	1.13	1.11	1.33	1.01	1.18
vw1-1.31-psh	0.52	0.50	0.49	0.60	0.72	0.75	1.03	0.84	0.95	1.03	1.08	1.15	1.00	1.13
vw1-1.72-pph	0.70	0.71	0.72	0.75	0.93	0.69	1.19	1.04	1.03	0.85	0.95	0.90	0.97	0.98
vw1-1.72-psh	0.69	0.63	0.63	0.75	0.83	1.02	1.35	0.95	1.23	1.54	1.43	1.70	1.26	1.63
vw1-1.90-pph-	0.71	0.72	0.70	0.77	0.91	0.78	1.14	0.91	0.95	0.94	0.96	0.93	0.86	0.95
vw-1-1.90-psh-	0.71	0.62	0.62	0.71	0.88	0.93	1.33	1.08	1.24	1.34	1.46	1.45	1.34	1.48
vw1-2.65-pph-	0.68	0.61	0.59	0.63	0.75	0.82	0.85	0.90	1.36	1.30	1.49	1.48	1.95	2.10
vw1-2.65-psh-	0.50	0.48	0.47	0.55	0.68	0.75	1.01	0.81	0.91	0.94	1.00	0.95	0.89	1.00
vw1-3.22-pph	0.85	0.96	0.99	1.14	1.46	1.34	1.92	1.58	1.67	1.62	1.65	1.58	1.45	1.50
vw1-3.22-psh	0.91	0.71	0.73	0.82	1.11	1.17	1.42	1.41	1.39	1.75	1.62	1.83	1.76	1.83
vw2a-0.5-pph-	0.66	0.67	0.66	0.74	0.90	0.92	1.21	0.98	1.06	1.06	1.09	1.05	0.99	1.08
vw2a-0.5-psh	0.66	0.64	0.49	0.72	0.86	0.96	1.35	1.11	1.26	1.43	1.50	1.70	1.37	1.73
vw2e-1.79-pph	0.63	0.78	0.62	0.69	0.86	0.88	1.17	0.96	1.05	1.04	1.08	1.03	0.96	1.00
vw2e-1.79-psh	0.46	0.45	0.34	0.51	0.59	0.67	0.94	0.84	0.89	1.04	1.10	1.13	0.96	1.21
vw2e-2.80-pph	0.65	0.64	0.63	0.73	0.90	0.96	1.31	1.08	1.20	1.28	1.36	1.33	1.26	1.43

Table A1.4. continues.

Sample	La	Ce	Pr	Nd	Sm	Eu	Gd	Tb	Dy	Ho	Er	Tm	Yb	Lu
vw2e-2.80-psh	0.62	0.56	0.43	0.64	0.75	0.85	1.19	1.06	1.13	1.31	1.39	1.43	1.21	1.53
vw36a2-0.98-pph	0.64	0.66	0.65	0.70	0.83	0.69	1.05	0.85	0.89	0.87	0.89	0.88	0.83	0.90
vw36a2-0.98-psh	0.58	0.56	0.54	0.67	0.82	0.80	1.11	0.84	1.07	1.17	1.31	1.05	1.16	1.13
VW13A-pph	0.55	0.59	0.58	0.68	0.86	0.94	1.21	1.01	1.12	1.13	1.17	1.13	1.04	1.13
VW23C-pph	1.06	1.26	1.41	1.72	2.29	2.46	3.26	2.75	3.00	3.06	3.21	3.15	2.81	2.98
vw461-bne	0.10	0.12	0.14	0.18	0.34	0.63	0.71	0.75	0.98	1.17	1.51	1.78	1.95	3.08
vw465-bne	0.43	0.60	0.75	1.07	1.84	2.35	3.21	2.78	3.30	3.69	4.10	4.20	3.96	4.60
vw466-bne	0.40	0.61	0.64	0.78	2.08	3.26	3.66	3.90	4.10	4.69	4.26	4.20	4.32	3.85
vw461 (bulk)	0.10	0.11	0.11	0.13	0.21	0.37	0.43	0.46	0.61	0.73	0.95	1.13	1.26	2.03
B1	0.03	0.03	0.03	0.03	0.04	0.04	0.05	0.04	0.04	0.05	0.05	0.06	0.06	0.08

Table A1.5. Samples from Langebaanweg and Bomgat (Hoedjiespunt) showing the indices Ce/Ce*, Eu/Eu*, Lu/La, Er/Nd, Sm/Nd and LREE/HREE (pph = peloidal phosphorite, psh = phosphatised shell fragments and bne=bone fragments).

Sample	Ce/Ce*	Eu/Eu*	(Lu/La)n	(Er/Nd)n	(Sm/Nd)n	LREE/HREE
vw1A3 (bulk)	1.03	0.93	1.72	1.48	1.23	0.37
vw1A3-pph-	0.99	0.83	2.54	2.15	1.66	0.31
vw1A3-psh-	0.99	0.87	2.12	1.90	1.21	0.31
vw1-0.2-pph-	1.12	0.87	1.51	2.03	1.29	0.39
vw1-0.2-psh-	1.11	1.02	1.48	1.42	1.35	0.44
vw1-1.31-pph	1.02	0.77	1.39	1.20	1.16	0.44
vw1-1.31-psh	0.97	0.86	2.15	1.81	1.20	0.32
vw1-1.72-pph	1.00	0.65	1.39	1.27	1.23	0.44
vw1-1.72-psh	0.95	0.93	2.34	1.91	1.12	0.29
vw1-1.90-pph-	1.02	0.76	1.33	1.25	1.18	0.45
vw-1-1.90-psh-	0.93	0.84	2.08	2.06	1.24	0.30
vw1-2.65-pph-	0.95	1.02	3.07	2.37	1.19	0.27
vw1-2.65-psh-	1.00	0.88	2.00	1.83	1.24	0.32
vw1-3.22-pph	1.05	0.79	1.77	1.45	1.29	0.38
vw1-3.22-psh	0.87	0.93	2.00	1.98	1.36	0.30
vw2a-0.5-pph-	1.02	0.87	1.62	1.48	1.22	0.38
vw2a-0.5-psh	1.12	0.87	2.63	2.07	1.19	0.27
vw2e-1.79-pph	1.25	0.87	1.59	1.56	1.23	0.39
vw2e-1.79-psh	1.11	0.88	2.63	2.18	1.17	0.27
vw2e-2.80-pph	1.01	0.87	2.20	1.85	1.22	0.32
vw2e-2.80-psh	1.08	0.88	2.48	2.17	1.17	0.27
vw36a2-0.98-pph	1.02	0.74	1.41	1.27	1.18	0.44
vw36a2-0.98-psh	1.00	0.83	1.94	1.96	1.23	0.33
VW13A-pph	1.03	0.90	2.05	1.71	1.26	0.33
VW23C-pph	1.02	0.89	2.81	1.86	1.33	0.29
vw461-bne	1.03	1.19	31.49	8.17	1.82	0.07
vw465-bne	1.03	0.93	10.71	3.83	1.72	0.15
vw466-bne	1.16	1.14	9.61	5.46	2.67	0.12
vw461 (bulk)	1.03	1.16	20.30	7.29	1.65	0.08
B1	0.96	0.84	3.03	1.64	1.24	0.34

A2. Laser ablation Inductively Coupled Plasma – Mass Spectroscopy (LA-ICP-MS)

Table A2.1. Abundance of trace elements of varying grain types from phosphorites and phosphate rocks by LA-ICP-MS. All values in ppm.

1. GRAVEL MEMBER, LANGEBAANWEG

Sample	Sr	Y	Pb	Th	U	V	Rb	Zr
				Peloidal grains				
vw01-pph-1	1476	41.6	43.9	14.2	9.8	128	239	769
vw01-pph-2	1950	56.7	21.6	8.7	14.5	78.6	126	384
vw01-pph-3	1985	65.6	32.2	10.7	21.0	55.9	181	505
vw02-pph-1	1955	29.0	50.7	13.8	8.5	34.0	238	636
vw02-pph-2	1299	18.5	21.5	7.0	6.0	63.7	113	282
vw02-pph-3	1860	22.0	32.5	10.0	5.7	33.6	171	446
gm01-pph-1	3492	753	20.2	87.6	31.0	68.5	49.5	218
gm01-pph-2	2657	106	18.1	12.9	39.0	62.3	50.7	157
gm01-pph-3	2122	152	18.3	17.9	23.9	68.9	90.0	247
gm02-pph-1	3338	127	21.0	13.7	27.6	61.9	71.9	174
gm02-pph-2	2672	91.5	16.2	13.8	19.4	168	58.7	251
gm02-pph-3	2619	39.2	13.9	4.1	19.4	99.8	48.4	133
gm02-pph-4	478	36.1	50.6	17.4	8.6	44.9	327	855
gm03-pph-2	3344	167	31.5	29.1	42.4	37.8	190	502
gm03-pph-3	1719	274	16.5	19.2	71.5	30.1	88.4	268
gm04-pph-1	2382	48.4	8.9	6.4	19.7	59.5	30.2	96.1
gm04-pph-2	1735	360	4.4	27.7	22.5	44.1	6.7	55.5
gm04-pph-3	2145	229	11.0	33.4	12.8	69.5	48.4	189
				Biogenic grains				
gm02-psh-1	3311	33.7	16.9	8.6	10.2	64.6	67.1	173
				CFA cement				
vw01-cmt-1	1866	116	44.2	19.8	30.4	50.5	215	662
vw01-cmt-2	1884	52.4	32.1	12.2	14.3	106	184	592
vw01-cmt-3	2023	50.6	34.2	13.2	12.6	43.8	208	652
vw02-cmt-1	2282	33.0	31.5	11.2	77.0	62.4	161	426
vw02-cmt-2	943	19.8	28.1	9.3	5.4	34.9	152	417
vw02-cmt-3	1638	23.0	27.4	9.4	10.0	55.3	138	371
gm01-cmt-1	2278	31.6	22.9	11.0	5.5	58.1	112	314
gm01-cmt-2	3073	33.5	22.5	11.2	7.0	42.8	119	325
gm01-cmt-3	2244	206	20.6	18.3	24.3	31.8	68.2	212
gm01-cmt-4	1375	32.1	36.6	14.6	5.3	3.0	224	621
gm01-cmt-5	866	15.4	15.8	6.3	3.8	49.2	94.1	258
gm01-cmt-6-darkrim	809	38.6	76.6	19.3	13.8	33.7	376	908
gm01-cmt-7-darkrim	1046	39.7	51.2	16.5	12.2	14.5	356	772
gm02-cmt-1	2098	26.7	27.4	9.4	11.8	60.5	147	348
gm02-cmt-2	3432	33.8	11.0	9.4	8.1	46.9	60.7	169
gm02-cmt-3	3148	34.7	15.4	10.3	10.8	54.5	68.9	199
gm03-cmt-4	4386	86.8	29.3	15.6	37.5	53.1	203	537
gm03-cmt-5	5525	112	32.3	15.9	51.4	56.6	191	497

Table A2.1. continues.

Sample	Sr	Y	Pb	Th	U	V	Rb	Zr
gm03-cmt-6	3059	67.6	40.3	22.3	24.0	45.1	254	697
gm04-cmt-1	1596	35.9	161	15.8	80.9	396	210	274
gm04-cmt-2	1686	32.4	17.8	10.1	3.8	77.2	63.5	181
gm04-cmt-3	1361	35.8	25.5	11.3	5.0	58.4	108	349
gm02-cmt-7	243	-	949	2.5	20.6	217	1051	82.2

2. PELLETAL PHOSPHORITE MEMBER, LANGEBAANWEG

Sample	Sr	Y	Pb	Th	U	V	Rb	Zr
				Peloidal grains				
vw16a-pph-1	2324	37.4	36.2	7.4	21.4	-	-	-
vw16a-pph-2	1966	20.8	11.7	2.3	26.6	-	-	-
vw16a-pph-3	1884	25.8	30.2	6.1	34.6	-	-	-
vw16a-pph-4	2335	60.7	22.1	6.2	33.9	-	-	-
vw16a-pph-5	2180	95.2	38.3	14.1	24.2	-	-	-
vw16a-pph-6	2097	96.4	41.4	9.8	42.6	-	-	-
vw16a-pph-7	1831	36.4	30.3	9.8	15.8	-	-	-
vw16a-pph-8	4679	328	33.1	38.8	71.1	-	-	-
vw19b-pph-1	2426	23.4	23.5	3.2	29.3	-	-	-
vw19a-pph-1	1226	200	41.8	27.5	19.7	-	-	-
vw19a-pph-2	2180	236	31.9	17.4	39.9	-	-	-
vw19a-pph-3	2348	66.9	23.9	3.9	39.8	-	-	-
vw19a-pph-4	1808	156	13.4	10.3	43.1	-	-	-
vw16b-pph-1	2112	152	26.5	10.6	29.7	-	-	-
vw16b-pph-2	2141	93.3	23.8	5.5	26.3	-	-	-
				Biogenic grains				
vw16a-psh-1	2123	78.3	35.8	3.4	32.8	-	-	-
vw16a-psh-2	2242	17.7	16.6	2.6	28.3	-	-	-
vw16a-psh-3	1248	56.1	14.2	3.3	39.4	-	-	-
vw16a-psh-4	1381	72.1	15.6	3.8	46.6	-	-	-
vw16a-psh-5	1544	9.9	17.2	4.4	54.3	-	-	-
vw16a-psh-6	1762	13.0	24.2	7.7	28.7	-	-	-
vw16b-psh-1	2248	34.3	17.6	3.4	30.4	-	-	-
vw16b-psh-2	2249	19.5	19.6	2.9	21.3	-	-	-
vw16b-psh-3	3509	315	13.0	3.6	53.9	-	-	-
				CFA cement				
vw16a-cmt-1	773	10.3	17.0	5.3	2.7	-	-	-
vw16a-cmt-2	1263	80.1	20.6	7.6	23.4	-	-	-
vw16a-cmt-3	1671	63.1	36.7	7.3	23.3	-	-	-
vw16a-cmt-4	932	8.5	10.7	3.5	5.8	-	-	-
vw19b-cmt-1	2009	367	27.4	21.2	18.3	-	-	-
vw19b-cmt-2	664	5.5	6.5	1.7	1.7	-	-	-
vw19b-cmt-3	2076	104	30.2	5.6	53.3	-	-	-
vw19a-cmt-1	2318	53.9	10.4	1.7	59.4	-	-	-
vw19a-cmt-2	2269	41.2	18.4	3.0	52.0	-	-	-
vw19a-cmt-3	1575	60.1	21.0	8.0	21.0	-	-	-
vw19a-cmt-4	780	5.3	3.2	1.7	2.3	-	-	-
vw19a-cmt-5	546	8.0	4.0	3.0	2.5	-	-	-

Table A2.1. continues.

Sample	Sr	Y	Pb	Th	U	V	Rb	Zr
				Misc.				
vw16b-S1	1873	72.1	10.2	7.9	60.3	-	-	-
vw16b-S2	2523	169	7.7	3.4	49.1	-	-	-
vw19b-test	1160	30.7	32.1	35.5	9.2	-	-	-

3. BOMGAT, HOEDJIESPUNT

Sample	Sr	Y	Pb	Th	U	V	Rb	Zr
				Biogenic grains				
b1-cmt-1	3250	16.2	31.4	7.4	58.9	31.8	154	381
b1-cmt-2	3958	14.0	17.8	5.6	13.8	34.4	97.1	303
b1-cmt-3	3502	14.4	22.5	6.8	11.5	23.9	101	337
b1-cmt-4	5943	19.7	29.9	8.7	11.1	28.7	154	455
b2-cmt-1cfa	7278	21.2	29.8	9.2	7.4	26.4	148	444
b2-cmt-2cfa	2176	8.7	11.1	3.3	10.4	24.4	49.6	227
b2-cmt-3cfa	3936	9.1	20.1	3.7	8.3	26.1	65.8	187
b3-cmt-1	2170	66.3	6.8	1.8	68.3	29.8	12.2	62.5
b3-cmt-2	2600	29.7	5.0	0.7	25.3	19.4	6.2	26.5
b3-cmt-3	889	23.0	25.7	9.6	26.6	7.6	184	462.1
b3-cmt-4	2731	320	24.1	16.8	35.8	23.8	5.9	82.1
				Biogenic grains				
b3-bio-1	2517	3.9	7.8	0.9	20.0	50.7	14.7	53.5
b3-bio-2	2450	3.4	5.0	0.8	15.0	37.0	11.7	40.3
b3-bio-3	2853	30.9	12.3	2.0	45.3	63.2	31.1	99.5
b3-bio-5	1642	15.0	11.3	1.8	11.0	93.3	16.4	47.7
b3-bio-6	2274	528	12.5	4.9	93.9	40.9	16.1	74.9

4. ALIMINIUM PHOSPHATES

Sample	Sr	Y	Pb	Th	U	V	Rb	Zr
kr204-cmt-1	724	96.6	2235	907	129	1196	348	1456
kr204-cmt-2	911	82.6	2689	1671	145	1231	302	2287
kr204-cmt-3	2436	94.3	803	595	71.9	377	304	1331
kr204-cmt-4	2268	66.2	292	173	35.3	117	324	933

5. OFFSHORE PHOSPHORITES/PHOSPHATES

Sample	Sr	Y	Pb	Th	U	V	Rb	Zr
3703-1-cfa-3	5612	215	146	82.2	18.0	1003	736	841
3703-1-cfa-4	3943	94.4	37.2	18.7	42.8	198	186	325
3700-3-cfa-1	1819	28.3	36.7	11.0	310	56.8	192	469
3700-3-cfa-2	1922	25.0	29.6	10.3	175	50.9	186	436
3700-3-cfa-3	1671	23.2	31.0	10.6	169	50.7	197	457
mjm025gtd-cfa-1	6572	1488	111	17.6	212	171	208	870
mjm025gtd-cfa-2	6060	1079	41.9	16.5	262	168	203	813
mjm025gtd-cfa-3	7956	1494	43.1	18.6	281	207	192	1332
mjm025gtd-cfa-4	6640	1526	47.5	15.7	264	141	182	827
mjm025gN-cfa-1	1441	185	40.1	13.5	26.1	82.2	214	628
mjm025gN-cfa-2	432	49.8	74.7	27.5	7.8	14.7	438	1335

Table A2.1. continues.

Sample	Sr	Y	Pb	Th	U	V	Rb	Zr
mjm025gN-cfa-3	494	57.1	72.9	26.7	21.1	26.6	442	1297
mjmb25d-cmt-1	431	31.9	45.0	15.8	37.0	33.4	321	775
mjmb25d-cmt-2	527	33.0	37.9	15.3	62.5	26.2	299	730
mjmb25d-cmt-3	516	31.2	41.5	14.9	82.2	29.5	305	742
mjmb25d-cmt-4	473	31.7	66.4	16.1	70.4	30.6	332	764

Table A2.2. Abundance of rare-earth elements in varying grain types from phosphorites and phosphate rocks by LA-ICP-MS. All values in ppm.

1. GRAVEL MEMBER, LANGEBAANWEG

Sample	La	Ce	Pr	Nd	Sm	Eu	Gd	Tb	Dy	Ho	Er	Tm	Yb	Lu
PAAS	**38.2**	**79.6**	**8.8**	**33.9**	**5.6**	**1.1**	**4.7**	**0.8**	**4.7**	**1**	**2.9**	**0.4**	**2.8**	**0.4**
Peloidal grains														
vw01-pph-1	46.9	85.7	8.85	35.1	6.87	0.99	5.46	0.70	6.20	1.54	4.64	0.58	3.48	0.57
vw01-pph-2	26.1	48.3	5.19	20.5	4.20	0.92	4.04	0.72	6.40	1.31	4.33	0.60	5.46	0.85
vw01-pph-3	47.7	77.8	7.85	33.6	6.61	0.73	5.03	0.90	6.14	1.39	4.20	0.47	4.92	0.70
vw02-pph-1	47.0	87.2	8.76	36.6	4.29	0.40	3.33	0.08	2.54	0.50	1.14	0.44	1.27	0.27
vw02-pph-2	24.1	48.9	4.45	20.8	3.66	0.39	1.93	0.25	2.36	0.31	0.83	0.01	1.12	0.06
vw02-pph-3	35.7	68.6	6.89	30.5	4.02	0.01	2.51	0.16	2.49	0.22	0.28	0.13	0.65	0.01
gm01-pph-1	170	401	53.1	267	75.2	17.3	84.4	14.3	91.3	20.3	56.5	7.57	53.5	7.48
gm01-pph-2	66.0	122	13.9	62.3	13.2	2.70	13.1	1.85	11.7	2.49	6.59	0.89	6.59	0.87
gm01-pph-3	99.8	187	21.3	95.6	19.5	3.70	18.3	2.57	17.4	3.77	9.91	1.29	10.52	1.32
gm02-pph-1	70.8	156	18.8	86.0	19.1	4.32	19.0	2.73	17.5	3.43	9.53	1.23	7.98	1.21
gm02-pph-2	53.5	107	12.3	54.7	12.3	2.62	12.2	1.92	11.8	2.45	7.19	0.97	6.59	1.02
gm02-pph-3	26.6	42.6	4.69	21.4	4.42	0.86	4.06	0.67	3.98	0.92	2.77	0.36	2.70	0.38
gm02-pph-4	54.6	108	10.00	44.5	8.86	2.60	5.48	1.08	5.00	1.35	3.28	0.82	4.46	0.94
gm03-pph-1	207	648	121	646	225	43.5	291	83.6	667	135	386	60.89	424	42.6
gm03-pph-2	81.7	184	20.8	109	24	5.70	25.8	3.58	21.5	4.60	13.8	1.67	12	1.58
gm03-pph-3	37.2	98.8	13.7	78.4	26.5	6.82	31.6	5.15	33.1	7.28	21.0	2.84	19.7	3.16
gm04-pph-1	28.7	49.0	5.65	24.5	5.43	0.95	5.66	0.79	4.53	1.09	3.51	0.45	3.43	0.51
gm04-pph-2	195.1	396	44.9	202	44.9	9.27	46.5	6.96	44.7	9.72	27.1	3.66	24.0	3.51
gm04-pph-3	65.3	137	16.6	75.9	21.0	4.70	23.4	4.02	27.4	6.07	18.5	2.35	18.6	2.53
Biogenic grains														
gm02-psh-1	28.42	57.56	6.04	26.84	5.14	1.34	5.15	0.69	5.03	1.09	2.97	0.41	2.5	0.36
CFA cement														
vw01-cmt-1	46.1	92.0	10.1	43.3	10.9	1.63	8.61	2.04	13	3.23	8.39	1.66	10.78	1.39
vw01-cmt-2	37.1	67.0	7.21	30.3	6.02	1.57	5.24	1.04	5.91	1.4	4.95	0.72	5.09	0.82
vw01-cmt-3	39.1	74.7	8.12	33.4	6.08	1.7	6.21	0.74	5.32	1.44	4.14	0.64	4.78	0.61
vw02-cmt-1	37.0	72.7	7.46	31.1	5.3	0.93	3.73	0.42	3.63	0.57	1.42	0.09	2.64	0.22
vw02-cmt-2	29.9	57.4	5.7	26.1	3.73	0.28	2.57	0.13	1.83	0.29	0.74	0.23	1.35	0.1
vw02-cmt-3	28.7	56.8	5.75	23.3	3.64	0.21	2.77	0.3	1.9	0.36	0.4	0.16	0.73	0.11
gm01-cmt-1	34.3	65.8	6.65	28.4	5.07	0.35	3.15	0.34	2.65	0.67	1.56	0.07	2.29	0.09
gm01-cmt-2	36.6	69.6	7.35	26.7	4.07	0.8	4.13	0.53	3.57	0.55	2.12	0.06	1.69	0.12
gm01-cmt-3	129	236	27.5	121	25.2	5.08	26.1	3.65	24.8	5.06	14.8	1.76	12.6	1.72
gm01-cmt-4	48.0	88.5	9.27	37.2	4.56	0.02	3.82	0.05	2.37	0.2	1.05	0.37	1.68	0.21
gm01-cmt-5	21.5	38.8	4.26	16.9	1.71	0.07	0.21	0.8	1.18	0.14	0.32	0.09	0.99	0.07

Table A2.2. continues.

Sample	La	Ce	Pr	Nd	Sm	Eu	Gd	Tb	Dy	Ho	Er	Tm	Yb	Lu
gm01-cmt-6-darkrim	59.8	118	11.7	44.8	4.99	0.79	2.91	0.41	2.33	0.13	0.81	0.85	1.25	0.18
gm01-cmt-7-darkrim	56.9	116	11.7	42.6	7.14	0.7	5.02	0.43	3.18	0.62	2.39	0	2.3	0.02
gm02-cmt-1	32.0	62.2	6.07	26.3	5.33	1.22	3.94	0.72	4.11	0.94	2.19	0.44	2.71	0.42
gm02-cmt-2	27.4	53.2	5.55	26.9	5.48	1.36	5.69	0.73	5.11	1.06	2.43	0.38	2.17	0.36
gm02-cmt-3	34.8	70.1	7.6	32.2	5.7	1.63	5.39	0.78	4.26	1.04	2.89	0.34	2.44	0.38
gm03-cmt-4	61.1	119	14.0	81.4	15.3	3.26	15.9	1.95	11.3	2.8	7.52	0.78	6.37	1.1
gm03-cmt-5	64.7	157	17.8	97.6	21.4	5.47	18.1	2.68	12.5	3.41	8.49	1.32	7.63	0.96
gm03-cmt-6	62.4	130	14.1	70.9	14.4	3.33	13.0	1.95	11	2.41	6.48	0.86	7.56	1.16
gm04-cmt-1	158	97.1	131	179	32.3	19.8	7.89	3.11	7.7	1.89	7.57	1.6	5.09	1
gm04-cmt-2	27.5	53.2	5.93	25.5	5.74	1.03	4.28	0.65	4.67	0.99	2.26	0.31	2.44	0.24
gm04-cmt-3	33.2	62.1	7.25	30.8	6.22	1	5.56	0.89	5.42	1.13	2.86	0.52	2.6	0.31
gm02-cmt-7	31.7	184	1.24	181	12.84	-	2.89	0.23	2.7	15.47	-	-	15.5	-

2. PELLETAL PHOSPHORITE MEMBER, LANGEBAANWEG

Sample	La	Ce	Pr	Nd	Sm	Eu	Gd	Tb	Dy	Ho	Er	Tm	Yb	Lu
Peloidal grains														
vw16a-pph-1	34.4	61.7	7	28.0	5.51	1.14	4.47	0.91	3.87	0.97	2.85	0.52	2.4	0.43
vw16a-pph-2	12.6	23.5	2.37	11.2	2.45	0.54	2.17	0.38	2.41	0.48	1.66	0.2	1.43	0.24
vw16a-pph-3	22.4	38.6	4.22	16.4	3.23	0.67	3.07	0.48	3.01	0.76	2.22	0.48	1.99	0.4
vw16a-pph-4	33.1	66.1	7.43	32.2	7.17	1.42	7.04	1.14	7.06	1.45	4.5	0.64	4.3	0.66
vw16a-pph-5	75.1	130	14.6	64.1	13.3	3.06	14.1	2.02	12.4	2.52	7.64	1.06	7.79	1.2
vw16a-pph-6	51.8	104	11.6	48.5	10.4	2.13	10.8	1.69	10.3	2.48	7.31	0.9	6.57	1.08
vw16a-pph-7	37.7	73.3	8.27	31.6	6.3	1.24	4.87	0.78	5.28	1.03	2.95	0.5	3.33	0.46
vw16a-pph-8	104	280	35.1	156.2	38.8	9.48	38.9	7.11	42.6	8.91	24.5	3.22	22.4	3.19
vw19b-pph-1	17.0	27.2	3.23	12.4	2.84	0.55	2.52	0.38	2.32	0.51	1.96	0.23	1.73	0.27
vw19a-pph-1	135	297	32.9	145	31.5	6.26	29.8	4.51	26.4	5.42	15.2	2.04	14.1	2.03
vw19a-pph-2	137	290	31.4	142	33.5	6.28	31.6	4.96	29.4	6.41	17.2	2.37	15.9	2.31
vw19a-pph-3	43.8	78.0	8.27	37.0	7.56	1.73	7.9	1.11	6.67	1.55	4.4	0.61	3.9	0.65
vw19a-pph-4	81.0	156	17.2	76.3	16.9	3.45	17.3	2.59	16.9	3.79	10.3	1.47	10.2	1.48
vw16b-pph-1	74.1	142	16.0	71.2	16.2	3.45	17.3	2.68	15.7	3.76	10.5	1.51	10.5	1.65
vw16b-pph-2	40.3	78.0	8.79	41.3	9.06	1.98	9.93	1.54	9.7	2.35	6.8	0.92	6.56	0.96
Biogenic grains														
vw16a-psh-1	35.9	57.7	6.21	27.6	6.11	1.19	6.61	1.04	6.53	1.65	4.99	0.73	4.84	0.83
vw16a-psh-2	11.7	23.8	2.48	9.8	2.62	0.52	2.01	0.31	2.35	0.45	1.52	0.23	1.44	0.25
vw16a-psh-3	21.7	41.5	4.97	25.2	5.49	1.36	6.36	0.97	5.72	1.4	4.22	0.64	4.04	0.67
vw16a-psh-4	26.7	54.0	6.85	32.8	7.36	1.59	8.27	1.22	7.71	1.86	5.51	0.81	5.42	0.95
vw16a-psh-5	13.2	24.6	2.5	11.4	2.24	0.46	1.27	0.25	1.47	0.28	1.16	0.15	0.61	0.22
vw16a-psh-6	23.7	45.7	4.75	20	3.9	0.72	2.36	0.47	2.05	0.37	1.31	0.12	1.32	0.16
vw16b-psh-1	19.7	33.5	3.78	16.5	3.62	0.78	3.18	0.5	3.23	0.84	2.49	0.38	2.37	0.44
vw16b-psh-2	13.8	22.2	2.49	10.3	1.99	0.42	1.76	0.32	2	0.47	1.25	0.19	1.47	0.25
vw16b-psh-3	15.7	33.8	4.09	22.9	8.69	2.7	19.4	3	23.9	7.43	26.2	4.06	28.8	5.07
CFA cement														
vw16a-cmt-1	16.2	30.1	3.09	11.7	2.41	0.62	2.31	0.31	2.14	0.4	1.23	0.14	0.85	0.17
vw16a-cmt-2	35.2	68.7	8.37	39.3	9.26	1.89	9.77	1.39	9.17	2.13	6.28	0.83	6.73	1.01
vw16a-cmt-3	41.7	78.1	8.51	34.7	7.07	1.64	7.29	1.21	7.58	1.53	4.69	0.68	4.72	0.69
vw16a-cmt-4	11.57	22.4	2.57	9.47	1.76	0.5	1.29	0.29	1.45	0.23	0.65	0.12	0.78	0.13
vw19b-cmt-1	171	336	38.5	174	39.1	7.91	40.4	6.45	39.5	9.01	24.2	3.43	21.7	3.43

Table A2.2. continues.

Sample	La	Ce	Pr	Nd	Sm	Eu	Gd	Tb	Dy	Ho	Er	Tm	Yb	Lu
vw19b-cmt-2	6.53	12.1	1.23	4.86	1.03	0.22	0.67	0.16	0.97	0.17	0.6	0.1	0.62	0.07
vw19b-cmt-3	59.9	97.6	10.8	49.4	10.2	2.38	11.3	1.7	10.4	2.64	6.55	0.89	5.72	1
vw19a-cmt-1	28.5	43.8	5	24	4.89	1.07	5.88	0.78	5.05	1.18	3.57	0.49	3.54	0.53
vw19a-cmt-2	28.0	49.7	5.5	25.2	5.01	1.08	5.35	0.8	4.45	1.03	2.75	0.38	2.7	0.38
vw19a-cmt-3	40.1	80.3	8.56	37.5	7.56	1.62	7.29	1.09	7.12	1.56	4.77	0.54	4.26	0.73
vw19a-cmt-4	5.28	10.5	1.24	4.9	0.94	0.18	0.76	0.15	0.88	0.13	0.51	0.04	0.46	0.13
vw19a-cmt-5	7.8	15.41	1.93	7.35	1.4	0.34	1.6	0.25	1.3	0.23	0.76	0.11	0.7	0.15
						Misc.								
vw16b-S1	32.1	70.5	8.81	40.2	9.31	2.13	9.26	1.4	9.27	1.96	5.48	0.75	5.24	0.76
vw16b-S2	10.4	26.6	5.05	23.6	7.51	2.28	12.7	2.19	16.0	4.44	12.0	1.66	12.4	2.07
vw19b-test	32.3	65.5	6.54	25.2	5.76	2.19	4.28	0.69	4.82	1.01	3.35	0.76	5.56	1.12

3. BOMGAT, HOEDJIESPUNT

Sample	La	Ce	Pr	Nd	Sm	Eu	Gd	Tb	Dy	Ho	Er	Tm	Yb	Lu
						CFA cement								
b1-cmt-1	32.0	49.8	4.47	22.4	6	1.08	3.41	0.77	3.06	0.6	1.47	0.3	3.32	0.35
b1-cmt-2	18.1	35.1	3.55	15.6	3.16	0.71	2.79	0.4	1.83	0.49	1.31	0.39	1.84	0.21
b1-cmt-3	22.1	39.0	4.58	18.1	4.12	0.88	4.23	0.73	5.3	1.04	2.84	0.53	2.53	0.69
b1-cmt-4	28.9	54.1	5.58	22.9	4.52	0.93	3.29	0.51	3.06	0.59	1.52	0.09	2.28	0.2
b2-cmt-1cfa	29.5	52.8	5.66	24.7	5.9	2.24	6.17	1.1	4.35	1.12	2.55	0.82	4.87	0.94
b2-cmt-2cfa	9.59	18.3	2.04	8.17	2	0.81	1.59	0.31	1.71	0.41	0.86	0.17	1.42	0.32
b2-cmt-3cfa	13.0	23.6	2.77	11.1	2.66	0.73	2.42	0.4	2.18	0.46	1.36	0.29	1.71	0.31
b3-cmt-1	48.5	49.0	4.25	18.1	2.39	0.43	3.06	0.41	3.53	0.94	3.09	0.36	3.48	0.52
b3-cmt-2	12.1	17.9	2.13	10.8	2.11	0.23	2.18	0.24	2.03	0.44	1.31	0.1	1.22	0.14
b3-cmt-3	30.7	60.4	6.06	22.5	2.52	-	2.24	-	2	0.19	-	-	1.23	-
b3-cmt-4	123	255	32.2	151	34.97	7.21	37.4	5.74	36.6	8.2	23.65	3.29	23.6	3.65
						Biogenic grains								
b3-bio-1	3.45	5.71	0.53	2.4	0.34	-	-	-	0.34	-	-	-	0.08	-
b3-bio-2	2.88	4.71	0.47	1.63	-	-	-	-	-	-	-	-	0.11	-
b3-bio-3	15.3	23.6	2.69	12.8	1.89	0.28	2.51	0.25	2.03	0.47	1.3	0.07	0.93	0.15
b3-bio-5	10.1	17.5	1.81	7.66	1.21	0.14	1.36	0.15	1.33	0.22	0.67	0.03	0.63	0.05
b3-bio-6	281	396	46.17	212	41.4	8.96	48.3	7.15	48.1	11.3	31.3	4.19	29.2	4.5

4. ALIMINIUM PHOSPHATES

Sample	La	Ce	Pr	Nd	Sm	Eu	Gd	Tb	Dy	Ho	Er	Tm	Yb	Lu
kr204-cmt-1	122	257	30.2	102	20.7	6.85	14.9	2.82	22.1	2.86	10.6	3.11	20.6	3.67
kr204-cmt-2	56.8	120	14.5	47.5	11.6	4.67	13.1	2.58	14.3	2.41	10.2	1.82	17.0	3.48
kr204-cmt-3	80.1	183	23.8	76.7	21.6	6.51	15.1	3.91	24.5	3.85	10.8	1.97	14.0	2.09
kr204-cmt-4	74.9	143	25.7	62.3	16.6	4.25	12.9	2.46	14.8	2.66	8.39	1.17	10.3	1.22

5. OFFSHORE PHOSPHORITES/PHOSPHATES

Sample	La	Ce	Pr	Nd	Sm	Eu	Gd	Tb	Dy	Ho	Er	Tm	Yb	Lu
3703-1-cfa-3	227.7	389	44.9	155	32.4	7.81	23.5	3.4	24.6	5.42	12.9	2.14	12.9	1.45
3703-1-cfa-4	47.8	83.7	9.53	37.1	8.92	1.86	14.5	2.29	14.4	3.13	6.47	0.88	6.82	0.98
3700-3-cfa-1	40.1	69.6	7.2	30	4.41	0.89	3.43	0.63	3.48	0.94	2.06	0.17	3	0.24
3700-3-cfa-2	36.7	66.2	7	28.0	5.35	0.77	4.64	0.58	3.97	0.69	1.83	0.18	2.7	0.35

Table A2.2. continues.

Sample	La	Ce	Pr	Nd	Sm	Eu	Gd	Tb	Dy	Ho	Er	Tm	Yb	Lu
3700-3-cfa-3	36.7	66.6	7.1	29.8	5.02	0.95	3.75	0.5	4.35	0.8	2.14	0.27	2.27	0.35
mjm025gtd-cfa-1	704	946	91.7	407	84.1	25.4	140	22.2	158	40.9	115	16.3	103	15.4
mjm025gtd-cfa-2	646	836	80.5	348	68.4	18.4	106	16.0	111	27.5	78	10.6	75	11.0
mjm025gtd-cfa-3	846	1134	111	487	90.4	25.3	149	22.9	158	37.9	113	15.2	105	15.7
mjm025gtd-cfa-4	762	1158	119	530	109	29.9	158	26.0	177	42.2	120	16.0	107	15.9
mjm025gN-cfa-1	106	159	14.9	66.0	12.2	2.09	15.9	2.45	17.3	4.5	12.9	1.54	11.8	1.61
mjm025gN-cfa-2	84.9	158	15.7	69.4	8.04	-	5.13	0.09	3.3	1.17	0.4	-	4.04	-
mjm025gN-cfa-3	92.6	177	22.2	63.5	9.27	0.1	0.97	0.52	5.82	0.99	0.31	-	5.8	-
mjmb25d-cmt-1	53.9	98.8	9.13	40.9	7.11	1.98	5.08	0.82	4.8	1.13	3.64	0.7	3.27	0.72
mjmb25d-cmt-2	52.1	96.8	8.72	36.9	6.08	1.57	5.29	0.66	5.88	1.08	3.43	0.74	3.31	0.6
mjmb25d-cmt-3	51.6	105	9.53	39.7	7.88	1.84	4.94	0.95	5.63	1.28	2.82	0.54	4.28	0.5
mjmb25d-cmt-4	52.1	120	9.04	39.3	6.89	1.94	6.76	1.05	5.64	1.06	3.35	0.61	3.23	0.65

Table A2.3. PAAS-normalised rare-earth element ratios of varying grain type from phosphorites and phosphate rocks.

1. GRAVEL MEMBER, LANGEBAANWEG

Sample	La	Ce	Pr	Nd	Sm	Eu	Gd	Tb	Dy	Ho	Er	Tm	Yb	Lu
Peloidal grains														
vw01-pph-1	1.23	1.08	1.01	1.03	1.23	0.90	1.16	0.88	1.32	1.54	1.60	1.44	1.24	1.43
vw01-pph-2	0.68	0.61	0.59	0.60	0.75	0.84	0.86	0.90	1.36	1.31	1.49	1.49	1.95	2.11
vw01-pph-3	1.25	0.98	0.89	0.99	1.18	0.66	1.07	1.13	1.31	1.39	1.45	1.18	1.76	1.74
vw02-pph-1	1.23	1.10	1.00	1.08	0.77	0.36	0.71	0.10	0.54	0.50	0.39	1.11	0.45	0.67
vw02-pph-2	0.63	0.61	0.51	0.61	0.65	0.36	0.41	0.31	0.50	0.31	0.29	0.02	0.40	0.14
vw02-pph-3	0.93	0.86	0.78	0.90	0.72	0.01	0.53	0.20	0.53	0.22	0.10	0.33	0.23	0.02
gm01-pph-1	4.44	5.04	6.03	7.88	13.4	15.7	18	17.9	19.4	20.3	19.5	18.9	19.1	18.7
gm01-pph-2	1.73	1.54	1.58	1.84	2.35	2.46	2.78	2.31	2.49	2.49	2.27	2.22	2.35	2.19
gm01-pph-3	2.61	2.34	2.42	2.82	3.49	3.36	3.89	3.21	3.70	3.77	3.42	3.23	3.76	3.29
gm02-pph-1	1.85	1.96	2.13	2.54	3.41	3.93	4.05	3.41	3.71	3.43	3.29	3.07	2.85	3.02
gm02-pph-2	1.40	1.35	1.39	1.61	2.20	2.38	2.60	2.40	2.52	2.45	2.48	2.43	2.35	2.55
gm02-pph-3	0.70	0.53	0.53	0.63	0.79	0.78	0.86	0.84	0.85	0.92	0.95	0.89	0.96	0.95
gm02-pph-4	1.43	1.36	1.14	1.31	1.58	2.37	1.17	1.35	1.06	1.35	1.13	2.05	1.59	2.34
gm03-pph-1	5.41	8.14	13.7	19.1	40.2	39.5	61.9	105	142	135	133	152	151	107
gm03-pph-2	2.14	2.31	2.37	3.22	4.29	5.18	5.49	4.47	4.58	4.60	4.74	4.17	4.29	3.95
gm03-pph-3	0.97	1.24	1.56	2.31	4.72	6.20	6.73	6.44	7.05	7.28	7.23	7.10	7.04	7.90
gm04-pph-1	0.75	0.62	0.64	0.72	0.97	0.86	1.20	0.99	0.96	1.09	1.21	1.14	1.22	1.28
gm04-pph-2	5.11	4.97	5.10	5.96	8.02	8.43	9.90	8.70	9.51	9.72	9.34	9.14	8.56	8.78
gm04-pph-3	1.71	1.72	1.89	2.24	3.74	4.27	4.97	5.02	5.83	6.07	6.38	5.88	6.63	6.33
Biogenic grains														
gm02-psh-1	0.74	0.72	0.69	0.79	0.92	1.22	1.10	0.86	1.07	1.09	1.03	1.03	0.89	0.90
CFA cement														
vw01-cmt-1	1.21	1.16	1.15	1.28	1.95	1.48	1.83	2.55	2.76	3.23	2.89	4.15	3.85	3.46
vw01-cmt-2	0.97	0.84	0.82	0.89	1.07	1.43	1.12	1.30	1.26	1.40	1.71	1.80	1.82	2.04
vw01-cmt-3	1.02	0.94	0.92	0.99	1.09	1.55	1.32	0.92	1.13	1.44	1.43	1.60	1.71	1.53
vw02-cmt-1	0.97	0.91	0.85	0.92	0.95	0.85	0.79	0.53	0.77	0.57	0.49	0.22	0.94	0.56

Table A2.3. continues.

Sample	La	Ce	Pr	Nd	Sm	Eu	Gd	Tb	Dy	Ho	Er	Tm	Yb	Lu
vw02-cmt-2	0.78	0.72	0.65	0.77	0.67	0.25	0.55	0.16	0.39	0.29	0.26	0.59	0.48	0.24
vw02-cmt-3	0.75	0.71	0.65	0.69	0.65	0.19	0.59	0.37	0.40	0.36	0.14	0.40	0.26	0.28
gm01-cmt-1	0.90	0.83	0.76	0.84	0.91	0.31	0.67	0.43	0.56	0.67	0.54	0.18	0.82	0.23
gm01-cmt-2	0.96	0.87	0.84	0.79	0.73	0.73	0.88	0.66	0.76	0.55	0.73	0.14	0.60	0.29
gm01-cmt-3	3.38	2.96	3.13	3.56	4.51	4.62	5.55	4.56	5.28	5.06	5.09	4.39	4.51	4.30
gm01-cmt-4	1.26	1.11	1.05	1.10	0.81	0.02	0.81	0.06	0.50	0.20	0.36	0.94	0.60	0.53
gm01-cmt-5	0.56	0.49	0.48	0.50	0.31	0.06	0.05	0.99	0.25	0.14	0.11	0.22	0.35	0.18
gm01-cmt-6-darkrim	1.57	1.48	1.32	1.32	0.89	0.72	0.62	0.51	0.50	0.13	0.28	2.12	0.44	0.45
gm01-cmt-7-darkrim	1.49	1.46	1.32	1.26	1.28	0.64	1.07	0.53	0.68	0.62	0.83	0.01	0.82	0.05
gm02-cmt-1	0.84	0.78	0.69	0.77	0.95	1.11	0.84	0.90	0.87	0.94	0.75	1.09	0.97	1.06
gm02-cmt-2	0.72	0.67	0.63	0.79	0.98	1.24	1.21	0.92	1.09	1.06	0.84	0.96	0.78	0.89
gm02-cmt-3	0.91	0.88	0.86	0.95	1.02	1.48	1.15	0.97	0.91	1.04	1.00	0.85	0.87	0.94
gm03-cmt-4	1.60	1.49	1.59	2.40	2.73	2.97	3.39	2.44	2.41	2.80	2.59	1.94	2.28	2.76
gm03-cmt-5	1.69	1.97	2.03	2.88	3.81	4.97	3.85	3.35	2.66	3.41	2.93	3.30	2.72	2.40
gm03-cmt-6	1.63	1.64	1.61	2.09	2.57	3.02	2.78	2.44	2.33	2.41	2.23	2.16	2.70	2.89
gm04-cmt-1	4.15	1.22	14.84	5.28	5.77	18	1.68	3.89	1.64	1.89	2.61	3.99	1.82	2.51
gm04-cmt-2	0.72	0.67	0.67	0.75	1.03	0.93	0.91	0.81	0.99	0.99	0.78	0.78	0.87	0.61
gm04-cmt-3	0.87	0.78	0.82	0.91	1.11	0.91	1.18	1.11	1.15	1.13	0.99	1.30	0.93	0.78
gm02-cmt-7	0.83	2.31	0.14	5.33	2.29	-	0.61	0.29	0.57	15.47	-	-	5.55	-

2. PELLETAL PHOSPHORITE MEMBER, LANGEBAANWEG

Sample	La	Ce	Pr	Nd	Sm	Eu	Gd	Tb	Dy	Ho	Er	Tm	Yb	Lu
Peloidal grains														
vw16a-pph-1	0.90	0.78	0.80	0.83	0.98	1.04	0.95	1.14	0.82	0.97	0.98	1.30	0.86	1.09
vw16a-pph-2	0.33	0.30	0.27	0.33	0.44	0.49	0.46	0.47	0.51	0.48	0.57	0.50	0.51	0.60
vw16a-pph-3	0.59	0.48	0.48	0.48	0.58	0.61	0.65	0.60	0.64	0.76	0.77	1.21	0.71	1.00
vw16a-pph-4	0.87	0.83	0.84	0.95	1.28	1.29	1.50	1.43	1.50	1.45	1.55	1.59	1.54	1.64
vw16a-pph-5	1.97	1.63	1.66	1.89	2.37	2.78	3.00	2.53	2.64	2.52	2.63	2.66	2.78	2.99
vw16a-pph-6	1.35	1.31	1.32	1.43	1.85	1.94	2.29	2.11	2.18	2.48	2.52	2.26	2.35	2.69
vw16a-pph-7	0.99	0.92	0.94	0.93	1.12	1.13	1.04	0.98	1.12	1.03	1.02	1.25	1.19	1.14
vw16a-pph-8	2.73	3.51	3.99	4.61	6.93	8.61	8.28	8.88	9.05	8.91	8.45	8.04	7.99	7.97
vw19b-pph-1	0.44	0.34	0.37	0.37	0.51	0.50	0.54	0.48	0.49	0.51	0.68	0.58	0.62	0.68
vw19a-pph-1	3.53	3.73	3.74	4.29	5.63	5.69	6.35	5.64	5.61	5.42	5.24	5.09	5.03	5.08
vw19a-pph-2	3.58	3.64	3.56	4.19	5.98	5.71	6.72	6.21	6.25	6.41	5.93	5.92	5.68	5.77
vw19a-pph-3	1.15	0.98	0.94	1.09	1.35	1.57	1.68	1.39	1.42	1.55	1.52	1.53	1.39	1.63
vw19a-pph-4	2.12	1.96	1.96	2.25	3.01	3.13	3.69	3.23	3.60	3.79	3.54	3.68	3.63	3.71
vw16b-pph-1	1.94	1.79	1.82	2.10	2.89	3.14	3.69	3.35	3.34	3.76	3.60	3.78	3.76	4.11
vw16b-pph-2	1.06	0.98	1.00	1.22	1.62	1.80	2.11	1.93	2.06	2.35	2.35	2.29	2.34	2.40
Biogenic grains														
vw16a-psh-1	0.94	0.73	0.71	0.81	1.09	1.08	1.41	1.30	1.39	1.65	1.72	1.84	1.73	2.08
vw16a-psh-2	0.31	0.30	0.28	0.29	0.47	0.47	0.43	0.38	0.50	0.45	0.52	0.57	0.51	0.64
vw16a-psh-3	0.57	0.52	0.57	0.74	0.98	1.23	1.35	1.21	1.22	1.40	1.46	1.59	1.44	1.67
vw16a-psh-4	0.70	0.68	0.78	0.97	1.32	1.44	1.76	1.53	1.64	1.86	1.90	2.02	1.94	2.38
vw16a-psh-5	0.35	0.31	0.28	0.34	0.40	0.42	0.27	0.31	0.31	0.28	0.40	0.38	0.22	0.54
vw16a-psh-6	0.62	0.57	0.54	0.59	0.70	0.65	0.50	0.59	0.44	0.37	0.45	0.30	0.47	0.39
vw16b-psh-1	0.52	0.42	0.43	0.49	0.65	0.71	0.68	0.62	0.69	0.84	0.86	0.94	0.85	1.10
vw16b-psh-2	0.36	0.28	0.28	0.30	0.36	0.38	0.37	0.40	0.43	0.47	0.43	0.48	0.52	0.62
vw16b-psh-3	0.41	0.42	0.46	0.68	1.55	2.46	4.13	3.75	5.08	7.43	9.02	10.1	10.3	12.7

Table A2.3. continues.

Sample	La	Ce	Pr	Nd	Sm	Eu	Gd	Tb	Dy	Ho	Er	Tm	Yb	Lu
						CFA cement								
vw16a-cmt-1	0.43	0.38	0.35	0.34	0.43	0.56	0.49	0.38	0.46	0.40	0.42	0.35	0.30	0.43
vw16a-cmt-2	0.92	0.86	0.95	1.16	1.65	1.72	2.08	1.74	1.95	2.13	2.17	2.09	2.40	2.54
vw16a-cmt-3	1.09	0.98	0.97	1.02	1.26	1.49	1.55	1.51	1.61	1.53	1.62	1.70	1.69	1.74
vw16a-cmt-4	0.30	0.28	0.29	0.28	0.31	0.45	0.27	0.37	0.31	0.23	0.22	0.30	0.28	0.34
vw19b-cmt-1	4.49	4.22	4.38	5.13	6.97	7.19	8.60	8.06	8.40	9.01	8.34	8.56	7.76	8.58
vw19b-cmt-2	0.17	0.15	0.14	0.14	0.18	0.20	0.14	0.20	0.21	0.17	0.21	0.26	0.22	0.17
vw19b-cmt-3	1.57	1.23	1.23	1.46	1.82	2.16	2.39	2.12	2.21	2.64	2.26	2.23	2.04	2.50
vw19a-cmt-1	0.75	0.55	0.57	0.71	0.87	0.98	1.25	0.98	1.07	1.18	1.23	1.22	1.26	1.33
vw19a-cmt-2	0.73	0.62	0.62	0.74	0.89	0.98	1.14	0.99	0.95	1.03	0.95	0.94	0.96	0.96
vw19a-cmt-3	1.05	1.01	0.97	1.10	1.35	1.48	1.55	1.37	1.51	1.56	1.65	1.35	1.52	1.83
vw19a-cmt-4	0.14	0.13	0.14	0.14	0.17	0.16	0.16	0.19	0.19	0.13	0.18	0.11	0.17	0.32
vw19a-cmt-5	0.20	0.19	0.22	0.22	0.25	0.31	0.34	0.31	0.28	0.23	0.26	0.27	0.25	0.38
						Misc.								
vw16b-S1	0.84	0.89	1.00	1.18	1.66	1.94	1.97	1.75	1.97	1.96	1.89	1.87	1.87	1.89
vw16b-S2	0.27	0.33	0.57	0.70	1.34	2.07	2.70	2.74	3.40	4.44	4.13	4.15	4.42	5.18
vw19b-test	0.84	0.82	0.74	0.74	1.03	1.99	0.91	0.87	1.02	1.01	1.16	1.89	1.99	2.81

3. BOMGAT, HOEDJIESPUNT

Sample	La	Ce	Pr	Nd	Sm	Eu	Gd	Tb	Dy	Ho	Er	Tm	Yb	Lu
						CFA cement								
b1-cmt-1	0.84	0.63	0.51	0.66	1.07	0.99	0.73	0.97	0.65	0.60	0.51	0.74	1.18	0.86
b1-cmt-2	0.47	0.44	0.40	0.46	0.56	0.65	0.59	0.51	0.39	0.49	0.45	0.98	0.66	0.53
b1-cmt-3	0.58	0.49	0.52	0.53	0.74	0.80	0.90	0.91	1.13	1.04	0.98	1.31	0.90	1.74
b1-cmt-4	0.76	0.68	0.63	0.68	0.81	0.85	0.70	0.64	0.65	0.59	0.53	0.24	0.81	0.50
b2-cmt-1cfa	0.77	0.66	0.64	0.73	1.05	2.03	1.31	1.37	0.93	1.12	0.88	2.04	1.74	2.35
b2-cmt-2cfa	0.25	0.23	0.23	0.24	0.36	0.74	0.34	0.39	0.36	0.41	0.30	0.43	0.51	0.80
b2-cmt-3cfa	0.34	0.30	0.31	0.33	0.48	0.67	0.52	0.50	0.46	0.46	0.47	0.73	0.61	0.78
b3-cmt-1	1.27	0.62	0.48	0.53	0.43	0.39	0.65	0.52	0.75	0.94	1.06	0.91	1.24	1.29
b3-cmt-2	0.32	0.22	0.24	0.32	0.38	0.21	0.46	0.30	0.43	0.44	0.45	0.25	0.43	0.36
b3-cmt-3	0.80	0.76	0.69	0.66	0.45	-	0.48	-	0.43	0.19	-	-	0.44	-
b3-cmt-4	3.22	3.20	3.65	4.45	6.24	6.56	7.96	7.17	7.78	8.20	8.16	8.22	8.43	9.13
						Biogenic grains								
b3-bio-1	0.09	0.07	0.06	0.07	0.06	-	-	-	0.07	-	-	-	0.03	-
b3-bio-2	0.08	0.06	0.05	0.05	-	-	-	-	-	-	-	-	0.04	-
b3-bio-3	0.40	0.30	0.31	0.38	0.34	0.25	0.53	0.31	0.43	0.47	0.45	0.17	0.33	0.38
b3-bio-5	0.26	0.22	0.21	0.23	0.22	0.13	0.29	0.19	0.28	0.22	0.23	0.07	0.22	0.11
b3-bio-6	7.34	4.97	5.25	6.25	7.39	8.14	10.3	8.93	10.2	11.3	10.8	10.48	10.4	11.3

4. ALUMINIUM PHOSPHATES

Sample	La	Ce	Pr	Nd	Sm	Eu	Gd	Tb	Dy	Ho	Er	Tm	Yb	Lu
kr204-cmt-1	3.20	3.23	3.44	3.00	3.70	6.23	3.18	3.52	4.70	2.86	3.66	7.79	7.35	9.18
kr204-cmt-2	1.49	1.50	1.65	1.40	2.07	4.24	2.78	3.23	3.03	2.41	3.51	4.54	6.05	8.70
kr204-cmt-3	2.10	2.30	2.70	2.26	3.85	5.92	3.21	4.88	5.21	3.85	3.73	4.92	4.99	5.23
kr204-cmt-4	1.96	1.80	2.92	1.84	2.96	3.86	2.74	3.07	3.15	2.66	2.89	2.92	3.68	3.04

Table A2.3. continues.

5. OFFSHORE PHOSPHORITES/PHOSPHATES

Sample	La	Ce	Pr	Nd	Sm	Eu	Gd	Tb	Dy	Ho	Er	Tm	Yb	Lu
3703-1-cfa-3	5.96	4.88	5.10	4.57	5.79	7.10	4.99	4.25	5.24	5.42	4.43	5.35	4.61	3.62
3703-1-cfa-4	1.25	1.05	1.08	1.10	1.59	1.69	3.08	2.87	3.06	3.13	2.23	2.19	2.43	2.45
3700-3-cfa-1	1.05	0.87	0.82	0.89	0.79	0.81	0.73	0.79	0.74	0.94	0.71	0.44	1.07	0.59
3700-3-cfa-2	0.96	0.83	0.80	0.83	0.95	0.70	0.99	0.73	0.84	0.69	0.63	0.44	0.96	0.89
3700-3-cfa-3	0.96	0.84	0.81	0.88	0.90	0.86	0.80	0.63	0.93	0.80	0.74	0.67	0.81	0.87
mjm025gtd-cfa-1	18.4	11.9	10.4	12.0	15.0	23.1	29.9	27.8	33.7	40.9	39.8	40.7	36.9	38.6
mjm025gtd-cfa-2	16.9	10.5	9.1	10.3	12.2	16.7	22.7	20.0	23.5	27.5	26.9	26.5	26.7	27.6
mjm025gtd-cfa-3	22.1	14.2	12.6	14.4	16.1	23.0	31.8	28.6	33.6	37.9	39.0	38.1	37.6	39.1
mjm025gtd-cfa-4	20.0	14.6	13.5	15.6	19.5	27.2	33.6	32.5	37.7	42.2	41.3	39.9	38.2	39.7
mjm025gN-cfa-1	2.77	2.00	1.69	1.95	2.18	1.90	3.37	3.06	3.69	4.45	4.46	3.84	4.20	4.03
mjm025gN-cfa-2	2.22	1.98	1.79	2.05	1.44	-	1.09	0.11	0.70	1.17	0.14	-	1.44	-
mjm025gN-cfa-3	2.42	2.22	2.52	1.87	1.65	0.10	0.21	0.65	1.24	0.99	0.11	-	2.07	-
mjmb25d-cmt-1	1.41	1.24	1.04	1.21	1.27	1.80	1.08	1.03	1.02	1.13	1.25	1.75	1.17	1.80
mjmb25d-cmt-2	1.36	1.22	0.99	1.09	1.09	1.43	1.13	0.83	1.25	1.08	1.18	1.84	1.18	1.49
mjmb25d-cmt-3	1.35	1.32	1.08	1.17	1.41	1.68	1.05	1.19	1.20	1.28	0.97	1.35	1.53	1.24
mjmb25d-cmt-4	1.36	1.51	1.03	1.16	1.23	1.76	1.44	1.32	1.20	1.06	1.16	1.52	1.15	1.62

Table A2.4. Phosphorite and phosphate samples showing the indices Ce/Ce*, Eu/Eu*, Lu/La, Er/Nd, Sm/Nd and LREE/HREE.

1. GRAVEL MEMBER, LANGEBAANWEG

Sample	Ce/Ce*	Eu/Eu*	(Lu/La)n	(Er/Nd)n	(Sm/Nd)n	LREE/HREE
			Peloidal grains			
vw01-pph-1	0.96	0.76	1.16	1.55	1.19	0.48
vw01-pph-2	0.95	1.04	3.09	2.47	1.24	0.26
vw01-pph-3	0.91	0.59	1.4	1.46	1.19	0.45
vw02-pph-1	0.98	0.49	0.54	0.36	0.71	1.07
vw02-pph-2	1.08	0.67	0.22	0.47	1.06	1.1
vw02-pph-3	1	0.01	0.02	0.11	0.8	1.93
gm01-pph-1	0.96	1	4.21	2.47	1.71	0.22
gm01-pph-2	0.93	0.96	1.26	1.24	1.28	0.42
gm01-pph-3	0.93	0.91	1.26	1.21	1.24	0.43
gm02-pph-1	0.98	1.05	1.63	1.3	1.34	0.39
gm02-pph-2	0.96	0.99	1.83	1.54	1.36	0.36
gm02-pph-3	0.87	0.95	1.37	1.52	1.25	0.4
gm02-pph-4	1.06	1.72	1.64	0.86	1.21	0.47
gm03-pph-1	0.85	0.77	19.69	6.99	2.11	0.08
gm03-pph-2	1.03	1.06	1.85	1.47	1.33	0.35
gm03-pph-3	0.98	1.08	8.11	3.13	2.04	0.17
gm04-pph-1	0.88	0.79	1.7	1.67	1.34	0.37
gm04-pph-2	0.97	0.94	1.72	1.57	1.35	0.36
gm04-pph-3	0.96	0.98	3.7	2.85	1.67	0.22
			Biogenic grains			
gm02-psh-1	1.01	1.21	1.2	1.29	1.16	0.42

Table A2.4. continues.

Sample	Ce/Ce*	Eu/Eu*	(Lu/La)n	(Er/Nd)n	(Sm/Nd)n	LREE/HREE
			CFA cement			
vw01-cmt-1	0.98	0.78	2.87	2.26	1.52	0.26
vw01-cmt-2	0.94	1.3	2.1	1.91	1.2	0.33
vw01-cmt-3	0.96	1.29	1.5	1.45	1.1	0.39
vw02-cmt-1	1.01	0.97	0.58	0.53	1.03	0.8
vw02-cmt-2	1.01	0.42	0.31	0.33	0.86	1.12
vw02-cmt-3	1.02	0.3	0.37	0.2	0.95	1.16
gm01-cmt-1	1	0.4	0.26	0.64	1.08	0.96
gm01-cmt-2	0.97	0.91	0.31	0.93	0.92	0.78
gm01-cmt-3	0.91	0.92	1.27	1.43	1.27	0.4
gm01-cmt-4	0.96	0.02	0.42	0.33	0.74	1.33
gm01-cmt-5	0.93	0.37	0.32	0.22	0.61	0.99
gm01-cmt-6-darkrim	1.02	0.95	0.29	0.21	0.67	1.14
gm01-cmt-7-darkrim	1.04	0.55	0.04	0.66	1.01	1.3
gm02-cmt-1	1.02	1.24	1.26	0.97	1.23	0.47
gm02-cmt-2	0.99	1.13	1.25	1.06	1.23	0.42
gm02-cmt-3	0.99	1.36	1.04	1.05	1.07	0.5
gm03-cmt-4	0.93	0.97	1.73	1.08	1.14	0.42
gm03-cmt-5	1.06	1.3	1.42	1.02	1.32	0.42
gm03-cmt-6	1.01	1.13	1.77	1.07	1.23	0.42
gm04-cmt-1	0.13	4.83	0.61	0.49	1.09	0.82
gm04-cmt-2	0.96	0.96	0.85	1.04	1.36	0.5
gm04-cmt-3	0.92	0.79	0.9	1.09	1.22	0.47

2. PELLETAL PHOSPHORITE MEMBER, LANGEBAANWEG

Sample	Ce/Ce*	Eu/Eu*	(Lu/La)n	(Er/Nd)n	(Sm/Nd)n	LREE/HREE
			Peloidal grains			
vw16a-pph-1	0.91	1.07	1.21	1.19	1.19	0.47
vw16a-pph-2	0.99	1.09	1.82	1.73	1.32	0.36
vw16a-pph-3	0.91	1	1.7	1.59	1.2	0.38
vw16a-pph-4	0.97	0.93	1.9	1.63	1.35	0.35
vw16a-pph-5	0.9	1.04	1.52	1.39	1.25	0.39
vw16a-pph-6	0.98	0.93	1.99	1.76	1.29	0.35
vw16a-pph-7	0.96	1.04	1.15	1.09	1.21	0.5
vw16a-pph-8	1.05	1.13	2.92	1.83	1.5	0.29
vw19b-pph-1	0.84	0.95	1.54	1.85	1.39	0.4
vw19a-pph-1	1.03	0.95	1.44	1.22	1.31	0.43
vw19a-pph-2	1.02	0.9	1.61	1.41	1.43	0.38
vw19a-pph-3	0.94	1.04	1.42	1.39	1.24	0.4
vw19a-pph-4	0.96	0.93	1.75	1.57	1.34	0.35
vw16b-pph-1	0.95	0.95	2.12	1.72	1.37	0.32
vw16b-pph-2	0.95	0.97	2.27	1.92	1.33	0.3
			Biogenic grains			
vw16a-psh-1	0.88	0.87	2.21	2.11	1.34	0.3
vw16a-psh-2	1.02	1.05	2.08	1.81	1.62	0.37
vw16a-psh-3	0.92	1.06	2.94	1.96	1.32	0.27
vw16a-psh-4	0.92	0.94	3.4	1.96	1.36	0.27
vw16a-psh-5	0.98	1.26	1.57	1.19	1.19	0.54

Table A2.4. continues.

Sample	Ce/Ce*	Eu/Eu*	(Lu/La)n	(Er/Nd)n	(Sm/Nd)n	LREE/HREE
vw16a-psh-6	0.99	1.09	0.63	0.77	1.18	0.73
vw16b-psh-1	0.89	1.07	2.13	1.76	1.33	0.34
vw16b-psh-2	0.87	1.04	1.7	1.43	1.17	0.39
vw16b-psh-3	0.97	0.86	30.77	13.35	2.3	0.05
			CFA cement			
vw16a-cmt-1	0.98	1.22	1	1.23	1.25	0.51
vw16a-cmt-2	0.92	0.92	2.75	1.87	1.43	0.29
vw16a-cmt-3	0.95	1.06	1.59	1.58	1.23	0.37
vw16a-cmt-4	0.94	1.53	1.11	0.8	1.13	0.53
vw19b-cmt-1	0.95	0.92	1.91	1.62	1.36	0.34
vw19b-cmt-2	0.98	1.2	1.02	1.44	1.28	0.44
vw19b-cmt-3	0.88	1.02	1.6	1.55	1.25	0.36
vw19a-cmt-1	0.84	0.92	1.79	1.74	1.23	0.33
vw19a-cmt-2	0.92	0.96	1.31	1.27	1.2	0.41
vw19a-cmt-3	1	1.02	1.75	1.49	1.22	0.4
vw19a-cmt-4	0.94	0.98	2.29	1.21	1.16	0.46
vw19a-cmt-5	0.91	1.04	1.87	1.2	1.16	0.41
			Misc.			
vw16b-S1	0.96	1.07	2.26	1.59	1.4	0.33
vw16b-S2	0.79	1.03	18.99	5.93	1.92	0.1
vw19b-test	1.04	2.06	3.33	1.55	1.38	0.31

3. BOMGAT, HOEDJIESPUNT

Sample	Ce/Ce*	Eu/Eu*	(Lu/La)n	(Er/Nd)n	(Sm/Nd)n	LREE/HREE
			CFA cement			
b1-cmt-1	0.93	1.1	1.03	0.77	1.62	0.51
b1-cmt-2	1	1.12	1.11	0.98	1.23	0.45
b1-cmt-3	0.89	0.98	3	1.83	1.38	0.29
b1-cmt-4	0.98	1.12	0.66	0.78	1.2	0.65
b2-cmt-1cfa	0.94	1.72	3.04	1.21	1.45	0.28
b2-cmt-2cfa	0.95	2.13	3.18	1.23	1.48	0.31
b2-cmt-3cfa	0.9	1.35	2.3	1.43	1.45	0.34
b3-cmt-1	0.7	0.72	1.02	2	0.8	0.43
b3-cmt-2	0.8	0.49	1.12	1.42	1.18	0.44
b3-cmt-4	0.93	0.92	2.83	1.83	1.4	0.29
			Biogenic grains			
b3-bio-3	0.84	0.57	0.94	1.19	0.9	0.52
b3-bio-5	0.93	0.5	0.43	1.02	0.96	0.65
b3-bio-6	0.79	0.92	1.53	1.72	1.18	0.34

4. ALUMINIUM PHOSPHATES

Sample	Ce/Ce*	Eu/Eu*	(Lu/La)n	(Er/Nd)n	(Sm/Nd)n	LREE/HREE
kr204-cmt-1	0.97	1.81	2.87	1.22	1.23	0.34
kr204-cmt-2	0.96	1.75	5.85	2.51	1.47	0.21
kr204-cmt-3	0.96	1.68	2.49	1.65	1.7	0.32
kr204-cmt-4	0.74	1.36	1.55	1.57	1.61	0.41

Table A2.4. continues.

5. OFFSHORE PHOSPHORITES/PHOSPHATES

Sample	Ce/Ce*	Eu/Eu*	(Lu/La)n	(Er/Nd)n	(Sm/Nd)n	LREE/HREE
3703-1-cfa-1	0.98	0.94	1.38	1.23	1.2	0.43
3703-1-cfa-3	0.88	1.32	0.61	0.97	1.27	0.58
3703-1-cfa-4	0.9	0.73	1.96	2.04	1.45	0.26
3700-3-cfa-1	0.93	1.06	0.56	0.8	0.89	0.65
3700-3-cfa-2	0.95	0.73	0.92	0.76	1.16	0.64
3700-3-cfa-3	0.95	1.02	0.9	0.84	1.02	0.62
mjm025gtd-cfa-1	0.82	1.03	2.09	3.32	1.25	0.22
mjm025gtd-cfa-2	0.81	0.96	1.63	2.62	1.19	0.27
mjm025gtd-cfa-3	0.82	0.96	1.77	2.71	1.12	0.26
mjm025gtd-cfa-4	0.87	1.02	1.99	2.64	1.25	0.25
mjm025gN-cfa-1	0.9	0.68	1.45	2.29	1.12	0.32
mjm025gN-cfa-2	0.99	0	0	0.07	0.7	2.04
mjm025gN-cfa-3	0.9	0.1	0	0.06	0.88	2
mjmb25d-cmt-1	1.01	1.53	1.27	1.04	1.05	0.51
mjmb25d-cmt-2	1.03	1.29	1.09	1.09	1	0.5
mjmb25d-cmt-3	1.08	1.36	0.92	0.83	1.2	0.55
mjmb25d-cmt-4	1.26	1.32	1.19	1	1.06	0.51

A3. X- ray diffraction

The following section contains selected XRD profiles obtained from the analysis of the phosphate rocks, phosphorites and phosphatic sands. The major peaks have been identified and labelled in the figures.

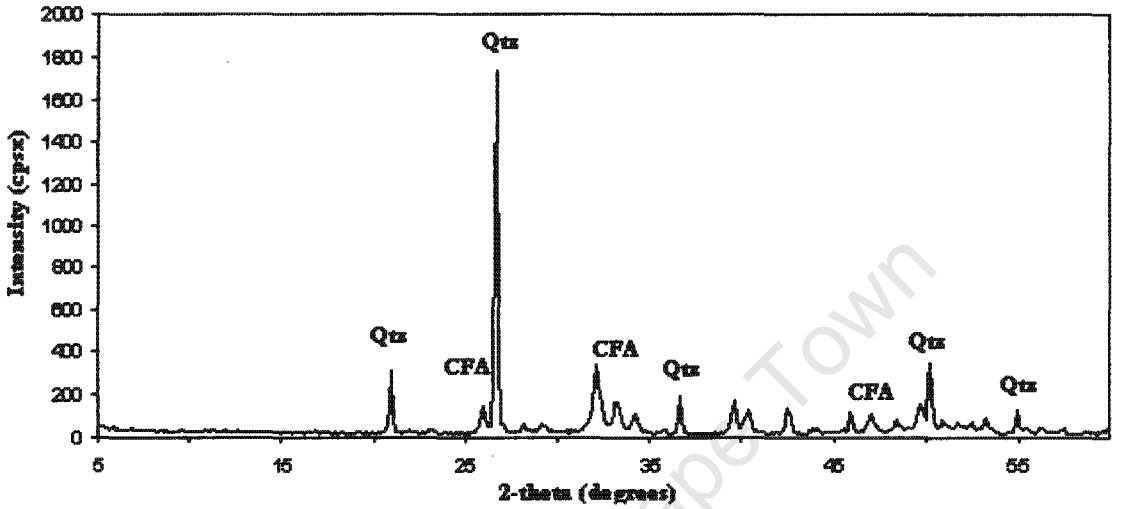

Figure A3.1. XRD profile obtained from the preferred orientation of minerals in the Gravel member sample VW43.

The diffractograms indicate that the samples contain predominantly quartz and francolite (CFA). Feldspar is also present but as a minor component. No attempt was made to determine the clay mineral assemblage. The most likely provenance of the quartz in the sediments is the underlying Elandsfontyn Formation and Table Mountain Group sandstones (TMS).

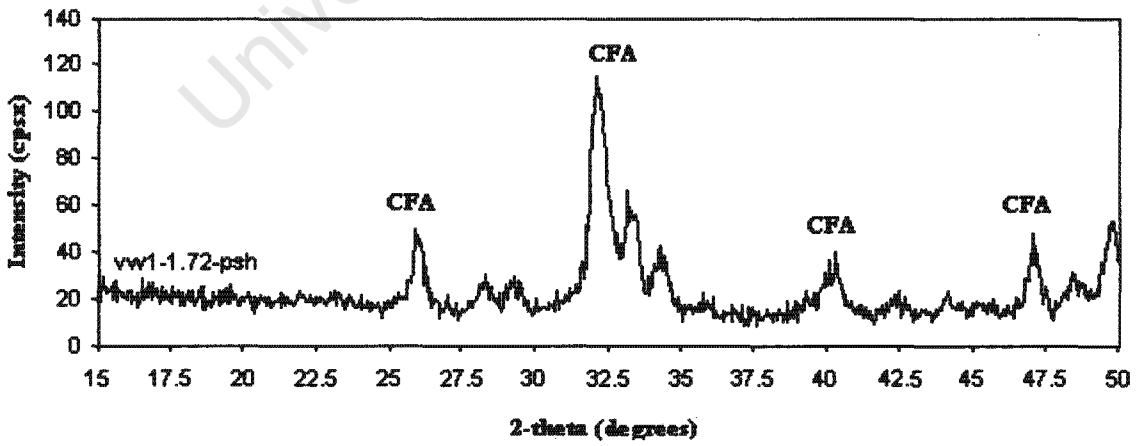

Figure A3.2. XRD profile obtained from the preferred orientation of minerals in Pelletal Phosphorite sample vw1-1.72-psh.

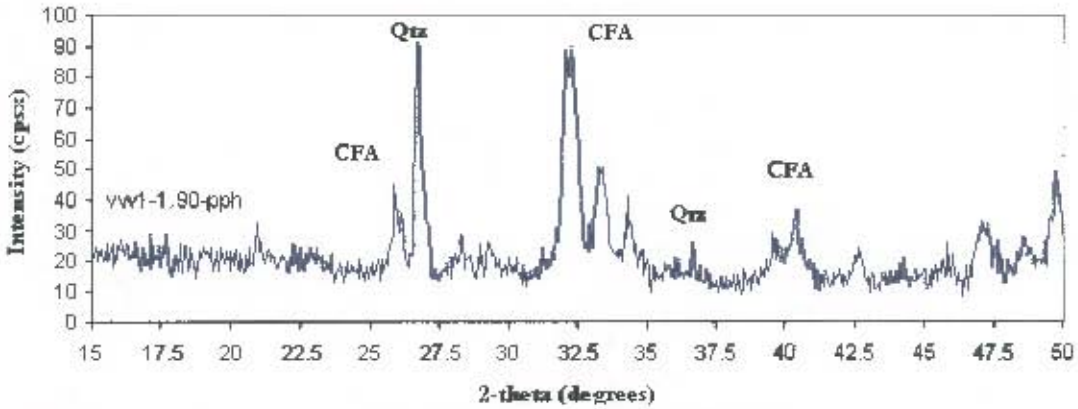

Figure A3.3. XRD profile obtained from the preferred orientation of minerals in Pelletal Phosphorite sample vw1-1.90-pph.

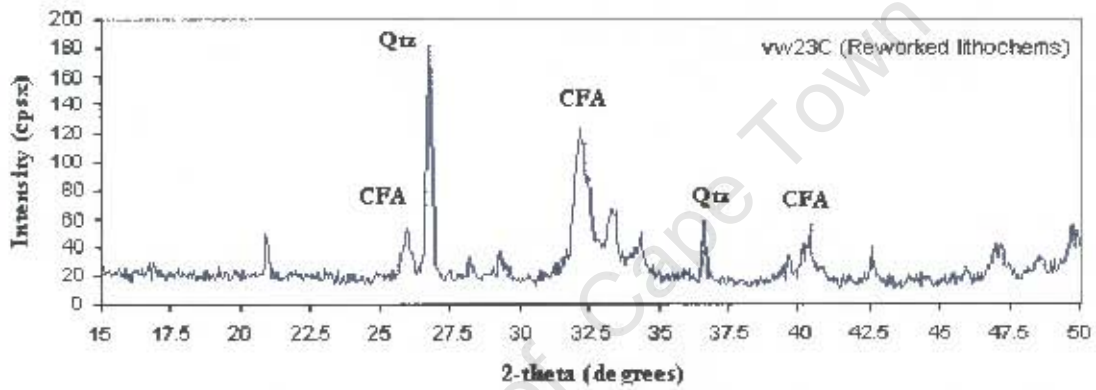

Figure A3.4. XRD profile obtained from the preferred orientation of minerals in Pelletal Phosphorite sample vw23C (reworked lithochems).

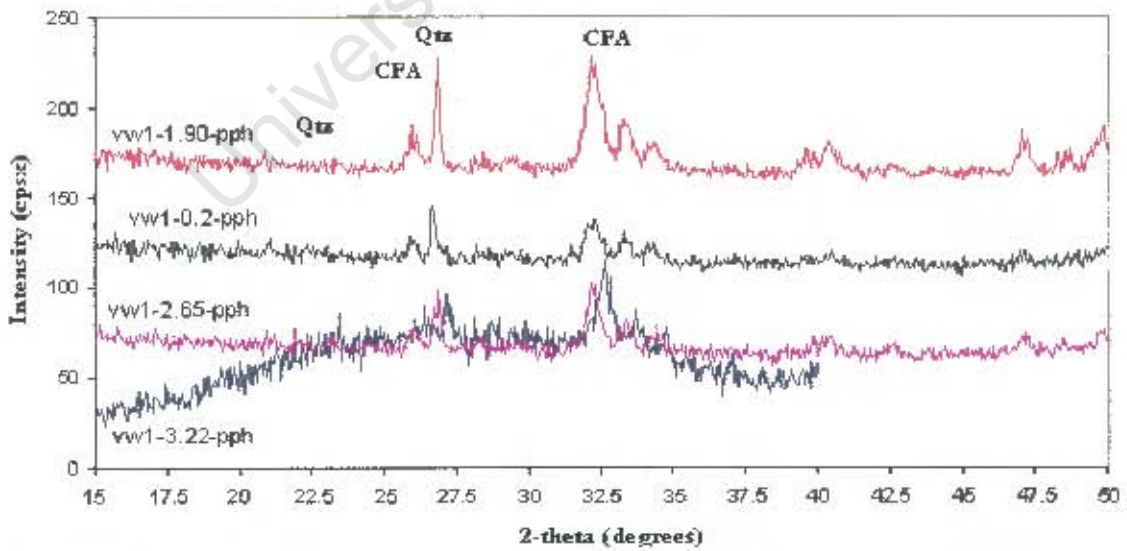

Figure A3.5. Selected XRD profiles obtained from the preferred orientation of minerals in the sub-samples. The grain type investigated is phosphorite peloids.

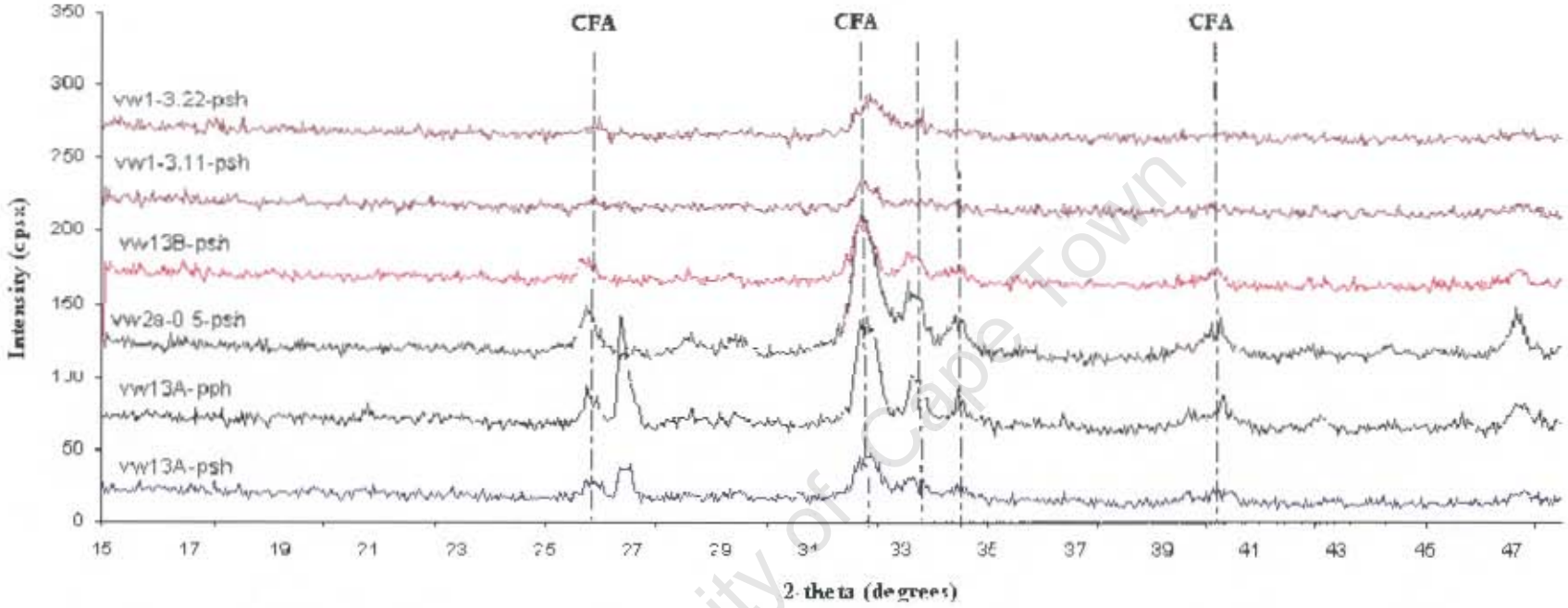

Figure A3.6. Selected XRD profiles obtained from the preferred orientation of minerals in the sub-samples. The grain type investigated was phosphatised shell fragments (PSh). The predominant mineral present is francolite (CFA) (no calcite was documented). Sub sample vw13A-pph is for comparison.

A4. Photomicroscopy

Phosphorite and phosphate rock thin sections were examined and photographed using the photomicroscope facility housed within the Department of Geological Sciences. Selected sediment samples were photographed using the photomacroscope facility housed within the Department of Archaeology.

A4.1. Results

The following pages contain the photomicrographs of various phosphorite samples. The photomicrographs document the mineralogy and the texture of the various components of the phosphorite rock samples. The phosphorite rock samples include samples taken from the basal Gravel member and Pelletal Phosphorite member at Langebaanweg. Other phosphorite samples include the Bomgat (Hoedjiespunt) phosphorite, Konstabelkop and Kreefte Bay samples and offshore phosphorites.

A4.2 Varswater Quarry (Langebaanweg)

A.4.2.1 The Basal Gravel Member

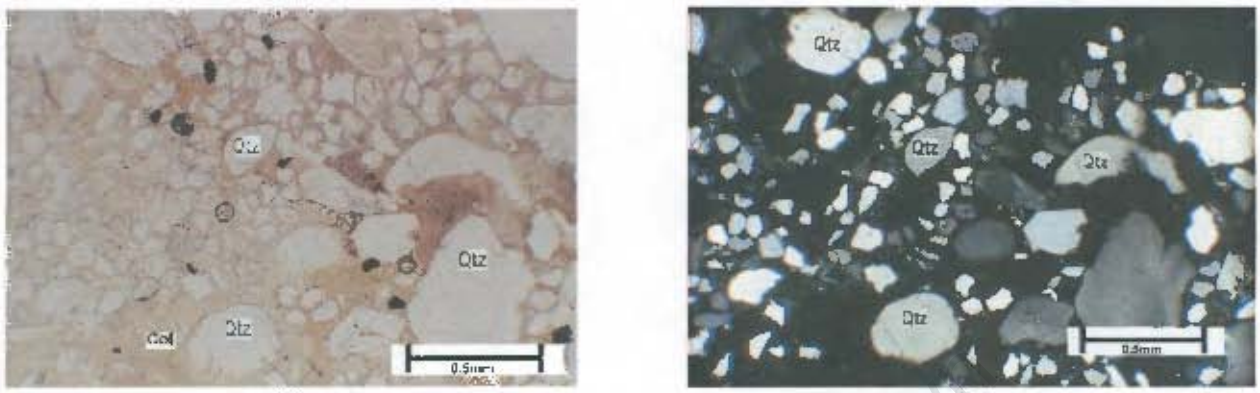

(a) (b)

Figure A4.1. Sample VW49 has a pale brown, fine grained matrix. The sample is composed of predominantly subrounded to rounded quartz grains. The highly variable CFA matrix suggests possible reworking and re-phosphatisation of the sample. In general Gravel member samples are composed of different intraclasts. (a) Sample VW49 under plane-polarised light (PPL) (b) Sample VW49 under cross polarised light (XPL), note the pseudo-isotropic properties of the carbonate fluorapatite.

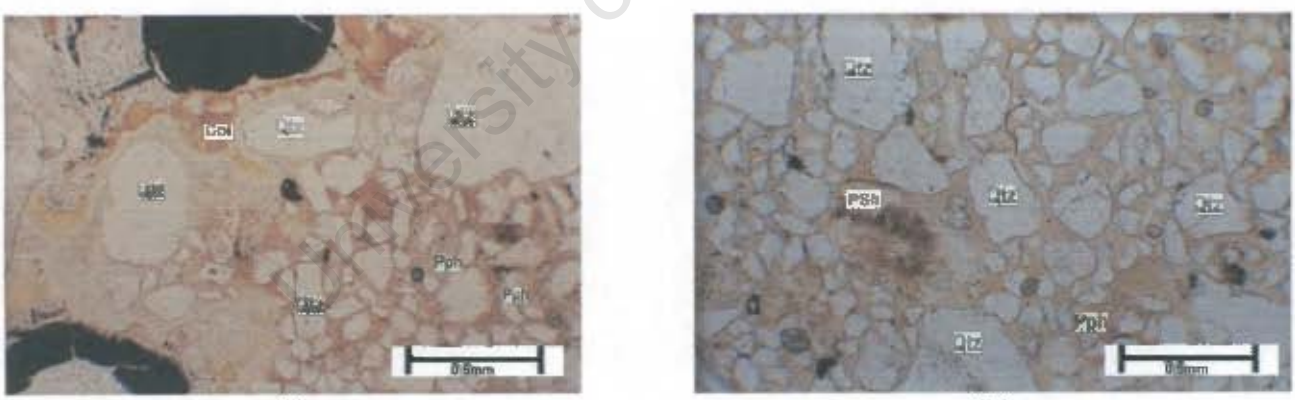

(a) (b)

Figure A4.2. Sample VW49, (a) showing the poorly sorted nature of the sample, the occurrence of phosphorite peloids (b) and the occasional phosphatised shell fragment. Phosphatised shell fragments in Gravel member samples are extremely rare (photomicrograph taken in plane-polarised light).

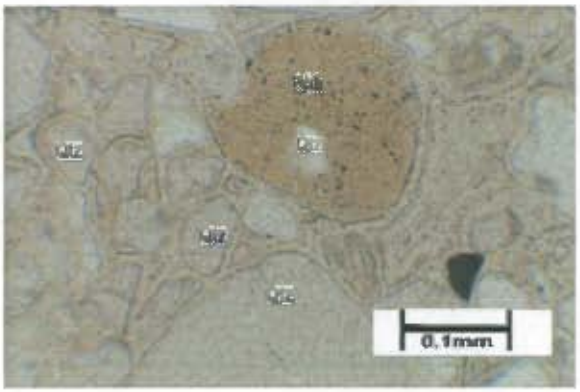

Figure A4.3. Sample VW49, showing a phosphorite peloid (Pph) with an included quartz grain. The peloid is structureless. According to Middleton (2000) benthic foraminifera also appear as nuclei for phosphorite peloids; however this may be limited to phosphorites from the Pelletal Phosphorite member. (photomicrograph taken in plane-polarised light).

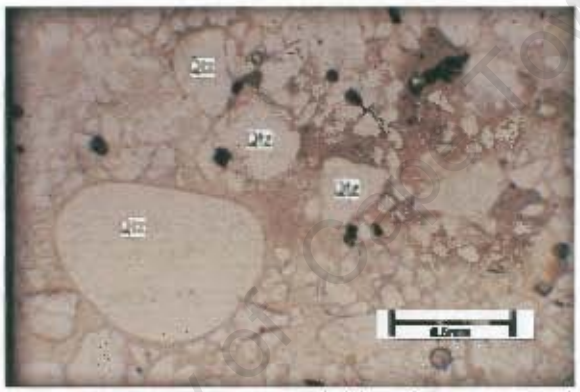

Figure A4.4. Sample VW49, showing poorly sorted, bimodal quartz grains with large well rounded and fine sub-angular a fine CFA cement (photomicrograph taken in plane-polarised light).

A.4.2.2 The Pelletal Phosphorite Member

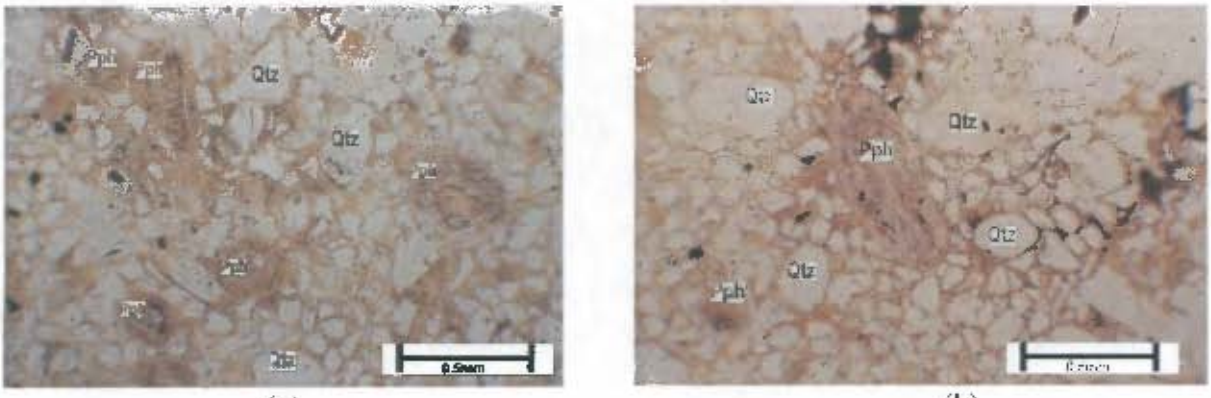

(a) (b)

Figure A4.5 Sample VW19 showing well-rounded phosphorite peloids (Pph) and quartz set within a fine cement of CFA (photomicrograph taken in plane-polarised light).

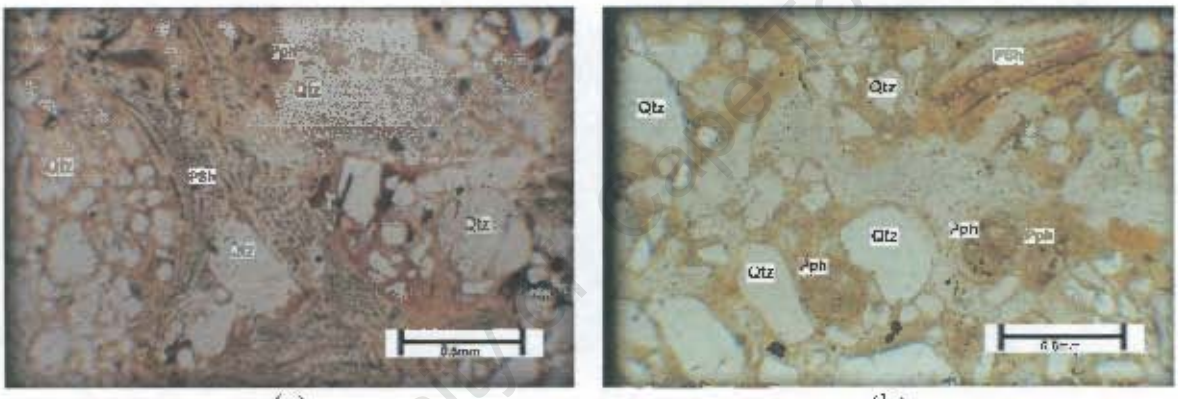

(a) (b)

Figure A4.6 Sample VW16(a) showing a phosphatised shell fragment (PSh) (b) and phosphorite peloids (photomicrograph taken in plane-polarised light).

A4.3 Bomgat (Hoedjiespunt)

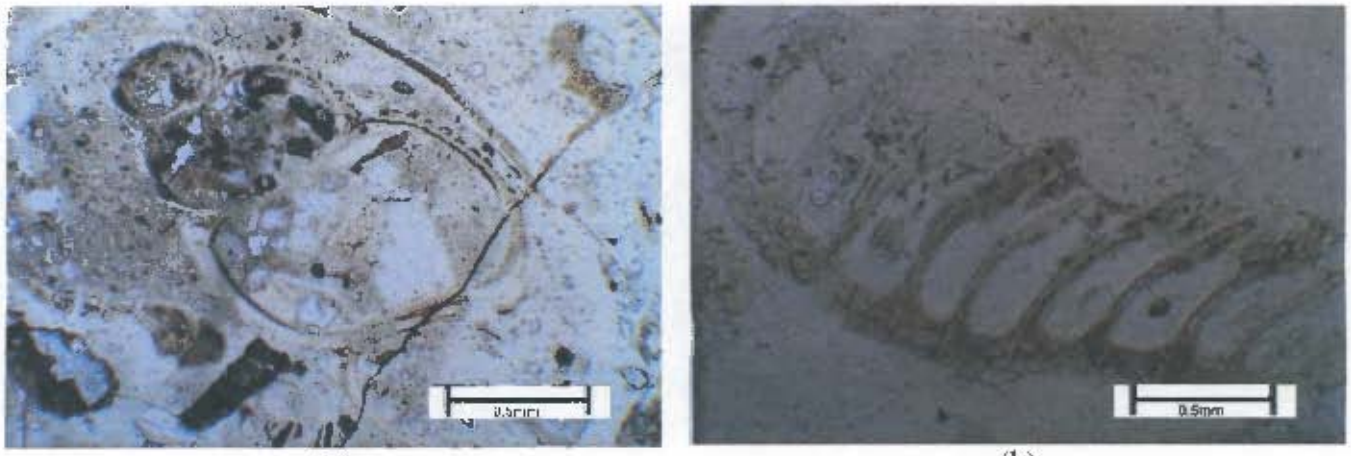

(a) (b)

Figure A4.7. Sample B1 is characterised by an extremely fine-grained homogenous, light brown CFA matrix. The sample shows biogenic grains, (a) gastropod (b) bivalve shell fragment (photomicrograph taken in plane-polarised light).

A4.4 Phosphorite nodules from offshore South Africa

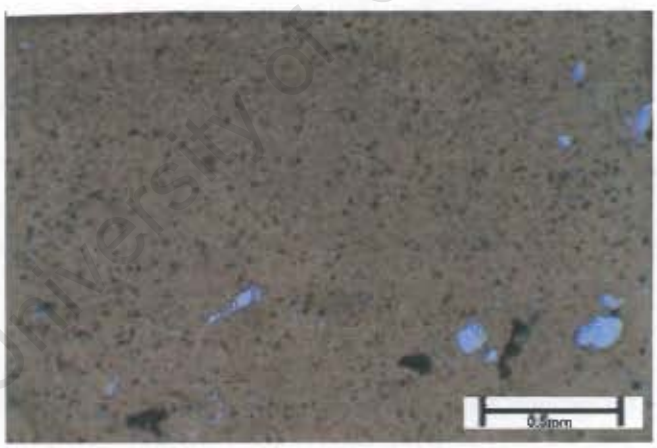

Figure A4.8. Sample Mjm3 is a Group A phosphorite and characterised by an extremely fine-grained homogenous, light brown collophane matrix. The minerals present are detrital quartz, mica and feldspar. Pyrite is also present (photomicrograph taken in plane-polarised light).

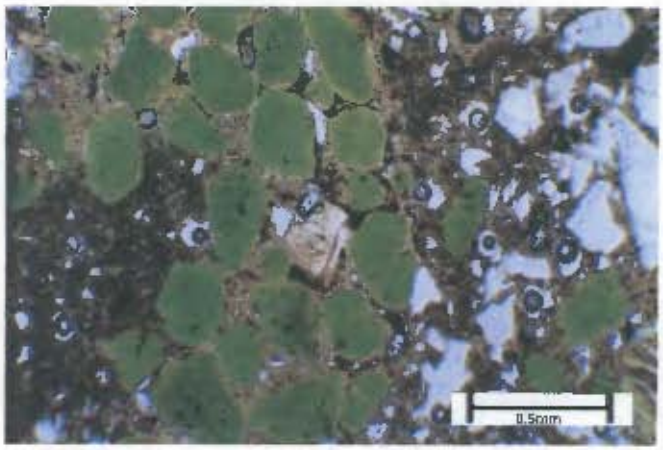

Figure A4.9. Sample 3700-3 can be classified as a Group B phosphorite or a glauco-phosphorite. The sample is characterised by predominantly authigenic glauconite (20 – 35%) and detrital quartz (35 – 40%) set within a CFA cement. Other mineral phases present are feldspar, calcite and possibly pyrite (photomicrograph taken in plane-polarised light).

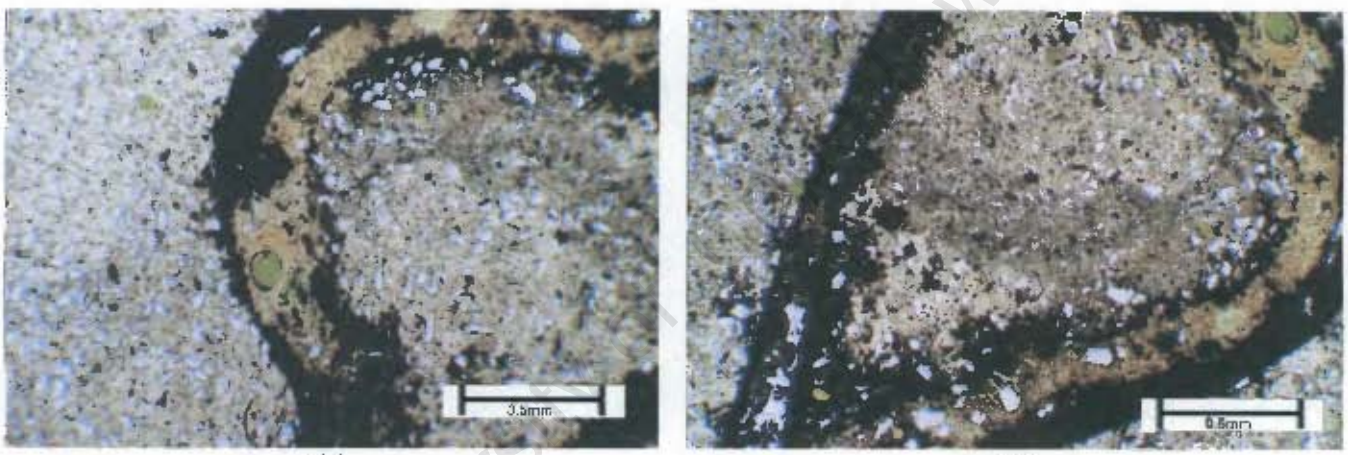

(a) (b)

Figure A4.10. Sample Mjm025(h) can be classified as a Group D phosphorite. The sample contains detrital quartz, minor amounts of glauconite set within a fine pseudo-isotropic CFA matrix (photomicrograph taken in plane-polarised light).

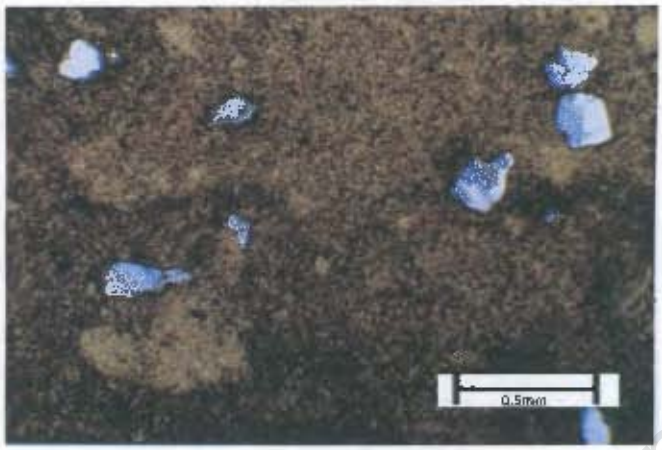

Figure A4.11. Sample Mjm028, Group E phosphorite with detrital quartz and feldspar grains. According to Mulabisana (1998) the type E phosphorites show well defined layering (photomicrograph taken in plane-polarised light).

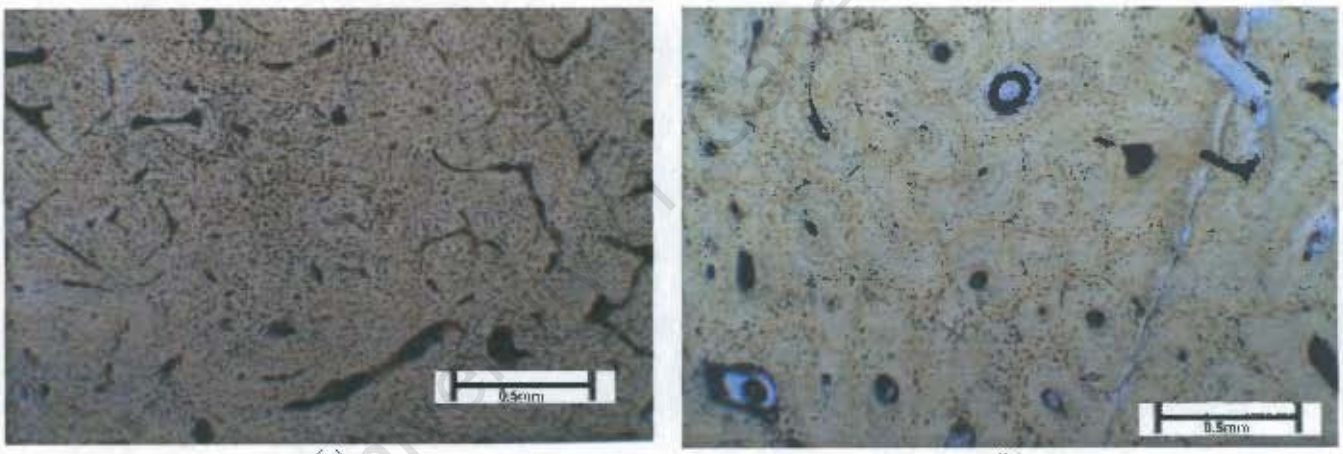

(a) (b)

Figure A4.12. Sample Mjm010 can be classified as a Group F phosphorite. Group F phosphorites are characterised by fine-grained fibrous carbonate fluorapatite, and characteristic bone honeycomb texture (photomicrograph taken in plane-polarised light).

A.4.5 Aluminium phosphate (Kreefte Bay and Konstabelkop)

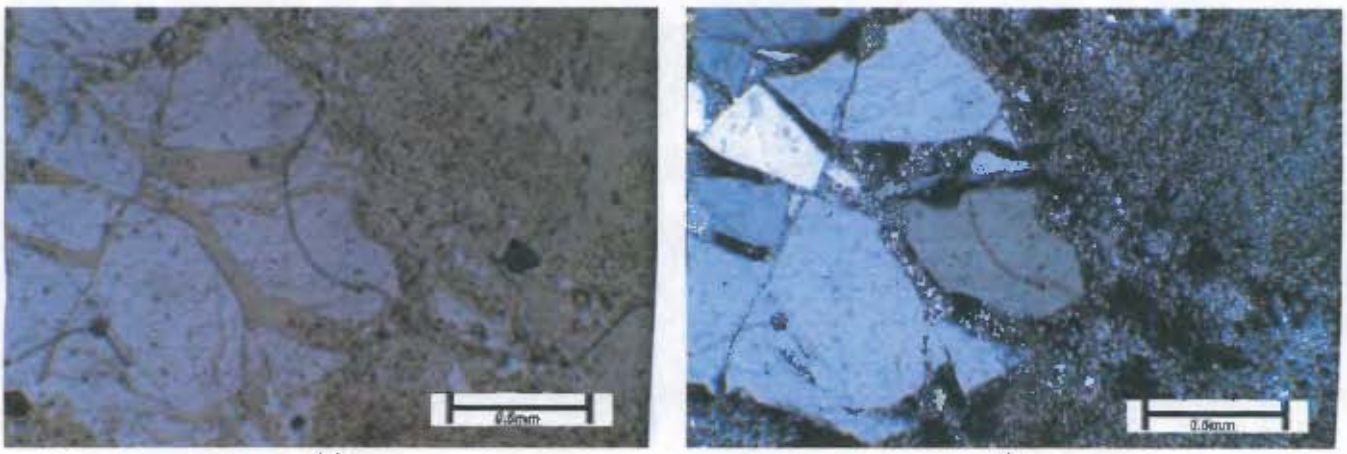

(a) (b)

Figure A4.13. Sample Ko1 shows a typical pale brown, fine grained matrix. (a) Sample Ko1 under plane-polarised light and (b) Sample Ko1 under cross polarised light (XPL).

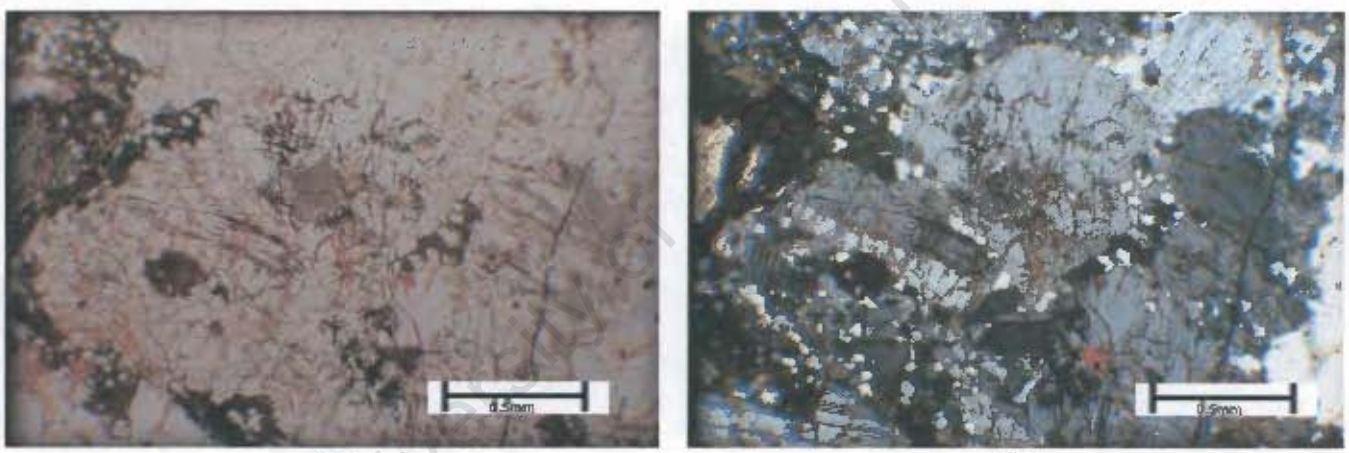

(a) (b)

Figure A4.14. KR203 is a sample of the weathered, replaced quartz porphyry. The sample shows anhedral to subhedral twinned phenocrysts of feldspar set within a ground mass of anhedral quartz. (a) Sample KR203 under plane-polarised light (PPL) (b) Sample KR203 under cross polarised light (XPL).

A5. Scanning electron microscope (SEM)

In order to document the surface textures and features of specific phosphorite grain-types (PSh, Pph, and bne) and selected phosphorite rock samples, the UCT Electron Microscope Unit's SEM (scanning electron microscope) facility housed within the R.W. James Building was used.

A5.1. Sample preparation

The sample or specimen is glued to a sample holder or "post" and coated with a thin layer of conductive material (typically gold or carbon). The gold acts as a conductor thus preventing any charge build up at the point of analysis. After the initial preparation the sample is placed in the SEM vacuum chamber and the electron gun is switched on. The high-resolution morphological images are obtained from the emission of secondary electrons.

A5.2. Results

The following pages contain the scanning electron microscope (SEM) photographs of various phosphorite samples. The SEM photographs document exterior surface textures as well as interior textures of various phosphorite rock samples and individual phosphorite grains. The phosphorite rock samples include samples taken from the Basal Gravel member and Pelletal Phosphorite member. Phosphorite grain types include phosphatised shell fragments, phosphatised bone fragments and phosphorite peloids (pellets).

A5.3. SEM Photographs

A5.3.1. SEM photographs of peloidal and biogenic phosphorite grains from the Pelletal Phosphorite Member.

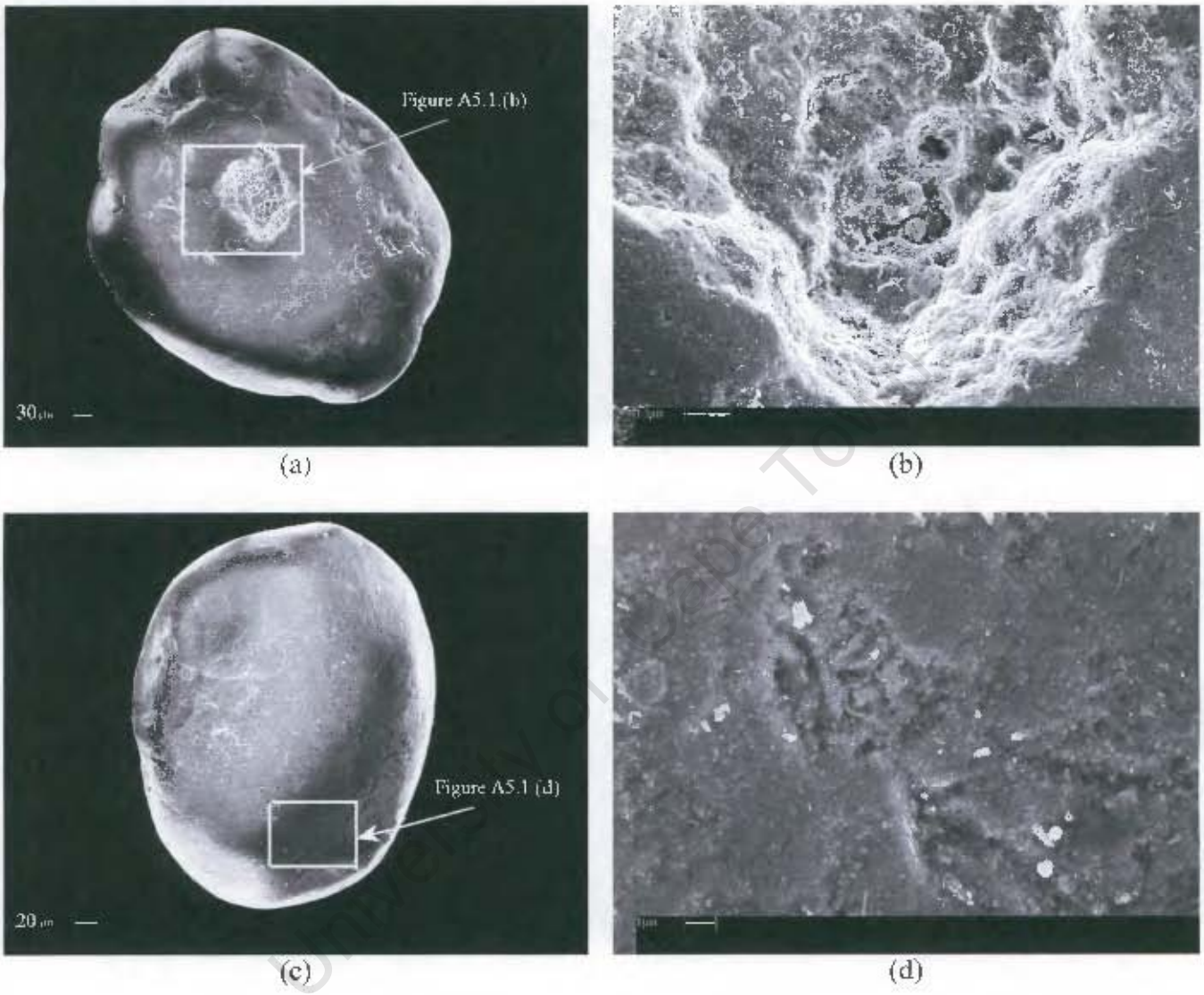

Figure A5.1. SEM photograph of sample VW1A3, showing (a) and (c) an overview of a smooth, subrounded to rounded phosphorite peloid with some surface pits, (b) a close-up image of a prominent cavity within the phosphate grain, and (d) a close-up image of the smooth and fine grained surface. The close-up images demonstrate that the surface texture and interior of the peloid is composed of very fine grained CFA (predominantly subhedral to anhedral francolite crystals).

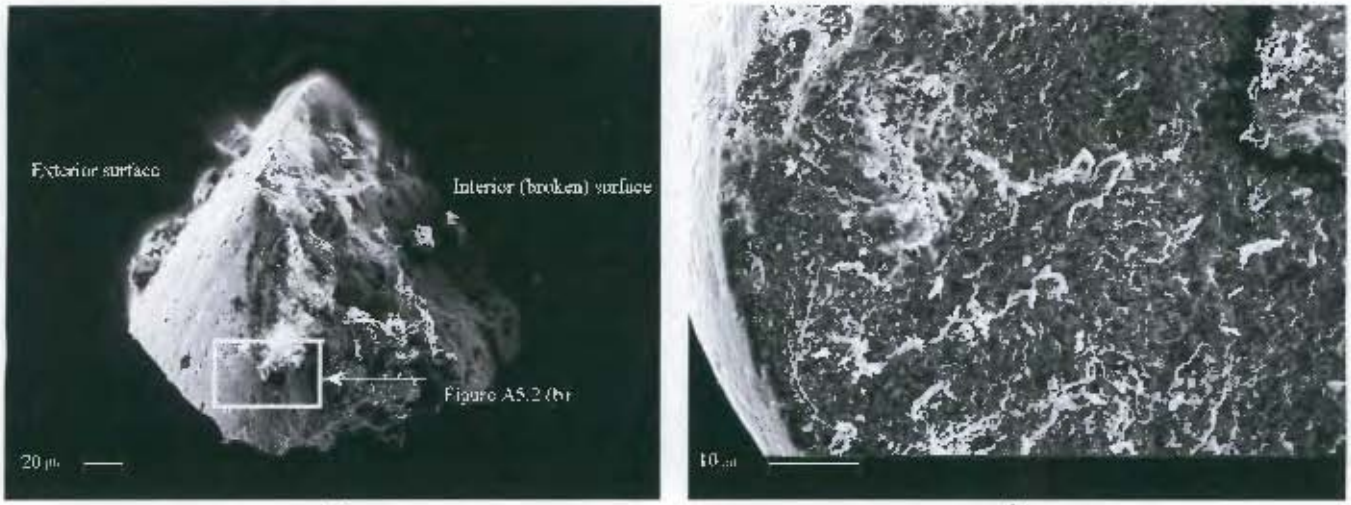

Figure A5.2. SEM photographs of a hand-crushed phosphorite peloid from sample VW1@1.20m, showing (a) an overview of a crushed well-rounded subspherical peloid and (b) a close-up image of the smooth rim and extremely fine grained, but extremely irregular fractured interior.

Figure A5.3. SEM photographs of a hand-crushed phosphorite peloid from sample VW1@1.20m, showing (a) a close-up of the interior of a phosphorite peloid and (b) a close-up image of a fractured surface on a peloid. SEM photograph (a) shows fine quartz grains set within the very fine grained CFA matrix. SEM photograph (b) shows the interior of the peloid , which is composed of anhedral to subhedral hexagonal francolite crystals.

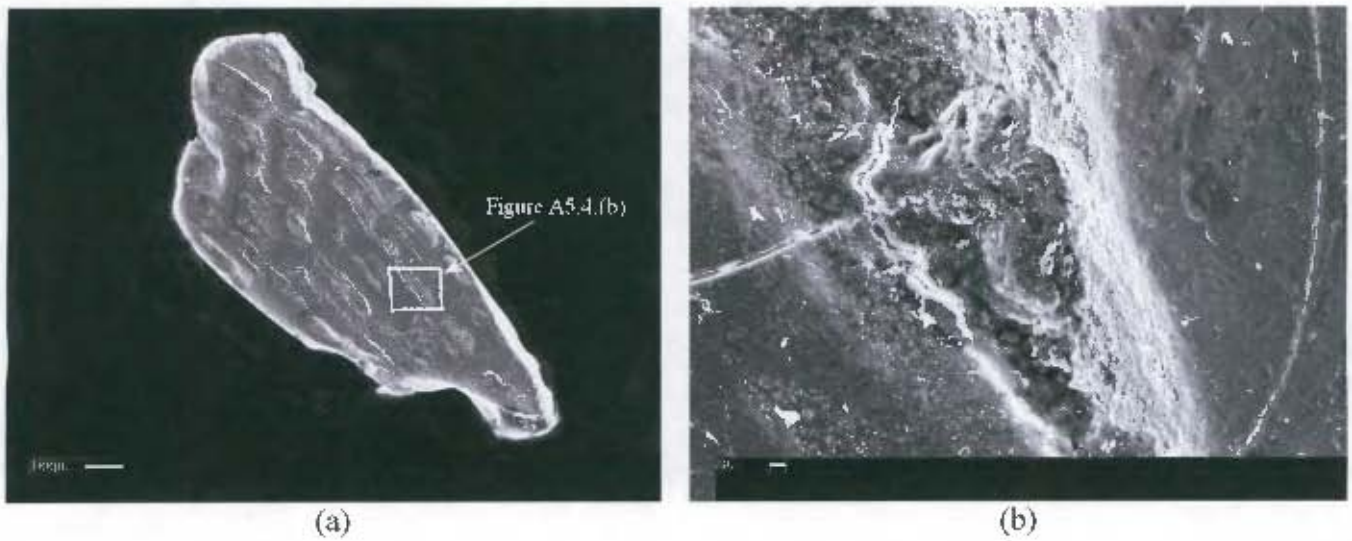

(a) (b)

Figure A5.4. SEM photographs of sample VW1A3, showing (a) an overview of an elongate, angular phosphatised shell fragment (PSh), with distinctive well rounded edges and (b) a close-up image of the micropitted, fine grained surface texture of the grain. Anhedral to subhedral francolite crystals are visible in the top left corner of the close-up SEM photograph.

(a) (b)

Figure A5.5. SEM photographs of sample VW1A3, showing (a) an overview of a phosphatised shell fragment (PSh) and (b) an overview of a heavily eroded phosphatised shell fragment (PSh). The distinctive platy shape of grain (b), which characterises phosphatised shell fragments, is however retained although the grain has been eroded and the edges rounded.

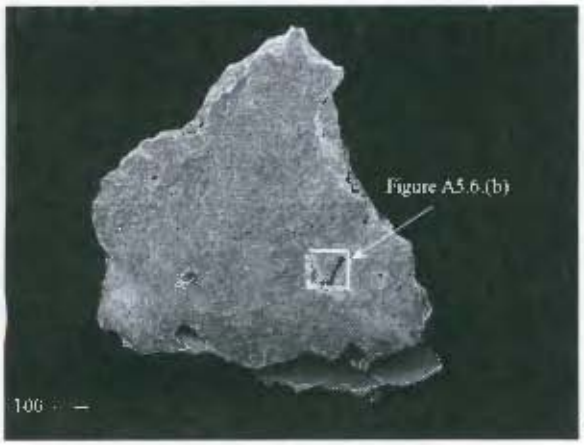

(a)

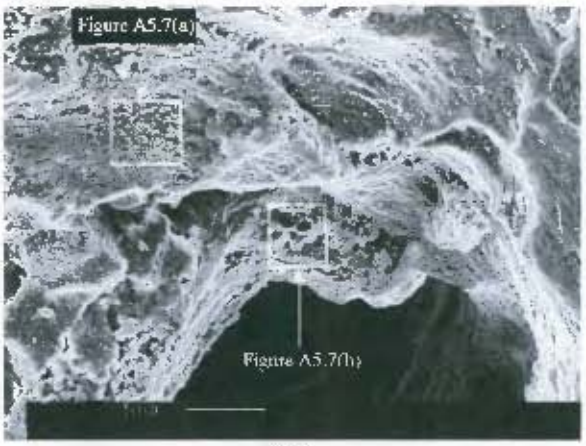

(b)

Figure A5.6. SEM photographs of sample VW463, showing (a) an overview of a phosphatised bone fragment (bnc) and (b) a close-up image of the cavity within the bone fragment. The phosphatised bone fragment is pitted with slightly rounded edges, however the general angularity of the grain indicates that it has not been reworked or transported significantly.

(a)

(b)

Figure A5.7. SEM photographs of sample VW463, showing (a & b) close-up images of voids within the phosphatised bone fragment (bnc) (from figure A5.4). The close-up images show the interior surfaces of one of the numerous cavities found on the bone fragment. The surface texture is very irregular, with globular aggregates. The irregular surface texture is caused by the aggregation of micron-sized crystals of francolite.

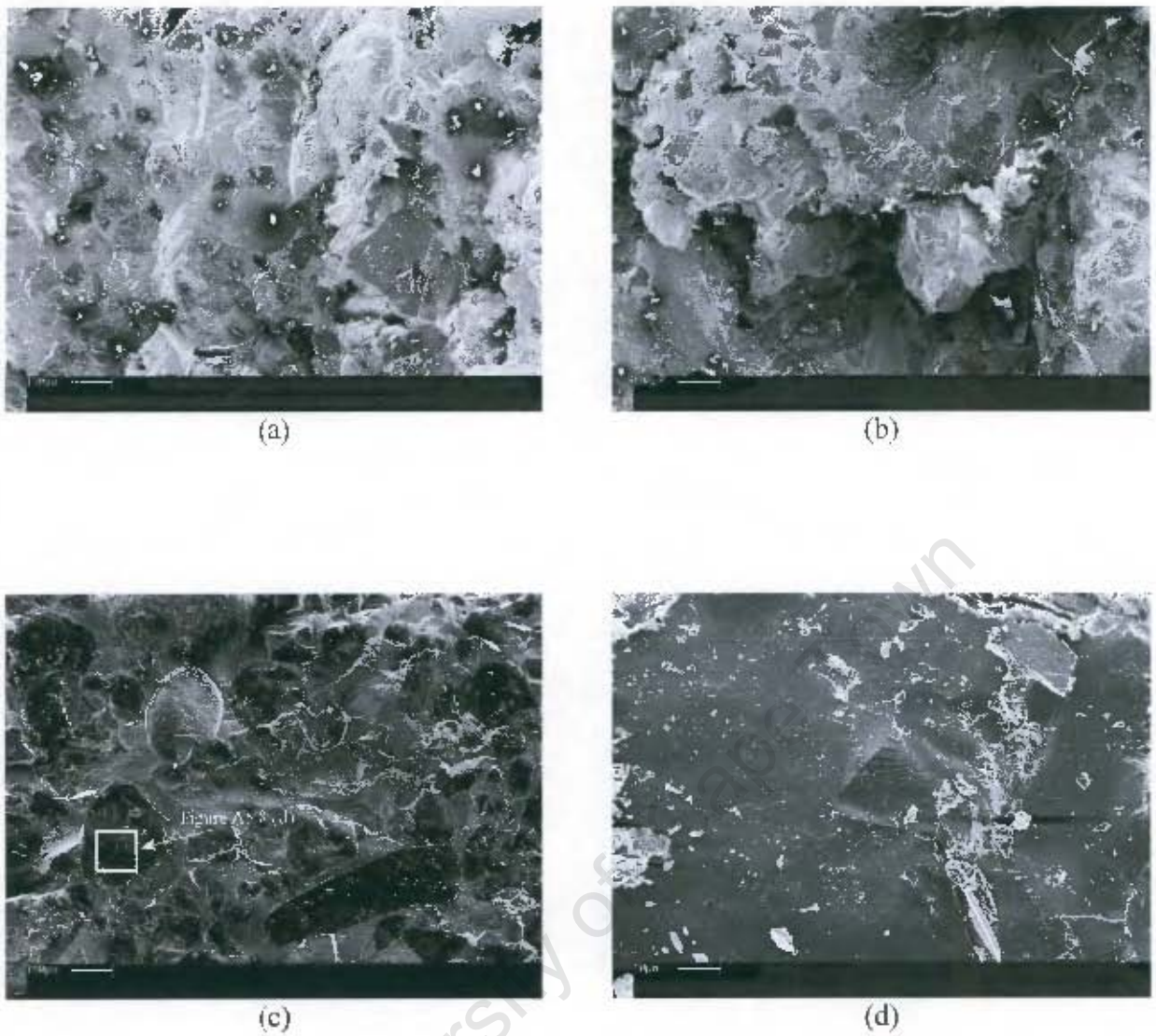

Figure A5.8. SEM photographs of the phosphorite lens sample VW19, showing (a, b & c) fine to medium grained, well rounded quartz and peloidal phosphorite in a fine CFA matrix and (d) a close-up of a quartz grain, showing characteristic conchoidal fracturing.

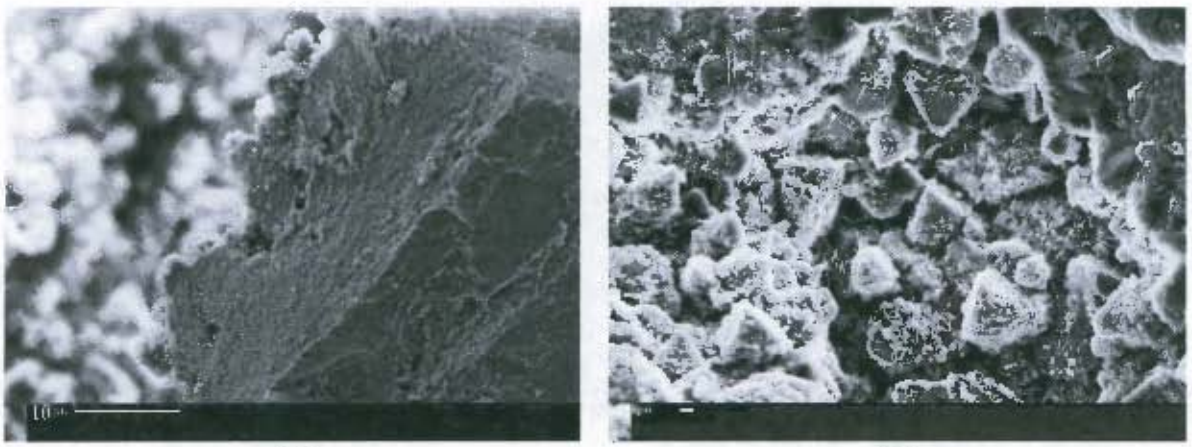

(a) (b)

Figure A5.9. SEM photographs of the phosphorite bed (lens) sample VW19, showing (a) the extremely fine grained nature of the CFA cement and the occurrence of euhedral dolomite rhombs, coated with CFA.

A5.3.2. SEM Photographs of surface textures on phosphorites from the Basal Gravel Member, Langebaanweg.

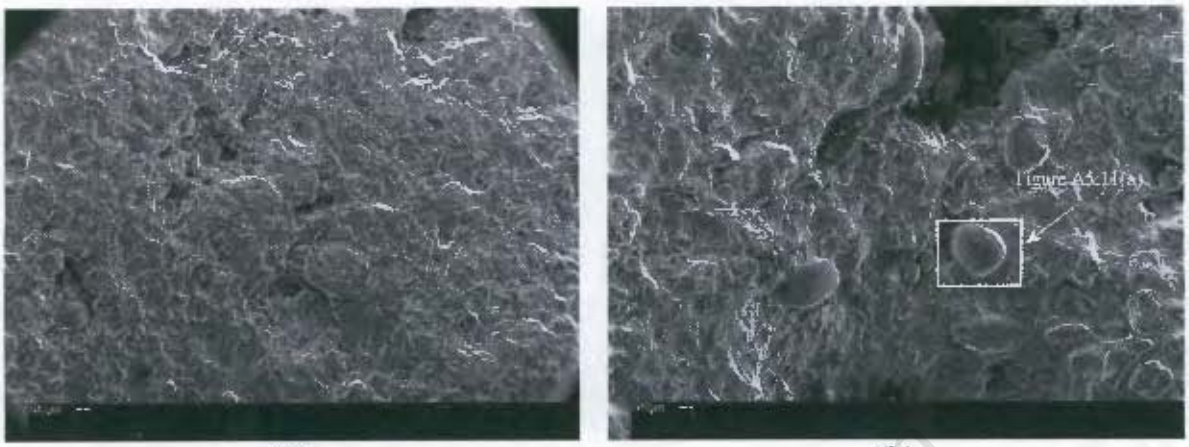

(a) (b)

Figure A5.10. SEM photograph of the interior of the phosphorite rock sample VW0-3, showing (a & b) an overview of the phosphorite rock sample. The phosphorite sample is characterised by being poorly sorted and composed of medium to fine grained, rounded to well rounded quartz grains set within a fine CFA cement.

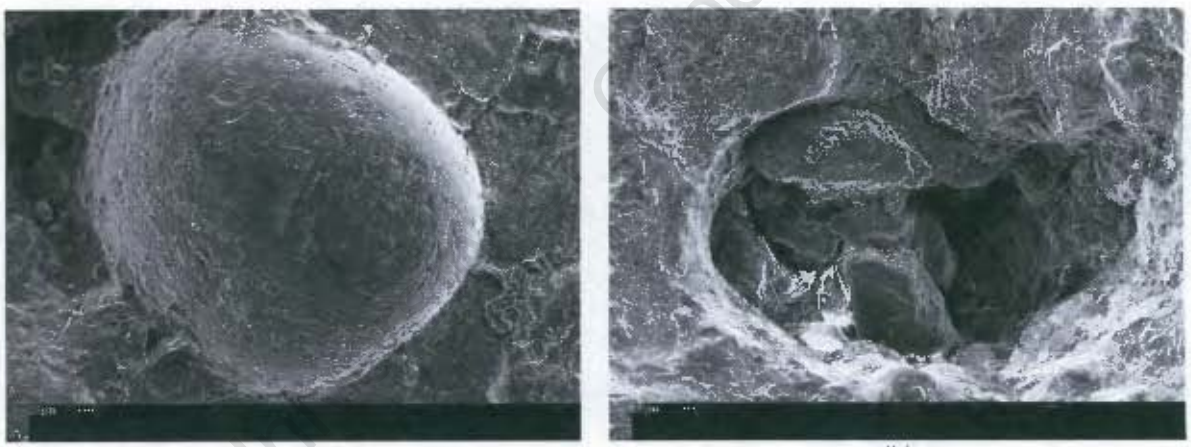

(a) (b)

Figure A5.11. SEM photograph of the interior of the phosphorite rock sample VW0-3, showing (a) a well rounded, spherical and pitted quartz grain and. (b) a close-up image of a cavity within the phosphorite sample. The cavity consists of medium to fine grained, subrounded to well rounded quartz grains set within a fine cement of CFA.

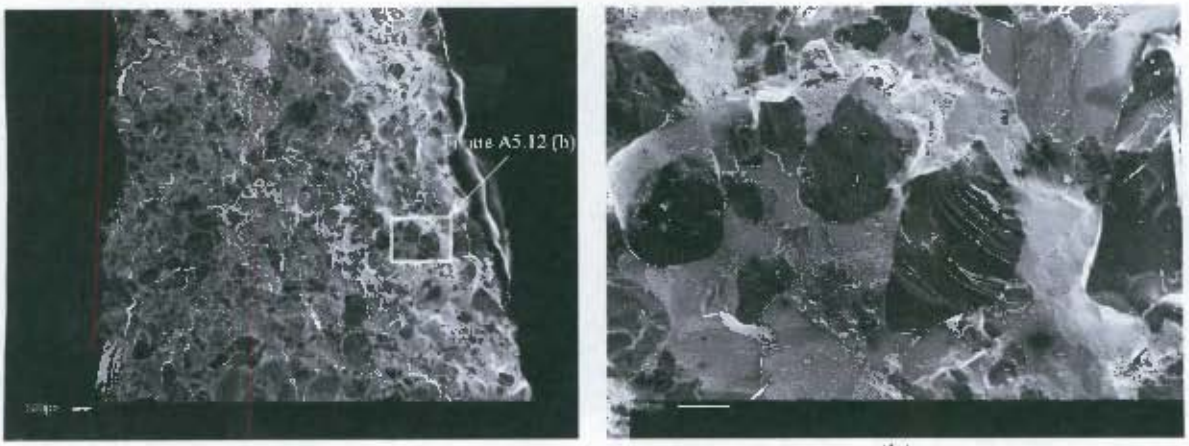

(a) (b)

Figure A5.12. SEM photograph of a phosphorite rock sample VW49, showing (a) an overview of the surface texture of the rock sample and (b) a close-up image of the surface features. The close-up image of the phosphorite reveals medium grained, subrounded to well rounded quartz grains set within a fine cement of CFA. The quartz grains show conchoidal fracturing.